MICROWAVE SPECTROSCOPY

C. H. TOWNES

University Professor of Physics
University of California

A. L. SCHAWLOW

Professor of Physics
Stanford University

DOVER PUBLICATIONS, INC.

NEW YORK

Copyright © 1975 by Dover Publications, Inc.
Copyright © 1955 by C. H. Townes and A. L. Schawlow.
All rights reserved under Pan American and International Copyright Conventions.

Published in Canada by General Publishing Company, Ltd., 30 Lesmill Road, Don Mills, Toronto, Ontario.
Published in the United Kingdom by Constable and Company, Ltd., 10 Orange Street, London WC 2.

This Dover edition, first published in 1975, is an unabridged and corrected republication of the work first published in 1955 by the McGraw-Hill Book Company, Inc.

International Standard Book Number: 0-486-61798-X
Library of Congress Catalog Card Number: 74-83620

Manufactured in the United States of America
Dover Publications, Inc.
180 Varick Street
New York, N.Y. 10014

PREFACE

This volume is concerned primarily with a relatively new field, the microwave spectroscopy of gases. The origins of microwave spectroscopy might be said to lie in the early high-frequency measurements of dielectric constants, or much more directly in the 1933 experiment of Cleeton and Williams on absorption of centimeter radiation by ammonia gas. However, a generally useful and accurate spectroscopy in the microwave region has come only after development of microwave oscillators and techniques and after demonstration in 1946 of the high resolution obtainable with low-pressure gases. Since 1946 microwave spectroscopy of gases has developed very rapidly and yielded a wide range of useful information in fields as far separated as nuclear physics, molecular structure, chemical kinetics, quantum electrodynamics, and astronomy. The purpose of this book is to present a systematic and fairly complete account of the large amount of theory, experimental data, and experimental know-how which has been developed, and to make this information more available to students, prospective research workers, and those interested in the many practical problems to which microwave spectroscopy may be applied.

The furious activity in microwave spectroscopy has made a book in this field both very desirable, because of the plethora of research work and results which need digestion and coordination, and at the same time very difficult because of the rapid development of ideas and outmoding of techniques. It is only now that microwave spectroscopy appears to have matured to the point where one can attempt a book of some perspective and lasting value.

Most microwave spectra are associated with molecules, although some important atomic microwave spectra occur and are treated here. Molecular spectra have previously been well described from the point of view of infrared spectroscopy; but the different frequency range, higher resolution, and greater accuracy of microwave spectroscopy makes available for study rather different types of phenomena such as hyperfine structure, pressure broadening, and Stark and Zeeman effects. The discussion is particularly full for those phases of the theory of molecular spectra which older types of spectroscopy have not been able to test adequately or which have been developed by persons interested in micro-

wave spectra. In addition, some attention is directed toward obtaining information about nuclear and molecular properties from the interpretation of molecular spectra.

Although a fairly complete account of microwave techniques is included, only those parts which are especially useful or somewhat peculiar to microwave spectroscopy are discussed in detail. The reader can obtain further elaboration on standard microwave techniques from the large number of excellent books on microwaves which have been published in the last few years. An attempt has been made to present not only the basic theory and properties of various types of microwave spectroscopes, but also some details of construction and specific operating characteristics which would be useful to the person faced with the problem of making and operating this type of instrument.

This volume is not primarily intended as a text, but rather as a readable reference which can be used both by students interested in one of the many aspects of microwave spectroscopy, and by those interested in research in this field. The authors have endeavored to discuss the material critically, systematically, and in the simplest way consistent with some completeness in a single volume. It is hoped that the simplicity of wording and mathematics (no group theory, as such, is used) will allow most of the discussion to be profitably read by those with a very elementary knowledge of quantum mechanics and atomic physics.

Considerable effort has been directed at making this volume valuable as a reference to a variety of users. Although the treatment is a continuously developed one, attention has been directed at making each chapter and section as independent of other sections as is practical. For example, certain expressions and definitions of symbols are often repeated in order to reduce the need for reference to other parts of the book. Appendixes give most of the tables and information needed in doing research and in interpreting microwave spectra. They also contain extensive data on nuclear and molecular constants, including essentially all those determined by microwave techniques. A complete list of publications concerning microwave spectroscopy and a subject index are included. The tables and appendixes include material published up to January 1, 1955.

Microwave spectra of solids and other closely related types of spectroscopy are not discussed because it appeared that justice to such a wide variety of fields could hardly be done in one volume. However, much of the material will be of use to those interested in types of microwave and radio-frequency spectroscopy not specifically discussed here.

The authors are grateful to their many colleagues in microwave physics who have provided information, criticism, and encouragement for this volume. These include the following, who have given helpful comments on certain sections of the manuscript:

P. W. Anderson, T. S. Benedict, R. Beringer, D. G. Burkhard, D. K. Coles, B. P. Dailey, H. M. Foley, R. A. Frosch, R. H. Hughes, C. K. Jen, C. M. Johnson, W. C. King, D. R. Lide, H. Lyons, A. H. Nethercot, R. Novick, W. V. Smith, M. W. P. Strandberg, and E. B. Wilson, Jr. In addition, they wish to thank the many students and members of the Columbia Radiation Laboratory who have uncovered errors and provided valuable discussion.

The appendixes and tables have profited from the cooperation and assistance of a number of others whose help it is a pleasure to acknowledge. Inclusion of the extensive table in Appendix IV was made both possible and convenient through the efforts of T. E. Turner and G. Reitwiesner. J. A. Klein and G. C. Dousmanis did a major part of the work involved in compiling the bibliography and Appendix VI, respectively. L. C. Aamodt, J. F. Lotspeich, M. McDermott, and B. Herzog performed many of the computations necessary for the appendixes. J. Kraitchman assisted with Appendix III, in addition to checking many of the formulas and derivations.

One of the authors (C.H.T.) would like to thank Columbia University for grant of the E. K. Adams Fellowship which assisted in preparation of this work. The other (A.L.S.) would also like to thank this University for its hospitality during the time when much of the book was written.

Charles H. Townes
Arthur L. Schawlow

CONTENTS

PREFACE v

LIST OF SYMBOLS xv

INTRODUCTION 1

CHAPTER 1. ROTATIONAL SPECTRA OF DIATOMIC MOLECULES 3

1-1. The Rigid Rotor 3
1-2. Energy Levels of the Diatomic Molecule 5
1-3. Mass Measurements 14
1-4. Absorption Intensities and Selection Rules 18

CHAPTER 2. LINEAR POLYATOMIC MOLECULES 25

2-1. Pure Rotational Spectra—General Considerations . . 25
2-2. *l*-Type Doubling 31
2-3. Perturbations between Vibrational States—Fermi Resonance 35
2-4. Moments of Inertia and Internuclear Distances . . . 40
2-5. Determination of Nuclear Masses 42

CHAPTER 3. SYMMETRIC-TOP MOLECULES 48

3-1. Introduction and General Features of Rotational Spectra. 48
3-2. Symmetric-top Wave Functions. 60
3-3. Symmetry and Inversion. 62
3-4. Effects of Nuclear Spins and Statistics 69
3-5. Intensities of Symmetric-top Transitions 73
3-6. Centrifugal Stretching in Symmetric Tops. 77
3-7. Rotation-Vibration Interactions and *l*-Type Doubling in Symmetric Tops 79
3-8. Dipole Moment Due to Degenerate Vibrations . . . 82

CHAPTER 4. ASYMMETRIC-TOP MOLECULES 83

4-1. Energy Levels of Asymmetric and Slightly Asymmetric Rotors 83
4-2. Symmetry Considerations and Intensities 92
4-3. Centrifugal Distortion 105
4-4. Structures of Asymmetric Rotors 109

CHAPTER 5. ATOMIC SPECTRA 115

5-1. The Hydrogen Atom 115
5-2. Atoms with More Than One Electron 118
5-3. Fine Structure, Electron Spin, and the Vector Model . 120

5-4. Atoms with More Than One Valence Electron . . . 123
5-5. Selection Rules and Intensities 124
5-6. Fine Structure—More Exact Treatment 126
5-7. Hyperfine Structure 130
5-8. Penetrating Orbits 143
5-9. Zeeman Effects for Atoms 143
5-10. Microwave Studies of Atomic Hyperfine Structure . . 145
5-11. Microwave Spectra from Astronomical Sources . . . 146

CHAPTER 6. QUADRUPOLE HYPERFINE STRUCTURE IN MOLECULES . . . 149

6-1. Introduction 149
6-2. Quadrupole Hyperfine Structure in Linear Molecules . 150
6-3. Quadrupole Hyperfine Structure in Symmetric Tops . 154
6-4. Second-order Quadrupole Effects 155
6-5. Asymmetric Tops 159
6-6. Hyperfine Structure from Two or More Nuclei in the Same Molecule 164

CHAPTER 7. MOLECULES WITH ELECTRONIC ANGULAR MOMENTUM . . . 174

7-1. Introduction 174
7-2. Hund's Coupling Cases 177
7-3. Rotational Energies 180
7-4. Spin Uncoupling 185
7-5. Λ-Type Doubling 188
7-6. Nonlinear Molecules 192

CHAPTER 8. MAGNETIC HYPERFINE STRUCTURE IN MOLECULAR SPECTRA . 194

8-1. Introduction 194
8-2. Coupling Schemes for Magnetic Hyperfine Structure . 196
8-3. Examples of Magnetic Hyperfine Structure in Molecules with Electronic Angular Momentum 199
8-4. Nonlinear Molecules 200
8-5. Spin-spin Interaction between Nuclei 202
8-6. Effect of Hyperfine Structure on Doubling—Hyperfine Doubling 203
8-7. Electronic Angular Momentum in $^1\Sigma$ Molecules and Its Contributions to Molecular Energy 207
8-8. Effect of Electronic Motion on Rotational Energy . . 212
8-9. Magnetic Hyperfine Interaction ($\mathbf{I} \cdot \mathbf{J}$) in $^1\Sigma$ Molecules . 215
8-10. Magnetic Hyperfine Structure of Nonlinear Molecules in $^1\Sigma$ States 219

CHAPTER 9. INTERPRETATION OF HYPERFINE COUPLING CONSTANTS IN TERMS OF MOLECULAR STRUCTURE AND NUCLEAR MOMENTS . . . 225

9-1. Introductory Remarks on Quadrupole Coupling . . . 225
9-2. Quadrupole Coupling in Atoms 226
9-3. Quadrupole Coupling in Molecules—General Considerations 228
9-4. Procedure for Calculating q in a Molecule 234
9-5. Quadrupole Coupling in Asymmetric Molecules . . . 241
9-6. Interpretation of Magnetic Hyperfine Coupling Constants 245

CHAPTER 10. STARK EFFECTS IN MOLECULAR SPECTRA 248

10-1. Introduction 248
10-2. Quantum-mechanical Calculation of Stark Energy for Static Fields 250
10-3. Relative Intensities of Stark Components and Identification of Transitions from Their Stark Patterns . . . 255
10-4. Stark Effect When Hyperfine Structure Is Present . . 258
10-5. Determination of Molecular Dipole Moments 264
10-6. Forbidden Lines and Change of Intensity Due to Stark Effect 269
10-7. Polarization of Molecules by Electric Fields 270
10-8. Stark Effects in Rapidly Varying Fields—Nonresonant Case 273
10-9. Stark Effects in Rapidly Varying Fields—Resonant Modulation 279

CHAPTER 11. ZEEMAN EFFECTS IN MOLECULAR SPECTRA 284

11-1. Introduction 284
11-2. Zeeman Effect in Weak Fields for Molecules Having Electronic Angular Momentum 284
11-3. Characteristics of Zeeman Splitting of Spectral Lines . 286
11-4. Intermediate Coupling and Intermediate Fields . . . 289
11-5. Zeeman Effect with Hyperfine Structure 289
11-6. Zeeman Effects in Ordinary Molecules ($^1\Sigma$ States) . . 290
11-7. Combined Zeeman-Stark Effects 296
11-8. Transitions between Zeeman Components 296

CHAPTER 12. THE AMMONIA SPECTRUM AND HINDERED MOTIONS 300

12-1. Introduction 300
12-2. Inversion Frequency of NH_3 302
12-3. Inversion of Other Symmetric Hydrides 307
12-4. Fine Structure of the Ammonia Inversion Spectrum—Rotation-Vibration Interactions 307
12-5. Asymmetric Forms of Ammonia 314
12-6. Hindered Torsional Motions in Symmetric Rotors . . 315
12-7. Heights of Hindering Barriers 322
12-8. Hindered Torsional Motions in Asymmetric Rotors . . 324
12-9. Selection Rules 331
12-10. Examples of Hindered Torsional Motion in Asymmetric Rotors 333

CHAPTER 13. SHAPES AND WIDTHS OF SPECTRAL LINES 336

13-1. Natural Line Breadth 336
13-2. Doppler Effect 337
13-3. Pressure Broadening 338
13-4. Absolute or Integrated Line Intensity 343
13-5. Comparison of the Van Vleck—Weisskopf Line Shape with Experiment 344
13-6. Pressure Broadening and Intermolecular Forces . . . 347
13-7. Comparison of Methods of Treating Pressure Broadening . 348
13-8. Impact Theory—Anderson's Treatment 355
13-9. Comparison of Theories with Experiment 361

13-10. Self-broadening of Linear Molecules 366
13-11. Oxygen Line Breadths 368
13-12. Temperature Dependence of Line Widths 368
13-13. Effect of Temperature on Intensities 369
13-14. High Pressures 370
13-15. Saturation Effects 371
13-16. Broadening by Collisions with Walls 374
13-17. Microwave Absorption in Nonpolar Gases 375

CHAPTER 14. MICROWAVE CIRCUIT ELEMENTS AND TECHNIQUES 376

14-1. Introduction. Electromagnetic Fields and Waves . . 376
14-2. Waveguides 379
14-3. Attenuation 383
14-4. Reflections in Waveguides 386
14-5. Cavity Resonators 390
14-6. Coupling of Cavities to Waveguide 392
14-7. Directional Couplers 394
14-8. Attenuators 397
14-9. Joints in Waveguide Systems 397
14-10. Waveguide Windows 398
14-11. Plungers 399
14-12. Other Types of Guided Waves 399
14-13. Microwave Applications of Ferrites 400
14-14. Microwave Generators 401
14-15. Klystrons 402
14-16. Magnetrons 405
14-17. Traveling-wave and Backward-wave Tubes 405
14-18. Detectors 407

CHAPTER 15. MICROWAVE SPECTROGRAPHS 411

15-1. General Principles and Ultimate Sensitivity 411
15-2. Source Modulation 416
15-3. Stark Modulation 418
15-4. Modulation-frequency Signal Amplifiers 420
15-5. Zeeman Modulation Spectrographs 424
15-6. Choice of Modulation Frequency for Spectrographs . 425
15-7. Superheterodyne Detection 425
15-8. Bridge Spectrographs 425
15-9. High-resolution Spectrometers 427
15-10. Some High-resolution Spectrometers 428
15-11. Cavity Spectrographs 435
15-12. Large Untuned Cavity 439
15-13. Spectrographs for Measurements of Zeeman Effect . . 441
15-14. Spectrometers for High and Low Temperatures . . . 443
15-15. Spectrographs for Intensity and Line-Shape Measurements 445
15-16. Gas Handling for Microwave Spectrographs 446
15-17. Spectrometers for Free Radicals 447
15-18. Microwave Radiometers 448

CHAPTER 16. MILLIMETER WAVES 451

16-1. Introduction 451
16-2. Spark Oscillators for Millimeter Waves 451

16-3. Vacuum-tube Generators 452
16-4. Harmonics from Vacuum Tubes 454
16-5. Detection of Millimeter Waves 455
16-6. Semi-conducting Crystal Harmonic Generators . . . 458
16-7. Propagation of Millimeter Waves 462
16-8. Frequency Measurement 463
16-9. Absorption Spectrographs for the Millimeter Region . . 464

CHAPTER 17. FREQUENCY MEASUREMENT AND CONTROL 466

17-1. Wavemeters 466
17-2. Quartz-crystal-controlled Frequency Standards . . . 468
17-3. Measurement of Frequency Differences 473
17-4. Frequency Stabilization of Microwave Oscillators . . 474
17-5. Control of Frequency by a Resonant Cavity 475
17-6. Stabilization of Microwave Oscillators by Absorption Lines 477
17-7. The Molecular-beam Maser 482
17-8. Realization of Atomic Frequency and Time Standards . 483

CHAPTER 18. THE USE OF MICROWAVE SPECTROSCOPY FOR CHEMICAL ANALYSIS 486

18-1. Microwave Spectroscopy for Analysis 486
18-2. Qualitative Analysis 488
18-3. Quantitative Analysis 492
18-4. Special Equipment and Techniques for Spectroscopic Analysis 497

APPENDIX I. Intensities of Hyperfine Structure Components and Energies Due to Nuclear Quadrupole Interactions 499

II. Second-order Energies Due to Nuclear Quadrupole Interactions in Linear Molecules and Symmetric Tops 517

III. Coefficients for Energy Levels of a Slightly Asymmetric Top . 522

IV. Energy Levels of a Rigid Rotor 527

V. Transition Strengths for Rotational Transitions 557

VI. Molecular Constants Involved in Microwave Spectra . . . 613

VII. Properties of the Stable Nuclei (Abundance, Mass, and Moments) 643

BIBLIOGRAPHY 649

AUTHOR INDEX 683

SUBJECT INDEX 689

FUNDAMENTAL CONSTANTS AND CONVERSION FACTORS 699

LIST OF SYMBOLS

English letters

a	magnetic hyperfine-structure interval factor
a_0	$a_0 = h^2/4\pi^2\mu e^2$ = radius of first Bohr orbit for hydrogen
A	largest rotational constant of an asymmetric rotor
$\mathbf{a}$	dyadic (tensor) connecting angular momentum and magnetic hyperfine structure
b	impact parameter, distance of closest approach of molecules
B	rotational constant; intermediate rotational constant (usually in cycles/sec.)
B_0	rotational constant in ground vibrational state
B_e	rotational constant in absence of zero-point vibrations
$\mathbf{B}$	magnetic induction
c	velocity of light
C	smallest rotational constant of an asymmetric rotor
C	$C = F(F + 1) - I(I + 1) - J(J + 1)$
D	dissociation energy
D_0, D_J, D_{JK}	centrifugal distortion constants
D	spectroscopic symbol for state with $l = 2$
$\mathbf{D}$	electric displacement
e	electron charge or, in some cases, the proton charge
e	subscript indicating equilibrium distance or conditions
E	electric field intensity
$\mathbf{E}$	electric field
f	fraction of molecules in state of interest
f_v	fraction of molecules in vibrational state of interest
F	quantum number for total angular momentum including nuclear spin
g	g factor = magnetic moment (in Bohr magnetons or sometimes in nuclear magnetons) divided by angular momentum (in units $h/2\pi$). This is negative for electron spin or orbital motion
g_I	nuclear g factor = nuclear magnetic moment (in nuclear magnetons) divided by angular momentum (in units $h/2\pi$)
h	Planck's constant

$\hbar$ $\hbar = h/2\pi$, where h is Planck's constant
$\mathbf{H}$ magnetic field intensity
H Hamiltonian
$\mathbf{i}$ electric current
I moment of inertia of molecule
I spin of nucleus in units of $h/2\pi$
J rotational quantum number
$\mathbf{J}$ total angular momentum excluding nuclear spin
k Boltzmann constant
K quantum number of component of angular momentum along molecular axis
l angular-momentum quantum number for polyatomic molecule with excited degenerate vibration
l electronic orbital angular-momentum quantum number for a single electron
$\mathbf{L}$ electronic orbital angular momentum of an entire atom or molecule
m mass of electron
m atomic magnetic quantum number
M mass of nucleus
M projection of $\mathbf{J}$ on fixed direction, magnetic quantum number
M molecular weight
M_F projection of total angular momentum, including nuclear spin, on space-fixed axis
M_I projection of nuclear spin angular momentum on space-fixed axis
M_J projection of total angular momentum, excluding nuclear spin, on space-fixed axis
M_L projection of electronic orbital angular momentum on space-fixed axis
M_S projection of electron spin on space-fixed axis
$\mathfrak{M}$ dyadic (tensor) connecting angular momentum and magnetic moment
n atomic principal quantum number
N number of molecules per cubic centimeter
$\mathbf{N}$ total orbital angular momentum including rotation of molecule
N_0 Avogadro's number; number of molecules in one molecular weight
$\mathbf{O}$ orbital angular momentum due to rotation of molecule
P associated Legendre function
$\mathbf{P}$ total angular momentum
P spectroscopic symbol for state with $l = 1$

q negative electric field gradient at nucleus $= \partial^2 V/\partial z^2$
q_J negative electric field gradient in the direction of J, or $(\partial^2 V/\partial z_J^2)_{\text{av}}$
q_l l-type doubling constant
q_Λ Λ-type doubling constant
Q nuclear quadrupole moment
Q resonator figure of merit
r internuclear distance
r intermolecular distance
r_e equilibrium distance between nuclei
R dipole moment matrix element
R Rydberg constant
s electron spin quantum number
s quantum number for internal torsional states
S degree of degeneracy for a symmetric top
S transition strength
S spectroscopic symbol for state with $l = 0$
S electron spin angular momentum
T absolute temperature
U potential energy
U_p number of unbalanced P electrons oriented along the bond
v vibrational quantum number
v linear velocity of molecule
V potential energy
W energy
x fractional importance of covalent bond
x_e anharmonicity vibrational constant
Y Dunham's molecular energy constant
Z nuclear charge, in units of the proton charge
Z characteristic impedance of a transmission line
Z_i effective nuclear charge

Greek letters

α attenuation constant
α rotation-vibration interaction constant
α fine-structure constant $2\pi e^2/hc$
α torsion angle of one part of a molecule with respect to another part
γ absorption coefficient
γ propagation constant
δ skin depth
$\Delta\nu$ line-breadth parameter
$\Delta\nu$ frequency bandwidth from which noise is passed by amplifier
ϵ dielectric constant

λ_g wavelength in waveguide
λ_0 wavelength in free space
η field gradient asymmetry
θ coordinate polar angle
κ Ray's asymmetry parameter $= (2B - A - C)/(A - C)$
Λ projection of electronic angular momentum on molecular axis
μ reduced mass
μ molecular electric dipole moment, or in some cases molecular magnetic dipole moment
μ magnetic permeability
$|\mu_{ij}|^2$ square of dipole moment matrix element, summed over directions
μ_n nuclear magneton $= he/4\pi Mc$, where M is proton mass
μ_0 Bohr magneton $= he/4\pi mc$, where m is electron mass
ν frequency
ν_0 resonant frequency; frequency absorbed by undisturbed molecule $= \omega_0/2\pi$
ν_1, ν_2, ν_3 frequencies of vibration of polyatomic molecule
π Zeeman components of line for transitions with $\Delta M = 0$
Π molecular state having one unit of electronic orbital angular momentum
ρ electric charge density
σ effective cross section area of molecule
σ Zeeman components of line for transitions with $\Delta M = \pm 1$
Σ molecular state having zero electronic orbital angular momentum
Σ projection of total electron spin on molecular axis
τ volume of space
τ integer used in specifying levels of asymmetric rotor
τ mean lifetime between collisions
τ resistivity
ψ wave function
ω angular frequency $= 2\pi\nu$
ω_e vibrational frequency (at equilibrium)
ω_0 2π times the natural molecular frequency $= 2\pi\nu_0$
Ω projection of total angular momentum, excluding nuclear spin, on molecular axis (absolute value)
Ω_I projection of nuclear spin angular momentum on molecular axis
Ω_F projection of total angular momentum, including nuclear spin, on molecular axis

INTRODUCTION

Some low-pressure gases selectively absorb electromagnetic radiation of particular wavelengths in the millimeter and centimeter range. This type of absorption can be observed in an experiment broadly represented by Fig. 1.

The source of microwaves (electromagnetic radiation of wavelength between 1 and 1000 mm) is usually an electronic tube, which emits radiation through a hollow metal pipe called a waveguide. The microwaves are detected after passage through a region of low-pressure gas (10 mm to 10^{-4} mm Hg pressure) by a silicon "crystal" or other detecting device. This detector produces an electrical signal proportional to the

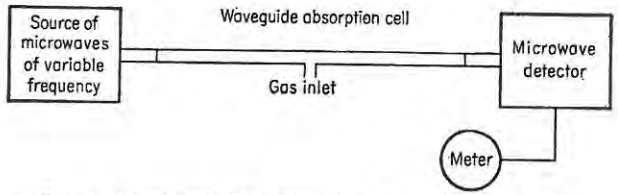

FIG. 1. Experiment for measuring microwave absorption.

microwave power which, after possible amplification, is observed on a meter or oscilloscope. As the frequency of the microwaves is varied, absorption appears as a sudden decrease in the voltage output of the detector.

Electronic techniques are characteristic of microwave spectroscopy, being involved in the production, detection, and amplification of microwaves. In some cases very sensitive electronic circuits are needed for proper detection and amplification, since the fractional power decrease may be quite small—as small as one part in 10^8 in an absorption path of 1 meter. In a few cases the absorption may be as much as 90 per cent in 1 meter path, and very easily detectable.

At gas pressures near 1 atm, a small microwave absorption may occur over a wide range of frequency. As the pressure is lowered, the range of frequency absorbed decreases proportionally down to pressures near 10^{-3} mm Hg, where the range is so small that the term absorption "line" is well merited. Very significantly, and contrary to experience in most

other types of spectroscopy, the intensity of absorption in the center of the line does not appreciably decrease with this enormous decrease in pressure.

Because of the narrowness of absorption lines at low pressures, and the flexibility and sensitivity of electronic techniques, this type of experiment and its many refinements and ramifications form a basis for the precise, widely applicable microwave spectroscopy of gases which is the subject of this volume.

Consider now the frequencies absorbed. These must be interpretable in terms of the structure and behavior of the absorbing molecules. The motions (or transitions) of electrons in atoms and molecules are known to produce characteristically spectra in the optical and ultraviolet region. The slower vibrational motions of atoms in molecules are primarily responsible for the rich infrared spectra. It is the still slower end-over-end rotation of molecules which have characteristic frequencies so low that they lie in the microwave range and dominate microwave spectra.

Discussion of the interpretation of microwave spectra will begin with the rather simple diatomic molecules and progress in following chapters to successively more complex cases of linear polyatomic molecules, symmetric-top molecules, and asymmetric-top molecules.

Superimposed on the frequencies associated with molecular rotation are many interesting fine and hyperfine effects, some of which have been observed clearly for the first time by microwave techniques. These will be discussed after the broader outlines of rotational spectra have been treated.

CHAPTER 1

ROTATIONAL SPECTRA OF DIATOMIC MOLECULES

1-1. The Rigid Rotor. If the distance between nuclei in a diatomic molecule is considered fixed, the possible frequencies of the end-over-end rotation of this "rigid rotor" can be rather simply obtained. Using assumptions of the "old" quantum mechanics, the angular momentum must be some integral multiple of $h/2\pi$, so that

$$2\pi\nu I = \frac{Jh}{2\pi}$$

where h is Planck's constant, I is the molecular moment of inertia about axes perpendicular to the internuclear axis, ν is the frequency of rotation, and J is a positive integer giving the angular momentum in units of $h/2\pi$. Hence the frequencies expected from such a system are

$$\nu = \frac{Jh}{4\pi^2 I} \tag{1-1}$$

The moment of inertia I comes largely from the nuclei, where most of the molecular mass is concentrated, and for diatomic molecules of ordinary masses is of such size that for small integral values of J, the frequency ν is of the order 10,000 to 100,000 Mc, or the wavelength in the region 3 cm to 3 mm.

On this simple basis one might expect a rotation about the molecular axis to occur also and to have characteristic frequencies a few thousand times greater because the moment of inertia about this axis is produced by electrons, which are very much lighter than the nuclei. These frequencies lie then near the optical region, and in a very rough way the electronic frequencies may be regarded as due to this type of rotation about the molecular axis. Since these frequencies are very high, they lie far beyond the microwave range and are not ordinarily excited at room temperature. They will therefore be neglected in most of the following treatment. A somewhat more sophisticated and rigorous determination of the frequencies produced by a rigid diatomic molecule can be obtained by finding the permitted energy levels from wave mechanics (see [62], p. 271, or [305], p. 60). As the molecule rotates about its center of gravity, its orientation in space may be specified by the spherical

polar coordinates θ and ϕ. The wave equation may then be written

$$\frac{h^2}{8\pi^2 I}\left[\frac{1}{\sin\theta}\frac{\partial}{\partial\theta}\left(\sin\theta\frac{\partial\psi}{\partial\theta}\right)+\frac{1}{\sin^2\theta}\frac{\partial^2\psi}{\partial\phi^2}\right]+W\psi=0 \qquad (1\text{-}2)$$

where ψ is the wave function and W the rotational energy of the molecule. The variables θ and ϕ may be separated by substituting

$$\psi = \Theta(\theta)\Phi(\phi)$$

which gives

$$\frac{d^2\Phi}{d\phi^2} = -M^2\Phi \qquad (1\text{-}3)$$

and

$$\frac{h^2}{8\pi^2 I}\left[\frac{1}{\sin\theta}\frac{d}{d\theta}\left(\sin\theta\frac{d\Theta}{d\theta}\right)-\frac{M^2\Theta}{\sin^2\theta}\right]+W\Theta=0 \qquad (1\text{-}4)$$

where M^2 is an arbitrary constant.

Solutions of these equations which are single-valued and normalized can be obtained only when

$$W = \frac{h^2}{8\pi^2 I}J(J+1)$$

where J is a positive integer and M is an integer such that $|M| \leq J$. Such solutions are

$$\Phi_M = \frac{1}{\sqrt{2\pi}}e^{iM\phi} \qquad (1\text{-}5)$$

$$\Theta_{MJ} = \left[\frac{(2J+1)(J-|M|)!}{2(J+|M|)!}\right]^{\frac{1}{2}} P_J^{|M|}(\cos\theta) \qquad (1\text{-}6)$$

where $P_J^{|M|}(\cos\theta)$ is an associated Legendre function. $[J(J+1)](h^2/4\pi^2)$ is the square of the total angular momentum, so that the angular momentum may for convenience be designated by J. Similarly the projection of the angular momentum on the polar axis is given by $M(h/2\pi)$, or simply by the integer M.

The frequency observed when the molecule makes a transition between a lower state of energy W_1 and an upper state of energy W_2 is given by

$$\nu = \frac{W_2 - W_1}{h} = \frac{h}{8\pi^2 I}[J_2(J_2+1) - J_1(J_1+1)] \qquad (1\text{-}7)$$

From the correspondence principle, these frequencies may be expected to approximately equal the frequencies given by expression (1-1); hence J_2 should equal $J_1 + 1$, and

$$\nu = 2B(J+1) \qquad (1\text{-}8)$$

where J is the angular-momentum quantum number for the lower state (J_1), and $B = (h/8\pi^2 I)$ is called the rotational constant. The quantity

B is often expressed in units of cm^{-1} for infrared spectroscopy. In that case $B = (h/8\pi^2 Ic)$. For microwave spectroscopy, B will generally be given in cycles per second, or $B = h/8\pi^2 I$. However, numerical values will usually be quoted in megacycles, or 10^6 cycles/sec. The selection rule that $J_2 = J_1 + 1$ or $\Delta J = \pm 1$ for dipole radiation of a diatomic molecule will be more rigorously demonstrated in the discussion of intensities later in this chapter.

1-2. Energy Levels of the Diatomic Molecule. From Eq. (1-8) it is seen that the spectrum of a rigid rotor consists of absorption lines equally spaced in frequency with an interval $2B$. Although the rigid rotor is an idealization to which actual molecules conform to a good approximation, accurate spectroscopic measurement reveals many deviations from this approximation. As J increases and the molecule rotates faster, it stretches so that the moment of inertia increases. Moreover, the nuclei vibrate back and forth along the line joining them even in the lowest vibrational state. A much greater difficulty from the point of view of obtaining a complete theoretical treatment is that the entire molecular system, composed of interacting electrons as well as nuclei, is so complicated that an exact quantum-mechanical solution is impossible.

However, since the electrons are very much lighter than the nuclei and move in electric fields of approximately the same intensity, the electron motion is very much faster than that of the nuclei; *i.e.*, many cycles of the electronic motion occur during a small portion of a cycle of the nuclear motion. It is therefore reasonable to treat first the electronic motion, considering the nuclei as fixed. Then the internuclear distance r appears as a parameter. In this way the electrons are found to be capable of occupying several states, each giving the molecule a particular value of the energy U, for each internuclear distance. Generally in microwave spectroscopy only the lowest of these electronic states is important.

As the internuclear distance is slowly varied, the electronic energy varies. Because the electronic motion is so fast in comparison with the nuclear motion, at each instant the electronic energy may be considered to have reached its equilibrium value corresponding to that distance. Thus we are justified in treating the vibration and rotation of the nuclei separately from the electronic motion. In this treatment $U(r)$, which is the sum of the electron energy plus energy of electrostatic interaction between the two nuclei, appears as the potential energy. The validity of this approximation was discussed by Born and Oppenheimer ([8]; see also [62], pp. 259–274, and [21], Chap. I). They showed that the entire molecular energy, including that due to electronic motion, can be expanded in powers of $(m/M)^{\frac{1}{4}}$, where m is the electronic mass and M an average nuclear mass. Separation of nuclear and electronic motions hence corresponds to selecting the larger terms of the series expansion

and neglecting those which are smaller by $(m/M)^{\frac{1}{2}}$ or more. In some cases the neglected terms lead to observable effects, but they can only with difficulty be taken into account.

Using the approximation that the variation in electron energy with nuclear motion may be included in the potential $U(r)$, the wave equation for vibration and rotation of a diatomic molecule becomes

$$\frac{1}{M_1}\nabla_1^2\psi + \frac{1}{M_2}\nabla_2^2\psi + \frac{8\pi^2}{h^2}[W - U(r)]\psi = 0 \tag{1-9}$$

in which ψ is the wave function for the nuclear motion, M_1 and M_2 are the nuclear masses, and

$$\nabla_i^2 = \frac{\partial^2}{\partial x_i^2} + \frac{\partial^2}{\partial y_i^2} + \frac{\partial^2}{\partial z_i^2} \qquad \text{where } i = 1 \text{ or } 2 \tag{1-10}$$

x_i, y_i, and z_i being Cartesian coordinates of the ith nucleus relative to axes fixed in space.

Transforming to spherical polar coordinates r, θ, ϕ of the second nucleus relative to the first as origin (*cf.* [62], p. 264),

$$\frac{1}{r^2}\frac{\partial}{\partial r}\left(r^2\frac{\partial\psi}{\partial r}\right) + \frac{1}{r^2\sin\theta}\frac{\partial}{\partial\theta}\left(\sin\theta\frac{\partial\psi}{\partial\theta}\right) + \frac{1}{r^2\sin^2\theta}\frac{\partial^2\psi}{\partial\phi^2} + \frac{8\pi^2\mu}{h^2}[W - U(r)]\psi = 0 \tag{1-11}$$

where μ is the reduced mass, $M_1M_2/(M_1 + M_2)$. The variables may be separated by the substitution

$$\Psi = R(r)\Theta(\theta)\Phi(\phi) \tag{1-12}$$

$\Theta(\theta)$ and $\Phi(\phi)$ turn out to be the same as the wave functions found above for the rigid rotor.

The radial wave function $R(r)$ obtained by the separation process is given by

$$\frac{1}{r^2}\frac{d}{dr}\left(r^2\frac{dR}{dr}\right) + \left\{\frac{8\pi^2\mu}{h^2}[W - U(r)] - \frac{J(J+1)}{r^2}\right\}R = 0 \tag{1-13}$$

The term $J(J + 1)/r^2$ may be regarded as a potential energy associated with the centrifugal force due to the rotational angular momentum J. Substituting the expression

$$R(r) = \frac{1}{r}S(r) \tag{1-14}$$

we get

$$\frac{d^2S}{dr^2} + \left\{-\frac{J(J+1)}{r^2} + \frac{8\pi^2\mu}{h^2}[W - U(r)]\right\}S = 0 \tag{1-15}$$

The solutions of Eq. (1-15) will obviously depend on the form of $U(r)$. Since it is seldom possible actually to solve the electronic wave equation, it is customary to use an empirical expression for $U(r)$.

From experimental studies of molecular spectra and from calculations on simple molecules, the general form of $U(r)$ is known to be that of Fig. 1-1 (see [471]). At large distances the atoms are independent, and the force between them is negligible. Their energy is then just the sum of the energies of the individual atoms. At very small distances, when the atoms are "in contact," they must repel each other. At some intermediate distance there must be a potential minimum, corresponding to the equilibrium distance of the atoms.

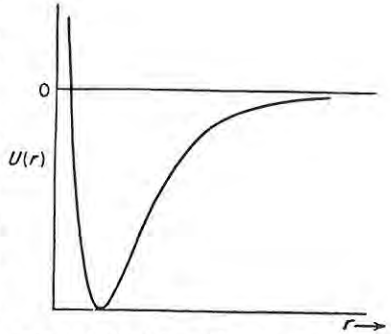

FIG. 1-1. Variation of molecular potential energy $U(r)$ with internuclear distance r.

Solution for Morse Potential. A potential which fulfills these requirements is the Morse function [16]

$$U(r) = D(1 - e^{-a(r-r_e)})^2 \tag{1-16}$$

where D = dissociation energy of the molecule
r_e = equilibrium distance between nuclei
a = a constant

The Morse function differs from the true potential at $r = 0$, where the actual potential would be extremely large. However, the Morse potential is also quite large at $r = 0$ and this is a region where the wave function of the vibrating rotor is expected to be small so that the discrepancy is not serious.

Using the Morse potential function, the radial equation (1-15) becomes

$$\frac{d^2S}{dr^2} + \left[-\frac{J(J+1)}{r^2} + \frac{8\pi^2\mu}{h^2}(W - D - De^{-2a(r-r_e)} + 2De^{-a(r-r_e)})\right]S = 0 \tag{1-17}$$

The solution of this equation for $J = 0$ has been given by Morse [16] and for any J by Pekeris [52]. Substituting

$$y = e^{-a(r-r_e)} \qquad \text{and} \qquad A = J(J+1)\frac{h^2}{8\pi^2\mu r_e^2} \tag{1-18}$$

in Eq. (1-17), we obtain

$$\frac{d^2S}{dy^2} + \frac{1}{y}\frac{dS}{dy} + \frac{8\pi^2\mu}{a^2h^2}\left(\frac{W - D}{y^2} + \frac{2D}{y} - D - \frac{Ar_e^2}{y^2r^2}\right)S = 0 \tag{1-19}$$

For $A \neq 0$, it is necessary to expand r_e^2/r^2 in terms of y:

$$\frac{r_e^2}{r^2} = \frac{1}{[1 - (\ln y)/ar_e]^2} = 1 + \frac{2}{ar_e}(y - 1) + \left(-\frac{1}{ar_e} + \frac{3}{a^2r_e^2}\right)(y - 1)^2 + \cdots \quad (1\text{-}20)$$

If the first three terms of this Taylor expansion are retained, Eq. (1-19) becomes

$$\frac{d^2S}{dy^2} + \frac{1}{y}\frac{dS}{dy} + \frac{8\pi^2\mu}{a^2h^2}\left(\frac{W - D - c_0}{y^2} + \frac{2D - c_1}{y} - D - c_2\right)S = 0 \quad (1\text{-}21)$$

in which

$$\begin{aligned} c_0 &= A\left(1 - \frac{3}{ar_e} + \frac{3}{a^2r_e^2}\right) \\ c_1 &= A\left(\frac{4}{ar_e} - \frac{6}{a^2r_e^2}\right) \\ c_2 &= A\left(-\frac{1}{ar_e} + \frac{3}{a^2r_e^2}\right) \end{aligned} \quad (1\text{-}22)$$

Eq. (1-21) can be further simplified by the substitutions

$$\begin{aligned} S(y) &= e^{-z/2}z^{b/2}F(z) & z &= 2dy \\ d^2 &= \frac{8\pi^2\mu}{a^2h^2}(D + c_2) & b^2 &= -\frac{32\pi^2\mu}{a^2h^2}(W - D - c_0) \end{aligned} \quad (1\text{-}23)$$

so that it becomes

$$\frac{d^2F}{dz^2} + \left(\frac{b+1}{z} - 1\right)\frac{dF}{dz} + \frac{v}{z}F = 0 \quad (1\text{-}24)$$

where

$$v = \frac{4\pi^2\mu}{a^2h^2d}(2D - c_1) - \tfrac{1}{2}(b + 1) \quad (1\text{-}25)$$

As in the usual quantum-mechanical treatment of the simple harmonic oscillator or of the hydrogen atom (*cf.* [62]), for the solution of Eq. (1-24) to be finite and vanish at the ends of its range, it must be given by a terminating series, *i.e.*, a polynomial. In fact, Eq. (1-24) is identical in form with the equation for Laguerre polynomials found in the solution of the hydrogen atom. This requirement can be shown to restrict v to the values 0, 1, 2, ... Strictly speaking, the solutions thus obtained satisfy the boundary condition $S \to 0$ as $r \to -\infty$ rather than the proper condition $S \to 0$ as $r \to 0$. Ter Haar [156] has examined this approximation and shown that it is usually a good one.

It is possible to solve for W using Eqs. (1-25), (1-23), (1-22), and

(1-18), which give

$$W_{Jv} = D + c_0 - \frac{(D - \frac{1}{2}c_1)^2}{D + c_2} + \frac{ah(D - \frac{1}{2}c_1)}{\pi\sqrt{2\mu}\sqrt{D + c_2}}\left(v + \frac{1}{2}\right) - \frac{a^2h^2}{8\pi^2\mu}\left(v + \frac{1}{2}\right)^2 \quad (1\text{-}26)$$

Expanding Eq. (1-26) in powers of c_1/D and c_2/D, it takes the form:

$$\frac{W_{Jv}}{h} = \omega_e(v + \tfrac{1}{2}) - x_e\omega_e(v + \tfrac{1}{2})^2 + J(J + 1)B_e - D_eJ^2(J + 1)^2 - \alpha_e(v + \tfrac{1}{2})J(J + 1) \quad (1\text{-}27)$$

where

$$\begin{aligned} \omega_e &= \frac{a}{2\pi}\sqrt{\frac{2D}{\mu}} \qquad x_e = \frac{h\omega_e}{4D} \qquad B_e = \frac{h}{8\pi^2I_e} \\ D_e &= \frac{h^3}{128\pi^6\mu^3\omega_e^2r_e^6} = \frac{4B_e^3}{\omega_e^2} \\ \alpha_e &= \frac{3h^2\omega_e}{16\pi^2\mu r_e^2D}\left(\frac{1}{ar_e} - \frac{1}{a^2r_e^2}\right) = 6\sqrt{\frac{x_eB_e^3}{\omega_e}} - \frac{6B_e^2}{\omega_e} \end{aligned} \quad (1\text{-}28)$$

ω_e, α_e, B_e in (1-27) and (1-28) are expressed in cycles per second. The terms in Eq. (1-27) can be identified with the solutions of more specialized problems, so that each can be given a physical significance. Thus the first term involving $(v + \frac{1}{2})$ has the form of the solution of the wave equation of a pure vibrator with a harmonic potential. The second term is obtained when the vibrator potential is made anharmonic by the addition of a cubic term in the potential energy. A term of the form $BJ(J + 1)$ is just that obtained in Eq. (1-4), the solution of the rigid rotor problem, while the next to last term comes from centrifugal stretching of the rotating molecule. The last term allows for the change in average moment of inertia due to vibration and the consequent change in rotational energy.

Dunham's Solution for Energy Levels. Some other more refined potentials have been used for problems in optical spectra involving excited rotational or vibrational states ([471], pp. 102, 108). Dunham [34] has calculated the energy levels of a vibrating rotor, by a Wentzel-Kramers-Brillouin method, for any potential which can be expanded as a series of powers of $(r - r_e)$ in the neighborhood of the potential minimum. This treatment shows that the energy levels can be written in the form

$$F_{vJ} = \sum_{l,j} Y_{lj}(v + \tfrac{1}{2})^lJ^j(J + 1)^j \quad (1\text{-}29)$$

where l and j are summation indices, v and J are, respectively, vibrational and rotational quantum numbers, and Y_{lj} are coefficients which depend on molecular constants. The effective potential function of the vibrating

rotor may be written in the form

$$U = a_0\xi^2(1 + a_1\xi + a_2\xi^2 + \cdots) + B_eJ(J+1)(1 - 2\xi + 3\xi^2 - 4\xi^3 + \cdots) \quad (1\text{-}30)$$

where $\xi = (r - r_e)/r_e$, $B_e = h/8\pi^2\mu r_e^2$. The term involving $B_eJ(J+1)$ allows for the influence of the rotation on the effective potential.

Dunham [34] shows that the first 15 Y_{ij}'s are

$$\left.\begin{aligned}
Y_{00} &= B_e/8(3a_2 - 7a_1^2/4)\\
Y_{10} &= \omega_e[1 + (B_e^2/4\omega_e^2)(25a_4 - 95a_1a_3/2 - 67a_2^2/4\\
&\quad + 459a_1^2a_2/8 - 1155a_1^4/64)]\\
Y_{20} &= (B_e/2)[3(a_2 - 5a_1^2/4) + (B_e^2/2\omega_e^2)(245a_6 - 1365a_1a_5/2\\
&\quad - 885a_2a_4/2 - 1085a_3^2/4 + 8535a_1^2a_4/8 + 1707a_2^3/8\\
&\quad + 7335a_1a_2a_3/4 - 23{,}865a_1^3a_3/16 - 62{,}013a_1^2a_2^2/32\\
&\quad + 239{,}985a_1^4a_2/128 - 209{,}055a_1^6/512)]\\
Y_{30} &= (B_e^2/2\omega_e)(10a_4 - 35a_1a_3 - 17a_2^2/2 + 225a_1^2a_2/4\\
&\quad - 705a_1^4/32)\\
Y_{40} &= (5B_e^3/\omega_e^2)(7a_6/2 - 63a_1a_5/4 - 33a_2a_4/4 - 63a_3^2/8\\
&\quad + 543a_1^2a_4/16 + 75a_2^3/16 + 483a_1a_2a_3/8 - 1953a_1^3a_3/32\\
&\quad - 4989a_1^2a_2^2/64 + 23{,}265a_1^4a_2/256 - 23{,}151a_1^6/1024)
\end{aligned}\right\} \quad (1\text{-}31)$$

$$\left.\begin{aligned}
Y_{01} &= B_e\{1 + (B_e^2/2\omega_e^2)[15 + 14a_1 - 9a_2 + 15a_3 - 23a_1a_2\\
&\quad + 21(a_1^2 + a_1^3)/2]\}\\
Y_{11} &= (B_e^2/\omega_e)\{6(1 + a_1) + (B_e^2/\omega_e^2)[175 + 285a_1 - 335a_2/2\\
&\quad + 190a_3 - 225a_4/2 + 175a_5 + 2295a_1^2/8 - 459a_1a_2\\
&\quad + 1425a_1a_3/4 - 795a_1a_4/2 + 1005a_2^2/8 - 715a_2a_3/2\\
&\quad + 1155a_1^3/4 - 9639a_1^2a_2/16 + 5145a_1^2a_3/8\\
&\quad + 4677a_1a_2^2/8 - 14{,}259a_1^3a_2/16\\
&\quad + 31{,}185(a_1^4 + a_1^5)/128]\}\\
Y_{21} &= (6B_e^3/\omega_e^2)[5 + 10a_1 - 3a_2 + 5a_3 - 13a_1a_2\\
&\quad + 15(a_1^2 + a_1^3)/2]\\
Y_{31} &= (20B_e^4/\omega_e^3)[7 + 21a_1 - 17a_2/2 + 14a_3 - 9a_4/2 + 7a_5\\
&\quad + 225a_1^2/8 - 45a_1a_2 + 105a_1a_3/4 - 51a_1a_4/2 + 51a_2^2/8\\
&\quad - 45a_2a_3/2 + 141a_1^3/4 - 945a_1^2a_2/16 + 435a_1^2a_3/8\\
&\quad + 411a_1a_2^2/8 - 1509a_1^3a_2/16 + 3807(a_1^4 + a_1^5)/128]
\end{aligned}\right\} \quad (1\text{-}32)$$

$$\left.\begin{aligned}
Y_{02} &= -(4B_e^3/\omega_e^2)\{1 + (B_e^2/2\omega_e^2)[163 + 199a_1 - 119a_2 + 90a_3\\
&\quad - 45a_4 - 207a_1a_2 + 205a_1a_3/2 - 333a_1^2a_2/2 + 693a_1^2/4\\
&\quad + 46a_2^2 + 126(a_1^3 + a_1^4/2)]\}\\
Y_{12} &= -(12B_e^4/\omega_e^3)(\tfrac{19}{2} + 9a_1 + 9a_1^2/2 - 4a_2)\\
Y_{22} &= -(24B_e^5/\omega_e^4)[65 + 125a_1 - 61a_2 + 30a_3 - 15a_4\\
&\quad + 495a_1^2/4 - 117a_1a_2 + 26a_2^2 + 95a_1a_3/2 - 207a_1^2a_2/2\\
&\quad + 90(a_1^3 + a_1^4/2)]
\end{aligned}\right\} \quad (1\text{-}33)$$

$$\left.\begin{aligned}
Y_{03} &= 16B_e^5(3 + a_1)/\omega_e^4\\
Y_{13} &= (12B_e^6/\omega_e^5)(233 + 279a_1 + 189a_1^2 + 63a_1^3 - 88a_1a_2\\
&\quad - 120a_2 + 80a_3/3)\\
Y_{04} &= -(64B_e^7/\omega_e^6)(13 + 9a_1 - a_2 + 9a_1^2/4)
\end{aligned}\right\} \quad (1\text{-}34)$$

It should be noted that B_e is generally much smaller than ω_e. For most molecules the ratio B_e^2/ω_e^2 is of the order of 10^{-6}, although for light molecules such as H_2 it approaches more nearly to 10^{-3}. In such cases more terms are required in the expressions for the various coefficients.

If B_e/ω_e is small, the Y's can be related to the ordinary band spectrum constants as follows:

$$\begin{array}{lll}
Y_{10} \approx \omega_e & Y_{20} \approx -\omega_e x_e & Y_{30} \approx \omega_e y_e\\
Y_{01} \approx B_e & Y_{11} \approx -\alpha_e & Y_{21} \approx \gamma_e\\
Y_{02} \approx -D_e & Y_{12} \approx -\beta_e & Y_{40} \approx \omega_e z_e\\
Y_{03} \approx H_e & &
\end{array} \quad (1\text{-}35)$$

where these symbols refer to the coefficients in the Bohr theory expansion for the molecular energy levels:

$$F_{vJ} = \omega_e(v + \tfrac{1}{2}) - \omega_e x_e(v + \tfrac{1}{2})^2 + \omega_e y_e(v + \tfrac{1}{2})^3 + \omega_e z_e(v + \tfrac{1}{2})^4 + B_vJ(J+1) - D_eJ^2(J+1)^2 + H_eJ^3(J+1)^3 + \cdots \quad (1\text{-}36)$$

where $B_v = B_e - \alpha_e(v + \frac{1}{2}) + \gamma_e(v + \frac{1}{2})^2 \ldots$ (*cf.* [471], p. 92, pp. 107–108).

Sandeman [103] has extended Dunham's treatment to include other terms of the same order of magnitude which involve higher powers of the vibrational quantum number.

For the special case of the Morse potential function, Dunham shows that all the Y_{l0}'s except Y_{10} and Y_{20} vanish and all but the first terms in the expressions for Y_{10} and Y_{20} are zero. Because of the simplicity of the expressions obtained with the Morse function, and because it does give a quite good fit to the actual potential in the region of $r = r_e$, the Morse function has been widely used.

Dependence of Energy on Isotopic Masses. Since the frequencies of lines in microwave spectra can be measured with great precision, and since they can be used to evaluate the molecular moment of inertia, they permit an accurate evaluation of atomic or nuclear masses, or rather the mass ratios of isotopic nuclei.

To a good approximation we can use the Morse potential solution. The usual expansion for energy levels, appropriate to the Morse potential or other similar potentials, is given by (1-27), from which the frequency of a microwave rotational transition, where J changes by one unit, is easily shown to be

$$\begin{aligned}
\nu = \frac{W_{J+1} - W_J}{h} &= 2B_e(J+1) - 2\alpha_e(v + \tfrac{1}{2})(J+1) - 4D_e(J+1)^3\\
&= 2B_v(J+1) - 4D_e(J+1)^3
\end{aligned} \quad (1\text{-}37)$$

The constants B_e, α_e, and D_e are usually expressed in cm^{-1} in optical work. In the above formula they, and therefore the frequency, are in cycles per second, which may be divided by 10^6 to convert to megacycles, the most usual unit for microwave work.

B_e and α_e can be evaluated directly from microwave spectra if two lines can be measured with different values of v; for instance, the same rotational transition in the ground vibrational state and the first excited vibrational state. The term in $(J + 1)^3$ is often negligible because $D_e = (4B_e^3/\omega_e^2)$ is smaller in magnitude than B_e by $4(B_e/\omega_e)^2$, or approximately 10^{-5} for most molecules. However, for very light molecules or large J this term may be rather prominent. When required it can be calculated with sufficient accuracy from $B_0 \approx B_e$ and ω_e, which is usually obtainable from optical spectra.

If the nuclear masses are known from mass spectrographic or other measurements, a determination of B_e allows an evaluation of the internuclear distance r_e, since B_e is related to the moment of inertia I_e.

$$r_e = \sqrt{\frac{I_e}{\mu}} = \sqrt{\frac{h}{8\pi^2 B_e \mu}} \tag{1-38}$$

where $\mu = M_1M_2/(M_1 + M_2)$ is the reduced mass. The accuracy with which r_e can be determined for a diatomic molecule is limited mainly by the error in Planck's constant h, which is required to calculate I_e from B_e. The best available value of this constant is

$$h = (6.6252 \pm 0.0005) \times 10^{-27} \text{ erg-sec}$$

[795] so that r_e can be determined to an accuracy of about 1 part in 6000. It is often convenient to have B_e in megacycles, r_e in angstroms, and μ in atomic mass units. In these units

$$I_e = \frac{5.055 \times 10^5}{B_e} = \frac{I_e \text{ in cgs units}}{1.6598 \times 10^{-40}} \tag{1-39}$$

and

$$r_e = \sqrt{\frac{5.055 \times 10^5}{\mu B_e}} \quad \text{angstrom units} \tag{1-40}$$

Table 1*a* gives the constants of a number of representative diatomic molecules. Table 1*b* lists certain constants of one isotopic species of all diatomic molecules whose microwave rotational spectra have been studied.

If the spectroscopic constants have been measured for one isotopic species of a molecule, their values for other species may be found from the following relations which are deducible from Eq. (1-28):

$$\omega_e \propto \frac{1}{\sqrt{\mu}} \qquad B_e \propto \frac{1}{\mu} \qquad \alpha_e \propto \frac{1}{\mu^{3/2}} \qquad D_e \propto \frac{1}{\mu^2} \tag{1-41}$$

The values in Table 1*a* have been calculated with the aid of these relations in some cases.

TABLE 1-1*a*. MOLECULAR CONSTANTS OF SOME REPRESENTATIVE DIATOMIC MOLECULES

Molecule	Y_{01} (approx. B_e), Mc	Y_{01} (approx. B_e), cm^{-1}	α_e, Mc	I_e, $A^2 \times$ atomic mass units	r_e, A	ω_e, cm^{-1}	$D_e = \frac{4B_e^3}{\omega_e^2}$, Mc	μ, debyes	Reference
H^1Cl^{35}	317,510	10.591	9050	1.592	1.275	2989.74	15.94	1.18	[336*a*] [471]
DI^{127}	(B_0 = 97,537.2)	(B_0 = 3.25348)	1840	(I_0 = 5.183)	1.604	1630	1.56	0.38	[755*a*] [827*a*] [782*b*]
$C^{12}O^{16}$	57,897.5	1.93124	524.0	8.731	1.128	2170.21	0.1834	0.10	[336*a*] [457]
$C^{13}O^{16}$	55,344.9	1.84610	488.3	9.134	1.128	2074.81	0.1753	0.10	[457]
$Cl^{35}F^{19}$	15,483.69	0.516479	130.67	32.65	1.628	793.2	0.02626	0.88	[366]
$Cl^{37}F^{19}$	15,189.22	0.506657	126.96	33.28	1.628	778.6	0.02527	0.88	[366]
$Br^{79}F^{19}$	10,706.9	0.357143	156.3	47.21	1.759	671	0.0121	1.29	[534]
$Br^{81}F^{19}$	10,655.7	0.355435	155.8	47.44	1.759	670	0.0121	1.29	[534]
$K^{41}Cl^{35}$	3,767.394	0.125667	22.865	134.2	2.667	300	0.003	10.48	[835] [938]
$K^{39}Cl^{35}$	3,856.370	0.128634	23.680	131.1	2.667	300	0.003	10.48	[835] [938]
$K^{39}Cl^{37}$	3,746.583	0.124972	22.676	134.9	2.667	300	0.003	10.48	[835] [938]
$I^{127}Cl^{35}$	3,422.300	0.114155	16.06	147.7	2.321	384.2	0.00121	0.65	[330]
$I^{127}Cl^{37}$	3,277.365	0.109320	15.05	154.2	2.321	376	0.00111	0.65	[330]

TABLE 1-1b. MOLECULAR CONSTANTS OF DIATOMIC MOLECULES WHOSE ROTATIONAL SPECTRA HAVE BEEN MEASURED IN THE MICROWAVE REGION

Molecule	Y_{01} (approx B_e), Mc	α_e, Mc	r_e, 10^{-8} cm or angstroms	μ, 10^{-18} esu or debyes	Reference
DBr^{79}	(B_0 = 127,358.2)	2500	1.414	0.79	[336a] [676c] [927]
DI	(B_0 = 97,537.2)	1840	1.604	0.38	[755a] [782b] [827a]
FCl^{35}	15,483.69	130.67	1.628	0.881	[366]
$Br^{79}Cl^{35}$	4,570.92	23.22	2.138	0.57	[535]
ICl^{35}	3,422.300	16.06	2.321	0.65	[330]
FBr^{79}	10,706.9	156.3	1.759	1.29	[534]
$C^{12}O^{16}$	57,897.5	524.0	1.128	0.10	[336a] [457]
$C^{12}S^{32}$	24,584.352	177.544	1.535	2.0	[777]
$N^{14}O^{16}$	51,084.5	534	1.151	0.16	[336a] [782b] [924]
Li^6Br^{79}	19,161.51	208.8	2.170	6.19	[938]
Li^6I	15,381.45	152.6	2.392	6.25	[938]
$NaCl^{35}$	6,536.86	48.28	2.361	8.5	[751] [987]
$NaBr^{79}$	4,534.51	28.25	2.502	.....	[938]
NaI	3,531.76	19.44	2.712	.....	[938]
$K^{39}Cl^{35}$	3,856.370	23.680	2.667	10.48	[835] [987]
$K^{39}Br^{79}$	2,434.947	12.136	2.821	10.41	[799]
$K^{39}I$	1,825.01	8.034	3.048	11.05	[938]
$Rb^{85}Cl^{35}$	2,627.400	13.601	2.787	.....	[938]
$Rb^{85}Br^{79}$	1,424.83	5.578	2.945	.....	[938]
$Rb^{85}I$	984.31	3.281	3.177	.....	[938]
CsF	5,527.27	33.13	2.345	7.874	[423a] [938]
$CsCl^{35}$	2,161.20	10.085	2.906	10.40	[751] [606a] [938]
$CsBr^{79}$	1,081.34	3.718	3.072	.....	[938]
CsI	708.36	2.044	3.315	12.1	[938]

1-3. Mass Measurements. Once B_e has been measured for two isotopic species of a molecule, the reduced mass ratio is given directly by the ratio of the B_e's. That is,

$$\frac{\mu^{(1)}}{\mu^{(2)}} = \frac{B_e^{(2)}}{B_e^{(1)}} = \frac{M_1(M + M_2)}{M_2(M + M_1)} \tag{1-42}$$

or

$$\frac{M_1}{M_2} = \frac{(M/M_2)(B_e^{(2)}/B_e^{(1)})}{1 + M/M_2 - B_e^{(2)}/B_e^{(1)}} \tag{1-43}$$

where M_1 and M_2 are the masses of the two isotopes; M is the mass of the other nucleus in the molecule. From (1-43) and microwave measurements of $B_e^{(2)}/B_e^{(1)}$, the mass ratio M_1/M_2 can be obtained with great precision. The mass ratio M/M_2 need be known only moderately accurately since it enters into both the numerator and denominator. Planck's constant and the other constants required to compute r_e from B_e do not enter at all. By this procedure the mass ratio of the chlorine 35 to the

chlorine 37 isotope has been found from the spectra of ICl and FCl. The values obtained are compared in Table 1-2 with another microwave measurement in the triatomic molecule ClCN and with values from mass-spectroscopic and nuclear-disintegration work. It may be seen from this table that they agree well with other determinations and represent very accurate determinations of the Cl^{35}/Cl^{37} mass ratio.

TABLE 1-2. VALUE OF Cl^{35}/Cl^{37} MASS RATIO

Method	Value	Reference
Mass spectroscopy	0.9459777 ± 20	[562a]
Nuclear reaction	0.9459893 ± 110	[110a]
Microwave (ICl)	0.9459801 ± 50	[330]
Microwave (FCl)	0.9459775 ± 40	[366]
Microwave-molecular beam (KCl)	0.9459803 ± 15	[835]
Microwave (CsCl)	0.9459781 ± 30	[938]
Microwave (ClCN)	0.9459906 ± 120	[490]

Within the limits of error given in Table 1-2 for the microwave measurements, there seem to be no theoretical uncertainties which should affect mass ratios. However, microwave measurements can be made considerably more precise, so that it is important to examine even small effects which might possibly cause errors. Such effects have been observed in optical spectra of hydrides where the large mass ratio between H^1 and H^2, the rapid rotation, and vibration with large amplitudes make them unusually large (see, for example, [57], [58], and [71]).

The more important errors in measuring mass ratios from rotational spectra of diatomic molecules (other than simply inaccurate measurements of B_e) may be grouped under three causes:

1. Anharmonicity of the potential function
2. Uncertainties in electronic behavior, including L uncoupling
3. Inaccurate knowledge of the mass of the other atom in the molecule, or in M/M_2

Anharmonicity has been partly taken into account by the use of the Morse function, but if this is not a sufficiently good approximation to the potential curve, Dunham's method must be used.

The Dunham coefficient corresponding most nearly to B_e is Y_{01}, but actually

$$Y_{01} = B_e\{1 + B_e^2/2\omega_e^2[15 + 14a_1 - 9a_2 + 15a_3 - 23a_1a_2 + 21(a_1^2 + a_1^3)/2]\} \tag{1-31}$$

where $a_1, a_2, \ldots$ are the coefficients in the expansion for the potential curve in terms of powers of $(r - r_e)/r_e$ [*cf.* (1-30)]. Then

$$Y_{01} = B_e[1 + (B_e^2/\omega_e^2)\beta_{01}] \tag{1-44}$$

where β_{01} does not depend on M_1, M_2

$$Y_{01}(\mu_1)/Y_{01}(\mu_2) = \mu_2/\mu_1\left[1 + \beta_{01}\left(\frac{B_e^2}{\omega_e^2}\right)\left(\frac{\mu_2 - \mu_1}{\mu_2}\right)\right] \qquad (1\text{-}45)$$

β_{01} can be calculated from spectroscopically observable quantities, as Dunham shows.

$$\beta_{01} = Y_{10}^2 Y_{21}/4Y_{01}^3 + 16a_1 Y_{20}/3Y_{01} - 8a_1 - 6a_1^2 + 4a_1^3 \qquad (1\text{-}46)$$
$$a_1 = Y_{11}Y_{10}/6Y_{01}^2 - 1$$

Since β_{01} is multiplied by B_e^2/ω_e^2 in the expression for Y_{01}, it will enter as a small correction, and it is sufficiently accurate to replace the coefficients entering into it by their approximate values from (1-35), *i.e.*,

$$Y_{10} \approx \omega_e \qquad Y_{01} \approx B_e \qquad Y_{21} \approx \gamma_e \qquad Y_{20} \approx -\omega_e x_e \qquad Y_{11} \approx -\alpha_e$$
$$a_1 \approx (-\alpha_e\omega_e/6B_e^2) - 1$$

For example, in the case of ICl, β_{01} is approximately 50, so that the fractional correction to the mass ratio deduced from the microwave measurements is $50(B_e^2/\omega_e^2)[(\mu^{37} - \mu^{35})/\mu^{35}] = 2 \times 10^{-7}$. Since the accuracy of the present measurements is about 2×10^{-6}, an improvement by a factor of 10 would make this correction appreciable.

It is customary in calculating the moment of inertia of a molecule to assume each atom has the proper number of electrons to make it neutral, and that the entire mass of the atom is concentrated at a point. Thus for diatomic molecules the moment of inertia is generally written $I_e = [M_1M_2/(M_1 + M_2)]r_e^2$, where M_1 and M_2 are the masses of neutral atoms. Such an approximation is good only because the electrons are very light compared with the atomic nuclei which are, indeed, concentrated within a very small radius. However, uncertainties in the location and behavior of electrons in a rotating molecule do appreciably affect the moment of inertia. In NaCl, for example, it would be more correct to associate with Cl the mass of one electron more than the neutral atom and with Na one electron less since the molecule is largely ionic or $\overset{+}{\mathrm{N}}\mathrm{a}\overset{-}{\mathrm{Cl}}$. In the case of LiBr and LiI, it has been shown [938] that the rotational spectrum gives a mass ratio for the two Li isotopes which is in agreement with other measurements of this ratio only if the Li is assumed to have lost one electron and be $\overset{+}{\mathrm{L}}\mathrm{i}$.

Electrons are certainly not concentrated at the nuclei, but are arranged more or less spherically about their respective nuclei. Hence the moments of inertia might be expected to be greater than those calculated from the point mass assumption by an amount approximately equal to the moments of inertia of the electrons about their respective nuclei. This last contribution to the moment of inertia would be rather large, but fortunately it is not really present because a completely spherical shell

of electrons around an atom would not, in fact, rotate as the molecule rotates. This is known as the "slip effect," for the spherical shells of electrons appear to remain fixed in orientation or slip as the molecule rotates (*cf.* [339] and discussion of this effect in Chap. 8). The valence shell of electrons, however, is not completely spherical, and part of it must be considered to rotate with the molecule, giving a contribution of approximately nmr^2, where n is the number of rotating valence electrons, m the electron mass, and r some average of their distance from the nuclei with which they are supposed to be associated. This is of approximately the same magnitude as the uncertainty in moment of inertia due to an uncertainty of the position in the molecule of one electron. If n is taken as 1 and $r = r_e$, the error in moment of inertia is of the order mr_e^2, or a fractional error of $m(M_1 + M)/M_1M$. This is less than 1 part in 10,000 for almost all atoms, and hence would not affect a calculation of r_e from B_e. On the other hand, it does affect a determination of mass ratios, giving a fractional error in the mass ratio M_1/M_2 of $m(M_1 - M_2)/M_1M_2$. For ICl, this fractional error is 8×10^{-7}, which is of the same general magnitude as the other errors discussed above. However, for the light nucleus of Li in LiI, such an effect would be as large as 10^{-5}, and easily detectable.

L uncoupling also involves the behavior of electrons during rotation and is very closely related to the above effects, although it may be described in somewhat different language. The rotational momentum of the molecule can to a very small extent be transferred to the molecular electrons. Rotation tends to excite the valence electrons from their normal $^1\Sigma$ state of zero angular momentum to excited $^1\Pi$ states, which have unit angular momentum, and hence slightly change the rotational energy. This process, known as L uncoupling, is very difficult to evaluate quantitatively from theory, since little exact knowledge of the electronic wave functions and excited states is available. However, it can be approximately evaluated from experimental results. Since a Π state has an electronic angular momentum and magnetic moment, even a small excitation of this state contributes a considerable part of the magnetic moment of the rotating molecule, which is of the order of a nuclear magneton, or one two-thousandth that of an electron. Hence a measurement of the molecular magnetic moment allows a rough estimate of the extent of L uncoupling or of its effect on the rotational energy.

Electrons in a Π state also produce a large magnetic field at the positions of the nuclei and hence a magnetic hyperfine interaction with the nuclei. Although this is not the only source of magnetic hyperfine interactions in a rotating molecule, it is probably a major contributor, so that measurement of the magnetic hyperfine interactions allow an estimate of the L uncoupling.

It is estimated that L uncoupling in ICl or FCl produces uncertain-

ties in the mass ratio Cl^{35}/Cl^{37} of about 1 part in 10^6. This is again large enough to be of importance in accurate microwave measurements. Lighter molecules, which rotate faster, would in general involve larger errors from L uncoupling.

These electronic effects and their interrelations will be discussed in some detail in Chap. 8. That chapter shows that the entire contribution of electrons to the kinetic energy of rotation of a $^1\Sigma$ molecule can be evaluated by a measurement of the rotational magnetic moment of the molecule. The magnetic moment of a $^1\Sigma$ molecule is due to the rotation of both nuclear and electronic charges. The nuclear effect can be calculated by assuming that the nuclei form a rigid rotating frame. If their effect is subtracted from the measured magnetic moment, the electronic contribution to the moment can be determined. The change in rotational energy due to electron motion is, from (8-29) and (11-15),

$$W_R = g_e J(J + 1)hB_e \tag{1-47}$$

where $g_e J$ is the magnetic moment in Bohr magnetons due to the motion of all the electrons. This expression allows the possibility of precise corrections for all effects due to electron motion [type (2) above].

Finally, it is of interest to examine how accurately the mass M must be known for the atom whose mass is not being measured. In determining the ratio M_1/M_2, it may be seen from Eq. (1-42) that M/M_2 is assumed known. A fractional error ϵ in this ratio will give a fractional error δ in the determination of M_1/M_2 which is

$$\delta = \frac{(M_2 - M_1)\epsilon}{M + M_2} \tag{1-48}$$

It is evident that, when the fractional change in weight of the molecule, $(M_2 - M_1)/(M + M_2)$, is small, the ratio M/M_2 need not be known with high accuracy. The error produced by uncertainties in M/M_2 is not, of course, due to theoretical uncertainties in the behavior of the molecule as are errors (1) and (2) on page 15. However, inaccurate knowledge of M/M_2 may often give errors in M_1/M_2 of the same order as those of type (1) and (2).

So far microwave mass measurements are just at the threshold of difficulties of the types discussed here. Since the measurements of B_e with microwaves can be rather easily improved by another factor of 10, these difficulties will provide an ultimate limit to the accuracy of most mass ratio measurements of about 1 part in 10^6. This limit, of course, represents a very good accuracy and one which cannot always be obtained by other methods, *i.e.*, an error of 10^{-4} mass unit for nuclei of atomic mass 100.

1-4. Absorption Intensities and Selection Rules. A molecule interacts appreciably with a microwave electromagnetic field to emit or absorb

radiation only if it has an electric or magnetic dipole moment μ. Usually the dipole is an electric moment due to the positive and negative charges in the molecule. In the ICl molecule, for example, the Cl has an excess negative charge and the I an excess positive charge, so that the molecule is a small rotating dipole which acts in many ways like a small antenna in radiating or receiving electromagnetic waves whose frequency coincides with its frequency of rotation. The rate of radiation is small because the molecule is so small (approximately 10^{-8} cm) compared with the wavelengths radiated (approximately 1 cm).

As will be discussed in some detail in Chap. 13, the intensity of a narrow microwave absorption line in a gas may usually be written

$$\gamma = \frac{8\pi^2 N f |\mu_{ij}|^2 \nu^2 \, \Delta\nu}{3ckT[(\nu - \nu_0)^2 + (\Delta\nu)^2]} \tag{1-49}$$

where N = the number of molecules per cc in absorption cell
f = fraction of these molecules in the lower of the two states involved in the transition
$|\mu_{ij}|^2$ = square of the dipole moment matrix element for the transition, summed over the three perpendicular directions in space
ν = frequency
ν_0 = resonant frequency or, to a good approximation, the center frequency of the absorption line
$\Delta\nu$ = half width of the line at half maximum, or line-breadth parameter
c = velocity of light
k = Boltzmann constant
T = absolute temperature

The peak absorption of the line occurs very near to $\nu = \nu_0$, and is

$$\gamma_{max} = \frac{8\pi^2 N f |\mu_{ij}|^2 \nu_0^2}{3ckT \, \Delta\nu} \tag{1-50}$$

The fraction of molecules in a particular vibrational state of energy $h\omega_e(v + \frac{1}{2})$ is given by

$$f_v = \frac{e^{-h\omega_e(v+\frac{1}{2})/kT}}{\sum_{n=0}^{\infty} e^{(h\omega_e/kT)(n+\frac{1}{2})}} = e^{-vh\omega_e/kT}(1 - e^{-h\omega_e/kT}) \tag{1-51}$$

since

$$1 + e^{-h\omega_e/kT} + e^{-2h\omega_e/kT} + e^{-3h\omega_e/kT} + \cdots = \frac{1}{1 - e^{-h\omega_e/kT}} \tag{1-52}$$

Of the molecules in a particular vibrational state, we must find the fraction f_J in a particular rotational state J in order to obtain the fraction $f = f_v f_J$ in the particular state of interest for expression (1-50). The

angular momentum J may be oriented in space $2J + 1$ different ways, corresponding to the different values of the magnetic quantum number $M = J, J - 1, J - 2, \ldots, -J$. The fraction having angular momentum J is then

$$f_J = \frac{(2J + 1)e^{-hBJ(J+1)/kT}}{\sum_{n=0}^{\infty} (2n + 1)e^{-hBn(n+1)/kT}} \tag{1-53}$$

If B/kT is sufficiently small, the sum, often called the partition function, may be replaced by an integral,

$$\sum_{n=0}^{\infty} (2n + 1)e^{-hBn(n+1)/kT} = \int_0^{\infty} (2x + 1)e^{-hBx(x+1)/kT}\, dx = \frac{kT}{hB} \tag{1-54}$$

In case B/kT is large enough that a more accurate value of the rotational partition function is needed, it may be written as an expansion

$$\sum_{n=0}^{\infty} (2n + 1)e^{-hBn(n+1)/kT} = \frac{kT}{hB} + \frac{1}{3} + \frac{1}{15}\frac{hB}{kT} + \frac{4}{315}\left(\frac{hB}{kT}\right)^2 + \frac{1}{315}\left(\frac{hB}{kT}\right)^3 + \cdots \tag{1-55}$$

Using only the first term of this expansion,

$$f_J = \frac{(2J + 1)hBe^{-hBJ(J+1)/kT}}{kT} \tag{1-56}$$

In most cases of microwave rotational spectra, $hB/kT \approx \frac{1}{200}$ at room temperature, so that not only is hB/kT small, but $e^{-hBJ(J+1)/kT}$ can usually be approximated as unity for low values of J. Hence

$$f = (2J + 1)\frac{hB}{kT} e^{-vh\omega_e/kT}(1 - e^{-h\omega_e/kT}) \tag{1-57}$$

Dipole Moment Matrix Elements. The dipole moment of a macroscopic linear array of charges oriented along the z axis would be defined as

$$\mu = \sum_i e_i z_i \text{ or } \int \rho(z) z\, dz \tag{1-58}$$

where e_i is the size of the ith charge and z_i is its coordinate. In the integral form, $\rho(z)$ is the charge density per unit length. A linear molecule may be thought of as having an inherent or permanent dipole moment of the same type oriented along its axis. However, the molecular orientation is not fixed in space, so that its average dipole moment in any one direction is zero unless it is subjected to external electric fields or other constraining forces.

A measure of the effectiveness of an electric field along the z axis in exerting a torque on a rotating molecule, or in inducing a transition between states JM and $J'M'$ is given by the dipole moment matrix elements

$$\mu_z(JMJ'M') = \int \psi_{JM}^* \mu_z \psi_{J'M'}\, d\tau \tag{1-59}$$

where μ_z is the projection of the molecular dipole moment on the z axis. ψ_{JM} represents the molecular wave function for a total angular momentum J and magnetic quantum number M. Similarly, for electric fields in the x or y directions the dipole matrix elements

$$\mu_x(JMJ'M') = \int \psi_{JM}^* \mu_x \psi_{J'M'}\, d\tau \tag{1-60}$$
$$\mu_y(JMJ'M') = \int \psi_{JM}^* \mu_y \psi_{J'M'}\, d\tau \tag{1-61}$$

are important. The intensity of absorption or emission of radiation polarized with the electric vector in x, y, or z directions due to a transition between the states JM and $J'M'$, is just proportional to $|\mu_x(JMJ'M')|^2$, $|\mu_y(JMJ'M')|^2$, or $|\mu_z(JMJ'M')|^2$, respectively. In expression (1-50) giving the intensity of an absorption line, in which either the radiation is unpolarized or the molecules are randomly distributed in various M states, the quantity $|\mu_{ij}|^2$ is given by

$$|\mu_{ij}|^2 = \sum_{M'} |\mu_x(JMJ'M')|^2 + |\mu_y(JMJ'M')|^2 + |\mu_z(JMJ'M')|^2 \tag{1-62}$$

In terms of spherical polar coordinates fixed in space, the components of the dipole moment are

$$\mu_x = \mu \sin\theta \cos\phi \qquad \mu_y = \mu \sin\theta \sin\phi \qquad \mu_z = \mu \cos\theta \tag{1-63}$$

In these coordinates the matrix elements become:

$$\begin{aligned} \mu_x(JMJ'M') &= \mu \int \psi_{JM}^* \sin\theta \cos\phi\, \psi_{J'M'}\, d\tau \\ \mu_y(JMJ'M') &= \mu \int \psi_{JM}^* \sin\theta \sin\phi\, \psi_{J'M'}\, d\tau \\ \mu_z(JMJ'M') &= \mu \int \psi_{JM}^* \cos\theta\, \psi_{J'M'}\, d\tau \end{aligned} \tag{1-64}$$

where ψ_{JM} is an eigenfunction for the rotating molecule.

For the rigid rotator, on substituting the eigenfunctions from (1-5) and (1-6) and using $d\tau = \sin\theta\, d\phi\, d\theta$, we get

$$\mu_z(JMJ'M') = \mu N_{JM} N_{J'M'} \int_0^{\pi} P_J^{|M|}(\cos\theta) \cos\theta\, P_{J'}^{|M'|}(\cos\theta) \sin\theta\, d\theta \int_0^{2\pi} e^{-iM\phi} e^{iM'\phi}\, d\phi \tag{1-65}$$

where N_{JM} and $N_{J'M'}$ are the normalization factors for ψ_{JM} and $\psi_{J'M'}$, or

$$N_{JM} = \frac{1}{\sqrt{2\pi}}\left[\frac{(2J + 1)(J - |M|)!}{2(J + |M|)!}\right]^{\frac{1}{2}} \tag{1-66}$$

The second integral in (1-65) has the value of 2π if $M = M'$; otherwise it is zero. The first integral may be obtained from the properties of the

Legendre polynomials ([471], p. 73; [62], p. 307; [537], p. 136)

$$\cos\theta\, P_J^{|M|}(\cos\theta) = \frac{J + |M|}{2J + 1} P_{J-1}^{|M|}(\cos\theta) + \frac{J - |M| + 1}{2J + 1} P_{J+1}^{|M|}(\cos\theta) \quad (1\text{-}67)$$

so that, remembering that M must equal M',

$$\mu_z(JMJ'M) = 2\pi\mu N_{JM} N_{J'M} \left[\frac{J + M}{2J + 1} \int P_{J-1}^{|M|}(\cos\theta) P_{J'}^{|M|}(\cos\theta) \sin\theta\, d\theta + \frac{J - |M| + 1}{2J + 1} \int P_{J+1}^{|M|}(\cos\theta) P_{J'}^{|M|}(\cos\theta) \sin\theta\, d\theta \right] \quad (1\text{-}68)$$

These integrals vanish unless $J' = J \pm 1$, giving the selection rule that for a transition $\Delta J = \pm 1$. Taking J as the lower state so that

$$J' = J + 1$$

the first integral vanishes and

$$\mu_z(JMJ'M) = 2\pi\mu \frac{N_{JM}}{N_{J+1,M}} \frac{J - |M| + 1}{2J + 1} \int N_{J+1,m}^2 [P_{J+1}^{|M|}(\cos\theta)]^2 \sin\theta\, d\theta \quad (1\text{-}69)$$

The integral remaining is just the normalization integral and equals $1/2\pi$ with our choice of normalization factor. Putting in values of N_{JM} and $N_{J+1,M}$,

$$\mu_z(J,M,J + 1,M) = \mu \sqrt{\frac{(J + 1)^2 - M^2}{(2J + 1)(2J + 3)}} \quad (1\text{-}70)$$

Similarly, μ_x and μ_y are zero unless $J = J' \pm 1$ and $M = M' \pm 1$. Then

$$\mu_x(J,M,J + 1,M + 1) = -i\mu_y(J,M,J + 1,M + 1) = \frac{-\mu}{2} \sqrt{\frac{(J + M + 2)(J + M + 1)}{(2J + 1)(2J + 3)}} \quad (1\text{-}71)$$

$$\mu_x(J,M,J + 1,M - 1) = i\mu_y(J,M,J + 1,M - 1) = \frac{\mu}{2} \sqrt{\frac{(J - M + 1)(J - M + 2)}{(2J + 1)(2J + 3)}} \quad (1\text{-}72)$$

The signs or "phases" of the matrix elements (1-71) and (1-72) are usually not important and may be positive or negative according to one's definition of $P_J^M(\cos\theta)$. The signs given are those adopted by Condon and Shortley [56] but are not used by all authors.

The probability of inducing an absorption in a particular molecule in a state JM by radiation with the electric field in the z direction is then

proportional to

$$|\mu_z|^2 = \mu^2 \frac{(J + 1)^2 - M^2}{(2J + 1)(2J + 3)} \quad (1\text{-}73)$$

and only the transition $J + 1,M \leftarrow JM$ can occur. Here the arrow indicates that the absorption process produces a transition from the state JM to the state $J + 1,M$.* Probability of emission of radiation of the same polarization due to the transition $J + 1,M \rightarrow JM$ is proportional to the same quantity. For radiation with the electric vector in the x or y direction, the absorption probability is proportional to

$$|\mu_x|^2 = \frac{\mu^2}{4} \frac{(J + M + 2)(J + M + 1)}{(2J + 1)(2J + 3)} \quad (1\text{-}74)$$

for a transition $J + 1,M + 1 \leftarrow JM$ and

$$|\mu_x|^2 = \frac{\mu^2}{4} \frac{(J - M + 1)(J - M + 2)}{(2J + 1)(2J + 3)} \quad (1\text{-}75)$$

for $J + 1,M - 1 \leftarrow JM$.

For an electric vector in the z direction, the result that M, the angular momentum about the z axis, cannot change is easily understood because there can then be no torque on the molecule about the z axis. For electric fields in the x or y directions, however, there is a torque about the z axis and M changes by one unit.

For any particular initial state JM, it can be shown from (1-73), (1-74), and (1-75) that

$$\begin{aligned} |\mu_{ij}|^2 &= \sum_{M'} |\mu_x(JMJ'M')|^2 + |\mu_y(JMJ'M')|^2 + |\mu_z(JMJ'M')|^2 \\ &= \mu^2 \frac{(J + 1)}{2J + 1} \quad \text{for the transition } J + 1 \leftarrow J \\ &= \mu^2 \frac{J + 1}{2J + 3} \quad \text{for the transition } J + 1 \rightarrow J \end{aligned} \quad (1\text{-}76)$$

The expression is independent of M, as it should be since it represents the probability of absorption of unpolarized radiation, which should be independent of molecular orientation.

It should be noted that, although the individual matrix elements are identical for reverse transitions $J'M' \leftarrow JM$ and $JM \leftarrow J'M'$, the average matrix element given by (1-76) for a transition $J + 1 \leftarrow J$ is greater than that for the reverse transition $J + 1 \rightarrow J$. This must be true in

* In spectroscopy it is conventional to denote transitions by writing first the state having higher energy. For an absorption process, which is the common type of transition in microwave work, this involves writing the final state before the initial one. We follow the common convention for the sake of uniformity with other branches of spectroscopy, although the lower state is written first in much of the previous microwave literature.

order to maintain thermal equilibrium when transitions take place, since there are $2J + 3$ states of angular momentum $J + 1$, but only $2J + 1$ states of the lower angular momentum J.

Peak Intensities of Absorption Lines. Combining (1-57) and(1-76) for an absorption in which $J + 1 \leftarrow J$

$$|\mu_{ij}|^2 f = \mu^2 \frac{hB(J+1)}{kT} f_v = \frac{\mu^2 f_v}{2kT} h\nu_0$$

where f_v is the fraction of molecules in the vibrational state being considered. The peak intensity of an absorption line of a diatomic molecule given by (1-50) becomes

$$\gamma_{\max} = \frac{4\pi^2 h N f_v \mu^2 \nu_0^3}{3c(kT)^2 \Delta\nu} \tag{1-77}$$

Since the line-breadth parameter $\Delta\nu$ is proportional to the molecular density N at low pressures, $N/\Delta\nu$ and therefore $\gamma_{\max}$ is quite constant for pressures from about 1 to 10^5 microns or 10^{-3} to 100 mm Hg. As a standard procedure, the value $\Delta\nu$ is often given for 1 mm Hg pressure. Then the universal constants of (1-77) may be evaluated and rewritten

$$\gamma_{\max} = 5.48 \times 10^{-17} f_v \frac{\mu^2 \nu_0^3}{\Delta\nu} \tag{1-78}$$

where μ is measured in debye units, or 10^{-18} esu, ν_0 and $\Delta\nu$ are measured in megacycles and T is taken as 300°K. Typical values would be $f_v \approx 1$, $\mu = 1$, $\nu_0 = 30{,}000$ ($\lambda = 1$ cm), $\Delta\nu = 15$, giving $\gamma_{\max} = 10^{-4}$/cm. This value of $\gamma_{\max}$ represents a conveniently strong absorption for microwave spectroscopic work, *i.e.*, 1 per cent absorption in one meter path length. Because of the rapid variation of intensity with ν_0, absorption-line intensities for wavelengths longer than 10 cm are usually too weak to be readily observed, while those for wavelengths as short as 1 mm are quite intense.

Measurements of intensity, combined with expression (1-78), can be used in some cases to evaluate $\Delta\nu$ if μ is known. Although dipole moments are usually measured most accurately by Stark effects (Chap. 10), they may be determined to an accuracy of a few per cent from (1-78) by a measurement of both intensity $\gamma_{\max}$ and the half width of the line $\Delta\nu$.

Expression (1-77) indicates that the absorption intensity $\gamma_{\max}$ increases rapidly with decreasing temperature T. For this reason it is often advantageous to strengthen absorption lines by decreasing the temperature of the gas to −78°C (dry ice) or lower if there is sufficient vapor pressure. The exact dependence of $\gamma_{\max}$ on T depends on how $\Delta\nu$ varies with T. $\Delta\nu$ will be shown in Chap. 13 to vary as T^n, where $-1 \leq n \leq -\frac{1}{2}$. Even when $n = -1$, $\gamma_{\max}$ can be increased by decreasing the gas temperature T.

CHAPTER 2

LINEAR POLYATOMIC MOLECULES

2-1. Pure Rotational Spectra—General Considerations. Except for the complication of more possible modes of vibration, the spectrum of a linear polyatomic molecule is much like that of a diatomic molecule. There is a very small moment of inertia about the molecular axis, and hence angular momentum about this axis is not easily excited, and the linear molecule rotates end over end with energies of the same form as for a diatomic molecule

$$W = \frac{h^2}{8\pi^2 I} J(J+1)$$

where I is the moment of inertia and vibrations are neglected. Wave functions and intensities for linear molecules are also similar to those for a diatomic molecule [Eqs. (1-5), (1-6), and (1-77)] if vibrations are neglected. Vibrations do, however, add considerably to the actual complexity of the spectra as well as introduce some new phenomena.

As an obvious extension of the effects of vibrations seen in diatomic molecules, the rotational constant $B = h/8\pi^2 I$ for a polyatomic linear molecule should be written

$$B = B_e - \sum_i \alpha_i (v_i + \tfrac{1}{2}) - J(J+1)D \tag{2-1}$$

where $-\alpha_i$ represents the change in the equilibrium value B_e due to excitation of the ith vibration, D the change due to centrifugal stretching, and v_i is the quantum number for the vibrational excitation. Even in the ground state, where all v_i are zero, the zero-point vibrations change the rotational constant by $-\sum_i \alpha_i/2$. A linear molecule has one or more degenerate modes of vibration, *i.e.*, modes which have the same frequency ω_i and the same value of α_i. If these are counted as a single vibration, then (2-1) is written:

$$B = B_e - \sum_i \alpha_i \left(v_i + \frac{d_i}{2}\right) - J(J+1)D$$

where d_i is the degree of the degeneracy, or the number of degenerate modes with the same value α_i. For the diatomic molecule where there

CHAPTER 3

SYMMETRIC-TOP MOLECULES

3-1. Introduction and General Features of Rotational Spectra. For the normal rotation of a linear molecule, no angular momentum occurs in the direction of the molecular axis because the moment of inertia about this axis is so small that one quantum of angular momentum represents a large excitation energy. For a more general type of molecule, however, there is no axis about which the moment of inertia is extremely small, and the normal rotational states of nonlinear molecules may involve rotation about any molecular axis.

The moments of inertia of a molecule (or of any system of masses) may be represented by an ellipsoid whose orientation is fixed in the molecule and whose center coincides with the center of mass. The shape of the ellipsoid is such that the molecular moment of inertia about any axis through the center of mass is just equal to half the distance between intersections of this axis and the ellipsoid. Every ellipsoid has three perpendicular principal axes, and if the coordinate system is oriented so that x, y, and z are along the principal axes of the ellipsoid of inertia, then the equation of the ellipsoid of inertia may be written simply

$$\frac{x^2}{I_x^2} + \frac{y^2}{I_y^2} + \frac{z^2}{I_z^2} = 1 \tag{3-1}$$

where I_x, I_y, and I_z are the moments of inertia along the directions of the principal axes, and are hence called the principal moments of inertia.

A molecular rotation can usually most simply be described in terms of motions about the principal axes. The special case of a linear molecule has an ellipsoid of inertia which is a flat disk, since the moment of inertia along the molecular axis, which we shall take as the z direction, is very small, and the other two principal moments of inertia are equal. The general rotating body where all three principal moments of inertia are different is called an asymmetric rotor or asymmetric top, and usually the principal moments of inertia are indicated by I_A, I_B, and I_C in increasing order of size. For some molecules, two moments of inertia, such as I_A and I_B or I_B and I_C, may be equal, in which case the molecule is called a symmetric rotor or symmetric top. The linear molecule is a special case of a symmetric rotor, since for it the two largest moments of inertia I_B and I_C are equal.

In many cases it is very easy to pick out the principal axes of a molecule and to see whether or not two principal moments of inertia are equal. If the molecule has an axis of symmetry, then this is always a principal axis of the molecule. An axis of symmetry is recognized if the distribution of atoms in space is unchanged when the molecule is rotated about some axis by an angle of $2\pi/n$, in which case the molecule is said to have an n-fold axis. For example, the water molecule, H_2O, has a configuration as follows

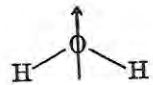

Symmetry axis

An axis in the plane of all three nuclei, passing through the oxygen nucleus lying halfway between the two hydrogens, is a twofold axis of symmetry, since the molecule will have just the same arrangement of atoms if it is rotated by π radians, or 180°, about this axis. Since the orientation of the ellipsoid of inertia must also remain unchanged as a result of this rotation, it is easy to see that this symmetry axis is a principal axis of inertia. The water molecule is not, however, a symmetric top, because its three principal moments of inertia are all different. If a molecule has an axis of three- or more fold symmetry, then it is always a symmetric top. An example would be NH_3, which is a pyramid-shaped molecule with the N at the apex and the three hydrogens equidistant from the nitrogen. An axis through the N and midway between the three hydrogens is a threefold axis of symmetry. It is also from the above discussion a principal axis of the ellipsoid of inertia and is usually taken as the z axis. If the molecule is rotated through an angle of $2\pi/3$ radians, or 120°, the ellipsoid of inertia must be unchanged. This is possible only if I_x and I_y are equal, so that the cross section of the ellipsoid of inertia in a plane perpendicular to the axis of symmetry z degenerates into a circle. The same argument would hold for any axis of symmetry greater than threefold. A linear molecule, for example, has an infinityfold axis of symmetry.

By far the most common varieties of symmetric tops are linear molecules, which have already been treated, and those with a threefold axis of symmetry. It can conceivably happen that a molecule with less symmetry than a threefold axis is a symmetric top, which would be called an "accidental" symmetric top. Since the high resolution and accuracy of microwave spectroscopy can detect even a very slight deviation from equality of two moments of inertia, it is extremely unlikely that two moments of inertia would be nearly enough equal by "acci-

dent" to make the molecule appear to be a symmetric top. Hence this variety of symmetric top with less than a threefold axis of symmetry will be ignored. Cases of this type which are almost symmetric will be treated in Chap. 4 as "slightly asymmetric" rotors.

Symmetric-rotor Spectra—Semiclassical Discussion. Much of the behavior—energy levels and selection rules—of a symmetric top can be deduced from classical mechanics and the correspondence principle. Figure 3-1 illustrates this classical motion. The axis of the molecule precesses around the total angular momentum P with a frequency that can be shown to be $P/2\pi I_B$. At the same time it may spin about its axis (see [130], p. 22). The energy of rotation would be given by

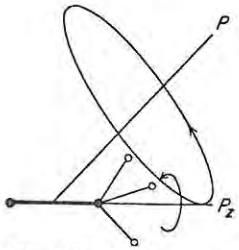

FIG. 3-1. Classical motion of a symmetric top. This is a combined rotation around the molecular axis associated with P_z and a precession of this axis around the total angular momentum P. The molecule represented is methyl chloride,

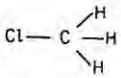

$$W = \tfrac{1}{2}I_x\omega_x^2 + \tfrac{1}{2}I_y\omega_y^2 + \tfrac{1}{2}I_z\omega_z^2 = \frac{P_x^2}{2I_x} + \frac{P_y^2}{2I_y} + \frac{P_z^2}{2I_z} \tag{3-2}$$

where x, y, and z are directions along the principal axes of inertia, z being the symmetry axis of the molecule. Now since the molecule is a symmetric top, I_x and I_y are equal and will be both called I_B, which is the normal symbol for the moment of inertia of intermediate size. I_z will be properly designated either I_A or I_C according to whether it is smaller or larger than I_B. If the relative sizes of the moments of inertia are unknown or unimportant, then I_z will always be designated as I_C. Using the fact that $I_x = I_y = I_B$ and that $P^2 = P_x^2 + P_y^2 + P_z^2$, (3-2) becomes

$$W = \frac{P^2}{2I_B} + P_z^2\left(\frac{1}{2I_C} - \frac{1}{2I_B}\right) \tag{3-3}$$

The square of the total angular momentum P^2 is quantized and must equal $J(J+1)h^2/4\pi^2$, where J is an integer. Similarly, the component of the angular momentum along some direction, say the z axis, is quantized, so that $P_z^2 = K^2h^2/4\pi^2$, where K is an integer. Hence (3-3) becomes

$$W = \frac{J(J+1)h^2}{8\pi^2 I_B} + \left(\frac{h^2}{8\pi^2 I_C} - \frac{h^2}{8\pi^2 I_B}\right)K^2$$

or, defining the rotational constants

$$A = \frac{h}{8\pi^2 I_A} \qquad B = \frac{h}{8\pi^2 I_B} \qquad C = \frac{h}{8\pi^2 I_C} \tag{3-4}$$

$$\frac{W}{h} = BJ(J+1) + (C - B)K^2 \tag{3-5}$$

The expression (3-5) gives the correct allowed energy levels for a symmetric top, which are illustrated in Fig. 3-2. If K is zero, the energy levels are just those previously found for a linear molecule. For a given value of J, however, K may have a number of values. K cannot, of course, be larger than J since K represents a component of J. It can therefore be one of the integers

$$K = J, J - 1, \ldots, -J \tag{3-6}$$

or have $2J + 1$ different values. Since the energy is independent of the sign of K, levels with the same absolute magnitude of K coincide, so that all levels for which K is greater than zero are doubly degenerate, and there

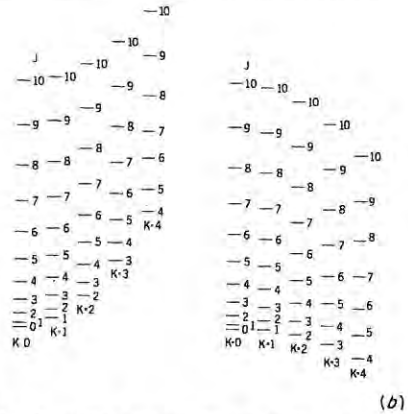

FIG. 3-2. Energy levels of typical symmetric-top molecules. (*a*) prolate; (*b*) oblate symmetric top.

are only $J + 1$ different energy values for each possible value of J. For each particular K, there is an infinite series of levels with different values of J. These are identical in relative spacing with the linear molecule levels except that the series must start with $J = K$ rather than $J = 0$.

A prolate symmetric top is one in which the molecule is more or less elongated like a cigar, and for which the moment of inertia about the symmetry axis I_z is smaller than the moment of inertia about the other principal axes. In that case $h/8\pi^2 I_z - h/8\pi^2 I_B$, which is the coefficient of K^2 in (3-5), is positive, so that the energy levels for the same J increase with increasing K as in Fig. 3-2*a*. An oblate symmetric top, which might be represented by a pancake shape, would have I_z larger than I_B, and hence the coefficient of K^2 in (3-5) would be negative. In this case energy levels for the same J decrease in energy with increasing K as in Fig. 3-2*b*. For a spherical top, with all moments of inertia equal, the coefficient of K^2 in (3-5) is zero and the energy depends only on the total angular momentum J.

In order to determine the spectrum to be expected, the selection rules in addition to the energy levels are needed. Because of the symmetry, there can be no dipole moment perpendicular to the axis of a symmetric top, and hence no torque along the axis due to electric fields associated with radiation. This indicates from the correspondence principle that the angular momentum along the molecular axis cannot change due to radiation, or $\Delta K = 0$. The dipole moment lies along the molecular axis and this axis precesses around the total angular momentum, which is fixed in direction, with a frequency $P/2\pi I_B$ as mentioned above. Hence the frequency to be expected classically is just $P/2\pi I_B$, which is identical with what would be expected from a linear molecule. This frequency can be obtained approximately with the selection rule $\Delta J = \pm 1$, which is identical with the rigorous result of a quantum-mechanical calculation.

It is important to note that, because of the above selection rules, as long as centrifugal stretching and other small effects are neglected, the frequencies observed for a symmetric top do not depend in any way on K or the moment of inertia about the symmetry axis. They are given simply by

$$\nu = \frac{2h(J+1)}{8\pi^2 I_B} = 2B(J+1) \tag{3-7}$$

The fact that the frequencies observed do not depend on I_C is an advantage in simplifying the spectrum; it is a disadvantage, however, in preventing any direct determination from the spectrum of the moment of inertia about the axis of a symmetric top.

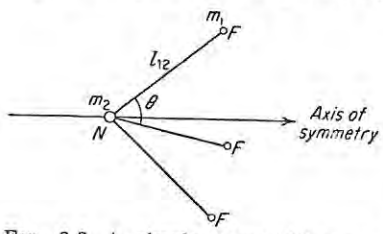

FIG. 3-3. A simple pyramidal symmetric-top molecule, NF_3.

The simplest type of symmetric top (other than a linear molecule or an "accidental" symmetric top, which never is exactly symmetric) is composed of three identical atoms arranged in an equilateral triangle, and another atom equidistant from these three. The fourth atom may be in the plane of the three identical atoms, or out of this plane so that the molecule is pyramidal. Planar molecules of this type include the trihalides of elements of the third column of the periodic table such as BF_3, BCl_3, and $AlCl_3$. Symmetric planar molecules give no pure rotational spectrum because they have no permanent dipole moment. Simple pyramidal symmetric molecules include the trihydrides and trihalides of the fifth-column elements such as NH_3, NF_3, PH_3, PCl_3, or AsF_3 (see Fig. 3-3). In order for these molecules to be symmetric rotors, the three like atoms must of course be of the same isotopic mass—NH_2D, where one hydrogen has been replaced with deuterium, is by no means a symmetric rotor.

Moments of Inertia. The moment of inertia about the symmetry axis is given by

$$I_C = 2m_1 l_{12}^2(1 - \cos\theta) \tag{3-8}$$

where m is the mass of one of the three identical atoms, l_{12} the distance from one of them to the fourth atom, and θ is the angle between two lines joining the fourth atom with two of the other atoms, *i.e.*, the angle of one face of the pyramid at its apex. The angle θ is usually called the bond angle because the chemical bonds are represented as straight lines between each of the three identical atoms and the fourth atom. The two equal moments of inertia perpendicular to the axis of symmetry are given by

$$I_B = m_1 l_{12}^2(1 - \cos\theta) + \frac{m_1 m_2 l_{12}^2}{3m_1 + m_2}(1 + 2\cos\theta) \tag{3-9}$$

TABLE 3-1. ROTATIONAL CONSTANT AND STRUCTURE OF SYMMETRIC PYRAMIDAL MOLECULES

l_{12} and θ are defined as in Fig. 3-2. Where errors in l_{12} and θ are not listed, the errors have not been estimated.

Molecule	B_0, Mc	l_{12}, angstroms	θ	Reference
NH_3	298,000	1.014	106°47′	[130] [662]
NF_3	10,680.96	1.371	102°9′	[527]
PH_3	133,478.3	1.421	93°27′	[606] [736] [866] [909]
PF_3	7,819.90	1.55	102°	[367] [947]
PCl_3^{35}	2,617.1	2.043 ± 0.003	100°6′ ± 20′	[481]
PBr_3^{79}	996.8	.....	.....	[551]
AsH_3	111,620	1.523	92°0′	[606] [735]
AsF_3	5,878.971	1.712 ± 0.006	102° ± 2°	[266] [824]
$AsCl_3^{35}$	2,147.2	2.161 ± 0.004	98°25′ ± 30′	[481]
$Sb^{121}H_3$	88,000	1.712	91°30′	[606] [736]
$Sb^{121}Cl_3^{35}$	1,754	2.325 ± 0.005	99°30′ ± 1°30′	[597] [947]

Since the frequencies of allowed rotational transitions depend only on I_B, observation of the rotational spectrum of this type of molecule does not allow determination of both parameters l_{12} or θ, which give the complete molecular configuration. If, however, spectra of two different isotopic species of the same molecule are observed, such as $N^{14}F_3$ and $N^{15}F_3$, then two different moments I_B are measured giving two equations of the type (3-9), and both molecular parameters l_{12} and θ may be determined. Structural information about these molecules may also be obtained from their nonsymmetric isotopic forms, *i.e.*, NH_2D, $AsCl_2^{35}Cl^{37}$, etc. These asymmetric molecules will be discussed in Chap. 4. Table 3-1 includes the best data available on the structure of symmetric

pyramidal molecules. The internuclear distances and angles are subject to the same type of uncertainties due to zero-point vibrations as are the internuclear distances in linear molecules. Where estimates of these or other errors have been made, they are included in Table 3-1.

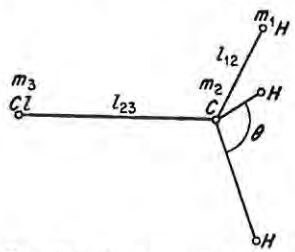

FIG. 3-4. A common type of symmetric-top molecule illustrated by methyl chloride.

Another common type of symmetric-top molecule involves elements of the fourth column of the periodic table bonded to three like atoms and a fourth different atom or group of atoms. Methyl chloride, an example of this type, is shown in Fig. 3-4. The moment of inertia I_C for this type of molecule is of course also given by (3-8), and the moment of inertia perpendicular to the axis of symmetry is

$$I_B = m_1 l_{12}^2(1 - \cos\theta) + \frac{m_1(m_2 + m_3)l_{12}^2}{3m_1 + m_2 + m_3}(1 + 2\cos\theta)$$
$$+ \frac{m_3 l_{23}}{3m_1 + m_2 + m_3} \times \left[(3m_1 + m_2)l_{23} + 6m_1 l_{12}\left(\frac{1 + 2\cos\theta}{3}\right)^{\frac{1}{2}}\right] \quad (3\text{-}10)$$

For these molecules three isotopic species must be measured in order to determine the three structural parameters l_{12}, l_{23}, and θ. In the rather common case where the three identical atoms of mass m are hydrogen, effects of zero-point vibrations can give rather large uncertainties in the positions of these hydrogens (l_{12} and θ). Variations in structural parameters of CH_3Cl as a result of using various combinations of effective moments of inertia of three isotopic species are indicated in Table 3-2. In this case variations in the hydrogen positions obtained are especially large. It has been shown that for methyl chloride the average C—H distance appears to be 0.009 A greater than the average C—D distance

TABLE 3-2. AN EXAMPLE OF SERIOUS VARIATIONS IN STRUCTURAL PARAMETERS FROM VARIOUS ISOTOPIC COMBINATIONS AS A RESULT OF ZERO-POINT VIBRATIONS

The best values are those in the last row obtained by using the asymmetric species CHD_2Cl. (Data from Miller *et al.* [729].)

Isotopic species used	Molecular parameters obtained		
	l_{12} (CH)	l_{23} (CCl)	θ (HCH)
$C^{12}H_3Cl^{35}$, $C^{12}H_3Cl^{37}$, $C^{13}H_3Cl^{37}$	1.123	1.7813	110°57′
$C^{12}H_3Cl^{35}$, $C^{12}H_3Cl^{37}$, $C^{12}D_3Cl^{37}$	1.128	1.7872	112°31′
$C^{12}H_3Cl^{37}$, $C^{13}H_3Cl^{37}$, $C^{12}D_3Cl^{37}$	0.949	1.7850	104°09′
$C^{12}H_3Cl^{35}$, $C^{13}H_3Cl^{35}$, $C^{12}HD_2Cl^{35}$	1.101	1.7815	110°13′

of the deuterated compound, and that the HCH angle is smaller than the DCD angle by about $\frac{1}{5}$° [729]. Symmetric-top molecules of the methyl chloride type (containing five atoms) which have so far been measured are listed in Table 3-3. In some cases all structural parameters have not been determined from microwave measurements because a sufficient number of isotopic species were not measured. In these cases one or two structural parameters have been estimated by other means.

TABLE 3-3. SYMMETRIC TOPS OF FIVE ATOMS FOR WHICH MICROWAVE SPECTRA ARE KNOWN

For definition of l_{12}, l_{23}, and θ see Fig. 3-4.

Molecule	B_0, Mc	l_{12}, angstroms	l_{23}, angstroms	θ	Reference
CH_3F	25,536.12	1.11	1.39	110°	[367] [946]
CH_3Cl^{35}	13,292.95	1.113	1.781	110°31′	[280] [412] [496] [729]
CH_3Br^{79}	9,568.19	1.113	1.939	111°14′	[280] [531] [533] [729]
CH_3I	7,501.31	1.113	2.1392	111°25′	[531] [729]
$Si^{28}H_3F$	14,327.9	1.46	1.5946	109°20′	[522] [772]
$Si^{28}H_3Cl^{35}$	6,673.8	1.44	2.050	110°	[315] [362] [727] [772]
$Si^{28}H_3Br^{79}$	4,321.72	1.57 ± 0.03	2.209 ± 0.001	111°20′ ± 1°	[409] [521]
$Ge^{74}H_3Cl^{35}$	4,333.91	1.52	2.148	111°	[362] [727]
$Ge^{74}H_3Br^{79}$	2,375.88	1.55 ± 0.05	2.297 ± 0.001	112° ± 1°	[521]
CF_3H	10,348.74	1.332	1.098	108°48′	[367] [690]
CF_3Cl^{35}	3,335.56	1.32	1.77	109°	[358]
CF_3Br^{79}	2,098.06	1.33	1.91	108°	[520] [743]
CF_3I	1,523.23	1.33	2.13	108°	[743]
$CCl_3{}^{35}H$	3,301.94	1.767	1.073	110°24′	[545] [690]
$CBr_3{}^{79}H$	1,247.61	1.930 ± 0.003	1.07	110°48′ ± 16′	[764]
SiF_3H	7,207.98	1.46	1.565	108°17′	[525]
$Si^{28}F_3Cl^{35}$	2,477.7	1.560	1.989	108°30′	[525] [641]
$Si^{28}F_3Br^{79}$	1,549.9	1.56	2.15	109°	[525] [641]
$Ge^{74}F_3Cl^{35}$	2,166.60	1.69 ± 0.02	2.067 ± 0.005	107°40′ ± 1°30′	[555]
PF_3O	4,594.25	1.52	1.45 ± 0.03	102°30′ ± 2°	[518] [765]
PF_3S	2,657.63	1.53	1.87	100°20′	[686] [765]
$PCl_3{}^{35}O$	2,015.20	1.99	1.45 ± 0.03	103°30′ ± 2°	[765]
$PCl_3{}^{35}S$	1,402.64	2.02	1.85 ± 0.02	100°30′ ± 2°	[765]
MnO_3F	4,129.11	1.586 ± 0.005	1.724 ± 0.005	108°27′ ± 7′	[943*a*]
ReO_3F	3,566.75	.....	.....	.....	[943*a*]
ReO_3Cl^{35}	2,094.20	1.761	2.230	108°20′ ± 1°	[665] [943*a*]

More complex symmetric tops which have been studied in the microwaves are listed in Table 3-4. In many of these cases some structural parameters are estimated.

Isotopic mass ratios may be determined from microwave measurements on the moments of inertia of symmetric-top molecules. As in

TABLE 3-4. SYMMETRIC-TOP MOLECULES OF MORE THAN FIVE ATOMS

Molecule	B_0	Structure	Reference
CH_3CN	9,198.83	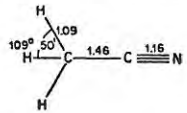	[446] [480] [543]
CH_3NC	10,052.90	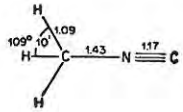	[480] [543]
CH_3CCH	8,545.84	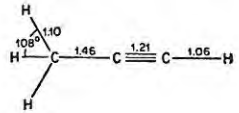	[544]
CH_3CCBr^{79}	1,561.11	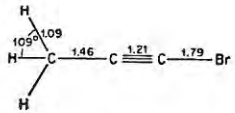	[744]
CH_3CCI	1,259.02	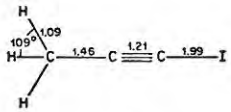	[744]
$CH_3Hg^{202}Cl^{35}$	2,076.20	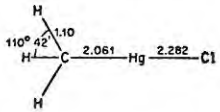	[462] [928]
$CH_3Hg^{202}Br^{79}$	1,139.88	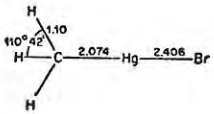	[462] [928]
$CH_3Hg^{202}I$	788.0	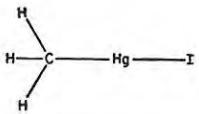	[462]

TABLE 3-4. SYMMETRIC-TOP MOLECULES OF MORE THAN FIVE ATOMS (*Continued*)

Molecule	B_0	Structure	Reference
$CH_3Hg^{202}CN$	1,747	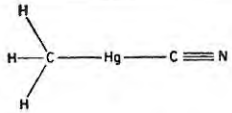	[712b]
CH_3CF_3	5,185	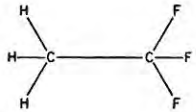	[268]
CH_3SiH_3	10,968.96	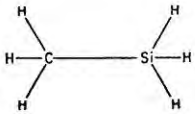	[604]
CH_3SiF_3	3,715.63	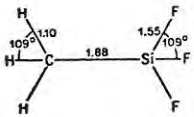	[498] [641]
$CH_3SiCl_3^{35}$	1,769.84	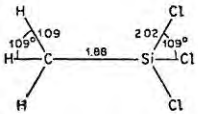	[847]
$CH_3Sn^{120}H_3$	6,890.2	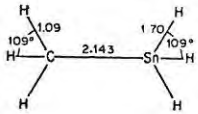	[603]
CF_3CN	2,945.54	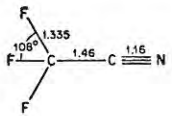	[743]
CF_3CCH	2,877.95	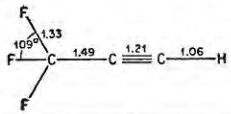	[557]

TABLE 3-4. SYMMETRIC-TOP MOLECULES OF MORE THAN FIVE ATOMS
(Continued)

Molecule	B_0	Structure	Reference
CF_3SF_5	1,097.6	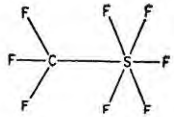	[713]
$B^{11}H_3CO$	8,657.22	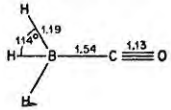	[461]
$(CN)_3P$	2,326	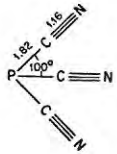	[712b]
$(CH_3)_3CCl^{35}$	3,016	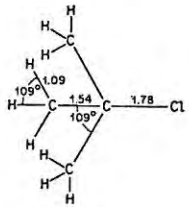	[550]
$(CH_3)_3CBr^{79}$	2,044	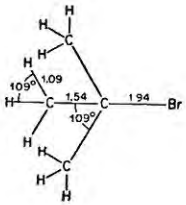	[550]
$(CH_3)_3CI$	1,562	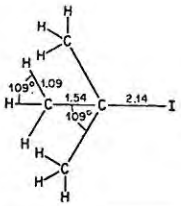	[550]

TABLE 3-4. SYMMETRIC-TOP MOLECULES OF MORE THAN FIVE ATOMS
(Continued)

Molecule	B_0	Structure	Reference
$(CH_3)_3SiCl^{35}$	2,197.44	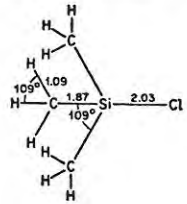	[847]
$C_3H_6O_3$	5,273.6	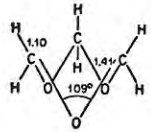	[553]
$C_8H_{12}Cl^{35}$	1,090.90	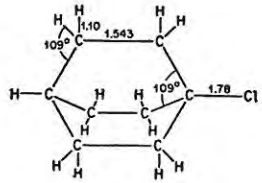	[851]
$C_8H_{12}Br^{79}$	725.9	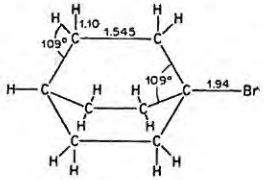	[851]
$B_5{}^{11}H_9$*	7,002.85	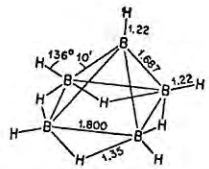	[939]

* Angle between plane containing two equivalent borons and the apical boron, and that containing the same equivalent borons and the hydrogen bonded to them is 196°.

polyatomic linear molecules, accurate determination of all the rotation-vibration effects and their dependence on mass is almost impossible, but mass difference ratios as given by (2-32) may be obtained

$$\frac{m_1 - m_0}{m_2 - m_0} = \frac{M_1}{M_2}\frac{I_1 - I_0}{I_2 - I_0} \tag{2-32}$$

It was shown in Chap. 2 that this expression is valid for any type of molecule as long as the moments of inertia I represent the various values for an axis of fixed orientation with respect to the molecule and for the several isotopic masses m_0, m_1, and m_2. If a molecule is to be a symmetric top with changes of the mass of one atom, this atom must necessarily be on the molecular axis, and hence the desired moments of inertia are simply given by the measured values of B, so that (2-32) becomes

$$\frac{m_1 - m_0}{m_2 - m_0} = \frac{M_1}{M_2}\frac{B^{(2)}}{B^{(1)}}\frac{(B^{(0)} - B^{(1)})}{(B^{(0)} - B^{(2)})} \tag{3-11}$$

Zero-point vibrations may be expected to give approximately the same types and magnitudes of errors in evaluation of masses from (3-11) as in the case of linear molecules. Mass difference ratios which have been measured from observations on symmetric tops are listed in Table 3-5.

TABLE 3-5. MASS-RATIO DETERMINATIONS FROM MEASUREMENTS OF ROTATIONAL CONSTANTS OF SYMMETRIC TOPS
(From Geschwind, Gunther-Mohr, and Townes [924a])

Molecule	Ratio of mass differences	Other determinations
GeH_3Cl^{35}	$\frac{Ge^{72} - Ge^{70}}{Ge^{74} - Ge^{70}} = 0.49985 \pm 0.00003$	0.49978 ± 0.00002
	$\frac{Ge^{76} - Ge^{74}}{Ge^{74} - Ge^{70}} = 0.50013 \pm 0.00003$	0.50011 ± 0.00002
SiH_3Cl^{35}	$\frac{Si^{30} - Si^{29}}{Si^{30} - Si^{28}} = 0.49941 \pm 0.00005$	0.49934 ± 0.00020 0.49943 ± 0.00003
SiD_3F	$\frac{Si^{30} - Si^{29}}{Si^{30} - Si^{28}} = 0.49934 \pm 0.00003$	

3-2. Symmetric-top Wave Functions. Discussion of energy levels and selection rules has been so far on a semiclassical basis. A quantum-mechanical treatment of course starts with the Hamiltonian and hence the wave equation for a symmetric top. The motion of a top is usually described in terms of Euler's angles, which are illustrated in Fig. 3-5. θ and ϕ are equivalent to the usual polar angles between an axis fixed in space and some axis fixed in the molecule, and χ (often designated ψ where there is no chance of confusion with the wave function) is the angle of rotation around the axis fixed in the molecule. For a symmetric top, this chosen axis is naturally the molecular or symmetry axis. Eulerian

angles are specified in several ways by various authors. Here they are defined as follows in agreement with Casimir [24]. Axes x, y, and z are fixed in the body; X, Y, and Z in space. The position of the body is specified from a starting position in which the two sets of axes coincide. The body is first rotated an angle ϕ about the Z axis, then through an angle θ about the x axis, and finally through an angle χ about the z axis. It can be shown ([81], p. 230) that the wave equation can be written in the above coordinates

$$\frac{1}{\sin\theta}\frac{\partial}{\partial\theta}\left(\sin\theta\frac{\partial\psi}{\partial\theta}\right) + \frac{1}{\sin^2\theta}\frac{\partial^2\psi}{\partial\phi^2} + \left(\frac{\cos^2\theta}{\sin^2\theta} + \frac{C}{B}\right)\frac{\partial^2}{\partial\chi^2}\psi - \frac{2\cos\theta}{\sin^2\theta}\frac{\partial^2\psi}{\partial\chi\,\partial\phi} + \frac{W}{hB}\psi = 0 \tag{3-12}$$

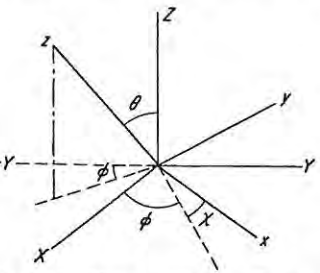

FIG. 3-5. Diagram showing Euler's angles for specifying the position of a rotating body. One dashed line is the line of nodes, or intersection between the xy and XY planes. Another is the projection of the z axis on the XY plane.

where C is the rotational constant for the symmetry axis and B is the rotational constant $h/8\pi^2 I_B$ for an axis perpendicular to the symmetry axis. The variables in (3-12) may be separated, and the solutions written in the form

$$\psi = \Theta(\theta)e^{iM\phi}e^{iK\chi} \tag{3-12a}$$

where M and K must be integers $0, \pm 1, \pm 2, \ldots$ in order to make the wave function single-valued. Θ satisfies the equation

$$\frac{1}{\sin\theta}\frac{d}{d\theta}\left(\sin\theta\frac{\partial\Theta}{\partial\theta}\right) - \left[\frac{M^2}{\sin^2\theta} + \left(\frac{\cos^2\theta}{\sin^2\theta} + \frac{C}{B}\right)K^2 - 2\frac{\cos\theta}{\sin^2\theta}KM - \frac{W}{hB}\right]\Theta = 0 \tag{3-13}$$

by introducing the variables

$$x = \tfrac{1}{2}(1 - \cos\theta) \tag{3-14}$$

and letting

$$\Theta(\theta) = x^{\frac{1}{2}|K-M|}(1 - x)^{\frac{1}{2}|K+M|}F(x) \tag{3-15}$$

the equation for F may be found to be

$$x(1 - x)\frac{d^2F}{dx^2} + (\alpha - \beta x)\frac{dF}{dx} + \gamma F = 0 \tag{3-16}$$

where

$$\begin{aligned}\alpha &= |K - M| + 1\\ \beta &= |K + M| + |K - M| + 2\\ \gamma &= \frac{W}{hB} - \frac{CK^2}{B} + K^2 - (\tfrac{1}{2}|K + M| + \tfrac{1}{2}|K - M|)\\ &\quad\times(\tfrac{1}{2}|K + M| + \tfrac{1}{2}|K - M| + 1)\end{aligned} \tag{3-17}$$

This is a well-known form of equation called the hypergeometric equation. Its solution, known as a hypergeometric function, can be obtained as a power series

$$F(x) = \sum_{n=0}^{\infty} a_n x^n \tag{3-18}$$

where

$$a_{n+1} = \frac{n(n-1) + \beta n - \gamma}{(n+1)(n+\alpha)} a_n \tag{3-19}$$

For ψ to be a satisfactory normalizable wave function, the series must terminate and become just a polynomial, which requires that the energy W is

$$\frac{W}{h} = BJ(J+1) + (C - B)K^2 \tag{3-20}$$

with

$$J = n_{\max} + \tfrac{1}{2}|K + M| + \tfrac{1}{2}|K - M| \tag{3-21}$$

$n_{\max}$ = the largest value of n in Eq. (3-18) for which a_n does not vanish.

In order for ψ to be normalized and to give matrix elements with signs or "phases" consistent with those of Condon and Shortley [56], the first term a_0 of the series (3-18) for $F(x)$ must be taken as (cf. [931])

$$e^{\frac{i\pi}{2}|K-M|}\left[\frac{(2J+1)(J+\frac{1}{2}|K+M|+\frac{1}{2}|K-M|)!(J-\frac{1}{2}|K+M|+\frac{1}{2}|K-M|)!}{8\pi^2(J-\frac{1}{2}|K+M|+\frac{1}{2}|K-M|)!\,|K-M|!\,(J+\frac{1}{2}|K+M|-\frac{1}{2}|K-M|)!}\right]^{1/2} \tag{3-22}$$

This expression may be regarded as a normalization and phase factor for ψ.

From (3-21) J must be a positive integer which is equal to or larger than $|K|$ or $|M|$, so that

$$\begin{aligned} J &= 0, 1, 2, \ldots \\ K &= 0, \pm 1, \pm 2, \ldots, \pm J \\ M &= 0, \pm 1, \pm 2, \ldots, \pm J \end{aligned} \tag{3-23}$$

As the reader may suspect, $J(J+1)h^2/4\pi^2$ can be shown to be the square of the total angular momentum; $Kh/2\pi$ is its projection on the molecular axis, and $Mh/2\pi$ its projection on the polar axis fixed in space. The energy (3-20) can be seen to be identical with Eq. (3-5) which was obtained from a semiclassical approach.

3-3. Symmetry and Inversion. The energy or behavior of a rotating molecule remains unchanged after certain types of changes of coordinates or symmetry operations, and hence the quantum-mechanical wave functions describing the molecule might be expected to remain unchanged. The wave equation may be written

$$H_{op}\psi = W\psi \tag{3-24}$$

where H_{op} represents the Hamiltonian operator for the energy which, for a symmetric top, takes the form (3-12) if Eulerian angles are used as coordinates. If Cartesian coordinates are used, H_{op} is easily seen to be unchanged when the coordinate system is inverted about the origin, *i.e.*, when x is replaced by $-x$, y by $-y$, and z by $-z$. This is shown by the fact that terms in H_{op} do not involve odd powers of the coordinates, but only terms of the type $\partial^2/\partial x^2$, $x(\partial/\partial y)$, etc.

If the coordinate change $x \to -x'$, $y \to -y'$, and $z \to -z'$ is made on (3-24), then H_{op} is unchanged, and the new ψ' must be a solution of(3-24), for the same energy W. If this energy does not represent a degenerate level, for which there are several different solutions of (3-24), then the new ψ' must be the same as the old ψ, or differ only by a multiplicative constant. Let this constant be c. If now another such transformation is made, $x' \to -x''$, $y \to -y''$, $z' \to -z''$, the new ψ'' is $\psi'' = c\psi' = c^2\psi$, but it also must be identical with ψ since this is just the reverse of the original transformation. Hence $c^2 = 1$, or $c = \pm 1$. If $c = +1$, ψ is unchanged by inversion about the origin, is said to be symmetric with respect to this operation, and is designated as an even (+) level. If $c = -1$, ψ simply changes sign on inversion, is said to be antisymmetric, and is designated as an odd (−) level.

One reason for the importance of the symmetry of the wave function with respect to inversion is its connection with the dipole matrix elements which determine the intensities of transitions. These have the form

$$\int \psi_1 x \psi_2 \, d\tau, \ \int \psi_1 y \psi_2 \, d\tau, \text{ and } \int \psi_1 z \psi_2 \, d\tau \tag{3-25}$$

where ψ_1 and ψ_2 are wave functions for the two states between which transitions occur and $d\tau$ is a volume element.

The integrals are to be taken over all values of the coordinates. Each integral may be equated to the sum of two integrals, the first over all positive values of x, y, z and the second over all negative values. The second integral is obtained from the first by the transformation $x \to -x'$, $y \to -y'$, and $z \to -z'$. In this transformation, the integrals will not of course change value, but may be seen to change sign unless ψ_1 and ψ_2 have opposite symmetries. Thus if ψ_1 and ψ_2 have the same symmetry, the integral over all space is the sum of two integrals which are equal in magnitude and opposite in sign, and so is zero. This establishes the selection rule

$$+ \longleftrightarrow - \qquad + \leftarrow\!|\!\rightarrow + \qquad - \leftarrow\!|\!\rightarrow -$$

The transitions of a diatomic molecule, for which the matrix elements vanish unless $J \pm 1 \leftarrow J$ (page 22), must of course obey the above selection rule and will be found to do so. We shall examine the symmetry of symmetric-top wave functions, but before doing so, the coordinate system for a symmetric top must be more completely described.

Consider a planar symmetric top such as BF_3 with three like atoms and a fourth atom equidistant from them. The orientation of this molecule can be specified in terms of an axis through the center of mass and perpendicular to the plane of the molecule. In order to define the positive direction of this axis, the three like (fluorine) atoms must be labeled with the numbers 1, 2, 3. The positive direction is then taken as the direction of advance of a right-handed screw rotated in the direction of successive nuclei 1, 2, 3. This is illustrated in Fig. 3-6*a*, or in Fig. 3-6*b* where the positive direction is into the page. θ and ϕ are the usual polar angles between the molecular axis and a fixed polar axis (z), and χ, illustrated in Fig. 3-6*b*, is the angle of rotation around the molecular axis. If the coordinates of each atom in the molecule are inverted about the origin, then Fig. 3-6*b* shows that the positive direction of the molecular axis does not change, so that θ and ϕ are unaffected. However, χ is changed into $\chi + \pi$.

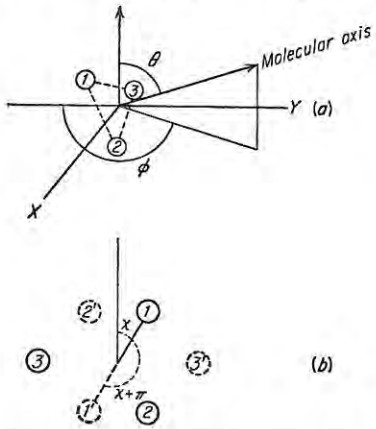

FIG. 3-6. Coordinates for a symmetric-top molecule. (*a*) The positive direction of the molecular axis of a symmetric-top molecule (*e.g.*, BF_3) and the polar angles θ and ϕ. The three identical nuclei are labeled 1, 2, and 3. (*b*) A symmetric-top molecule viewed along the positive direction of the molecular axis showing the angle χ which indicates rotation around the molecular axis. The vertical line is the "line of nodes." The solid circles represent the nuclear positions before an inversion through the origin, and the dotted circles are their positions after such an inversion.

The rotational wave functions for a symmetric top are from (3-12*a*), of the form

$$\psi_{JKM} = e^{iM\phi}e^{iK\chi}\Theta_{JKM}(\theta) \quad (3\text{-}26)$$

so that when the coordinates undergo an inversion about the origin, the new wave function becomes

$$\psi = \psi e^{iK\pi} = (-1)^K\psi \quad (3\text{-}27)$$

Hence the rotational wave function is even (+) or odd (−) with respect to inversion according to whether K is even or odd.

In addition to the rotational part of the wave function, the electronic, vibrational, and spin coordinates must be considered. The complete wave function may be indicated by a product

$$\psi_{\text{total}} = \psi_e\psi_v\psi_R\psi_I \quad (3\text{-}28)$$

where ψ_e, ψ_v, ψ_R, and ψ_I represent the parts of the wave function dependent, respectively, on electronic, vibrational, rotational, and spin coordinates. The behavior of ψ_{total} with respect to any symmetry operation

depends on the behavior of each of these four parts. The electronic wave functions for almost all polyatomic molecules in the ground state are symmetric, so they may be neglected in considering the symmetry of ψ_{total}. The spin wave functions ψ_I may usually be either symmetric or antisymmetric, but consideration of them will be postponed until later.

The vibrational wave function for a molecule in the ground vibrational state is always symmetric, so in this case the symmetry of ψ_{total} depends only on ψ_R (if ψ_I is neglected). Consider excited states of the vibration for which the central boron atom in the symmetric top illustrated by Fig. 3-6 moves perpendicularly to the plane of the three fluorines. The coordinate for this motion will be called h. It indicates the distance moved by the boron from the center of mass and will be called positive when the boron has moved along the positive direction of the molecular axis, negative if the boron moves in the opposite direction. The wave functions for a harmonic vibration of this type are ([62], p. 74)

$$\psi_v(h) = c_1e^{-c_2^2h^2/2}H_v(c_2h) \quad (3\text{-}29)$$

where c_1 and c_2 are constants, and H_v is a Hermite polynomial of order n. The lowest energy level corresponds to $v = 0$, with higher integral values $v = 1, 2, \ldots$ being successively higher in energy. H_v involves only odd or even powers of h according to whether v is odd or even. Hence when an inversion about the origin occurs, which changes h into $-h'$, the new vibrational wave function is

$$\psi_v' = (-1)^v\psi_v \quad (3\text{-}30)$$

The rotation-vibration wave functions hence have symmetries with respect to inversion as shown in Fig. 3-7, where the ground and first excited vibration states are indicated.

There are many symmetric tops such as CH_3Cl or NH_3 which are not normally considered planar molecules, but which have the same symmetry with respect to inversion as BF_3. NH_3 may actually be considered planar, but with a potential function which differs so much from a simple harmonic potential that as a result of vibration the nitrogen spends most of its time some distance from the plane of the three hydrogens. The energy levels of a particle moving in a parabolic potential are equally spaced as on the left side of Fig. 3-8. If the potential is distorted by a hill being gradually raised in the center, the energy levels approach each other in pairs as shown in Fig. 3-8. For a very high potential hill, the particle again has equally spaced energy levels, but two sets of them corresponding to oscillations on either one side of the hill or the other. However, even when the hill is so high that the particle does not have enough energy to go to its top, a quantum-mechanical "tunnel effect" occurs which allows the particle to oscillate slowly from one side of the potential barrier to the other. (This will be discussed more fully in

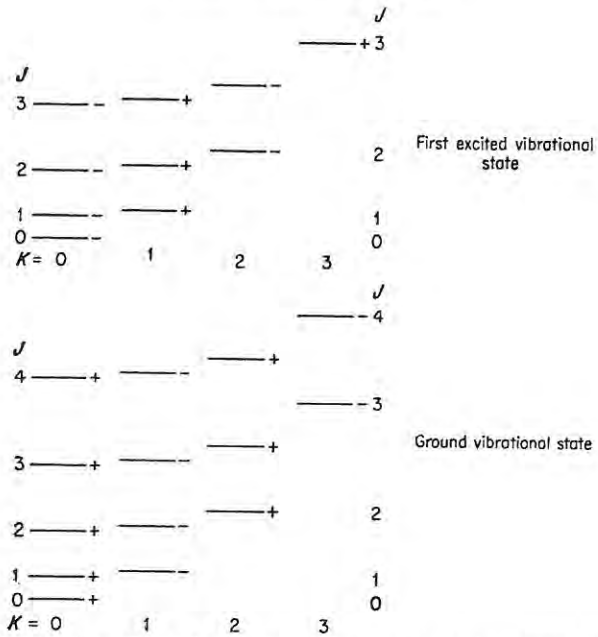

FIG. 3-7. Levels of a symmetric top and their symmetry with respect to inversion. The vibration is a nondegenerate mode in which atoms on the molecular axis move parallel to this axis.

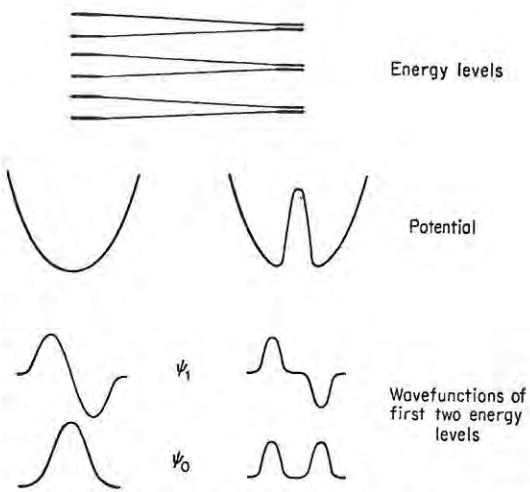

FIG. 3-8. Behavior of a vibration with introduction of a potential barrier.

Chap. 12 on the ammonia spectrum.) The rise of the central potential hill modifies the wave functions as is shown in Fig. 3-8, but does not destroy their symmetry. For BF_3 there is no potential hill and the potential minimum occurs when the boron is in the plane of the fluorines, so the energy levels are those on the left of Fig. 3-8. NH_3, on the other hand, is a pyramidal molecule. Potential minima occur when the nitrogen is on either side of the plane of the hydrogens, and the energy levels correspond to those on the right-hand side of Fig. 3-8. In NH_3, the central potential hill is only moderately high, and the two lowest vibrational levels are separated by an energy gap such that a transition between them falls in the microwave region. In the case of NF_3, CH_3Cl, or almost any other nonplanar top, the potential hill is so high that the two lowest vibrational levels have almost coalesced, their separation corresponding to frequencies which are so low that usually many years are required for an oscillation period.

For nonplanar symmetric tops, the transition between these two lowest levels is often referred to as inversion, for the classical motion corresponds to the molecule being turned inside out. This is not identical, however, with inversion of the molecule about the center of mass. Let the position of nitrogen with respect to the plane of the hydrogens in NH_3 be given by wave functions ψ_0 and ψ_1 as shown on the right side of Fig. 3-8. The energy for ψ_0 is W_0, so that it varies with time as $\psi_0 e^{2\pi i W_0 t/h}$, and similarly ψ_1 varies as

$$\psi_1 e^{2\pi i (W_0+\Delta) t/h}$$

where Δ is the energy separating the two lowest levels. If at time $t = 0$ the nitrogen is on the negative side of the hydrogens, then the wave function for the system may be written

$$\psi = \frac{1}{\sqrt{2}} (\psi_0 + \psi_1 e^{2\pi i \Delta t/h}) e^{2\pi i W_0 t/h} \tag{3-31}$$

which at time $t = 0$ is $(\psi_0 + \psi_1)/\sqrt{2}$, and at time $h/2\Delta$ is $(\psi_0 - \psi_1)/\sqrt{2}$, corresponding to the nitrogen being on the positive side. Hence the NH_3 molecule inverts itself with a frequency (for a complete cycle) $\nu = \Delta/h$, which happens to be about 2.4×10^{10} times per second. CH_3Cl, on the other hand, exists for some time with Cl on one particular side of the molecular axis, and inverts only very slowly.

Symmetry and spacing of the rotation and inversion levels of NH_3 are indicated in Fig. 3-9. Possible transitions, allowed by the rules $+ \longleftrightarrow -$, $\Delta J = 0, \pm 1$, $\Delta K = 0$, are also shown. Figure 3-10 shows the same things for CH_3Cl, where the inversion levels are so close together as to be indistinguishable, and the rule $+ \longleftrightarrow -$ is no longer of importance since $+$ and $-$ levels coincide in pairs. Some levels in Fig. 3-9 for which $K = 0$ are drawn as dashed lines. These levels cannot occur

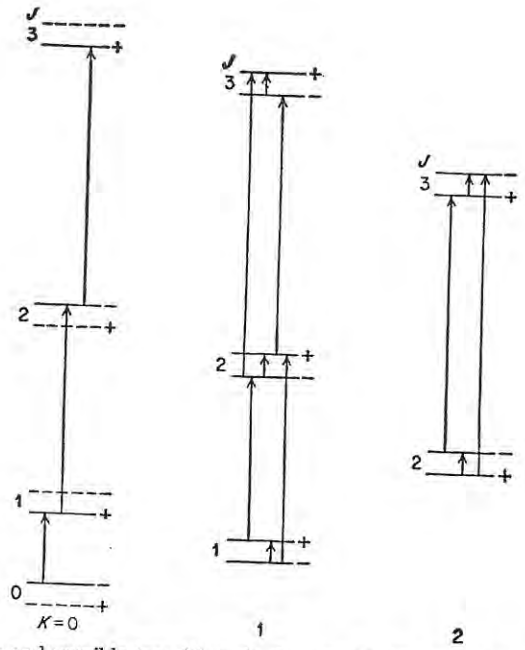

FIG. 3-9. Levels and possible transitions in the rotation-inversion spectrum of NH_3. The dotted levels for $K = 0$ are forbidden by the exclusion principle.

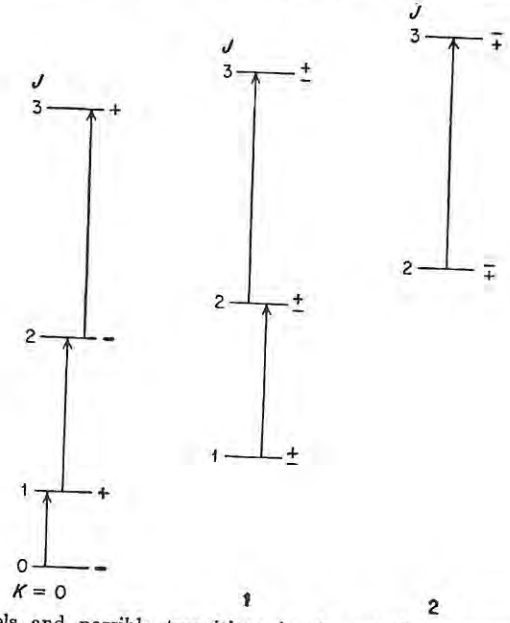

FIG. 3-10. Levels and possible transitions in the rotation-inversion spectrum of CH_3Cl, where the inversion frequency is negligibly small.

because of certain properties of the spin wave functions to be discussed below.

For NH_3, the doubling of each level due to inversion produces a doubling of the rotational lines with a separation between doublet components of twice the inversion frequency. This rotational spectrum lies in the infrared region. In addition, transitions between inversion levels with $\Delta J = 0$, $\Delta K = 0$ occur and produce lines which occur in the normal microwave range near 1 cm. In the case of CH_3Cl, the pure rotational spectrum is observed in the microwave range, and although each rotational line is split by twice the inversion frequency, this splitting is so small that it is completely unobservable even with the high resolution of microwave spectroscopy.

3-4. Effects of Nuclear Spins and Statistics. Other types of symmetry operations in addition to inversion about the center of mass may also be considered. For a symmetric top with a threefold axis of symmetry such as NH_3 or BF_3, a rotation of 120° about the symmetry axis should leave the molecule essentially unchanged, and reasoning similar to that applied above to inversion about the origin shows that this rotation must either leave the wave function unchanged or change only its sign if the state is not degenerate. Similarly an interchange of two H nuclei in NH_3 or two F nuclei in BF_3 is another permissible symmetry operation which must affect the wave function in the same way.

Symmetry considerations may also be applied to the case of interchanging two identical particles in any type of system. It is found experimentally that H^1, F^{19}, and any other nucleus of odd nuclear mass always occur in antisymmetric wave functions. These nuclei are said to obey Fermi-Dirac statistics. Nuclei of even mass always occur in symmetric wave functions and are said to obey Einstein-Bose statistics. Hence it is essential that any true and permissible wave function for NH_3 changes sign when two H nuclei are exchanged.

Consider just rotation of 120° around the symmetry axis of NH_3. This is equivalent to exchanging two pairs of H nuclei, say first numbers 1 and 2, then 2 and 3. Since there are two exchanges, the wave function must be unchanged by a rotation of 120° if H obeys either Fermi-Dirac or Bose-Einstein statistics. The only one of Euler's angles which changes with such a rotation is χ, which enters the wave function as $e^{iK\chi}$ or $e^{-iK\chi}$. Hence after a 120°, or $2\pi/3$, rotation,

$$\psi' = \psi e^{\pm(2\pi/3)Ki} \tag{3-32}$$

If K is a multiple of 3, then the exponential in (3-32) equals 1, and $\psi' = \psi$, so that the wave function is symmetric. If K is not a multiple of 3, then ψ is neither symmetric nor antisymmetric. This indicates that the state is degenerate, which is true since the same energy is obtained for $+K$ as for $-K$. In order to make wave functions of the

correct symmetry when K is not a multiple of 3, the spin wave function ψ_I must be considered, for when nuclei are exchanged not only their spatial coordinates are changed, but also their spins.

Before discussing spin wave functions, consider the symmetry operation of exchanging only one pair of nuclei, *e.g.*, 2 and 3. An interchange of these two nuclei changes the positive direction of the molecular axis as defined above, since it changes the relative order of the nuclei. The molecular variables are transformed as follows:

$$\begin{aligned} \theta' &\to \pi - \theta \qquad & \phi' &\to \phi + \pi \\ \chi' &\to \pi - \chi \qquad & h' &\to -h \end{aligned} \tag{3-33}$$

Detailed examination of the wave functions given by (3-12*a*) shows that for $\theta \to \theta' - \pi$, $\chi \to \pi - \chi'$, and $\phi \to \phi' - \pi$, the wave function changes as

$$\psi'_{JKM} \to (-1)^J \psi_{J,-K,M} \tag{3-34}$$

For this change of variables, ψ is neither symmetric nor antisymmetric but the wave functions are degenerate. They can be put in symmetric or antisymmetric form by choosing a wave function $\psi_{JKM} + \psi_{J,-K,M}$ or $\psi_{JKM} - \psi_{J,-K,M}$. In exchanging nuclei 2 and 3, χ changed to $\pi - \chi$. If, instead of interchanging 2 and 3, 1 and 3 had been interchanged, then the variables would have transformed as

$$\begin{aligned} \theta' &\to \pi - \theta \qquad & \phi' &\to \phi + \pi \\ \chi' &\to \pi - \chi + \frac{2\pi}{3} \qquad & h' &\to -h \end{aligned} \tag{3-35}$$

The new symmetrized forms $e^{iK\chi} \pm e^{-iK\chi}$ would then for this exchange no longer be symmetric or antisymmetric unless K is a multiple of 3. Spin wave functions are needed to produce ψ_{total} which has the correct type of symmetry for all possible interchanges of nuclei.

Spin Wave Functions. The spin wave function for a nucleus needs to tell the projection of the spin on some fixed direction, which in the case of hydrogen can take on only two values, $+\frac{1}{2}$ and $-\frac{1}{2}$. The $+\frac{1}{2}$ value will be indicated graphically by a vector pointed up, and $-\frac{1}{2}$ by a vector pointed down. Various possible spin functions which exactly specify the spin orientation of three H nuclei are then represented by Fig. 3-11.

The spin wave functions I and VIII of Fig. 3-11 are clearly symmetric with respect to interchange of any two nuclei, since they do not change. Spin function II, however, is symmetric with respect to interchange of 2 and 3, but it changes into III if 1 and 2 are interchanged, or into IV if 1 and 3 are interchanged. All spin functions shown in Fig. 3-11 are of this type except I and VIII, and hence are degenerate. Functions which are symmetric or antisymmetric with respect to interchange of any nuclei can be formed by combining the variation with χ and spin. Such functions automatically are symmetric for a 120° rotation, which corresponds to successive interchange of two pairs of nuclei. If K is not a

multiple of 3, they are

$$\begin{aligned} &\psi_{JKM}(\mathrm{II} + e^{2\pi Ki/3}\mathrm{III} + e^{4\pi Ki/3}\mathrm{IV}) \pm \psi_{J,-K,M}(\mathrm{II} + e^{-2\pi Ki/3}\mathrm{III} + e^{-4\pi Ki/3}\mathrm{IV}) \\ &\psi_{JKM}(\mathrm{V} + e^{2\pi Ki/3}\mathrm{VI} + e^{4\pi Ki/3}\mathrm{VII}) \\ &\qquad \pm \psi_{J,-K,M}(\mathrm{V} + e^{-2\pi Ki/3}\mathrm{VI} + e^{-4\pi Ki/3}\mathrm{VII}) \end{aligned} \tag{3-36}$$

If K is a multiple of 3, these reduce to

$$\begin{aligned} &(\psi_{JKM} \pm \psi_{J,-K,M})(\mathrm{II} + \mathrm{III} + \mathrm{IV}) \\ &(\psi_{JKM} \pm \psi_{J,-K,M})(\mathrm{V} + \mathrm{VI} + \mathrm{VII}) \end{aligned} \tag{3-37}$$

and two additional functions have the correct symmetry,

$$\begin{aligned} &(\psi_{JKM} \pm \psi_{J,-K,M})\mathrm{I} \\ &(\psi_{JKM} \pm \psi_{J,-K,M})\mathrm{VIII} \end{aligned} \tag{3-38}$$

Nucleus	1	2	3
I	↑	↑	↑
II	↓	↑	↑
III	↑	↓	↑
IV	↑	↑	↓
V	↑	↓	↓
VI	↓	↑	↓
VII	↓	↓	↑
VIII	↓	↓	↓

FIG. 3-11. The eight possible spin states for three nuclei with spin $\frac{1}{2}$.

In all these expressions, when J is even the + sign produces a function which is symmetric with respect to interchange of two identical nuclei, and the − sign gives an antisymmetric function [*cf.* Eq. (3-34)]. When J is odd, the symmetries are reversed.

Not all the functions (3-36) or (3-37) and (3-38) are permitted for a particular rotation-inversion state. In the lowest inversion state, the vibrational (inversion) part of the wave function does not change sign for a transformation of the type (3-33) or (3-35), which reverses the sign of h. The parts of the wave function involving h, θ, and ϕ are symmetric with respect to interchange of two nuclei if $J + K$ is even [*cf.* (3-34)]. For these cases antisymmetric forms, with the − sign, must be chosen from (3-36), or (3-37) and (3-38) to make the total wave function change sign with exchange of two nuclei, *i.e.*, if J is odd, the − sign is chosen in these equations, or if J is even, the + sign is needed. In the upper inversion state, the vibrational part of the wave function is antisymmetric for interchange of two nuclei, and the choice of + or − signs in (3-36), or (3-37) and (3-38) must be just reversed.

When $K = 0$, the functions of the form (3-37) or (3-38) become zero when the − sign is used, and hence no such wave function exists. This is the reason why half the levels are nonexistent when $K = 0$ as indicated in Fig. 3-9. In the lowest inversion state, when $K = 0$ and $J = 0$, a − sign in (3-37) or (3-38) would be called for, but this makes the wave function zero. In the upper inversion state, however, when $K = 0$ and $J = 0$, a + sign is called for and such a wave function is not zero. When $K = 0$ and J is odd, however, the ground inversion level requires the + sign and hence is the state in which molecules can exist.

Statistical Weights. It is evident that, with the exception of the case $K = 0$, there are twice as many acceptable wave functions from (3-37) and (3-38) for the case where K is a multiple of 3 as can be obtained from (3-36) for the cases where K is not a multiple of 3. This gives the states for which K is a multiple of 3 twice the statistical weight and hence approximately twice the population of otherwise similar states for which K is not a multiple of 3.

The above discussion has been specialized to the case of three identical atoms with spins $\frac{1}{2}$, which is by far the most common case. If there are three identical atoms with spin I, the statistical weights are given by Table 3-6 [25], [43]. Regardless of the type of statistics, the levels with K a multiple of 3 always have a greater weight, the ratio between these and other values of K being 2:1 in the case of spin $\frac{1}{2}$ as was found above.

If $K = 0$, we have seen that alternate inversion levels on the level diagram of Fig. 3-9 are missing, beginning with the lowest inversion level for $J = 0$. If the spin I of the identical nuclei had been zero, Bose-Einstein statistics would apply instead of Fermi-Dirac, and for $K = 0$ the role of permitted and forbidden levels on Fig. 3-9 would be just

TABLE 3-6. STATISTICAL WEIGHTS

Statistical weights due to nuclear spin for rotational levels of a symmetric-top molecule with three identical nuclei of spin I. These apply to molecules in a nondegenerate vibrational state. For a degenerate vibrational state, K should be replaced by $K - l$.

	Statistical weights	Nuclear spin, I
K a multiple 3, but not 0	$\frac{1}{3}(2I + 1)(4I^2 + 4I + 3)$	$0 \quad \frac{1}{2} \quad 1 \quad \frac{3}{2}$
K not a multiple of 3	$\frac{1}{3}(2I + 1)(4I^2 + 4I)$	
Ratio	$\dfrac{4I^2 + 4I + 3}{4I^2 + 4I}$	$\infty \quad \frac{2}{1} \quad \frac{11}{8} \quad \frac{6}{5}$
$K = 0$, J even lower inversion level or J odd upper inversion level, Fermi-Dirac statistics	$\frac{1}{3}(2I + 1)(2I - 1)I$	
$K = 0$, J odd, lower inversion level or J even, upper inversion level, Fermi-Dirac statistics	$\frac{1}{3}(2I + 1)(2I + 3)(I + 1)$	
Ratio Fermi-Dirac statistics	$\dfrac{(2I - 1)I}{(2I + 3)(I + 1)}$	$0 \quad \frac{1}{5}$
Ratio Bose-Einstein statistics	$\dfrac{(2I + 3)(I + 1)}{(2I - 1)I}$	$\infty \quad \frac{10}{1}$

reversed. If the spin is greater than $\frac{1}{2}$, none of these $K = 0$ levels is forbidden: their statistical weights for the case of Fermi-Dirac statistics are given in Table 3-6. For Bose-Einstein statistics, these formulas for statistical weights of alternate levels are just reversed.

For symmetric-top molecules with four identical nuclei equidistant around the axis, the statistical weights are as follows [43]:

For $K \neq 0$:

$(I + 1)(2I + 1)(2I^2 + I + 1)$
for K a multiple of 4, Bose-Einstein statistics or for K even, not a multiple of 4 and Fermi-Dirac statistics.

$I(2I + 1)(2I^2 + 3I + 2)$
for K a multiple of 4, Fermi-Dirac statistics or for K even, not a multiple of 4 and Bose-Einstein statistics.

$I(I + 1)(2I + 1)^2$
for K odd.

For $K = 0$:

$\frac{1}{2}(I + 1)(2I + 1)(2I^2 + 3I + 2)$
for J even, Bose-Einstein statistics.

$\frac{1}{2}I(I + 1)(2I - 1)(2I + 1)$
for J odd, Bose-Einstein statistics.

$\frac{1}{2}I(2I + 1)(2I^2 + I + 1)$
for J even, Fermi-Dirac statistics.

$\frac{1}{2}I(I + 1)(2I + 1)(2I + 3)$
for J odd, Fermi-Dirac statistics.

In this case, the inversion levels are considered to coincide, so statistical weights of the $K = 0$ levels refer to the sum of both inversion levels.

The above considerations about statistical weights apply only to molecules in nondegenerate vibrational states. When a degenerate vibrational mode is excited, a new angular momentum l is introduced (*cf.* l-type doubling in Chap. 2 and below). In this case similar statistical weights apply, but with K replaced by $K - l$ [943*a*]. Thus levels with $K - l$ a multiple of 3 have greater statistical weights than do other levels for molecules with a threefold axis.

Nuclear spins are important in a wide variety of other types of molecules. Some of these are discussed by Placzek and Teller [43], Wilson ([64] and [90]), and Minden [730].

3-5. Intensities of Symmetric-top Transitions. Intensities of symmetric-top absorption lines may be calculated from the basic formula (1-49). Some of the quantities in this expression, however, such as the matrix element μ and the fraction of molecules f in a given state, must be evaluated for the symmetric-top case.

Selection rules for dipole radiation of a nonplanar symmetric top (dipole moment taken only along the molecular axis since it is a truly symmetric top) are

$$\Delta J = 0, \pm 1 \qquad \Delta K = 0 \qquad + \rightarrow - \tag{3-39}$$

The last selection rule, taken from symmetry considerations above, is needed to specify the inversion levels involved in a transition, and may be

applied by referring to Fig. 3-9. Matrix elements may be calculated as indicated in (1-59), (1-60), and (1-61). However, since wave functions for a symmetric top are considerably more complex than those for a linear molecule, actual evaluation of these integrals is more difficult. The matrix elements are of course nonzero only for transitions given by the selection rules (3-39). The nonzero matrix elements are as follows:

$J + 1 \leftarrow J,\ K \leftarrow K$:

$$|\mu_{ij}|^2 = \mu^2 \frac{(J+1)^2 - K^2}{(J+1)(2J+1)} \tag{3-40}$$

$J \leftarrow J,\ K \leftarrow K$:

$$|\mu_{ij}|^2 = \frac{\mu^2 K^2}{J(J+1)} \tag{3-41}$$

$J - 1 \leftarrow J,\ K \leftarrow K$:

$$|\mu_{ij}|^2 = \mu^2 \frac{J^2 - K^2}{J(2J+1)} \tag{3-42}$$

These are the matrix elements appropriate for substitution into (1-49), and represent the sum of the components $|R_x|^2$, $|R_y|^2$, and $|R_z|^2$ for a particular molecule orientation specified by M, the projection of J on the z axis, to all possible final M states. The components $|R_x|^2$, $|R_y|^2$, and $|R_z|^2$ and their dependence on M are given in Table 4-4.

The quantity μ in the above equations is the usual dipole moment of the molecule. One might question whether a symmetric top has a dipole moment, since we have been considering inversion as a type of vibration and even a pyramidal molecule as an oscillating planar molecule. This dipole moment μ, however, is to be evaluated without considering inversion, but taking the symmetric top in its normal pyramidal configuration. Thus although NH_3 is inverting approximately 3×10^{10} times per second, μ is called a "permanent" dipole moment and is to be calculated when N is on one side only of the three hydrogens. This is the NH_3 dipole moment which commonly enters into other physical and chemical measurements. Quantum-mechanically, μ should be evaluated in the state $(\psi_0 + \psi_1)/\sqrt{2}$, where ψ_0 and ψ_1 represent wave functions for the two inversion levels.

The fraction of molecules f in a particular initial state is also needed to calculate absorption intensities from (1-49). This fraction f is the product of the fraction f_v in the vibrational state of interest and the fraction of these f_{JK} in a particular rotational state. If statistical weight due to nuclear spin is neglected, the probability of a molecule's being in a state J, K is proportional to

$$(2J + 1)e^{-[BJ(J+1)+(C-B)K^2]h/kT} \tag{3-43}$$

$2J + 1$ is the statistical weight due to the different orientations of J.

The fraction of molecules in this rotational state would be

$$f_{JK} = \frac{(2J+1)e^{-[BJ(J+1)+(C-B)K^2]h/kT}}{\sum_{J=0}^{\infty} \sum_{K=-J}^{J} (2J+1)e^{-[BJ(J+1)+(C-B)K^2]h/kT}} \tag{3-44}$$

Here B and C are in cycles per second as in (3-4). When Bh and Ch are small compared with kT the sums may be replaced by integrals, giving

$$f_{JK} = (2J+1)e^{-[BJ(J+1)+(C-B)K^2]h/kT} \sqrt{\frac{B^2Ch^3}{\pi(kT)^3}} \tag{3-45}$$

It should be noted that (3-45) applies to one particular value of K, and does not allow for K degeneracy. A more accurate evaluation of the sum has been made ([130], p. 506) but is not of much interest to us because the error in approximating the sum as an integral is usually very small and in addition (3-44) does not allow for the statistical weights introduced by the spins of the like particles which must always be considered in a symmetric top.

The usual type of symmetric top has threefold symmetry about the axis and the separation between inversion levels is negligible. In that case, from Table 3-6 the degeneracy due to spin and inversion levels (or spin and K degeneracy) for each value of J and K is proportional to (omitting a constant factor $(2I + 1)/3$):

For K a multiple of 3, but not 0,

$$S(I,K) = 2(4I^2 + 4I + 3) \tag{3-46a}$$

For $K = 0$,

$$S(I,K) = (4I^2 + 4I + 3) \tag{3-46b}$$

For K not a multiple of 3,

$$S(I,K) = 2(4I^2 + 4I) \tag{3-46c}$$

Allowing for this degeneracy, (3-44) becomes

$$f_{JK} = \frac{S(I,K)(2J+1)e^{-[BJ(J+1)+(C-B)K^2]h/kT}}{\sum_{J=0}^{\infty} \sum_{K=0}^{J} S(I,K)(2J+1)e^{-[BJ(J+1)+(C-B)K^2]h/kT}} \tag{3-47}$$

It is evident that (3-47) is unaffected by the omission of a constant factor $(2I + 1)/3$ in the degeneracy $S(I,K)$ associated with spin and inversion as given in (3-46). Again assuming B and C to be much smaller than kT, the sums in (3-47) may be changed to integrals, so that one obtains

$$f_{JK} = \frac{S(I,K)(2J+1)}{4I^2 + 4I + 1} \sqrt{\frac{B^2Ch^3}{\pi(kT)^3}}\, e^{-[BJ(J+1)+(C-B)K^2]h/kT} \tag{3-48}$$

For low values of J and K, the exponential in (3-48) is very close to 1, so that

$$f_{JK} = \frac{S(I,K)(2J+1)}{4I^2+4I+1}\sqrt{\frac{B^2Ch^3}{\pi(kT)^3}} \tag{3-49}$$

The fraction of molecules in a given vibrational state may be obtained analogously to (1-51) as

$$f_v = e^{-W_v/kT}\prod_n (1 - e^{-h\omega_n/kT})^{d_n} \tag{3-50}$$

where d_n is the degeneracy of a vibrational mode of frequency ω_n and $\prod_n$ represents the product

$$(1 - e^{-h\omega_1/kT})^{d_1}(1 - e^{-h\omega_2/kT})^{d_2}(1 - e^{-h\omega_3/kT})^{d_3} \cdots$$

for all vibrational modes. Since a symmetric top has a number of vibrational modes, the product $\prod_n$ is sometimes appreciably less than 1, but in simple symmetric tops not usually less than about 0.5. Substituting (3-49) and (3-40) into (1-49), and setting $2B(J+1) = h\nu_0$, the intensity for a transition $J+1 \leftarrow J$, $K \leftarrow K$ is

$$\gamma = \frac{4\pi hNf_vS(I,K)}{(4I^2+4I+1)3c(kT)^2}\sqrt{\frac{\pi Ch}{kT}}\,\mu^2\left[1 - \frac{K^2}{(J+1)^2}\right]\frac{\nu_0\nu^2\,\Delta\nu}{(\nu-\nu_0)^2+(\Delta\nu)^2} \tag{3-51}$$

It may be seen that γ increases, as in a linear molecule, approximately as ν^3. However, for a symmetric top γ is more strongly dependent on the temperature T than it is for the linear molecule. The expression (3-51) might be summed over all possible K for a particular J transition, since transitions for the various values of K coincide in frequency (approximately—see discussion of centrifugal distortions in Sec. 3-6). Summing over the K values, assuming J is large, and letting $\frac{S(I,K)}{4I^2+4I+1}$ be approximately 2,

$$\gamma_{\text{total}} = \frac{2\pi h^2Nf_v}{9c(kT)^2B}\sqrt{\frac{\pi Ch}{kT}}\,\mu^2\frac{(4J+3)(J+2)}{(J+1)^2}\,\frac{\nu_0^2\nu^2\,\Delta\nu}{(\nu-\nu_0)^2+(\Delta\nu)^2} \tag{3-52}$$

This shows that the entire intensity for a transition $J+1 \leftarrow J$ summed over all K increases approximately as ν^4, even more rapidly than intensities of transitions for linear molecules.

The maximum absorption coefficient of a symmetric-top transition $J+1 \leftarrow J$ may also be written from (3-51), after some numerical

evaluation,

$$\gamma_{\max} = \frac{1.23\times 10^{-20}f_vS(I,K)\sqrt{C}}{4I^2+4I+1}\,\mu^2\left[1 - \frac{K^2}{(J+1)^2}\right]\frac{\nu_0^3}{\Delta\nu} \quad \text{cm}^{-1} \tag{3-53}$$

where C = rotational constant about the symmetry axis, Mc
μ = dipole moment, debye units (10^{-18} esu)
$\Delta\nu$ = half width at half maximum at a pressure of 1 mm Hg, Mc
ν_0 = resonant frequency, Mc
the temperature is assumed to be 300°K

For symmetric tops with more than three identical nuclei, the statistical weight factor $\frac{S(I,K)}{4I^2+4I+1}$ in (3-53) must be adjusted, but this factor is of the order of 1 and may be set equal to 2 if an approximate evaluation of $\gamma_{\max}$ is all that is required. The only other type of transition, $J \leftarrow J$, which occurs for a symmetric top is rather rarely of interest since it is a transition between inversion levels which usually corresponds to a negligibly small frequency. However, these inversion transitions are important in the case of NH_3 and will be discussed in more detail in Chap. 13-

It may be noted that (3-51) or (3-53) does not reduce to the corresponding expression for a linear molecule when $K = 0$ and C is infinite. This is because C has been assumed much smaller than kT in deriving these expressions, and hence they are no longer valid when C is allowed to be large. Because of the additional possible rotation around the symmetry axis, symmetric-top molecules are generally distributed throughout more states than are linear molecules and individual transitions are usually less intense by a factor of approximately 10. Typical intensity of a symmetric-top absorption at 1 cm wavelength is $\gamma_{\max} = 10^{-6}$ cm^{-1}.

Since variations in intensity with K depend on the nuclear spins (*cf.* [3-53] and Table 3-6), they may be used as a means of determining nuclear spins when several identical nuclei occur in the same molecule. This method of spin measurement has very limited utility, however, since molecules of this type are normally found only for abundant isotopes of common elements such as H and the halogens whose spins are already well known [233].

3-6. Centrifugal Stretching in Symmetric Tops. The discussion so far has assumed a rigid symmetric top, with no effects of vibration or centrifugal distortion. Centrifugal stretching of symmetric tops is somewhat more complicated than that for linear molecules because it involves both angular momentum quantum numbers J and K. It is fairly obvious that the amount of centrifugal distortion of the molecule cannot depend on the sign of the angular rotation (*e.g.*, whether it is clockwise or counterclockwise). Hence the change in rotational energy must involve only even powers of the momentum, such as the square of the total angular momentum $J(J+1)$ or of the component of momentum along the sym-

metry axis K^2. The rotational energy W including centrifugal effects may therefore be written

$$W(J,K) = BJ(J+1) + (C-B)K^2 - D_J J^2(J+1)^2 - D_{JK}J(J+1)K^2 - D_K K^4 \quad (3\text{-}54)$$

plus terms of higher order in $J(J+1)$ and K^2 where the centrifugal distortion constants D_J, D_{JK}, and D_K are of the order of B^2/ω, ω being a molecular vibrational frequency. The distortion constants are hence very small compared with the rotational constants B and C. The frequency due to a rotational transition $J+1 \leftarrow J$, $\Delta K = 0$ is, from (3-54),

$$\nu = 2(J+1)(B - D_{JK}K^2) - 4D_J(J+1)^3 \quad (3\text{-}55)$$

Without centrifugal distortion, the rotational transitions for a symmetric top are all equally spaced, and for a given transition of J, the various possible values of K all give identical frequencies. From expression (3-55), it may be seen that centrifugal distortion destroys both these simple relations, although the previous approximation of a rigid rotor is still an extremely good one. Because of the term D_{JK}, molecules with different values of K have effectively slightly different values of the rotational constant B, so that their rotational transitions are not precisely superimposed. A high-resolution microwave spectroscope usually resolves separate rotational lines due to molecules with different values of K, so that D_{JK} is easily evaluated.

Centrifugal distortion for molecules of this type was first observed in the infrared rotational spectrum of NH_3 and PH_3 [44*a*]. In this case the lines due to different values of K were not resolved, but the center of gravity of successive J transitions could be fitted by an expression of the form

$$\nu = 2(J+1)B - 4D(J+1)^3$$

The constants D_J, D_{JK}, and D_K depend of course on the various molecular force constants and the moments of inertia. The calculation from observed vibrational frequencies and rotational constants is both tedious and uncertain, since some of the force constants needed cannot always be accurately determined. However, Slawsky and Dennison [94*a*] obtained theoretical values of the centrifugal distortion constants of NH_3, ND_3, and PH_3 which fit experimental measurements of infrared spectra. These values are listed in Table 3-7. Chang and Dennison [783*a*] have succeeded in calculating D_J and D_{JK} for CH_3Cl to an accuracy of a few per cent. Nielsen [624] has given general expressions for the centrifugal stretching constants of symmetric molecules of the type XY_3. Appropriate force constants must be evaluated, however, before numerical results can be obtained from these expressions.

Values of D_J and D_{JK} for a number of molecules are given in Table 3-7.

It can be expected that D_J will always be positive as is illustrated in the table, since centrifugal forces due to rotation about any given axis will always tend to increase the moment of inertia about that axis or decrease the effective rotational constant. The sign of D_{JK} may in principle be either positive or negative. It is striking that all molecules of the type XY_3 which have so far been examined have D_{JK} negative, while molecules involving a methyl group or its derivatives have a positive D_{JK}.

TABLE 3-7. VALUES OF CENTRIFUGAL STRETCHING CONSTANTS FOR REPRESENTATIVE SYMMETRIC-TOP MOLECULES

Molecule	D_J, Mc	D_{JK}, Mc	Reference
NH_3	19	−28	[94*a*]
ND_3	5.2	− 7.8	[94*a*]
PH_3	3.7	− 4.6	[94*a*]
AsF_3	.....	0.009 ± 0.002	[824]
CH_3Cl^{35}	0.0181	0.189	[531] [913]
CH_3I	0.0080	0.0994	[531]
H_3CCCl	.....	0.0072	[744]
F_3CCCH	0.00024	0.0063	[557]
F_3GeCl	~0.0006	$\lvert D_{JK}\rvert < 0.001$	[555]
$H_3B^{11}CO$	.....	0.00036	[461]

3-7. Rotation-Vibration Interactions and *l*-Type Doubling in Symmetric Tops. The rotation-vibration constants α for symmetric tops have been discussed theoretically by Shaffer [109*a*] and an extensive and systematic treatment has been given by Nielsen [624]. However, theoretical evaluation of these rotation-vibration constants involves knowing so many different force constants that as yet essentially no comparison between theory and experimental values of α has been possible. There are a number of experimentally determined values of the α's in various symmetric tops. In many cases, however, the multiplicity of vibrational modes makes it difficult to assign uniquely a given observed rotational line due to an excited state to a particular vibrational mode, and hence to assign uniquely measured values of α.

There are always a number of degenerate vibrational modes in symmetric tops. Even the simplest types (of the form XY_3) have two sets of doubly degenerate vibrational modes, and each of these modes can produce an angular momentum which reacts in an interesting way with the angular momentum of rotation. If a degenerate vibrational mode involves only motion perpendicular to the molecular axis, then as in the case of the degenerate modes of a linear molecule, the vibration produces an angular momentum $l\hbar$ about the molecular axis, where l is an integer and $\hbar = h/2\pi$. In general, the vibrational motion may not be entirely perpendicular to the axis, and it produces angular momentum $\zeta l\hbar$ about

the axis of symmetry, where $|\zeta| \leq 1$ (*cf.* [130]). The molecule may at the same time be rotating about the axis of symmetry, and it is the sum of the vibrational angular momentum plus that due to rotation of the molecular frame which is quantized and equal to $K\hbar$, where K is an integer. These two types of motions are illustrated in Fig. 3-12.

A given value of the angular momentum may be produced in a variety of ways. For example, if the molecule is excited to the first excited state of a degenerate mode for which $\zeta = 1$, then a momentum $K = 1$ may be formed entirely of vibrational momentum ($l = 1$) or it may be a combination of vibrational momentum $l = -1$ and an angular momentum of the molecular frame of two units in the positive direction.

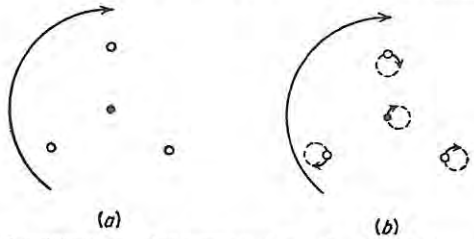

FIG. 3-12. Angular momentum along symmetry axis of XY_3 molecule. (*a*) Rotation of molecular frame only; (*b*) rotation of molecular frame plus angular momentum produced by degenerate vibration.

Similarly $K = -1$ can be formed in two ways. The angular momentum due to rotation of the molecular frame is $K - \zeta l$, and the energy associated with this momentum is hence not CK^2, but $C(K - \zeta l)^2$ or

$$C(K^2 - 2\zeta lK + \zeta^2 l^2)$$

Since $\zeta^2 l^2$ does not vary with rotational state, it may be omitted so that the rotational energy is written

$$W_R = BJ(J + 1) + (C - B)K^2 - 2K\zeta lC \qquad (3\text{-}56)$$

The energy levels with $l = \pm 1$ are compared in Fig. 3-13 with those for $l = 0$, assuming $\zeta = 1$.

When $K = l = \pm 1$, the molecule may be regarded as having no overall rotational motion about the symmetry axis. This is strictly true only if $\zeta = 1$, when the entire angular momentum K is provided by vibrational motion very much as in the case of a linear molecule with an angular momentum $l = \pm 1$ due to a degenerate vibration. In this case, it is not hard to understand why l-type doubling occurs just as in a linear molecule [503], [624].

If the symmetric top is the common variety with a threefold symmetry axis, then levels for which $K = -l = \pm 1$ are not split, nor is there appreciable splitting when $|K| > 1$. Since these cases correspond to the

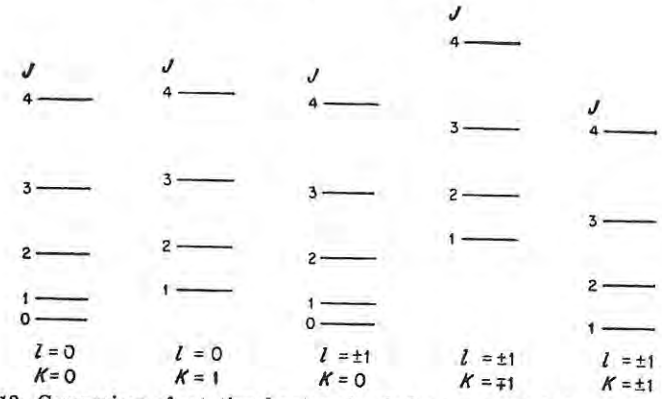

FIG. 3-13. Comparison of rotational energy levels for a symmetric top in the ground state with $l = 0$ and those for an excited degenerate vibrational mode with $l = \pm 1$. The vibrational energy has been disregarded. Each level indicated by $l = \pm 1$ is actually two which may be slightly different in energy due to l-type doubling. ζ is assumed to be positive.

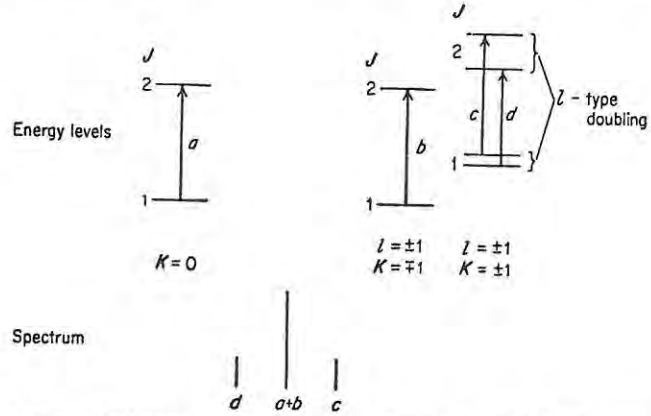

FIG. 3-14. l-type doubling in a symmetric rotator with three-fold symmetry axis. Energy levels and allowed transitions are shown above, and the resulting spectrum below. ζ is assumed to be negative. Note that the transitions a and b are between doubly degenerate levels and are superimposed to a good approximation, although some splitting due to centrifugal distortion may occasionally be observed.

framework of the molecule rotating as a whole, any change in the effective values of B due to vibration may be thought of as equivalent for all orientations of the angular momentum J because of the averaging effect of the rotation. However, this qualitative explanation cannot be taken too seriously, since de Heer has shown [568] that, for a molecule with a fourfold axis of symmetry, the levels $K = -l = \mp 1$ are split by an amount similar to those for which $K = l = \pm 1$.

Energy levels and allowed transitions for a $J = 2 \leftarrow 1$ rotational line of a symmetric top with an excited degenerate vibration are shown in Fig. 3-14. The resulting spectrum is also shown.

3-8. Dipole Moment Due to Degenerate Vibrations. There are many symmetric molecules which have zero dipole moment because of their symmetry and hence one would not normally expect microwave absorption due to pure rotational transitions of these molecules. Mizushima and Venkateswarlu [846] have shown, however, that if certain types of symmetric molecules with zero dipole moment are excited to degenerate vibrational states, it is possible to observe pure rotational transitions due to an effective dipole moment resulting from the vibrations. Such an effect should occur in molecules like allene, C_3H_4, or spherical tops such as CF_4.

CHAPTER 4

ASYMMETRIC-TOP MOLECULES

An asymmetric top is a rotor with no two principal moments of inertia equal. General principles involved in the motion of such rotors are of course the same as for symmetric tops, but the details turn out to be much more complex. This complexity shows up not only in the quantum-mechanical behavior of an asymmetric top, but also in its classical motion. The classical motion is well known and closely parallels the quantum-mechanical behavior; but it is not simple enough to afford any generally useful model for the quantum-mechanical case. For this reason the discussion below will begin immediately with a quantum-mechanical approach. Much of the discussion follows the recent extensive work of King, Hainer, and Cross on asymmetric rotors [118], [122], [215], [372].

4-1. Energy Levels of Asymmetric and Slightly Asymmetric Rotors. A general picture of the behavior of the energy levels of an asymmetric top may be had from examining their behavior as the rotor begins to deviate from the two simple extremes, the prolate and the oblate symmetric top. As in (3-2), the energy is

$$W = \frac{P_x^2}{2I_x} + \frac{P_y^2}{2I_y} + \frac{P_z^2}{2I_z} = \frac{4\pi^2 A}{h} P_x^2 + \frac{4\pi^2 B}{h} P_y^2 + \frac{4\pi^2 C}{h} P_z^2$$

where for an asymmetric rotor the constants A, B, and C are all different. If the three rotational constants are, in decreasing order of size, A, B, and C, a prolate symmetric top corresponds to $B = C$, and an oblate symmetric top to $B = A$. The range of values of B between A and C correspond to various conditions of asymmetry. If B differs from A or from C by only a small amount, the rotor may be called a slightly asymmetric top. Figure 4-1 shows in a qualitative way how the energy levels vary as B varies from C to A so that on the left-hand side the levels are just those of a prolate symmetric top ($B = C$) and on the right they correspond to an oblate symmetric top ($B = A$). A slight asymmetry splits the levels $\pm K$ which are degenerate for symmetric tops. Note that, as the value of B changes, no two levels of the same J cross. Levels of different J values may cross, however.

Various parameters may be used to indicate the degree of asymmetry.

Here $\nu/\Delta\nu = 3 \times 10^4$ due to Doppler effect has been used and λ is the wavelength. For a temperature change as large as 1°C, the number of molecules NL which must be in the path of observation is

$$NL = 2 \times 10^{18}\lambda \tag{5-71}$$

Since the longest dimension of the Milky Way is approximately 10^{23} cm, an interstellar gas must have a density as high as about $N = 2 \times 10^{-5}\lambda$ to be detected by microwave emission if the transition involved is due to a magnetic dipole moment. Since hydrogen has a density of approximately 1 atom/cm^3 in interstellar space, its radiation is clearly observable. In fact, in this case γL is larger than unity in most directions through our galaxy, and the galaxy is opaque at the center of the hydrogen line. On the other hand, deuterium would be very difficult to observe, since it probably has a density of only 10^{-3} or 10^{-4} atom/cm^3, and the transition between hyperfine levels falls at longer wavelengths.

If the transition is due to an electric dipole moment, then the dipole matrix element is approximately 1 debye, which is 100 times larger than the matrix element due to a magnetic dipole transition, and the minimum observable density of interstellar gas would be approximately

$$N = 2 \times 10^{-9}\lambda$$

A few molecules with dipole moments, such as the radical OH, are thought to have densities as high as $N = 10^{-6}$, and hence their spectra may possibly be observed.

Transitions between several other hyperfine levels in atoms may eventually be observed from astronomical objects. The hyperfine structure of N^{14} in several states of ionization may be sufficiently intense for observation since the density of nitrogen in interstellar gas is approximately 10^{-3} atom/cm^3. However, frequencies for the hyperfine structure of N^{14} are known experimentally only for the ground state of the neutral atom. The hyperfine structure of N^{14} in high states of ionization may possibly also be observed in the sun's atmosphere.

The microwave line emitted by interstellar hydrogen has been particularly valuable for astronomy. For example, its observation has shown that, in certain directions through our galaxy, there are several strips of gas each moving systematically at velocities appropriate to the successive arms of a rotating spiral nebula. This seems to give the clearest evidence so far available that our galaxy is a spiral nebula.

CHAPTER 6

QUADRUPOLE HYPERFINE STRUCTURE IN MOLECULES

6-1. Introduction. In most atoms, the predominant hyperfine structure is due to interaction between a nuclear magnetic moment and magnetic fields of the atomic electrons. Effects of a nuclear quadrupole moment are smaller and give small deviations from the expected magnetic hyperfine intervals. However, for most molecules in the ground state, the magnetic fields due to various electrons almost completely cancel, giving zero or only very small magnetic fields at the nucleus. Electric quadrupole effects in molecules may still be sizable, however, and they become the dominating source of hyperfine structure.

The cancellation of magnetic fields in molecules due to electronic motions is simply because the electrons are paired; *i.e.*, for each electron with an angular momentum and hence magnetic field, there is another electron in a similar state but with oppositely directed angular momentum. The net electronic angular momentum for the electrons in the ground state of most molecules is indicated by the spectroscopic term $^1\Sigma_0$, which signifies that the net electronic spin and orbital angular momentum are both zero. It is not surprising that electronic momenta are paired off in a molecule if the nature of molecular bonds is considered. Generally an atom forms chemical bonds with each of its unpaired electrons, each one pairing with an electron from another atom in the molecule to give a net zero angular momentum. For the rare molecules such as NO, ClO_2 and NO_2 having an odd number of electrons, a complete pairing of electron spins is impossible. These molecules are hence paramagnetic and have large magnetic hyperfine structures. There are in addition a few cases of molecules having an even number of electrons in which the chemical bonds are unusual and the electron spins are not paired. The most notable example of this case is O_2, which is in a $^3\Sigma_1$ state, having two parallel electron spins.

For the overwhelming majority of molecules, however, magnetic hyperfine effects are extremely small, and it is electric quadrupole hyperfine structure that is evident when molecular spectra are examined with high resolution.

The discussion given in the preceding chapter of interaction between a nuclear electric quadrupole moment and a surrounding charge distribution is of course as valid for a molecular system as for an atomic system

since the charge distribution assumed is a general one. Expression (5-45), which is

$$W_Q = \frac{1}{2}\frac{eq_JQ}{I(2I-1)J(2J-1)}[\tfrac{3}{4}C(C+1) - I(I+1)J(J+1)] \quad (6\text{-}1)$$

may be applied to the molecular case if J is taken as the angular momentum of the molecule, and q_J, given by (5-42), is

$$q_J = \int \rho_{JJ}\frac{(3\cos^2\theta - 1)}{r^3}\,d\tau = \left(\frac{\partial^2 V}{\partial z_J^2}\right)_{\text{av}}$$

where the charge density ρ applies to all charges in the molecule outside of a small sphere around the nucleus considered. It may be seen that the integral is just the average value of the second derivative of the potential at the nucleus due to all extranuclear charges ρ_{JJ}, taken along the direction of J, which is fixed in space and labeled z_J. The only problem peculiar to the molecular case is the particular evaluation of q_J, which will depend not only on the charge distribution in the molecule, but also on an average of the orientation of the molecule with respect to J. For a molecule of little symmetry, such as an asymmetric top, evaluation of q_J in terms of the various molecular axes and rotational quantum numbers can be rather tedious. We therefore begin by considering the much simpler and fortunately common case of a linear molecule.

6-2. Quadrupole Hyperfine Structure in Linear Molecules. In a linear molecule, the charge distribution is symmetric around the molecular axis, and hence if z_m indicates the direction of the molecular axis,

$$\frac{\partial^2 V}{\partial x_m^2} = \frac{\partial^2 V}{\partial y_m^2} = -\frac{1}{2}\frac{\partial^2 V}{\partial z_m^2}$$

using Laplace's equation and the equivalence of the x and y directions. A transformation of coordinates allows a reexpression of q_J.

$$\begin{aligned} q_J &= \left(\frac{\partial^2 V}{\partial z_J^2}\right)_{\text{av}} = \left(\frac{\partial^2 V}{\partial z_m^2}\cos^2\theta_{mJ} + \frac{\partial^2 V}{\partial x_m^2}\sin^2\theta_{mJ}\right)_{\text{av}} \\ &= \frac{\partial^2 V}{\partial z_m^2}\left(\frac{3\cos^2\theta_{mJ} - 1}{2}\right)_{\text{av}} \end{aligned} \quad (6\text{-}2)$$

where θ_{mJ} is the angle between the molecular axis and J. The quantity $\partial^2 V/\partial z_m^2$ is the second derivative of the potential at the nucleus under discussion along the direction of the molecular axis due to all charges outside a small sphere surrounding the nucleus. It is a property of the molecule independent of the rotational state of the molecule, and will be designated as q_m or simply q in analogy to q_J which is a similar quantity referred to the direction of J, and hence dependent on the rotational state.

In order to evaluate $[(3\cos^2\theta_{mJ} - 1)/2]_{\text{av}}$ we must use the molecular wave functions which have already been given in Chap. 1 as

$$\psi_{J,M=J} = \sqrt{\frac{2J+1}{4\pi(2J)!}}\,P_J^J(\cos\theta)e^{iJ\phi}$$

then

$$\begin{aligned} \left(\frac{3\cos^2\theta_{mJ} - 1}{2}\right)_{\text{av}} &= \frac{2J+1}{4\pi(2J)!}\int_0^\pi\int_0^{2\pi}[P_J^J(\cos\theta)]^2\frac{(3\cos^2\theta - 1)}{2}\sin\theta\,d\theta\,d\phi \\ &= \frac{-J}{2J+3} \end{aligned} \quad (6\text{-}3)$$

If J becomes very large, this result approaches the classical expectation that $[(3\cos^2\theta_{mJ} - 1)/2]_{\text{av}} = -\frac{1}{2}$, since classically the molecular axis should be perpendicular to the angular momentum and $\cos\theta_{mJ} = 0$. Hence from (6-1), (6-2), and (6-3), the quadrupole energy is

$$W_Q = -\frac{eq_mQ}{2I(2I-1)(2J-1)(2J+3)}[\tfrac{3}{4}C(C+1) - I(I+1)J(J+1)] \quad (6\text{-}4)$$

where $C = F(F+1) - I(I+1) - J(J+1)$. F is the quantum number for the total angular momentum, which takes on the values $I + J$, $I + J - 1, \ldots, |I - J|$.

The expression (6-4) gives the quadrupole energy for a single nucleus in a linear molecule in terms of the molecular constant q_m, the nuclear constant Q, and angular momentum quantum numbers I, J, F. It might be written $W = -eq_mQf(I,J,F)$, where eq_mQ or simply eqQ is called the quadrupole coupling constant and $f(I,J,F)$ might be called Casimir's function since it comes rather directly from theory developed by Casimir. This function is given in Appendix I for all values of I up to $\frac{11}{2}$ (excluding 0 and $\frac{1}{2}$, for which Q is necessarily zero, and 5 which is a rare case) and for values of J up to 10. It may be noted that, when F has its maximum or minimum values, corresponding to I and J parallel or antiparallel, respectively, Casimir's function is positive, whereas for intermediate values of F, the function is negative. This behavior corresponds roughly to the classically expected variation of $3\cos^2\theta_{IJ} - 1$.

From Appendix I and a knowledge of the quadrupole coupling constant eqQ the hyperfine energy levels can be easily determined. The constant eqQ may have an extremely wide range of values, but a representative value would be 100 Mc. To predict the hyperfine structure of a molecular transition, we need in addition some information about the selection rules and intensities. Selection rules for hyperfine structure are exactly the same as for fine structure assuming either type of inter-

action is very small compared with the separation between major energy levels. Thus if a microwave tends to change the angular momentum J of rotation of a molecule without acting on the nuclear spin I, this is an exact parallel to a light wave changing the orbital momentum L of electrons in an atom without acting on the electron spins S. The selection rules of Chap. 5 for fine structure then become for hyperfine structure

$$\Delta J = 0, \pm 1 \qquad \Delta F = 0, \pm 1 \qquad \Delta I = 0 \tag{6-5}$$

Relative intensities for the different possibilities are given by appropriate substitution of quantum numbers in expression (5-17) and (5-18).

For transitions $J \leftarrow J - 1$:

$$F \leftarrow F - 1: \frac{B(J+F+I+1)(J+F+I)(J+F-I)(J+F-I-1)}{F}$$

$$F \leftarrow F: \quad -\frac{B(J+F+I+1)(J+F-I)(J-F+1)(J-F-I-1)(2F+1)}{F(F+1)}$$

$$F \leftarrow F+1: \frac{B(J-F+I)(J-F+I-1)(J-F-I-1)(J-F-I-2)}{F+1} \tag{6-6a}$$

For transitions $J \leftarrow J$:

$$F \leftarrow F - 1: -\frac{A(J+F+I+1)(J+F-I)(J-F+I+1)(J-F-I)}{F}$$

$$F \leftarrow F: \quad \frac{A[J(J+1)+F(F+1)-I(I+1)]^2(2F+1)}{F(F+1)}$$

$$F \leftarrow F+1: -\frac{A(J+F+I+2)(J+F-I+1)(J-F+I)(J-F-I-1)}{F+1} \tag{6-6b}$$

Since the probability of exciting a transition between two states is independent of the direction of the transition, relative intensities for the components of the transition $J - 1 \leftarrow J$ may be obtained simply by reversing all arrows in the first group of three equations.

Appendix I gives relative intensities of the various possible hyperfine component transitions for low values of J and I up to $\frac{11}{2}$. Values given in this appendix are simply calculated from the formulas above, with their absolute values adjusted so that the sum of all hyperfine components of a particular J transition is one hundred. This is convenient because the sum of the intensities of hyperfine components of a transition should just equal the intensity of the transition if it had not been split.

Only very rarely is the hyperfine structure of rotational lines involving J greater than 10 of interest, since it is usually not prominent enough to be observed. For such large values of J, the more intense components of the hyperfine structure are always those for which F changes in the same way as J ($\Delta F = \Delta J$), and for these the hyperfine splitting is very small. Relative intensities of these components of a transition involving large J are approximately proportional to the statistical weights $2F + 1$ or, therefore, to F. For each of the weaker components, when J is larger than 10 the intensity is a small fraction of that of the entire transition. This fraction is given within a factor of about 2 by the following expressions:

When $J + 1 \leftarrow J$, $F \leftarrow F$, fraction of intensity $\approx 1/2J^2$

$J + 1 \leftarrow J$, $F - 1 \leftarrow F$, fraction of intensity $\approx 1/10J^4$

$J \leftarrow J$, $F \pm 1 \leftarrow F$, fraction of intensity $\approx 1/2J^2$

Changes in quadrupolar energies may be similarly approximated for large J. For the stronger components of the transition where $\Delta F = \Delta J$, the change in quadrupole energy is a small fraction of the quadrupole coupling constant, being in almost all cases smaller in size than $eqQ/4J^2$. For the other, very much weaker, components, the change in energy is larger and can be approximated by

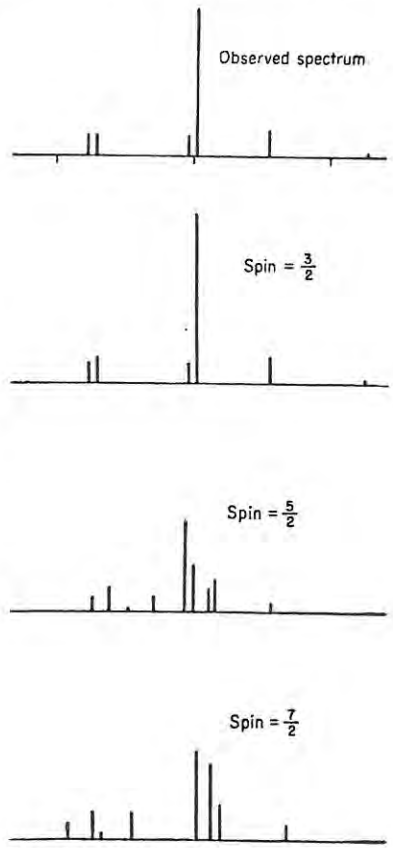

FIG. 6-1. Quadrupole hyperfine structure in the $J = 2 \leftarrow 1$ transition of $O^{16}C^{12}S^{33}$ due to S^{33}, showing the different patterns expected theoretically for various assumed values of the S^{33} spin. It is clear that the pattern for spin $\frac{3}{2}$ agrees well with the observed spectrum, and that other values of spin do not agree. For this case $eqQ = -29.2$ Mc.

$$\Delta W_Q(\Delta F = \Delta J \pm 1) = \mp \frac{3[2(F-J) \pm 1]eqQ}{8I(2I-1)} + \text{terms of order } \frac{eqQ}{2J}$$

The quantities given in Appendix I allow a ready calculation of quadrupole hyperfine structure such as is shown in Fig. 6-1. In this figure the

observed hyperfine structure in $O^{16}C^{12}S^{33}$ is compared with theoretically expected patterns assuming various values of the S^{33} spin. OCS is a linear molecule, and both O^{16} and C^{12} are known to have zero spins, and so produce no hyperfine structure. The quadrupole coupling constant assumed for S^{33} in OCS is chosen so that the computed hyperfine patterns will agree as closely as possible with the observed spectrum. It is evident that the observed structure agrees very well with the theory if the S^{33} spin is assumed to be $\frac{3}{2}$, whereas there is clear disagreement with the other calculated spectra. Thus a comparison of this type allows a determination of the S^{33} nuclear spin, its quadrupole coupling in OCS, and in addition the values of J involved in the transition, since both J and I determine the exact structure observed.

6-3. Quadrupole Hyperfine Structure in Symmetric Tops. For molecules which are not linear, the general theory of quadrupole coupling is unchanged, but the quantity q_J must be reevaluated. For the case of a nucleus on the axis of a symmetric top, this quantity is still rather simple in form. Because of the symmetry q_J may again be written, as in (6-2),

$$q_J = \frac{\partial^2 V}{\partial z_m^2}\left(\frac{3\cos^2\theta_{mJ} - 1}{2}\right)_{\text{av}}$$

where the direction z_m is as before along the molecular axis. For a symmetric top $[(3\cos^2\theta_{mJ} - 1)/2]_{\text{av}}$ has a somewhat different form, however.

$$\left(\frac{3\cos^2\theta_{mJ} - 1}{2}\right)_{\text{av}} = \int \psi^*_{J,K,M=J}\left(\frac{3\cos^2\theta_{mJ} - 1}{2}\right)\psi_{J,K,M=J}\,d\tau$$
$$= \left[\frac{3K^2}{J(J+1)} - 1\right]\frac{J}{2J+3} \qquad (6\text{-}7)$$

where $\psi_{J,K,M=J}$ is a symmetric-top wave function such as is given in Chap. 3. For J and K large, it can be seen that (6-7) gives the classically expected behavior, for then the cosine of the angle between J and the molecular axis ($\cos\theta_{mJ}$) is easily shown to be K/J or $K/\sqrt{J(J+1)}$ by use of the vector model.

The nuclear quadrupole energy for a nucleus on the axis of a symmetric top is, using (6-1), (6-2), and (6-7),

$$W_Q = \frac{eqQ\left[3\dfrac{K^2}{J(J+1)} - 1\right]}{2I(2I-1)(2J-1)(2J+3)}\left[\tfrac{3}{4}C(C+1) - I(I+1)J(J+1)\right] \qquad (6\text{-}8)$$

where q, or q_m, is the second derivative of the potential (excluding charges in a small sphere around the nucleus) along the direction of the molecular axis [143], [145]. This expression is identical with that for a linear molecule except for a factor $1 - 3K^2/J(J+1)$. The linear molecule is of course a special case of the symmetric top ($K = 0$). Appendix I may be used for the quadrupole energy levels of a symmetric top if energy values are multiplied by the factor $1 - 3K^2/J(J+1)$. Relative intensities of hyperfine components, which are also given by Appendix I, apply to this case.

It should be noted that, in deriving (6-8), the electric field was assumed to be symmetric about the molecular axis ($\partial^2 V/\partial x_m^2 = \partial^2 V/\partial y_m^2$ on the axis). This will be true in all cases for a nucleus on the axis of a symmetric top, since to make the moments of inertia about x_m and y_m exactly equal, a symmetric arrangement of atoms is required. However, there may occur very rare cases of "accidentally" nearly symmetric tops for which this condition is not fulfilled, and the quadrupole levels must be described by the somewhat more complex theory developed in the latter part of this chapter for asymmetric molecules rather than by (6-8). If the nucleus is in a symmetric top, but not on the axis, then there is always present the complication of other like nuclei with quadrupole coupling, which will be treated later in this chapter.

The hyperfine structure of a symmetric rotor transition $J + 1 \leftarrow J$ is usually more complex than that for a linear molecule because such a transition involves a number of different K values, each with its own hyperfine structure. An example is the structure of the $J = 2 \leftarrow 1$ transition of CH_3I, shown in Fig. 6-2. Iodine has a spin of $\frac{5}{2}$ and a rather large quadrupole coupling constant, whereas C and H have spins of 0 and $\frac{1}{2}$, respectively, and hence give no quadrupole effects.

6-4. Second-order Quadrupole Effects. The quadrupole hyperfine structure has so far been considered small by comparison with the frequency of the rotational transition. The quantity $[(3\cos^2\theta_{mJ} - 1)/2]_{\text{av}}$ has been calculated, for example, in (6-3) and (6-7) with so-called first-order perturbation theory, or by using rotational wave functions which are assumed to be unchanged by the existence of quadrupole effects. If the quadrupole coupling is not small compared with the rotational frequencies, however, the molecular rotational wave functions will be modified and the energies for quadrupole effects given above will not be exactly correct.

A strong quadrupole interaction produces some exchange of angular momentum between the nucleus and the molecule; so the state of the rotating molecule can no longer be accurately specified by a fixed angular momentum J. Allowing for quadrupole interactions which are not small, the state of the molecule can only approximately be described by J, and the wave functions and quadrupole energy must be calculated from second-order perturbation theory. However, the total angular momentum F and its projection on a fixed axis M_F are quantized and cannot be changed by interactions within the molecule.

For a general symmetric top the energy given by second-order perturbation theory is of the form

$$W_Q = (IJKFM_F|H_Q|IJKFM_F) + \sum_{J'K'} \frac{|(IJKFM_F|H_Q|IJ'K'FM_F)|^2}{W_{JK} - W_{J'K'}} \quad (6\text{-}9)$$

where H_Q is the part of the Hamiltonian which represents the quadrupole energy. It is given by $-\frac{1}{6}\mathbf{Q}:\nabla\mathbf{E}$, as discussed in Chap. 5. The quantities

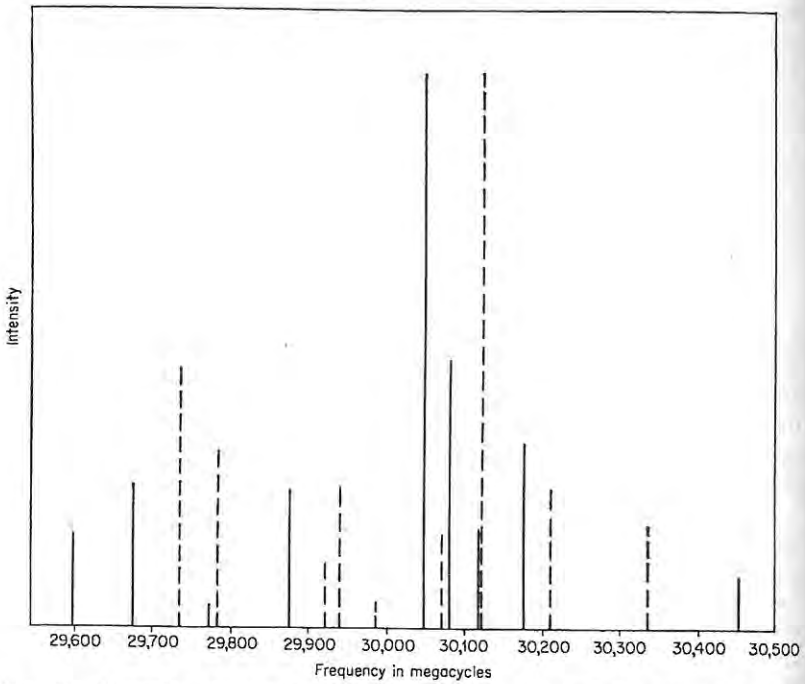

FIG. 6-2. Hyperfine structure in the $J = 2 \leftarrow 1$ transition of the symmetric rotor CH_3I due to the nuclear quadrupole moment of I^{127}. The spin of I^{127} is $\frac{5}{2}$ and its quadrupole coupling is -1934 Mc. Solid lines represent transitions due to molecules with $k = 0$, dashed lines those of molecules with $k = \pm 1$.

$(IJKFM_F|H_Q|IJ'K'FM_F)$ are matrix elements of H_Q for the symmetric-rotor wave functions specified by the quantum numbers I, J, K, F, M_F and I, J', K', F, M_F. The quantum numbers I, F, and M_F are not summed over since they are unaffected by the perturbation, or in other words the matrix of H_Q is diagonal in I, F, and M_F. The first term of (6-9) is just the previously calculated first-order quadrupole energy (6-8) which gives quite accurately the entire quadrupole energy when $W_{JK} - W_{J'K'}$ is much larger than eqQ. The only matrix elements in

the sum of (6-9) which are not identically zero are those for which $K' = K$ and either $J' = J \pm 1$ or $J' = J \pm 2$. They are [253]

$$(I,J,K,F,M_F|H_Q|I,J+1,K,F,M_F) = \frac{3eqQK[F(F+1) - I(I+1) - J(J+2)]}{8I(2I-1)J(J+2)}$$
$$\times \left\{\frac{\left[\left(1 - \frac{K^2}{(J+1)^2}\right)(I+J+F+2)(J+F-I+1)\times(I+F-J)(I+J-F+1)\right]}{(2J+1)(2J+3)}\right\}^{\frac{1}{2}}$$

$$(I,J,K,F,M_F|H_Q|I,J+2,K,F,M_F) = \frac{3eqQ}{16I(2I-1)(2J+3)}$$
$$\times \left\{\left[1 - \frac{K^2}{(J+1)^2}\right]\left[1 - \frac{K^2}{(J+2)^2}\right](I+J+F+3)(I+J+F+2)\right.$$
$$\times (I+J-F+2)(I+J-F+1)(J+F-I+2)$$
$$\left.\times \frac{(J+F-I+1)(I+F-J)(I+F-J-1)}{(2J+1)(2J+5)}\right\}^{\frac{1}{2}} \quad (6\text{-}10)$$

From the matrix elements (6-10) and expression (6-9) the modifications in the quadrupole energy due to second-order perturbations may be taken into account. They are usually rather small, for they are less than first-order energies (6-8) by a factor usually somewhat smaller than $eqQ/(W_{JK} - W_{J'K'}) \approx eqQ/\nu$, where ν is the frequency of the observed rotational transition. Usually eqQ is a few hundred megacycles, while ν is a few ten thousands of megacycles. However, in some cases, such as a large molecule with the atoms I or Hg in it, eqQ/ν may not be small; in fact it may possibly be so large that a still better approximation than that given by (6-9) will be needed in order to fit the experimentally measured hyperfine structure.

A linear molecule in the ground vibrational state is of course a special case of a symmetric top for which K equals zero. When $K = 0$, the matrix element given by (6-10) which connects J and $J + 1$ is zero, and the matrix element connecting J and $J + 2$ simplifies somewhat. If the linear molecule is excited in a degenerate vibrational mode so that there is an angular momentum $|l|$ around the axis of the molecule, then as seen in Chap. 2, its rotational wave functions are similar to those for a symmetric top with $|K|$ equal to $|l|$. Hence matrix elements (6-10) apply to a linear molecule excited to any vibrational mode if the value of l is substituted for K.

The molecule ICN is a case where eqQ/ν is as large as is normally encountered. For I^{127}, $eqQ = -2420$ Mc, and the transition $J = 4 \leftarrow 3$ occurs near 25,800 Mc. The N^{14} nucleus in ICN has a quadrupole coupling of -3.7 Mc which is so small that, unless the spectrum is observed under very high resolution, the quadrupole effects due to N

may be neglected. The effect of second-order corrections on the observed spectrum for the ground vibrational state is indicated in Table 6-1, which gives the first-order and second-order energies due to the I^{127} quadrupole coupling. It should be noted that the transitions $F = \frac{9}{2} \leftarrow \frac{7}{2}$ and $F = \frac{9}{2} \leftarrow \frac{9}{2}$ should, according to the usually first-order theory of quadrupole effects, exactly coincide. Second-order effects split these two lines by 6.32 Mc. Actual measurements of the hyperfine structure of the $J = 4 \leftarrow 3$ transition in ICN agree very well with the predicted combined first- and second-order effects.

TABLE 6-1. QUADRUPOLE SPLITTING OF THE $J = 4 \leftarrow 3$ TRANSITION OF ICN IN THE GROUND VIBRATIONAL STATE

Without quadrupole effects, the transition would occur at 25,804 Mc. The frequency contributions to the various possible hyperfine transitions due to an I quadrupole coupling of −2420 Mc are listed. F' represents the initial value of F associated with a J of 3, and F is the final value.

Transition $F \leftarrow F'$	Quadrupole coupling contribution, Mc	
	First order	Second order
$\frac{13}{2} \leftarrow \frac{11}{2}$	18.33	0.55
$\frac{11}{2} \leftarrow \frac{11}{2}$	−410.65	0.10
$\frac{11}{2} \leftarrow \frac{9}{2}$	33.02	0.49
$\frac{9}{2} \leftarrow \frac{9}{2}$	− 18.84	4.52
$\frac{9}{2} \leftarrow \frac{7}{2}$	− 18.84	−1.80
$\frac{7}{2} \leftarrow \frac{7}{2}$	150.87	−0.83
$\frac{7}{2} \leftarrow \frac{5}{2}$	− 74.98	−0.49
$\frac{5}{2} \leftarrow \frac{5}{2}$	189.01	−0.83
$\frac{5}{2} \leftarrow \frac{3}{2}$	− 93.32	0.65
$\frac{3}{2} \leftarrow \frac{3}{2}$	165.95	−0.60
$\frac{3}{2} \leftarrow \frac{1}{2}$	− 51.84	0.37

Transitions of ICN molecules in the first excited bending mode are split by l-type doubling, and each of the two l-type doublets is further split by the I quadrupole effects. First- and second-order quadrupole effects for these doublets are listed in Table 6-2. In this case $|l| = 1$, and the value of the corresponding quantum number K for the angular momentum around the symmetry axis is set equal to 1 in calculating second-order effects from the expressions (6-10).

The second-order effects of quadrupole coupling on the hyperfine structure as given in Tables 6-1 and 6-2 are not large, even though the quadrupole coupling constant for I^{127} in ICN is a rather large one. If the quadrupole coupling constant had been ten times smaller, or about 240 Mc, the second-order effects on frequency would have been 100 times smaller, since they depend on $(eqQ)^2$, and would then be detectable only by very accurate microwave frequency measurements.

In addition to changing the frequencies of hyperfine components, second-order quadrupole effects may affect their intensities. The quadrupole coupling modifies the molecular rotational wave functions, adding to the wave function of rotational quantum number J a small component of the wave functions for $J \pm 1$ (if $K \neq 0$) and $J \pm 2$. Because of this modification of the wave function, the matrix elements for the transitions and hence the intensities are slightly changed. This change is usually too small to be of significance for the normal transitions unless extremely accurate intensity measurements are made. More noticeable and important, however, is that the selection rules are modified to allow the occurrence of new transitions. Thus since a small component of the wave function for $J + 2$ is mixed with the wave function for J, a weak transition from this modified wave function to a $J + 3$ state may occur. If the modified wave function is still identified (approximately) by the quantum number J, this effect would allow weak transitions corresponding to $\Delta J = \pm 3$. Similarly, when K is not equal to zero and the quadrupole coupling is large, weak transitions corresponding to $\Delta J = \pm 2$ may be expected. These types of transitions have not yet been observed but could probably be found in the case of molecules with quadrupole couplings as large as is found in ICN. Their intensities may be calculated by evaluating the amounts of perturbation of the wave functions using the matrix elements given by (6-10).

TABLE 6-2. QUADRUPOLE SPLITTING OF THE $J = 4 \leftarrow 3$ TRANSITION OF ICN IN THE FIRST EXCITED BENDING MODE, FOR WHICH $|l| = 1$

Notation is as in Table 6-1. l-type doubling is not included in this table but produces two sets of hyperfine components separated by the l-type doubling.

Transition $F \leftarrow F'$	Quadrupole coupling contribution, Mc	
	First order	Second order
$\frac{13}{2} \leftarrow \frac{11}{2}$	54.08	1.61
$\frac{11}{2} \leftarrow \frac{9}{2}$	22.18	−0.72
$\frac{9}{2} \leftarrow \frac{7}{2}$	−21.90	0.28
$\frac{7}{2} \leftarrow \frac{5}{2}$	−47.03	−0.20
$\frac{5}{2} \leftarrow \frac{3}{2}$	−34.40	−0.45

6-5. Asymmetric Tops. In principle, evaluation of nuclear quadrupole effects in asymmetric rotors is straightforward. Expression (6-1) gives the energy, which is of the same form as for symmetric molecules, and q_J, the average second derivative of the potential along the direction of the angular momentum, is

$$q_J = \int \psi^*_{J_{K_{-1}K_1}, M=J} \left(\frac{\partial^2 V}{\partial z_J^2}\right) \psi_{J_{K_{-1}K_1}, M=J} \, d\tau \qquad (6\text{-}11)$$

where $\psi_{J_{K_{-1}K_1},M=J}$ is an asymmetric-rotor wave function. Evaluation of the integral in (6-11), however, is considerably more complex than evaluating the similar expression for symmetric rotors. We shall follow the method of Bragg [258].

For an evaluation of (6-11), we shall express $\partial^2 V/\partial z_J^2$ in terms of the second derivatives of the potential along the principal axes of inertia x_m, y_m, and z_m of the molecule and the direction cosines α between this set of axes and z_J which is fixed in space.

$$\frac{\partial^2 V}{\partial z_J^2} = \alpha^2_{z_J x_m}\left(\frac{\partial^2 V}{\partial x_m^2}\right) + \alpha^2_{z_J y_m}\left(\frac{\partial^2 V}{\partial y_m^2}\right) + \alpha^2_{z_J z_m}\left(\frac{\partial^2 V}{\partial z_m^2}\right) + 2\alpha_{z_J x_m}\alpha_{z_J y_m}\left(\frac{\partial^2 V}{\partial x_m\,\partial y_m}\right) + 2\alpha_{z_J x_m}\alpha_{z_J z_m}\left(\frac{\partial^2 V}{\partial x_m\,\partial z_m}\right) + 2\alpha_{z_J y_m}\alpha_{z_J z_m}\left(\frac{\partial^2 V}{\partial y_m\,\partial z_m}\right) \quad (6\text{-}12)$$

By an argument similar to that used to prove certain matrix elements of the dipole moment are zero (page 63), the integrals of the form

$$\int \psi^* \alpha_{z_J x_m}\alpha_{z_J y_m}\frac{\partial^2 V}{\partial x_m\,\partial y_m}\psi\, d\tau \quad (6\text{-}13)$$

may be shown to be zero. Because wave functions are either symmetric or antisymmetric with respect to a rotation around the principal axes, $\psi^*\psi$ is unchanged as a result of a 180° rotation about the axis x_m. However, α_{zy_m} is reversed in sign since the y_m direction has been reversed. Hence the integrand of (6-13) undergoes a reversal of sign due to this rotation and must be zero. Expression (6-11) becomes, therefore,

$$q_J = (\alpha^2_{zx_m})_{\text{av}}\frac{\partial^2 V}{\partial x_m^2} + (\alpha^2_{zy_m})_{\text{av}}\frac{\partial^2 V}{\partial y_m^2} + (\alpha^2_{zz_m})_{\text{av}}\frac{\partial^2 V}{\partial z_m^2} \quad (6\text{-}14)$$

where

$$(\alpha^2_{zx_m})_{\text{av}} = \int \psi^*_{J_{K_{-1}K_1},M=J}\alpha^2_{zx_m}\psi_{J_{K_{-1}K_1},M=J}\, d\tau \quad (6\text{-}15)$$

Matrix elements of the direction cosines have already been discussed and the line strengths $S_{J_{K_{-1}K_1}J'_{K'_{-1}K'_1}}$ derived from their squares are tabulated in Appendix V. Matrix elements of the squares of direction cosines such as (6-15) may be obtained by squaring the direction cosine matrices. Some manipulation (*cf.* [258]) shows that $(\alpha^2_{zx_m})_{\text{av}}$ may hence be expressed in terms of the quantities tabulated in Appendix V as follows:

$$(\alpha^2_{zx_m})_{\text{av}} = \frac{2J}{(2J+1)(2J+3)}\sum_{K'_{-1}K'_1} {}^xS_{J_{K_{-1}K_1}J_{K'_{-1}K'_1}} + \frac{1}{2J+3} \quad (6\text{-}16)$$

where x or x_m may refer to the direction of any one of the three principal axes a, b, or c. This gives

$$q_J = \frac{2J}{(2J+1)(2J+3)}\sum_{K'_{-1}K'_1}\frac{\partial^2 V}{\partial a^2}\,{}^aS_{J_{K_{-1}K_1}J_{K'_{-1}K'_1}} + \frac{\partial^2 V}{\partial b^2}\,{}^bS_{J_{K_{-1}K_1}J_{K'_{-1}K'_1}} + \frac{\partial^2 V}{\partial c^2}\,{}^cS_{J_{K_{-1}K_1}J_{K'_{-1}K'_1}} \quad (6\text{-}17)$$

where second derivatives of the potential along the three principal axes of inertia are indicated by $\partial^2 V/\partial a^2$, $\partial^2 V/\partial b^2$, and $\partial^2 V/\partial c^2$. This potential as before (page 135) is due to all charges outside a small sphere around the nucleus. The quantities S in (6-17) are tabulated in Appendix V for values of the asymmetry parameter $\kappa = -1.0, -0.5, 0, 0.5$, and 1.0 only. Interpolation must be used for other values of κ.

Another form in which q_J may be expressed is [352]

$$q_J = \frac{1}{(J+1)(2J+3)}\frac{\partial^2 V}{\partial a^2}\left[J(J+1) + E(\kappa) - (\kappa+1)\frac{\partial E(\kappa)}{\partial \kappa}\right] + \frac{2}{(J+1)(2J+3)}\frac{\partial^2 V}{\partial b^2}\frac{\partial E(\kappa)}{\partial \kappa} + \frac{1}{(J+1)(2J+3)}\frac{\partial^2 V}{\partial c^2}\left[J(J+1) - E(\kappa) + (\kappa-1)\frac{\partial E(\kappa)}{\partial \kappa}\right] \quad (6\text{-}18)$$

where $E(\kappa)$ is the energy parameter for an asymmetric rotor of asymmetry κ as defined in (4-10). In (6-18) $E_{J_{K_{-1}K_1}}(\kappa)$ appropriate to the particular state for which q_J is being evaluated is of course used. $E(\kappa)$ and $\partial E(\kappa)/\partial\kappa$ may be obtained from Appendix IV. Although interpolation must still be used to evaluate $E(\kappa)$ and $\partial E(\kappa)/\partial\kappa$, the tabulation in Appendix IV uses smaller steps of κ than does Appendix V, so that more accuracy may often be obtained from (6-18) than from (6-17).

Expression (6-18) is also very useful if q_J must be evaluated for states not tabulated in Appendices IV or V ($J > 12$), since all the approximate methods discussed in Chap. 4 for evaluating $E(\kappa)$ for large J are available. [See [352] for expression of (6-18) in terms of approximations for $E(\kappa)$.]

If better accuracy is needed than can be obtained by interpolation, the integral in (6-11) may be evaluated by expanding the wave function as a sum of symmetric-top functions as in (4-18). This leads to the expression [258]

$$q_J = \frac{q_m}{(J+1)(2J+3)}\sum_K a^2_{JK}[3K^2 - J(J+1)] - 2a_{JK}a_{JK+2}[f'(J,K+1)]^{\frac{1}{2}}\eta \quad (6\text{-}19)$$

where $f'(J,n) = \frac{1}{4}(J^2 - n^2)[(J+1)^2 - n^2]$ (6-20)

$q_m = \partial^2 V/\partial z_m^2$ is the second derivative of the potential along the principal axis which most nearly represents a symmetry axis of the moment of inertia ellipsoid

$$\eta = \frac{\partial^2 V/\partial x_m^2 - \partial^2 V/\partial y_m^2}{q_m} \quad (6\text{-}21)$$

If the molecule is considered an oblate top, z_m is the c axis, and x_m and y_m must be taken as the a and b axes, respectively. If it is prolate, z_m is the a axis, x_m the b axis, and y_m the c axis.

Expression (6-19) can give q_J exactly, but only after evaluation of the a_{JK}'s, which is troublesome. For small values of the asymmetry parameter b [for definition of b, see (4-2) and (4-3)] q_J can be satisfactorily obtained for various values of K from the expressions below. Terms of order b^3 or higher are omitted.*

For $K = 0$:

$$q_J = \frac{q_m}{(J+1)(2J+3)}\{-J(J+1) + (\tfrac{3}{2}b^2 - b\eta)f'(J,1)\} \tag{6-22a}$$

For $K = 1$:

$$q_J = \frac{q_m}{(J+1)(2J+3)}\left\{3 - J(J+1) \mp \frac{\eta}{2}J(J+1) + (\tfrac{3}{2}b^2 - b\eta)\frac{f'(J,2)}{4} \pm \tfrac{3}{128}b^2\eta J(J+1)f'(J,2)\right\} \tag{6-22b}$$

For $K = 2$:

$$q_J = \frac{q_m}{(J+1)(2J+3)}\left\{12 - J(J+1) + (\tfrac{3}{2}b^2 - b\eta)\left[\frac{f'(J,3)}{6} - \frac{f'(J,1)}{2} \mp \frac{f'(J,1)}{2}\right]\right\} \tag{6-22c}$$

For $K = 3$:

$$q_J = \frac{q_m}{(J+1)(2J+3)}\left\{27 - J(J+1) + (\tfrac{3}{2}b^2 - b\eta)\left[\frac{f'(J,4)}{8} - \frac{f'(J,2)}{4}\right] \mp \tfrac{3}{128}f'(J,2)J(J+1)b^2\eta\right\} \tag{6-22d}$$

For $K > 3$:

$$q_J = \frac{q_m}{(J+1)(2J+3)}\left\{3K^2 - J(J+1) + (\tfrac{3}{2}b^2 - b\eta)\left[\frac{f'(J,K+1)}{2(K+1)} - \frac{f'(J,K-1)}{2(K-1)}\right]\right\} \tag{6-22e}$$

where $f'(J,n) = \frac{1}{4}(J^2 - n^2)[(J+1)^2 - n^2]$

The upper signs apply to the upper-energy level of a K-type doublet for a prolate rotor or the lower doublet of an oblate rotor. The lower signs apply to the lower-energy level of a doublet for a prolate rotor, or the upper doublet of an oblate rotor. Since quadrupole effects are not usually measured to high fractional accuracy, the approximate expressions (6-22) (neglecting terms in b^3 and higher) are satisfactory in many cases, and when b is small they are more accurate than expressions (6-17) or (6-18) with interpolation.

* Expressions (6-22) were first given by G. Knight and B. T. Feld [379] but have been corrected by J. Kraitchman and A. Javan.

There can be no asymmetry in $\nabla\mathbf{E}$ about the axis for a nucleus on the axis of a real symmetric top. Nuclei off the axis of a symmetric top always occur as three or more equivalent nuclei, for the sum of which the asymmetry of the field, or of $\nabla\mathbf{E}$, cancels out. However, for a molecule which is accidentally very close to symmetric, an asymmetry of the electric field about the axis can give a sizable contribution to the quadrupole energy when $K = 1$. This shows up as the terms $\pm q_m J\eta/2J + 3$ in Eq. (6-22). In the case of $H_2C{=}CHCl$, for example, where the asymmetry $b = -0.006$, hyperfine structure of transitions between levels with $K = 1$ can be fitted rather well by omitting all terms involving b, but these terms dependent on the asymmetry of the field η must be kept. When $K \neq 1$, an asymmetry of the field affects the quadrupole energy only if at the same time the molecule is asymmetric ($b \neq 0$).

Hyperfine structure in an asymmetric rotor must be fitted by the two parameters $\partial^2V/\partial z_m^2$ and $\partial^2V/\partial x_m^2 - \partial^2V/\partial y_m^2$, or q_m and η instead of the one parameter q_m which is needed for symmetric tops. However, in many cases these two parameters can to a very good approximation be expressed in terms of a single property of the electric field, $\partial^2V/\partial z_b^2$, the second derivative of the electrostatic potential along the direction of the chemical bond which binds the nucleus in question to the molecule. This is because the electrostatic fields are in many cases almost symmetric about the bond axis.

A clear example of this is the field at the Cl nucleus in the asymmetric varieties of methyl chloride. For CH_3Cl, ∇E at the chlorine nucleus is symmetric about the C—Cl axis because of the threefold-symmetry axis of the molecule. In CH_2DCl, ∇E must still be symmetrical about the C—Cl axis, but the molecule has become an asymmetric top, and no principal axis coincides with the C—Cl bond. In such case the various second derivatives of the potential along principal axes may be readily obtained.

$$\begin{aligned}\frac{\partial^2V}{\partial z_m^2} &= \frac{\partial^2V}{\partial z_b^2}\,\frac{3\alpha_{z_bz_m}^2 - 1}{2}\\ \frac{\partial^2V}{\partial x_m^2} &= \frac{\partial^2V}{\partial z_b^2}\,\frac{3\alpha_{z_bx_m}^2 - 1}{2}\\ \frac{\partial^2V}{\partial y_m^2} &= \frac{\partial^2V}{\partial z_b^2}\,\frac{3\alpha_{z_by_m}^2 - 1}{2}\end{aligned} \tag{6-23a}$$

where $\alpha_{z_bz_m}$, etc., represent the cosines of angles between the various axes.

More generally, if the second derivatives of the potential with respect to one set of Cartesian coordinates x_1, x_2, x_3 are known, those along any

other set of axes x_1', x_2', x_3' may be obtained from the relations

$$\frac{\partial^2 V}{\partial x_1' \, \partial x_j'} = \sum_{kl} \alpha_{x'_1 x_k} \alpha_{x'_j x} \frac{\partial^2 V}{\partial x_k \, \partial x_l} \tag{6-23b}$$

Here $\alpha_{x'_1 x_k}$ represents the cosine of the angle between the two axes x_i' and x_k.

Very frequently, the electric field at a nucleus is to good accuracy symmetric about a bond, as in the case of CH_2DCl above. In CH_2Cl_2 it has been shown by Myers and Gwinn [732] that expressions (6-23) give the correct values for q_m and η to within the experimental accuracy of 1 per cent of $\partial^2 V/\partial z_b^2$. On the other hand, in cases where double bonds are involved, the fields may not be at all symmetric about the bond (see Chap. 9). $H_2C{=}CHCl$ is a molecule in which apparently the double-bond character of the C—Cl bond is sufficient to make the field appreciably asymmetric.

The quadrupole energy so far discussed for asymmetric rotors has been of the first-order type. As in symmetric rotors, the quadrupole energy is sometimes large enough compared with the separation between rotational energy levels that second-order perturbations are important. Corresponding to Eq. (6-9), the quadrupole energy is then

$$W_Q = (I,J_{K_{-1}K_1},F|H_Q|I,J_{K_{-1}K_1},F) + \sum_{J'K'_{-1}K'_1} \frac{|(I,J_{K_{-1}K_1},F|H_Q|I,J'_{K'_{-1}K'_1},F)|^2}{W_{J_{K_{-1}K_1}} - W_{J'_{K'_{-1}K'_1}}} \tag{6-24}$$

where $W_{J_{K_{-1}K_1}}$ is the rotational energy. The quantities in brackets are the matrix elements of the Hamilton for the quadrupole interaction H_Q, the first term being the first-order energy which has been discussed above. The sum is, of course, over all rotational states except the unperturbed state $J_{K_{-1}K_1}$.

It can be shown that all matrix elements involved in the sum of (6-24) are zero except those for which $J' = J \pm 1$ or $J' = J \pm 2$. These matrix elements have been discusssed by Bragg [258] but have not yet been evaluated in detail. In cases of near degeneracy where two asymmetric-top levels of appropriate symmetry lie close together, second-order quadrupole effects will, however, be of some importance.

6-6. Hyperfine Structure from Two or More Nuclei in the Same Molecule. A molecule may contain more than one nucleus which produces an observable hyperfine structure in its spectrum. This almost always occurs when more than one nucleus in the molecule has a spin greater than $\frac{1}{2}$ and hence is coupled by its quadrupole moment to the rotational motion of the molecule. In such cases the quadrupole energies are no longer given by expressions like (6-8), since the interaction between one nucleus and the molecule will affect the interaction between the second nucleus and the molecule, and vice versa. We shall consider first

the case of two such nuclei, which is the one of most importance. The treatment follows that of Bardeen and Townes [252].

If nucleus 1 is coupled to the molecule much more strongly than nucleus 2, the system can be fairly well described by the vector model. In that case, the spin $\mathbf{I}_1$ of nucleus 1 adds vectorially to the molecular angular momentum $\mathbf{J}$ to form a resultant $\mathbf{F}_1$, which is quantized with the possible values $J + I_1$, $J + I_1 - 1$, . . . , $|J - I_1|$. The spin $\mathbf{I}_2$ of the second, more weakly coupled nucleus then adds vectorially to $\mathbf{F}_1$ to form the total angular momentum $\mathbf{F}$ which may have the values $F_1 + I_2$, $F_1 + I_2 - 1$, . . . , $|F_1 - I_2|$. The two angular momenta $\mathbf{I}_1$ and $\mathbf{J}$ may be regarded as precessing around the vector $\mathbf{F}_1$ with a precessional frequency approximately equal to the energy difference between F_1 and $F_1 + 1$ divided by h. Similarly the vectors $\mathbf{I}_2$ and $\mathbf{F}_1$ precess about the vector $\mathbf{F}$, which is fixed in space. If the first nucleus is coupled to the molecule much more strongly than the second nucleus, then $\mathbf{I}_1$ precesses so much more rapidly than $\mathbf{I}_2$ that $\mathbf{F}_1$ and $\mathbf{I}_2$ may be thought of as stationary during a complete cycle of the motion of $\mathbf{I}_1$ and $\mathbf{J}$; hence the interaction between $\mathbf{I}_2$ and $\mathbf{J}$ is averaged over this motion. If the interaction between $\mathbf{I}_2$ and $\mathbf{J}$ is proportional to the cosine of the angle between them, then the vector model allows a rather simple and accurate calculation of this interaction energy, as will be seen from the discussion of magnetic hyperfine structure in Chap. 8. However, if the interaction is proportional to the square of the cosine between $\mathbf{I}_2$ and $\mathbf{J}$ as is the quadrupole interaction, a calculation from more rigorous quantum mechanics must be used. In addition, if the coupling of nucleus 1 and nucleus 2 is not widely different, then averaging over the precession of nucleus 1 is no longer a good approximation, and the vector model must be abandoned for a more sophisticated treatment such as that below.

First consider wave functions which are formed by combining the vectors $\mathbf{J}$ and $\mathbf{I}_1$ to produce $\mathbf{F}_1$, and then combining $\mathbf{F}_1$ and $\mathbf{I}_2$ to produce $\mathbf{F}$, and let wave functions of this type be represented by $\psi_1(F_1,F)$. The Hamiltonian for the two nuclear interactions may be written

$$H = H_1(\mathbf{I}_1,\mathbf{J}) + H_2(\mathbf{I}_2,\mathbf{J}) \tag{6-25}$$

The energy due to H_1 can be readily evaluated for wave functions of the type ψ_1. In the case of quadrupole interactions this energy is obtained simply by letting F_1 take the place of F in expression (6-9). (Here second-order quadrupole interaction will be neglected, so that J is a good quantum number.) There will be a number of wave functions $\psi_1(F_1,F)$ having the same F but different F_1 and hence different energies associated with the interaction H_1. There may also be several wave functions of the same F_1 and different F, which will have the same energy if H_2 is negligibly small. This degeneracy is removed if H_2 is appreciable, but

the energy associated with H_2 is not immediately calculable, since the wave function ψ_1 is not an eigenfunction of H_2.

Consider next wave functions formed by combining first the vectors $\mathbf{I}_2$ and $\mathbf{J}$ to make the vector which will be designated $\mathbf{F}_2$, then combining $\mathbf{F}_2$ and $\mathbf{I}_1$ to make the total angular momentum $\mathbf{F}$. These are eigenfunctions of H_2 and may be designated $\psi_2(F_2,F)$. The number of different wave functions with the same F will be the same as before, and the two sets of wave functions are linearly related. Their relation may be written

$$\psi_1(F_1,F) = \sum_{F_2} c(F_1,F_2)\psi_2(F_2,F) \tag{6-26}$$

The matrix $c(F_1,F_2)$ is unitary, and the phases of the wave functions may be chosen so that these coefficients are all real. Hence the reverse transformation is

$$\psi_2(F_2,F) = \sum_{F_1} c(F_1,F_2)\psi_1(F_1,F) \tag{6-27}$$

In case both interactions, H_1 and H_2, are appreciable, the eigenfunctions are not given by either $\psi_1(F_1,F)$ or $\psi_2(F_2,F)$ but by appropriate linear combinations of either set. Let the correct wave function be given by the general expansion

$$\psi(F) = \sum_{F_1} a(F_1)\psi_1(F_1,F) \tag{6-28}$$

The Hamiltonian equation $H\psi = W\psi$ becomes

$$\sum_{F_1} H_1(\mathbf{I}_1,\mathbf{J})a(F_1)\psi_1(F_1,F) + \sum_{F_1} H_2(\mathbf{I}_2,\mathbf{J})a(F_1)\sum_{F_2} c(F_1,F_2)\psi_2(F_2,F) = W\sum_{F_1} a(F_1)\psi_1(F_1,F) \tag{6-29}$$

in which use has been made of (6-25). Now ψ_1 is an eigenfunction of H_1 and ψ_2 of H_2, or

$$\begin{aligned} H_1(\mathbf{I}_1,\mathbf{J})\psi_1(F_1,F) &= W_1(F_1)\psi_1(F_1,F) \\ H_2(\mathbf{I}_2,\mathbf{J})\psi_2(F_2,F) &= W_2(F_2)\psi_2(F_2,F) \end{aligned} \tag{6-30}$$

Using these relations and replacing ψ_2 by (6-27), Eq. (6-29) becomes

$$\sum_{F_1}\Big\{[A(F_1,F_1) + W(F_1) - W]a(F_1) + \sum_{F_1'\neq F_1} A(F_1,F_1')a(F_1')\Big\}\psi_1(F_1,F) = 0 \tag{6-31}$$

where

$$A(F_1,F_1') = \sum_{F_2} c(F_1,F_2)c(F_1',F_2)W_2(F_2) \tag{6-32}$$

Since all the ψ_1's are orthogonal, (6-31) may be written as a group of homogeneous equations of the form

$$[A(F_1,F) + W(F_1) - W]a(F_1) + \sum_{F_1'\neq F_1} A(F_1,F_1')a(F_1') = 0 \tag{6-33}$$

for each value of F_1 which, when added to I_2, gives the same value F for the total angular momentum. In order for these equations to have a solution, the determinant of their coefficients must be zero. A solution of this secular determinant gives the possible values of the energy W. If the interaction H_2 is much smaller than H_1 and there is no degeneracy in W_1, then the energy values are given to the first order in H_2 by

$$W = W(F_1) + A(F_1,F_1)$$

or

$$W = W(F_1) + \sum_{F_2}[c(F_1,F_2)]^2 W_2(F_2) \tag{6-34}$$

This is the case when the eigenfunctions $\psi_1(F_1,F)$ are essentially correct. Then the energy is given by the sum of the energy $W(F_1)$ and the various possible energies $W_2(F_2)$ weighted by the probability $[c(F_1,F_2)]^2$ of finding $\psi_2(F_2,F)$ in the transformation (6-26) of the wave function $\psi_1(F_1,F)$.

The quantities $c(F_1,F_2)$ are given in terms of I_1, I_2, J_1, F_1, F_2, and F by Tables 6-3, 6-4, and 6-5. Table 6-3 gives these coefficients for an arbitrary I_1, J, F_1, F_2, and F when $I_2 = \frac{1}{2}$, and Tables 6-4 and 6-5 give them when $I_2 = 1$ and $\frac{3}{2}$, respectively.

TABLE 6-3. TRANSFORMATION COEFFICIENTS $c(F_1,F_2)$ for $I_1 = I$, $I_2 = \frac{1}{2}$, $\Sigma = I + J + F + \frac{1}{2}$

F_2	$F_1 = F - \frac{1}{2}$	$F_1 = F + \frac{1}{2}$
$J - \frac{1}{2}$	$\left[\frac{(\Sigma - 2F)(\Sigma - 2J)}{(2F+1)(2J+1)}\right]^{\frac{1}{2}}$	$\left[\frac{(\Sigma + 1)(\Sigma - 2I)}{(2F+1)(2J+1)}\right]^{\frac{1}{2}}$
$J + \frac{1}{2}$	$-\left[\frac{(\Sigma + 1)(\Sigma - 2I)}{(2F+1)(2J+1)}\right]^{\frac{1}{2}}$	$\left[\frac{(\Sigma - 2F)(\Sigma - 2J)}{(2F+1)(2J+1)}\right]^{\frac{1}{2}}$

These coefficients are related as follows to certain W functions defined by Racah [113]:

$$c(F_1,F_2) = (-1)^{F+J-I_1-I_2}[(2F_1+1)(2F_2+1)]^{\frac{1}{2}}W(F_1FJF_2;I_2I_1)$$

The W functions (W is not to be confused with the energy) have now been tabulated for most values of the variables which are of interest [674] [854a]. Hence the coefficients $c(F_1,F_2)$ for $I_2 > \frac{3}{2}$ may be obtained from them.

An Example of Two Nuclei with Hyperfine Structure. Calculation of a specific case may be helpful. Let $I_1 = \frac{3}{2}$, $I_2 = 1$, and $J = 2$. F_1 may

TABLE 6-4. TRANSFORMATION COEFFICIENTS $c(F_1, F_2)$ FOR $I_1 = I$, $I_2 = 1$. $\Sigma = I + J + F + 1$
(From Bardeen and Townes [252])

F_2	$F_1 = F - 1$	$F_1 = F$	$F_1 = F + 1$
$J - 1$	$\left(\frac{(\Sigma - 2F - 1)(\Sigma - 2F)(\Sigma - 2J - 1)(\Sigma - 2J)}{2J(2J+1)2F(2F+1)}\right)^{\frac{1}{2}}$	$\left(\frac{2(\Sigma - 2F - 1)(\Sigma - 2I - 1)\Sigma(\Sigma - 2J)}{2J(2J+1)2F(2F+1)}\right)^{\frac{1}{2}}$	$\left(\frac{(\Sigma - 2I - 1)(\Sigma - 2I)\Sigma(\Sigma + 1)}{2J(2J+1)(2F+1)(2F+2)}\right)^{\frac{1}{2}}$
J	$\left(\frac{2(\Sigma - 2F)(\Sigma - 2I - 1)\Sigma(\Sigma - 2J - 1)}{2J(2J+2)2F(2F+1)}\right)^{\frac{1}{2}}$	$\frac{(2J(2J+2)2F(2F+2))^{\frac{1}{2}}}{2F(F+1) + 2J(J+1) - 2I(I+1)}$	$-\left(\frac{2(\Sigma - 2I - 1)(\Sigma - 2I)(\Sigma - 2J)(\Sigma + 1)}{2J(2J+2)(2F+1)(2F+2)}\right)^{\frac{1}{2}}$
$J + 1$	$\left(\frac{(\Sigma - 2I - 1)(\Sigma - 2I)\Sigma(\Sigma + 1)}{(2J+1)(2J+2)2F(2F+1)}\right)^{\frac{1}{2}}$	$-\left(\frac{2(\Sigma - 2J - 1)(\Sigma - 2F)(\Sigma - 2I)(\Sigma + 1)}{(2J+1)(2J+2)2F(2F+2)}\right)^{\frac{1}{2}}$	$\left(\frac{(\Sigma - 2J - 1)(\Sigma - 2J)(\Sigma - 2F - 1)(\Sigma - 2F)}{(2J+1)(2J+2)(2F+1)(2F+2)}\right)^{\frac{1}{2}}$

TABLE 6-5. TRANSFORMATION COEFFICIENTS $c(F_1, F_2)$ FOR $I_1 = I$, $I_2 = \frac{3}{2}$. $\Sigma = I + J + F + \frac{3}{2}$
(From Bardeen and Townes [252])

F_2	$F_1 = F - \frac{3}{2}$	$F_1 = F - \frac{1}{2}$	$F_1 = F + \frac{1}{2}$
$J - \frac{3}{2}$	$\left(\frac{(\Sigma - 2F - 2)(\Sigma - 2F - 1)(\Sigma - 2F)(\Sigma - 2J - 2)(\Sigma - 2J - 1)(\Sigma - 2J)}{(2F-1)2F(2F+1)(2J-1)2J(2J+1)}\right)^{\frac{1}{2}}$	$\left(\frac{3(\Sigma - 1)(\Sigma - 2F - 2)(\Sigma - 2F - 1)(\Sigma - 2J - 1)(\Sigma - 2J)(\Sigma - 2J - 2)}{(2F-1)(2F+1)(2F+2)(2J-1)2J(2J+1)}\right)^{\frac{1}{2}}$	$\left(\frac{(3(\Sigma - 1)(\Sigma - 2F - 1) + (\Sigma - 2F)(-3I + 3J + F - \frac{1}{2}))((\Sigma - 2F - 1)(\Sigma - 2J - 1))^{\frac{1}{2}}}{[2(2F-1)(\Sigma - 2I - 1) + (\Sigma - 2F)(-3I + 3J - F + \frac{1}{2})](2J+1)}\right)$
$J - \frac{1}{2}$	$\left(\frac{3(\Sigma - 1)\Sigma(\Sigma - 2F)(\Sigma - 2J - 2)(\Sigma - 2I - 1)(\Sigma - 2J)}{(2F-1)2F(2F+1)(2J-1)(2J+2)}\right)^{\frac{1}{2}}$	$\left(\frac{3(\Sigma - 1)(\Sigma - 2F)(\Sigma - 2J - 2)(\Sigma - 2J - 1)(\Sigma - 2I - 2)}{(2F-1)2F(2F+1)(2J-1)(2J+2)}\right)^{\frac{1}{2}}$	$\left(\frac{((2F-1)(2F+1)(2F+2)2J(2J+1)(2J+2))^{\frac{1}{2}}}{[(2F-1)(\Sigma - 2I) + (\Sigma - 2F)(-3I + 3J - F + \frac{1}{2})](\Sigma)(\Sigma - 2I - 1)}\right)$
$J + \frac{1}{2}$	$\left(\frac{(\Sigma - 1)\Sigma(\Sigma + 1)(\Sigma - 2I - 2)(\Sigma - 2I - 1)(\Sigma - 2J)}{(2F-1)2F(2F+1)2J(2J+1)(2J+3)}\right)^{\frac{1}{2}}$	$\left(\frac{3\Sigma(\Sigma + 1)(\Sigma - 2F)(\Sigma - 2J - 2)(\Sigma - 2I - 1)(\Sigma - 2J)}{(2F-1)(2F+1)(2F+2)(2J+1)(2J+3)}\right)^{\frac{1}{2}}$	$-\left(\frac{((2F-1)(2F+1)(2F+2)2J(2J+1)(2J+3))^{\frac{1}{2}}}{[(\Sigma + 1)(\Sigma - 2F)(\Sigma - 2J - 2)(\Sigma - 2I - 1)(\Sigma - 2J)]}\right)$
$J + \frac{3}{2}$	$\left(\frac{(\Sigma - 1)\Sigma(\Sigma + 1)(\Sigma - 2I - 2)(\Sigma - 2I - 1)(\Sigma - 2J)}{(2F-1)2F(2F+1)(2J+1)(2J+2)(2J+3)}\right)^{\frac{1}{2}}$		
	$F_1 = F + \frac{1}{2}$		$F_1 = F + \frac{3}{2}$
$J - \frac{3}{2}$	$\left(\frac{3(\Sigma - 1)\Sigma(\Sigma - 2F - 2)(\Sigma - 2J)(\Sigma - 2I - 2)(\Sigma - 2I - 1)}{2F(2F+1)(2F+3)(2J-1)2J(2J+1)}\right)^{\frac{1}{2}}$		$\left(\frac{(\Sigma - 1)\Sigma(\Sigma + 1)(\Sigma - 2I - 2)(\Sigma - 2I - 1)(\Sigma - 2J)}{(2F+1)(2F+2)(2F+3)(2J-1)2J(2J+1)}\right)^{\frac{1}{2}}$
$J - \frac{1}{2}$	$\frac{[2F(-3I - J + 3F + \frac{1}{2}) + 3(\Sigma - 2F - 1)(\Sigma - 2I - 2)](\Sigma(\Sigma - 2I - 1))^{\frac{1}{2}}}{(2F(2F+1)(2F+3)(2J-1)(2J+1)(2J+2))^{\frac{1}{2}}}$		$-\left(\frac{3\Sigma(\Sigma + 1)(\Sigma - 2F - 2)(\Sigma - 2I - 2)(\Sigma - 2I - 1)(\Sigma - 2J)}{(2F+1)(2F+2)(2F+3)(2J-1)(2J+1)(2J+2)}\right)^{\frac{1}{2}}$
$J + \frac{1}{2}$	$-\frac{[2F(-3I + J + 3F + \frac{1}{2}) + 3(\Sigma - 2F)(\Sigma - 2I - 1)](\Sigma - 2F - 1)(\Sigma - 2J - 1))^{\frac{1}{2}}}{(2F(2F+1)(2F+3)2J(2J+1)(2J+3))^{\frac{1}{2}}}$		$\left(\frac{3(\Sigma + 1)(\Sigma - 2F - 2)(\Sigma - 2F - 1)(\Sigma - 2I - 1)(\Sigma - 2J)(\Sigma - 2J - 1)}{(2F+1)(2F+2)(2F+3)2J(2J+1)(2J+3)}\right)^{\frac{1}{2}}$
$J + \frac{3}{2}$	$\left(\frac{3(\Sigma + 1)(\Sigma - 2F - 1)(\Sigma - 2F)(\Sigma - 2I - 1)(\Sigma - 2J)(\Sigma - 2J - 1)}{2F(2F+1)(2F+3)(2J+1)2J(2J+3)}\right)^{\frac{1}{2}}$		$-\left(\frac{(\Sigma - 2F - 2)(\Sigma - 2F - 1)(\Sigma - 2F)(\Sigma - 2I - 1)(\Sigma - 2J)(\Sigma - 2J - 1)}{(2F+1)(2F+2)(2F+3)(2J+1)(2J+2)(2J+3)}\right)^{\frac{1}{2}}$

then have the values $\frac{1}{2}$, $\frac{3}{2}$, $\frac{5}{2}$, or $\frac{7}{2}$, F_2 the values 1, 2, or 3, and F may have values ranging from $\frac{1}{2}$ to $\frac{9}{2}$. There is only one possible wave function $\psi_1(F_1,F)$ or $\psi_2(F_2,F)$ which gives $F = \frac{9}{2}$, namely, $\psi_1(\frac{7}{2},\frac{9}{2})$ or $\psi_2(3,\frac{9}{2})$, which two functions must hence be identical. Therefore for $F = \frac{9}{2}$, all c's are zero except $c(\frac{7}{2},3)$ which is unity, as may be found from Table 6-4 or Table 6-5. The secular determinant for $F = \frac{9}{2}$ reduces to the single equation

$$W = W_1(\tfrac{7}{2}) + W_2(3)$$

There are two wave functions corresponding to $F = \frac{7}{2}$, linear combinations of $\psi_1(\frac{7}{2},\frac{7}{2})$ and $\psi_1(\frac{5}{2},\frac{7}{2})$, or of $\psi_2(3,\frac{7}{2})$ and $\psi_2(2,\frac{7}{2})$. The coefficients are, from Table 6-4 (or Table 6-5),

$$c(\tfrac{7}{2},3) = -\sqrt{\tfrac{1}{7}} \qquad c(\tfrac{7}{2},2) = \sqrt{\tfrac{6}{7}} \qquad c(\tfrac{5}{2},3) = \sqrt{\tfrac{6}{7}} \qquad c(\tfrac{5}{2},2) = \sqrt{\tfrac{1}{7}}$$

The secular determinant becomes, therefore

$$\begin{vmatrix} [W_1(\frac{7}{2}) + \frac{1}{7}W_2(3) + \frac{6}{7}W_2(2) - W] & \frac{\sqrt{6}}{7}[W_2(2) - W_2(3)] \\ \frac{\sqrt{6}}{7}[W_2(2) - W_2(3)] & [W_1(\frac{5}{2}) + \frac{6}{7}W_2(3) + \frac{1}{7}W_2(2) - W] \end{vmatrix} = 0 \qquad (6\text{-}35)$$

which gives two possible values of the energy E corresponding to the two different states with $F = \frac{7}{2}$. For $H_2 \ll H_1$, the first-order solutions derived from the diagonal terms are sufficiently accurate. They are

$$W = W_1(\tfrac{7}{2}) + \tfrac{1}{7}W_2(3) + \tfrac{6}{7}W_2(2)$$
and
$$W = W_1(\tfrac{5}{2}) + \tfrac{6}{7}W_2(3) + \tfrac{1}{7}W_2(2) \qquad (6\text{-}36)$$

If H_2 is not very small, then the quadratic equation (6-35) must be solved.

The energies given by (6-36), which are correct when the coupling of nucleus 2 is much less than that of nucleus 1, are the energies for nucleus 1 coupled to the molecule and slightly perturbed by nucleus 2. If the coupling of nucleus 2 were much greater than that of nucleus 1, then the energies would be given primarily by coupling nucleus 2 to the molecule and these energies would be slightly perturbed by nucleus 1. For intermediate coupling cases, where neither of these approximations holds, description of the energies is much more complex. The energies of the various states have been computed for the case $I_1 = \frac{3}{2}$, $I_2 = 1$, $J = 2$, and their behavior is shown in Fig. 6-3. Assuming the couplings between the nuclei and the molecule are due to quadrupole moments, the energy levels are plotted as a function of the ratio of the quadrupole couplings of the two nuclei. This ratio, $\alpha = (eqQ)_{I=1}/(eqQ)_{I=\frac{3}{2}}$, is measured along the axis of abscissas, the function $(1 + \alpha)/(1 + \alpha^2)^{\frac{1}{2}}$ being plotted linearly for positive α and $(1 - \alpha)/(1 + \alpha^2)^{\frac{1}{2}}$ linearly for negative α. Energy is

measured along the ordinate axis, $W/[(-eqQ)_{I=\frac{3}{2}}(1+\alpha^2)^{\frac{1}{2}}]$ being plotted linearly. Such a plot produces smooth curves and allows α a range from $-\infty$ to $+\infty$. Values of $1/\alpha$ rather than α are marked off in the region where $|\alpha| > 1$.

Near the line where $\alpha = 0$, the first-order approximation holds with the levels being close to those expected for a nucleus of spin $\frac{3}{2}$. Near the lines where $\alpha = \infty$, or $1/\alpha = 0$, the first-order approximation again holds, the levels being close to those expected for a nucleus of spin 1. It may

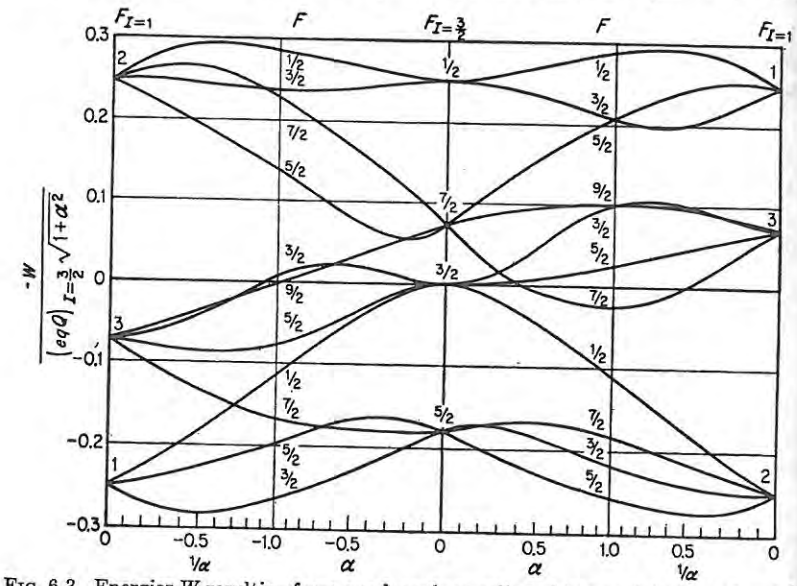

FIG. 6-3. Energies W resulting from quadrupole coupling of two nuclei of spin 1 and $\frac{3}{2}$, when $J = 2$. Parameter $\alpha = (eqQ_{I=1}/(eqQ)_{I=\frac{3}{2}}$. (*From Bardeen and Townes* [252].)

be seen that the first-order approximation is fairly accurate for $|\alpha| < 0.1$ or $|1/\alpha| < 0.1$, but that in intermediate ranges it can be very inaccurate, so that the secular equations must be solved in full. In these intermediate cases, the quantum numbers F_1 and F_2 do not have definite values for each state and the energy levels are designated in the figure only by the values of the total angular momentum F.

An example of a rotational spectrum with two quadrupole moments is given in Fig. 6-4. This is the $J = 2 \leftarrow 1$ transition of the ground state of the linear molecule $Cl^{35}C^{12}N^{14}$. In this case Cl has a spin of $\frac{3}{2}$ and a quadrupole coupling constant of -83.5 Mc, whereas N^{14}, with a spin of 1, has a coupling constant -3.83 Mc. Thus $\alpha \approx 0.05$ and the first-order theory is rather accurate, although some small deviations from it are noticeable.

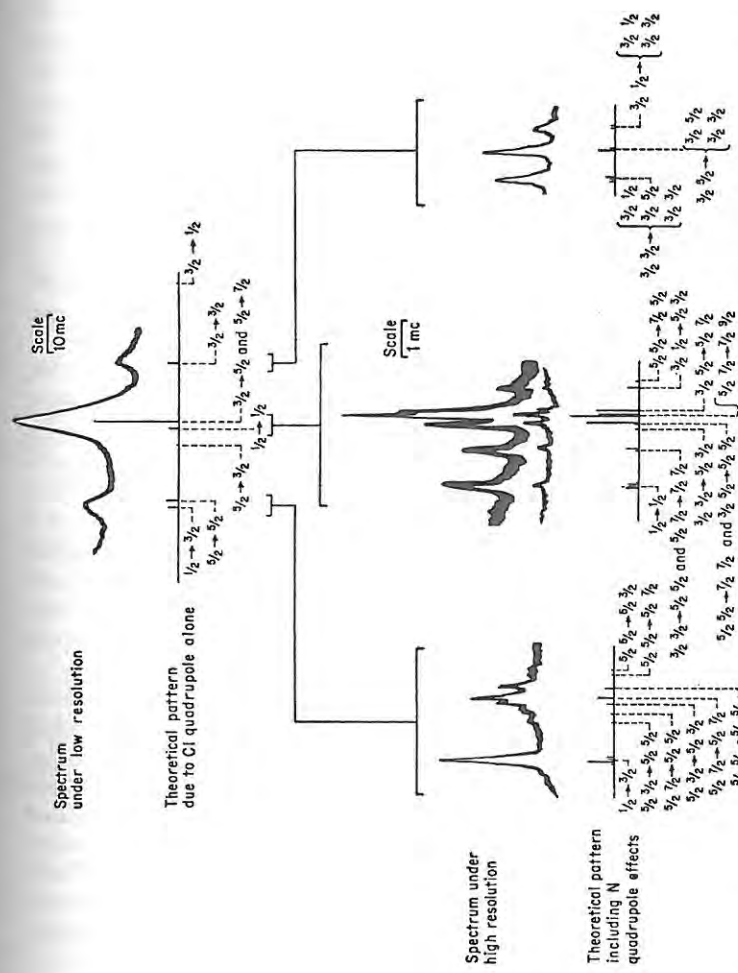

FIG. 6-4. Hyperfine structure of the $J = 2 \leftarrow 1$ transition of $Cl^{35}CN^{14}$ (ground vibrational state) with low and high dispersion and comparison with theoretical pattern. Spins for Cl^{35} and N^{14} are $\frac{3}{2}$ and 1, respectively. (*From Townes, Holden, and Merritt* [329].)

It should be noted that the technique for calculating the energies for the case of two nuclei given above is not restricted to quadrupole coupling but may be used for any case in which the energies W_1 and W_2, that is, the eigenvalues for the interaction between the individual nuclei and the molecule, can be obtained. The methods may thus also be used for magnetic coupling, which will be discussed in Chap. 8, or a combination of magnetic and quadrupole coupling.

Intensities of Hyperfine Components. In addition to energy levels, intensities are generally required. For the splitting of a line due to one nucleus alone, the fractional intensity in each hyperfine component may be formed from the fine- (or hyperfine-) structure intensity formulas (6-6), which are tabulated in Appendix I. If a second nucleus produces a hyperfine interaction, and its coupling is small compared with the coupling of the first nucleus, expressions (6-6) and the tables of Appendix I may again be applied to find intensities of all components of the still more finely split hyperfine structure. It is only necessary to replace J by F_1 and I by I_2 in order to use the tables. Appendix I does not list half-integral values of J, which will be needed when I_1 is half integral and J is replaced by F_1. However, values of intensities for such cases can usually be obtained to sufficient accuracy by interpolation between the nearest integral values. If the couplings of the two nuclei are not widely different, then true intensities cannot be found so directly, but a fair approximation to the intensities may be obtained by interpolating between the two extreme cases when coupling of the first nucleus is large compared with coupling of the second nucleus, and when it is small. Intensities for these extreme cases may be readily obtained from Appendix I.

Exact intensities may, of course, be obtained in cases of intermediate coupling by making use of the energy values obtained by the method described above and solving equations of the type (6-33) for $a(F_1)$. The matrix elements between hyperfine states for a single nucleus may be found in Condon and Shortley [56]. They may be designated $(I_1JF_1|\mu_J|I_1J'F_1')$ and their squares are proportional to the relative intensities given in Appendix I. A similar matrix element $(I_2F_1F|\mu_{F_1}|I_2F_1'F')$ for the transition between the states specified by I_2, F_1, and F can be obtained in the same way. For intermediate coupling cases, the relative intensity for a transition between states i and j would then be given by

$$\left|\sum_{F_1'}\sum_{F_1} a_i(F_1)a_j(F_1')(I_1JF_1|\mu_J|I_1J'F_1')(I_2F_1F|\mu_{F_1}|I_2F_1'F')\right|^2$$

Careful attention must be paid to the phases (see [56], p. 277). This procedure would at best be tedious and in most cases could be replaced by the more rapid approximate method of the preceding paragraph.

Hyperfine Structure Due to More Than Two Nuclei. The case of three nuclei coupled by quadrupole effects to a molecule is uncommon except in symmetric tops involving three halogens such as $AsCl_3$, $HCBr_3$, etc. The resulting hyperfine structure is so complex that so far only one example has been solved, the $J = 1 \leftarrow 0$ transition of $HCBr_3$ [620], [717]. Mizushima and Ito [620] give calculated patterns for the $J = 1 \leftarrow 0$ transition with a nuclear spin of 1, $\frac{3}{2}$, 2, or $\frac{5}{2}$.

For more than two nuclei coupled to the same molecule the method discussed above does not apply. Bersohn [437] has given a satisfactory technique for dealing with these more complicated cases by the use of a formulation due to Racah [113]. The state of a molecular system of angular momentum J with three nuclei of spins I_1, I_2, and I_3 may be designated by the vectors $\mathbf{I} = \mathbf{I}_1 + \mathbf{I}_2$, $\mathbf{I}^0 = \mathbf{I} + \mathbf{I}_3$, and $\mathbf{F} = \mathbf{I}^0 + \mathbf{J}$, or by the corresponding quantum numbers I, I^0, J, and F. Bersohn [437] obtains for the matrix elements of the quadrupole interactions H_Q for the three nuclei between states designated by the above quantum numbers, and when perturbations between different values of J are not important,

$$\begin{aligned}
&(II^0JF|H_{Q_1} + H_{Q_2} + H_{Q_3}|I'I^{0\prime}J'F)\\
&= \frac{(J|eQ_1\,\partial^2V_1/\partial z^2|J)(-1)^{I_2+I_3-I_1-I-I'+J'-F}}{8[J(2J-1)I_1(2I_1-1)]^{\frac{1}{2}}} \times [(2I+1)(2I'+1)(2I^0+1)\\
&\qquad (2I^{0\prime}+1)(2I_1+1)(2I_1+2)(2I_1+3)(2J+1)(2J+2)(2J+3)]^{\frac{1}{2}}\\
&\times W(I_1I_1II';2I_2)W(II'I^0I^{0\prime};2I_3)W(II'JJ';2F)\\
&+ \frac{(J|eQ_2\,\partial^2V_2/\partial z^2|J)(-1)^{I_1+I_3-I_2-I-I'+J'-F}}{8[J(2J-1)I_2(2I_2-1)]^{\frac{1}{2}}} \times [(2I+1)(2I'+1)(2I^0+1)\\
&\qquad (2I^{0\prime}+1)(2I_2+1)(2I_2+2)(2I+3)(2J+1)(2J+2)(2J+3)]^{\frac{1}{2}}\\
&\times W(I_2I_2II';2I_1)W(II'I^0I^{0\prime};2I_3)W(II'JJ';2F)\\
&+ \frac{(J|eQ_3\,\partial^2V_3/\partial z^2|J)(-1)^{I-I_3+I^0-I^{0\prime}+J'-F}}{[J(2J-1)I_3(2I_3-1)]^{\frac{1}{2}}}\,\delta_{II'} \times [(2I^0+1)(2I^{0\prime}+1)\\
&(2I_3+1)(2I_3+2)(2I_3+3)(2J+1)(2J+2)(2J+3)]^{\frac{1}{2}}\\
&\qquad\qquad \times W(I_3I_3I^0I^{0\prime};2I)W(I^0I^{0\prime}JJ';2F) \qquad (6\text{-}37)
\end{aligned}$$

$\delta_{II'}$ is unity for $I = I'$, and is otherwise zero. The matrix elements in (6-37) of the form $(J|eQ_1\,\partial^2V_1/\partial z^2|J')$ depend on matrix elements of the direction cosines as may be seen from (6-12). If the rotational state is not much perturbed so that J is a good quantum number, these take the form $e(q_JQ)_1$, where q_J is given by (6-17) or (6-18). The W functions of the particular form used in (6-37) may be found in tables by Biedenharn, Blatt, and Rose [674].

In order to solve a specific problem, secular equations must be set up by the use of matrix elements (6-37) and solved. These matrix elements may of course also be used for the case of two nuclei. However, techniques already discussed for handling this case are usually simpler to understand and to apply.

CHAPTER 8

MAGNETIC HYPERFINE STRUCTURE IN MOLECULAR SPECTRA

8-1. Introduction. Although hyperfine structure due to nuclear magnetic dipole moments is not so prominent in molecular spectra as that involving nuclear electric quadrupole moments, it is by no means insignificant. In molecules with electronic angular momentum, magnetic hyperfine structure is comparable in size with magnetic hyperfine structure in atoms and is usually much larger than that due to quadrupole moments. It is only because this type of molecule is uncommon that magnetic hyperfine structure is not prominent in molecular spectra. For molecules in $^1\Sigma$ states the average of each component of the electronic angular momentum is so small that it is usually considered zero. Even for these molecules, however, there are weak interactions involving nuclear magnetic moments. These include interaction between magnetic moments of two nuclei in the same molecule (spin-spin interactions), interaction between a nuclear magnetic moment and the rather small magnetic fields produced by molecular rotation ($\mathbf{I} \cdot \mathbf{J}$ interactions), and magnetic polarization of a molecule by a nuclear magnetic moment (pseudo quadrupole interaction).

When a molecule has electronic angular momentum, hence is in some state other than $^1\Sigma$, the magnetic fields associated with this momentum interact strongly with the nuclear moments present in the molecule, giving a magnetic hyperfine structure comparable in size with that found in atoms (10^3 Mc would be typical). The interaction is due either to electronic orbital angular momentum, $\mathbf{L}$ or Λ, or to spin angular momentum, $\mathbf{S}$ or Σ.

In the case of orbital angular momentum, the interaction energy is given by (5-49) if the spin is assumed to be zero, *i.e.*, if we let $\mathbf{j} = \mathbf{l}$. Then (5-49) and (5-51) give the energy as

$$H_{Il} = \frac{2\mu_0\mu_I}{Ir^3}\,\mathbf{I}\cdot\mathbf{l} \tag{8-1}$$

where μ_0 = the Bohr magneton
μ_I = nuclear magnetic moment
$\mathbf{I}$ = nuclear spin

r = distance between the electron and the nucleus
$\mathbf{l}$ = orbital angular momentum of an electron with respect to the nucleus in units of $h/2\pi$ (the quantity $h/2\pi$ will frequently be written $\hbar$)

To calculate the energy resulting from (8-1) in the first-order perturbation approximation, we need to average this expression (since in a molecule neither $\mathbf{l}$ nor r is constant) and to sum over all the electrons which contribute to the total orbital angular momentum $\mathbf{L}$. In the simplest cases, the nucleus may be assumed to lie on the molecular axis. $\mathbf{L}$ has an average nonzero value only if the molecule is linear, so that the average value of $\mathbf{L}$ is just $\mathbf{k}\Lambda$, where $\mathbf{k}$ is a unit vector along the molecular axis and Λ is as usual the component of $\mathbf{L}$ along this direction. Then if only one electron contributes to the orbital angular momentum $\mathbf{L}$,

$$H_{IL} = \frac{2\mu_0\mu_I\Lambda}{I}\left(\frac{1}{r^3}\right)_{\text{av}}\mathbf{I}\cdot\mathbf{k} \tag{8-2a}$$

If more electrons are involved,

$$H_{IL} = \frac{2\mu_0\mu_I}{I}\sum_n\left(\frac{1}{r_n^3}\right)_{\text{av}}\Lambda_n\mathbf{I}\cdot\mathbf{k} \tag{8-2b}$$

where the sum is over each electron contributing to the hyperfine structure and Λ_n is the average projection of the orbital angular momentum of the nth electron on the axis.

Interaction between a nuclear magnetic moment and an electron spin moment is somewhat more complex. There is the classical interaction between two dipoles $\boldsymbol{\mu}_1$ and $\boldsymbol{\mu}_2$ of the form

$$W_{\mu_1\mu_2} = \frac{\boldsymbol{\mu}_1\cdot\boldsymbol{\mu}_2}{r^3} - \frac{3(\boldsymbol{\mu}_1\cdot\mathbf{r})(\boldsymbol{\mu}_2\cdot\mathbf{r})}{r^5} \tag{8-3}$$

which for the nucleus $\left(\boldsymbol{\mu}_1 = \frac{\mu_I}{I}\mathbf{I}\right)$ and electron spin ($\boldsymbol{\mu}_2 = -2\mu_0\mathbf{S}$) becomes

$$(H_{IS})_1 = \frac{-2\mu_0\mu_I}{I}\left[\frac{\mathbf{I}\cdot\mathbf{S}}{r^3} - \frac{3(\mathbf{I}\cdot\mathbf{r})(\mathbf{S}\cdot\mathbf{r})}{r^5}\right] \tag{8-4}$$

In addition, there is an interaction of the type found between a nuclear magnetic moment and an S electron in atoms, which is not given simply by (8-4). It can be written approximately as in the atomic case from (5-49) and (5-54) as

$$(H_{IS})_2 = \frac{16\pi}{3}\frac{\mu_0\mu_I}{I}\psi^2(0)\mathbf{I}\cdot\mathbf{S} \tag{8-5}$$

Frosch and Foley [686] (*cf.* also [916*a*]) have discussed these magnetic interactions for a linear molecule, and obtain the sum of H_{IL}, $(H_{IS})_1$, and

$(H_{IS})_2$ in the common Hund's cases (a) and (b) as

$$H^1 = a\Lambda \mathbf{I} \cdot \mathbf{k} + b\mathbf{I} \cdot \mathbf{S} + c(\mathbf{I} \cdot \mathbf{k})(\mathbf{S} \cdot \mathbf{k}) \tag{8-6}$$

where

$$a = \frac{2\mu_0\mu_I}{I}\left(\frac{1}{r^3}\right)_{av}$$

and to a good approximation

$$b = \frac{2\mu_0\mu_I}{I}\left[\frac{8\pi}{3}\psi^2(0) - \frac{3\cos^2\theta - 1}{2r^3}\right]_{av}$$

$$c = \frac{3\mu_0\mu_I}{I}\left(\frac{3\cos^2\theta - 1}{r^3}\right)_{av}$$

Expression (8-6) applies accurately only when Λ is a "good" quantum number. Here θ is the angle between the molecular axis and the radius r from the nucleus to the electron. Λ and S are assumed to be good quantum numbers, since second-order terms involving changes of Λ or S give extremely small contributions to the energy by comparison with the first-order terms of (8-6). Some of these second-order terms will be discussed below, however, in connection with magnetic effects in $^1\Sigma$ molecules, where the first-order terms given by (8-6) are zero.

Expression (8-6) applies to each electron in the molecule. Of course, most of the electrons occupy orbits in pairs with oppositely directed spins so that the second and third parts of (8-6) cancel out, and the orbits are usually filled so that the orbital angular momentum Λ of most of the electrons cancel. Expression (8-6) need then only be applied to each of the "unpaired" electrons whose angular momentum is not cancelled. The quantity a refers only to electrons with orbital angular momentum. A spherical distribution of an electron around the nucleus would make $\left(\frac{3\cos^2\theta - 1}{2}\right)_{av}$ equal to zero, so that in this case the electron spin would interact with the nuclear magnetic moment only through the term in b proportional to $\psi^2(0)$. The probability $\psi^2(0)$ of the electron's being found at the nucleus is usually negligibly small for an electron in a p atomic orbit. For an S-type orbit, however, it is large enough so that $\frac{8\pi}{3}\psi^2(0)$ is much larger than $\left(\frac{3\cos^2\theta - 1}{2r^3}\right)_{av}$ for a p orbit and $b \gg a$. Hence, whenever there is an appreciable amount of S character to the wave function of an unpaired electron, the hyperfine interaction which is proportional to $\psi^2(0)$ may be expected to dominate.

8-2. Coupling Schemes for Magnetic Hyperfine Structure. Evaluation of the energy resulting from the interaction (8-6) depends on the coupling scheme which is followed by the particular case of interest. In addition to the electron angular momentum which is coupled according to the usual Hund's coupling cases (*cf.* Chap. 7) to the molecular axis or to the momentum of end-over-end rotation of the molecule, we have also

the nuclear spin momentum. The nuclear spin may be coupled with varying strength to the several molecular vectors, providing additional coupling possibilities. The commonly expected coupling schemes are shown in Fig. 8-1. They are classified according to Hund's scheme, with a subscript α indicating that the nuclear spin is most strongly coupled to the molecular axis [as is S in Hund's case (a)] and a subscript β indicating that the nuclear spin is not coupled to the molecular axis but to

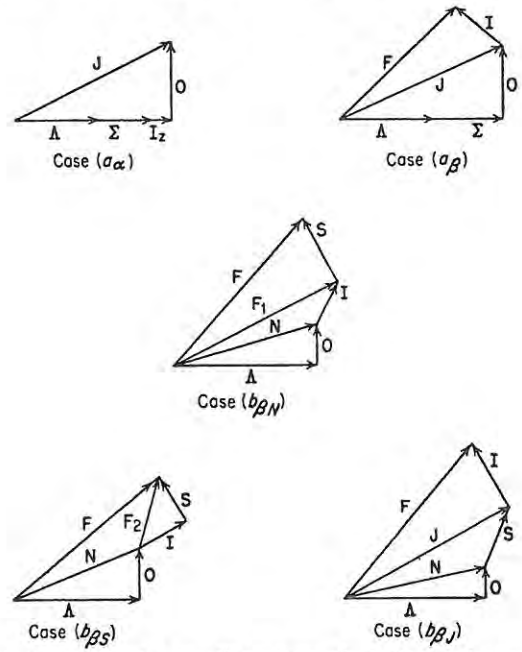

FIG. 8-1. Molecular coupling schemes including nuclear spin.

some other vector [as in case (b)]. For Hund's case (a), one may expect the nuclear spin to be coupled either to the molecular axis [case (a_α)] or to J [case (a_β)]. However, for Hund's case (b), where the electron spin is not coupled to the molecular axis, it is very unlikely that the nuclear spin will be coupled to the molecular axis since the interaction of its small nuclear magnetic moment with the molecular fields should be considerably less than that between the electron moment and the molecular fields. Hence only case (b_β) is expected to occur.

In case (a), (8-6) becomes (omitting the negligible perturbation of Λ by hyperfine interactions)

$$H^1 = [a\Lambda + (b + c)\Sigma]\mathbf{I} \cdot \mathbf{k} \tag{8-7}$$

since $\mathbf{S} \cdot \mathbf{k} = \Sigma$, and $\mathbf{I} \cdot \mathbf{S} = (\mathbf{I} \cdot \mathbf{k})(\mathbf{S} \cdot \mathbf{k})$ when $\mathbf{S}$ precesses about the

molecular axis **k**. The hyperfine energy for case (a_α) is the sum of a magnetic interaction given by (8-7) and a term dependent on the molecular moment of inertia. The entire effect of Ω_I, or $\mathbf{I}\cdot\mathbf{k}$, the projection of I on the axis, is

$$W = [a\Lambda + (b + c)\Sigma]\Omega_I - hB[\Omega_I + 2(\Lambda + \Sigma)]\Omega_I \tag{8-8}$$

All parts of this expression are constant for a given electronic level except Ω_I, which has one of the values $I, I - 1, \ldots, -I$. The second term of (8-8) may be obtained from (7-2), which gives the rotational energy in case (a) as $W_J = hB[J(J + 1) - \Omega^2]$. But in case (a_α), Ω may include Ω_I, which therefore affects the rotational energy. In case (a_β), the vector model gives

$$\mathbf{I}\cdot\mathbf{k} = \frac{(\mathbf{I}\cdot\mathbf{J})(\mathbf{J}\cdot\mathbf{k})}{J(J+1)}$$

or, since $\mathbf{J}\cdot\mathbf{k} = \Lambda + \Sigma = \Omega$,

$$W = [a\Lambda + (b + c)\Sigma]\frac{\Omega}{J(J+1)}\mathbf{I}\cdot\mathbf{J} \tag{8-9}$$

where

$$\mathbf{I}\cdot\mathbf{J} = \frac{F(F+1) - J(J+1) - I(I+1)}{2}$$

In this case, the hyperfine structure decreases with increasing J, since **I** becomes more and more nearly perpendicular to the molecular axis.

When neither the electronic nor nuclear spin is coupled to the molecular axis, one encounters the further complication of three possible coupling schemes:

1. Case $(b_{\beta N})$: **N** and **I** are coupled to form $\mathbf{F}_1$, then $\mathbf{F}_1$ and **S** couple to form the total angular momentum **F**.
2. Case $(b_{\beta S})$: **S** and **I** are coupled to form $\mathbf{F}_2$, then $\mathbf{F}_2$ and **N** couple to give **F**.
3. Case $(b_{\beta J})$: **N** and **S** are coupled to form **J**, then **J** and **I** couple to give **F**.

It may be noted that a subscript has been added to the designation of the coupling scheme which indicates the vector to which **I** is coupled. These three cases are illustrated in Fig. 8-1. Case $(b_{\beta N})$ is not expected to occur commonly because the much larger magnetic moment associated with the electron spin should couple much more strongly to N than does the nuclear magnetic moment.

The energy resulting from the first two terms of the interaction (8-6) can be obtained from the vector model for each of the three above cases. However, the last term of (8-6) requires a more complicated procedure such as multiplication of the matrices for $\mathbf{I}\cdot\mathbf{k}$ and $\mathbf{S}\cdot\mathbf{k}$. Frosch and Foley [686] have given all matrix elements necessary to evaluate the energy from (8-6) using the coupling schemes $(b_{\beta S})$ and $(b_{\beta J})$. For the

pure coupling case $(b_{\beta J})$, which is expected to be more common than $(b_{\beta S})$, the energies obtained are as follows:

When $S = \frac{1}{2}$:

$$\begin{aligned} W_{J=N+\frac{1}{2}} &= \left[\frac{2a\Lambda^2}{(N+1)(2N+1)} + \frac{b}{2N+1} + \frac{c}{(2N+1)(2N+3)}\left(1 + \frac{2\Lambda^2}{N+1}\right)\right]\mathbf{I}\cdot\mathbf{J} \\ W_{J=N-\frac{1}{2}} &= \left[\frac{2a\Lambda^2}{N(2N+1)} - \frac{b}{2N+1} + \frac{c}{(2N-1)(2N+1)}\left(1 - \frac{2\Lambda^2}{N}\right)\right]\mathbf{I}\cdot\mathbf{J} \end{aligned} \tag{8-10}$$

where

$$\mathbf{I}\cdot\mathbf{J} = \tfrac{1}{2}[F(F+1) - J(J+1) - I(I+1)]$$

When $S = 1$:

$$\begin{aligned} W_{J=N+1} &= \left[\frac{a\Lambda^2}{(N+1)^2} + \frac{b}{(N+1)} + \frac{c}{(N+1)(2N+3)}\left(1 + \frac{2\Lambda^2}{N+1}\right)\right]\mathbf{I}\cdot\mathbf{J} \\ W_{J=N} &= \left[\frac{a\Lambda^2(N^2+N-1)}{N^2(N+1)^2} + \frac{b}{N(N+1)} + \frac{c}{N(N+1)}\left(1 - \frac{2\Lambda^2}{N(N+1)}\right)\right]\mathbf{I}\cdot\mathbf{J} \\ W_{J=N-1} &= \left[\frac{a\Lambda^2}{N^2} - \frac{b}{N} + \frac{c}{N(2N-1)}\left(1 - \frac{2\Lambda^2}{N}\right)\right]\mathbf{I}\cdot\mathbf{J} \end{aligned} \tag{8-11}$$

Because of the accuracy of microwave measurements, noticeable deviations from the pure coupling cases listed above are to be expected, and intermediate coupling cases must be considered. In addition, when large coupling constants occur, N may not be a "good" quantum number, and second-order effects involving excitation of other N states must be considered. Frosch and Foley [686] give most of the matrix elements needed for calculation of the energy in these cases.

8-3. Examples of Magnetic Hyperfine Structure in Molecules with Electronic Angular Momentum. The molecule NO is a rather good example of Hund's case (a), its ground electronic state being $^2\Pi$. The nuclear magnetic moment of nitrogen and the molecular fields produce a hyperfine structure which follows case (a_β). The $^2\Pi_{\frac{3}{2}}$ state shows a hyperfine structure which is given by expression (8-9) with

$$a\Lambda + (b + c)\Sigma = 74.1 \text{ Mc}$$

[899], [686]. Hyperfine structure of the $^2\Pi_{\frac{1}{2}}$ state involves some additional effects which are discussed in Sec. 8-6. The common isotope of

oxygen, O^{16}, has zero spin and hence produces no hyperfine structure in NO. The spectrum of the $^2\Pi_{\frac{1}{2}}$ state of NO was actually measured in a strong magnetic field [435], [899] and will be discussed in more detail in Chap. 11 in connection with Zeeman effects.

The ground state of the oxygen molecule O_2 is $^3\Sigma$, and hence a good Hund's case (*b*). The coupling between S and N is approximately 60,000 Mc, whereas the hyperfine coupling between S and I for O^{17} in $O^{16}O^{17}$ is only a few hundred megacycles, so that $O^{16}O^{17}$ represents a rather good case ($b_{\beta J}$). For this molecule, having $S = 1$ and $\Lambda = 0$, the energies given by (8-11) simplify to

$$\begin{aligned} W_{J=N+1} &= \frac{\mathbf{I}\cdot\mathbf{J}}{N+1}\left(b + \frac{c}{2N+3}\right) \\ W_{J=N} &= \frac{\mathbf{I}\cdot\mathbf{J}}{N(N+1)}(b+c) \\ W_{J=N-1} &= \frac{\mathbf{I}\cdot\mathbf{J}}{N}\left(-b + \frac{c}{2N-1}\right) \end{aligned} \tag{8-12}$$

where

$$\mathbf{I}\cdot\mathbf{J} = \frac{F(F+1) - I(I+1) - J(J+1)}{2}$$

The expressions (8-11) or (8-12) have been found to fit very satisfactorily the observed hyperfine splitting of the microwave spectrum of $O^{16}O^{17}$ with the values $I = \frac{5}{2}$, $b = -102$ Mc, and $c = 140$ Mc [841]. Effects of the quadrupole moment of O^{17} and second-order effects involving decoupling of **S** from **N** can be shown to be less than about 1 Mc, which was the accuracy of the measurements, and hence were neglected.

Magnetic hyperfine structure has also been observed in OH [861], [971*a*], where coupling intermediate between case (*a*) and case (*b*) occurs.

The way in which a, b, and c depend on the electronic wave function of the molecule, and the information about NO and O_2 which can be derived from them are discussed in Chap. 9.

8-4. Nonlinear Molecules. Electrons in molecules which are not linear have no constant component of orbital angular momentum, since the molecular electric fields interfere with each component of the electrons' orbital motion. Hence in first-order approximation the interaction (8-1) is zero because the average value of each component of L is zero. The electron spin, however, may still be nonzero in such a molecule and may give a sizable hyperfine structure through interactions of types (8-3) and (8-5). No detailed evaluation of the energies resulting from (8-3) and (8-5) has been made for nonlinear molecules. However, coupling of the case ($b_{\beta J}$) type should be expected. For a given rotational state of angular momentum N due to end-over-end rotation, and given value of $\mathbf{J} = \mathbf{N} + \mathbf{S}$, the energy will have the form

$$W = 2C(\mathbf{I}\cdot\mathbf{J}) = C[F(F+1) - I(I+1) - J(J+1)] \tag{8-13}$$

Two examples of hyperfine structure in asymmetric molecules with electronic angular momentum have so far been observed, NO_2 and ClO_2. Both these molecules have an odd number of electrons and a value $S = \frac{1}{2}$. Selection rules for the hyperfine structure ($\Delta F = 0, \pm 1$) and relative intensities of the components are the same as with fine structure or other forms of hyperfine structure (see Chap. 5). Except for very small values of J, the dominantly strong hyperfine components are those for which ΔF is the same as ΔJ. Assuming ($b_{\beta J}$) coupling, the frequencies of the strong hyperfine components ($\Delta F = \Delta J$) for a particular transition can be obtained from (8-13) as

$$\nu = \nu_0 + \frac{F-J}{h}[(C_2 - C_1)(F-J) + C_2(2J_2+1) - C_1(2J_1+1)] \tag{8-14}$$

where J_1 and J_2 = total angular momentum exclusive of nuclear spin in lower and upper states, respectively
C_1 and C_2 = hyperfine constants in (8-13) for lower and upper states, respectively
ν_0 = a constant given primarily by the frequency of the rotational transition without hyperfine structure
$F - J$ = difference between F and J in either upper or lower states, which may have the values $I, I-1, \ldots, -I$

Expression (8-14) allows $2I + 1$ hyperfine components for each rotational transition and fine-structure component, *i.e.*, for each transition for given values of N and J in initial and final states, since $F - J$ can have $2I + 1$ different values. This is provided $I < J$; otherwise there are $2J + 1$ components. The components may be approximately equally spaced if $C_2 - C_1$ is small compared with

$$C_2(2J_2+1) - C_1(2J_1+1)$$

or may tend to converge when the two terms are comparable in magnitude. Figure 8-2 shows part of the spectrum of ClO_2, which can be seen to consist of two groups of four lines corresponding to the $\frac{3}{2}$ spin of the two Cl isotopes (O^{16} has zero spin). One group of hyperfine components in this spectrum has approximately equal spacings, whereas spacings of the second group increase markedly from left to right.

It has been suggested [497], [615] that two nearby sets of three lines in the spectrum of NO_2 are the $J = 6_{06} \longleftrightarrow 5_{15}$ transition, one set with $J = N + \frac{1}{2}$, and the other with $J = N - \frac{1}{2}$. Certainly each set of three must correspond to the hyperfine lines due to N^{14} ($I = 1$) of some rotational transition. However, the ratios of the separations between these

components has not yet been worked out in detail, and they do not seem to fit satisfactorily the approximate theoretical calculations which have been made. In addition, the Zeeman effect of these lines does not fit very well this assignment for the transitions [615].

8-5. Spin-spin Interaction between Nuclei. A nuclear magnetic moment may interact not only with an electron spin moment, but also with other nuclear magnetic moments which are present in a molecule. Expression (8-3) gives the interaction between two such dipole moments, from which the energy may be evaluated. This "spin-spin" interaction between nuclei is approximately 2000 times smaller than the hyperfine

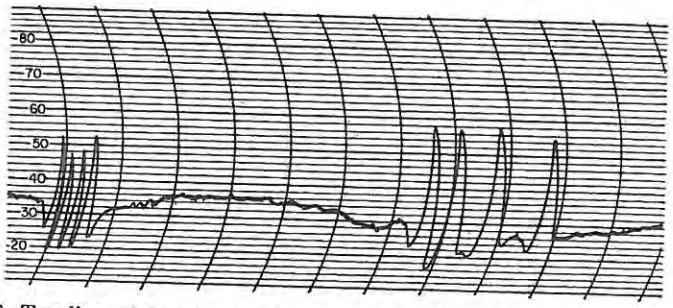

FIG. 8-2. Two lines of the asymmetric rotor ClO_2, each split into four components by magnetic hyperfine structure. (*From A. L. Schawlow and T. M. Sanders.*)

interactions in paramagnetic molecules because the magnetic moments associated with nuclei are this much smaller than those due to electrons. A rough magnitude for these effects can be obtained from μ_n^2/r^3, where μ_n is a nuclear magneton and r is the distance between two nuclei in a molecule. For a typical value of $r \approx 1.5$ A, μ_n^2/r^3 is only about 3 kc, which is so small that this "spin-spin" interaction is only rarely detected.

Because of their small size, nuclear "spin-spin" interactions will be of importance only for $^1\Sigma$ molecules, where the magnetic effect of electrons will also be very small. The vectors to be coupled are then the rotational angular momentum of the molecule J, and the spins of the two nuclei $\mathbf{I}_1$ and $\mathbf{I}_2$. If the nucleus having spin $\mathbf{I}_1$ is more strongly coupled to J than is the other nucleus, then the coupling scheme for a $^1\Sigma$ symmetric top is similar to case ($b_{\beta J}$) discussed above, but with N replaced by J, Λ by K, S by I, and J replaced by $\mathbf{F}_1 = \mathbf{I}_1 + \mathbf{J}$. This coupling scheme could occur when $\mathbf{I}_1$ is coupled by electric quadrupole effects to J, and would be the only pure coupling scheme of much interest for two nuclei. The energies are given for two nuclei in symmetric-top molecules by simplified forms of (8-10) and (8-11) or (8-12), or in more general form by Gunther-Mohr, Townes, and Van Vleck [931].

For $I_1 = \frac{1}{2}$:

$$W_{F_1=J+\frac{1}{2}} = \frac{2J\mu_1\mu_2(3\cos^2\theta - 1)}{(2J+1)(2J+3)I_2r^3}\left[\frac{3K^2}{J(J+1)} - 1\right]\mathbf{I}_2\cdot\mathbf{F}_1$$
$$W_{F_1=J-\frac{1}{2}} = \frac{-2(J+1)\mu_1\mu_2(3\cos^2\theta - 1)}{(2J-1)(2J+1)I_2r^3}\left[\frac{3K^2}{J(J+1)} - 1\right]\mathbf{I}_2\cdot\mathbf{F}_1 \tag{8-15a}$$

where r is the length of the vector between the two nuclei and θ is the angle between this vector and the molecular axis.

For $I_1 = 1$:

$$W_{F_1=J+1} = \frac{2J\mu_1\mu_2(3\cos^2\theta - 1)}{(J+1)(2J+3)I_2r^3}\left[\frac{3K^2}{J(J+1)} - 1\right]\mathbf{I}_2\cdot\mathbf{F}_1$$
$$W_{F_1=J} = -\frac{2\mu_1\mu_2(3\cos^2\theta - 1)}{J(J+1)I_2r^3}\left[\frac{3K^2}{J(J+1)} - 1\right]\mathbf{I}_2\cdot\mathbf{F}_1 \tag{8-15b}$$
$$W_{F_1=J-1} = -\frac{2(J+1)\mu_1\mu_2(3\cos^2\theta - 1)}{J(2J-1)I_2r^3}\left[\frac{3K^2}{J(J+1)} - 1\right]\mathbf{I}_2\cdot\mathbf{F}_1$$

A somewhat larger spin-spin effect, which occurs only when $K = 1$, will be discussed below in connection with the hyperfine structure of NH_3.

For intermediate coupling cases, the matrix elements given by Frosch and Foley [686] for the interaction of nuclear and electronic dipole moments may be used with a second nuclear moment replacing the electron spin S. The case of spin-spin interaction between two identical nuclei in a linear molecule, *i.e.*, two protons in H_2 or two deuterons in D_2, has been discussed in some detail by Kellogg, Rabi, Ramsey, and Zacharias [91], [98]. However, such cases are not of great interest to microwave spectroscopy because linear molecules in which two identical nuclei are found would usually have no dipole moment.

8-6. Effect of Hyperfine Structure on Λ Doubling—Hyperfine Doubling. So far we have discussed only those types of hyperfine structure which would be identical for the two energy levels of a Λ-type doublet. However, for Π states certain additional hyperfine effects may occur which are different for the two Λ-doubled states.

Different hyperfine structure for two members of a Λ doublet arises only from electron spin–nuclear spin interactions. A general understanding of the phenomenon can be obtained from a consideration of the distribution of electron density in the two Λ-doubled states of a $^2\Pi$ case (b) molecule. The part of the electron wave function depending on angle ϕ of rotation about the symmetry axis has the form $e^{i\phi} \pm e^{-i\phi}$ for the two Λ-doublet states of a Π electron. The probability distributions for the electron are then proportional to $\cos^2\phi$ and $\sin^2\phi$ for the two

states, giving large probabilities in the regions shown as shaded in Fig. 8-3. In Fig. 8-3*a*, corresponding to the lower Λ-doublet state with a $\sin^2 \phi$ distribution, the field of the electron at the nucleus is parallel to I (the electron magnetic moment is antiparallel to its spin S). In Fig. 8-3*b*, corresponding to the upper Λ-doublet state, the electron's field is directed oppositely to I. Hence the spin-spin interaction energy is quite different for the two cases. A reversal of I or S with respect to the

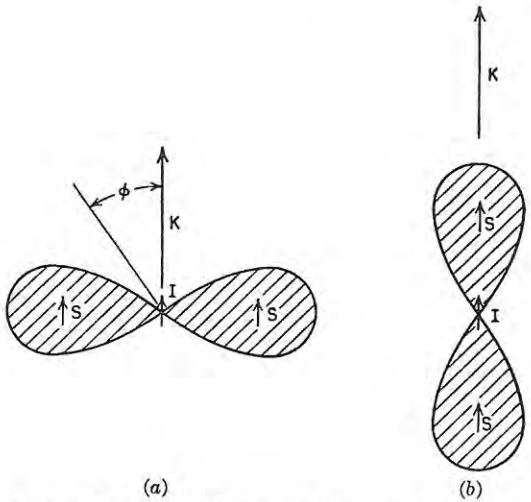

FIG. 8-3. Distribution of an unpaired electron in a $^2\Pi$ case (*b*) molecule for the two Λ-doublet states. The molecular axis is perpendicular to the page. Interaction energy between magnetic moments associated with the electron spin **S** and the nuclear spin **I** is different for the two cases. **K** is the angular momentum due to rotation of the molecule.

rotational angular momentum K of course reverses the sign of the hyperfine interaction energy for both Λ-doublet levels.

More formal reasoning shows that these effects are possible because the matrix elements of hyperfine interactions may connect states with a difference in Λ of ± 2 (and hence with differences in Ω [686]). The two Λ-doubled states actually involve equal mixtures of states with positive and negative values of Λ, in exact analogy with the *l*-doubled states discussed in Chap. 2 or the inversion states of Chap. 3. Hence in Hund's case (*a*) matrix elements connecting states with a difference in Ω of ± 1 or ± 2 give first-order (diagonal) effects for a $^2\Pi_{\frac{3}{2}}$ state but for no others. In case (*b*), first-order effects of such matrix elements are found for $^2\Pi$ or $^1\Pi$ states, but for no others.

The actual magnitude of the spin-spin interaction of the type described here, with case (*a*), case (*b*), or intermediate coupling, is given for a $^2\Pi$

state by [971*a*]

$$\Delta W = \pm \frac{d(X + 2 - A/B)}{4XJ(J+1)} (J + \tfrac{1}{2}) \mathbf{I} \cdot \mathbf{J} \tag{8-16}$$

where A = the fine-structure constant (energy = $A\mathbf{S} \cdot \mathbf{\Lambda}$)
B = the rotational constant
$X = \pm[(A/B)(A/B - 4) + 4(J + \frac{1}{2})^2]^{\frac{1}{2}}$
$d = 3\mu_0 \frac{\mu_I}{I} \left(\frac{\sin^2 \theta}{r^3}\right)_{av}$
r = distance from nucleus to electron
θ = angle between molecular axis and radius from nucleus to electron

The signs in (8-16) need explanation. When the constant A is positive (regular fine structure), then a positive sign for X is for the state which approaches $^2\Pi_{\frac{3}{2}}$ in case (*a*), and a negative sign for X for the state which approaches $^2\Pi_{\frac{1}{2}}$. When A is negative (inverted fine structure), a negative X gives the $^2\Pi_{\frac{3}{2}}$ state, and a positive X the $^2\Pi_{\frac{1}{2}}$ state. The upper (positive) sign in front of d in (8-16) applies to the upper Λ-doublet level of the state for which $J = N + \frac{1}{2}$ in the limiting case (*b*) or for both of the $^2\Pi_{\frac{3}{2}}$ and $^2\Pi_{\frac{1}{2}}$ states in case (*a*), and the lower sign to the lower state. The appropriate signs in front of d are the reverse in the state for which $J = N - \frac{1}{2}$ in the limiting case (*b*).

In case (*a*), $X = \pm A/B$, and (8-16) gives

$$\Delta W = \pm \frac{d(J + \frac{1}{2})}{2J(J+1)} \mathbf{I} \cdot \mathbf{J}$$

for the $^2\Pi_{\frac{1}{2}}$ state and $\Delta W = 0$ for the $^2\Pi_{\frac{3}{2}}$ state. The upper sign in front of d applies to the upper Λ-doublet state. In case (*b*), (8-16) gives

$$\Delta W = \pm \frac{d(J - \frac{1}{2})}{4J(J+1)} \mathbf{I} \cdot \mathbf{J} \qquad \text{for } J = N + \tfrac{1}{2}$$

and

$$\Delta W = \mp \frac{d(J + \frac{3}{2})}{4(J+1)} \mathbf{I} \cdot \mathbf{J} \qquad \text{for } J = N - \tfrac{1}{2}$$

This type of hyperfine effect we shall call hyperfine doubling, since it can remove the degeneracy from or further split Λ-type doublets. For hyperfine doubling to occur, one of the interacting spins must lie off the axis of the molecule [$\theta > 0$ in the definition of d under expression (8-16)]. This doubling can also occur in a symmetric-top molecule in a $^1\Sigma$ state if there is interaction between a nuclear spin on the axis and one off the axis. An example is NH_3, which will be discussed more fully below. Here interaction between the N and H nuclear moments splits the otherwise degenerate levels $K = \pm 1$.

Hyperfine doubling has been found in OH [861], which is a case of

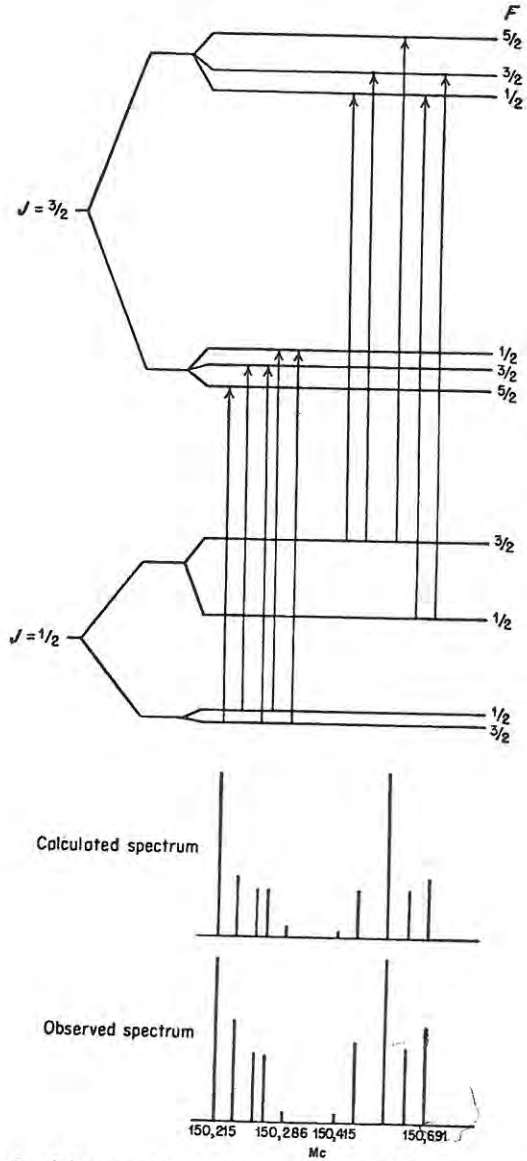

FIG. 8-4. Energy-level diagram and spectrum of the $J = \frac{3}{2} \leftarrow \frac{1}{2}$ rotational transition of the $^2\Pi_{\frac{3}{2}}$ state of $N^{14}O^{16}$. (*After Gallagher, Bedard, and Johnson* [924].)

intermediate coupling, and in the $^2\Pi_{\frac{3}{2}}$ state of NO [782*b*], [924], which is rather close to case (*a*). For OH, $d = 57$ Mc and for NO, $d = 112.6$ Mc. In both OH and NO, the hyperfine doubling is superimposed on a hyperfine structure of the form (8-6) which is identical for the two Λ doublets. Structures of the two lowest rotational states of NO are illustrated in Fig. 8-4. Here the hyperfine doubling is somewhat larger than other hyperfine effects and consequently has interchanged the order of the hyperfine levels in the two Λ-type doublets of each rotational state.

8-7. Electronic Angular Momentum in $^1\Sigma$ Molecules and Its Contributions to Molecular Energy. Although molecules in $^1\Sigma$ states are often said to have no electronic angular momentum, there is in fact a small electronic angular momentum when a molecule of this type is rotating. For example, consider the motion of closed shells of electrons associated with a nucleus. These move with the nucleus during rotation of the molecule and hence possess angular momentum. Their rotation produces magnetic fields which can give magnetic hyperfine structure. A more interesting and complex case is a valence electron which is not definitely associated with one nucleus. Valence electrons may only partly rotate with the molecule, but still usually produce the dominating magnetic fields at the nuclei. Their behavior also produces complications in the purely mechanical rotational energy of the molecule.

In order to examine the behavior of electrons in a rotating molecule, we shall start with the energy or Hamiltonian for electrons in a molecule with fixed nuclei, which is of the form

$$\begin{aligned} H_e &= \frac{1}{2m} \sum_n [p_{nx}^2 + p_{ny}^2 + p_{nz}^2] + V \\ &= \frac{1}{2m} \sum_n \sum_g p_{ng}^2 + V \end{aligned} \tag{8-17}$$

where m is the electron mass, p_{ng} is the gth component of the momentum of the nth electron in Cartesian coordinates, and V is the potential energy of all the electrons. The energy of the electrons in the ground state may be found in principle by solving Schrödinger's equation with (8-17) as the Hamiltonian. Let this energy be W_{e0}.

If the molecule rotates, the Hamiltonian for the electrons is of the same form, but p_{ng} refers then to a Cartesian component of the generalized momentum of the nth electron referred to a set of axes fixed in the molecule and rotating with it. This momentum is not simply the mass times the velocity in the rotating coordinates, and must be found by the general method of differentiating the Lagrangian with respect to the velocity. The important point for our purposes, however, is that the Hamiltonian in rotating coordinates has the same form (8-17) as long as the coordinate system is Cartesian. The nuclei also acquire kinetic energy as a result of

rotation, which may be written

$$H_n = \tfrac{1}{2}\sum_g \frac{O_g^2}{A_g} \tag{8-18}$$

where A_g is the moment of inertia of the system of nuclei in the molecule about one of the principal axes, and O_g is their angular momentum about this axis. We shall for simplicity assume that the nuclei are rigidly fixed in the molecule and disregard possible vibrational energies. The component J_g of the total angular momentum about a principal axis of inertia is the sum of that due to the nucleus O_g and the small angular momentum L_g of the electrons, or

$$O_g = (J_g - L_g)\hbar \tag{8-19}$$

where J_g and L_g are in units of $\hbar$.

Combining (8-17), (8-18), and (8-19), the Hamiltonian for the rotating system becomes

$$H = \tfrac{1}{2}\sum_g \frac{\hbar^2 J_g^2}{A_g} - \sum_g \frac{\hbar^2 J_g L_g}{A_g} + \tfrac{1}{2}\sum_g \frac{\hbar^2 L_g^2}{A_g} + \frac{1}{2m}\sum_n\sum_g p_{ng}^2 + V \tag{8-20}$$

If the electrons are truly in a $^1\Sigma$ state, there is no electronic angular momentum and L_g is zero, so that the energy given by (8-20) is just the sum of the energy due to the last two terms, and that due to the first term. This first term gives the rotational energies W_R of a rigid rotor, but one without electrons since A_g is the moment of inertia of the nuclei only. The total energy in this approximation is then just

$$W_0 = W_R + W_{e0} \tag{8-21}$$

It is only by allowing for perturbations of the ground $^1\Sigma$ electron states by the term $\sum_g (\hbar^2 J_g L_g/A_g)$ that the energy associated with the contribution of the electrons to the moment of inertia of the molecule can be obtained. This perturbation introduces a small probability for electronic angular momentum states other than $^1\Sigma$; hence it produces some electronic angular momentum which affects the rotational energy of the molecule. To a good approximation, the third term of (8-20), $\frac{1}{2}\sum_g (\hbar^2 L_g^2/A_g)$, is a constant of the molecular rotation. Rotation will indeed produce perturbations of this term, but they are too small to be significant at present.

Since the perturbation $\sum_g (\hbar^2 J_g L_g/A_g)$ introduces electronic angular momentum, we must take into account the various other types of energy terms connected with electronic angular momentum in order to complete the Hamiltonian (8-20). One of these is the interaction between a

nuclear magnetic moment and the magnetic fields produced by an electronic angular momentum. Such interactions are similar in principle to the magnetic hyperfine structure due to orbital motion of an electron in an atom, and may be written as in (5-49) after letting $\mathbf{j} = \mathbf{L}$,

$$a\mathbf{I}\cdot\mathbf{L}' = a\sum_g I_g L_g' \tag{8-22}$$

where $\mathbf{L}'$ is the electronic orbital angular momentum about the nucleus of spin $\mathbf{I}$, and $a = (2\mu_I\mu_0/I)(1/r^3)_{av}$. However, in a molecule, $\mathbf{L}$ is not a constant of the motion, and hence both $\mathbf{L}'$ and $(1/r^3)_{av}$ must be averaged over the electronic wave function. It should be noted too that (8-22) contains $\mathbf{L}'$, the angular momentum about a particular nucleus, rather than $\mathbf{L}$, the angular momentum with respect to the center of mass of the molecule. $\mathbf{L}'$ and $\mathbf{L}$ are, of course, closely related.

Another common interaction associated with electronic angular momentum is the Zeeman effect due to an external applied field H. The interaction energy is given by

$$\mu_0\mathbf{H}\cdot\mathbf{L} = \mu_0\sum_g H_g L_g \tag{8-23}$$

where μ_0 is the Bohr magneton.

Although we shall not be concerned here with all possible types of magnetic interaction, still another interaction which we shall include is the direct interaction between the magnetic moment of the nucleus and the external field H. This is

$$-\boldsymbol{\mu}_I\cdot\mathbf{H} = -\sum_g \mu_g H_g \tag{8-24}$$

where μ_I is the nuclear magnetic moment. Adding the three terms (8-22), (8-23), and (8-24) and omitting the constant term $\frac{1}{2}\sum_g \hbar^2(L_g^2/A_g)$ in (8-20), the Hamiltonian becomes

$$H = \frac{1}{2m}\sum_n\sum_g p_{ng}^2 + V + \tfrac{1}{2}\sum_g \frac{\hbar^2 J_g^2}{A_g} + \sum_g\left(\mu_0 H_g - \frac{\hbar^2 J_g}{A_g}\right)L_g + a\mathbf{I}\cdot\mathbf{L} - (\boldsymbol{\mu}_I\cdot\mathbf{H}) = H_0 + H' \tag{8-25}$$

Here H_0 represents the first three terms which are the main parts of the Hamiltonian. H' consists of the remaining small perturbing terms.

It may be seen from (8-25) that the effect of a magnetic field on electrons is just equivalent to that of molecular rotation since they both enter (8-25) only in the factor $\left(\mu_0 H_g - \frac{\hbar^2 J_g}{A_g}\right)$. Thus the effect of a mag-

netic field H_g is equivalent to a rotation $\frac{-\hbar^2 J_g}{\mu_0 A_g}$. Since $\hbar J_g = \omega A_g$, where ω is the angular velocity, the rate of angular rotation which produces an effect on the molecular electrons precisely the same as that of the field H_g is $\omega_g = \frac{eH_g}{2mc}$. This is Larmor's theorem, and is responsible for the direct connection (1 − 47) between L uncoupling and the molecular g factor due to electrons.

The first-order correction to the energy given by H_0 is the average value of H' in the $^1\Sigma$ state of the molecule. The parts of H' proportional to L have an average value of zero, so that the only term of H' which gives an energy in first order is $-\boldsymbol{\mu}_I \cdot \mathbf{H}$. The second-order correction to the energy is given as usual by

$$W' = \sum_n \frac{|(0|H'|n)|^2}{W_0 - W_n} \tag{8-26}$$

where W_0 is the energy of the unperturbed state, and W_n the energy of the nth excited electronic state. $(0|H'|n)$ is the matrix element of H' between the unperturbed and an excited electronic state.

To illustrate the nature of the various terms in (8-26), let us assume that only one excited state is of importance so the sum over n may be omitted. Second-order terms in $\boldsymbol{\mu}_I \cdot \mathbf{H}$ will be assumed negligible, as they usually are.

$$\begin{aligned} W' = {} & \frac{|(0|a\mathbf{I}\cdot\mathbf{L}|n)|^2}{W_0 - W_n} + \sum_g \sum_{g'} \hbar^4 J_g J_{g'} \frac{(0|L_g|n)(n|L_{g'}|0)}{A_g A_{g'}(W_0 - W_n)} + \frac{|(0|\mu_0 \mathbf{H}\cdot\mathbf{L}|n)|^2}{W_0 - W_n} \\ & + \sum_{g'} \sum_g \mu_0 I_g H_{g'} \frac{(0|aL_g'|n)(n|L_{g'}|0) + (0|L_{g'}|n)(n|aL_g'|0)}{W_0 - W_n} \\ & - \sum_{g'} \sum_g \frac{\hbar^2 I_g J_{g'}}{A_{g'}} \frac{(0|aL_g'|n)(n|L_{g'}|0) + (0|L_{g'}|n)(n|aL_g'|0)}{W_0 - W_n} \\ & - 2\sum_{g'} \sum_g \mu_0 \frac{\hbar^2 J_g H_{g'}}{A_g} \frac{(0|L_g|n)(n|L_{g'}|0)}{W_0 - W_n} \end{aligned} \tag{8-27}$$

Expression (8-27) appears rather formidable partly because it applies to the general asymmetric top and hence the sums over coordinate directions g and g' cannot be very much simplified. Its complexity is due also to the fact that each of the six terms of (8-27) corresponds to a different physical effect. These may be and usually are discussed separately.

The second term in (8-27) is the only one which does not involve magnetic effects. It is proportional to the square of the molecular angular momentum J, and represents the contribution of the electrons to the moment of inertia of the molecule or to the kinetic energy of rotation. Since $W_0 - W_n$ is negative, this term is negative and corresponds to a

decrease in the energy of rotation. This is to be expected since the electrons should add to the moments of inertia A_g of the bare nuclei. It will be shown below that, at least for electrons closely bound to the nuclei, this term does in fact have the magnitude to be expected from the electronic contribution to the moment of inertia.

The first term in (8-27) is called the pseudo quadrupole effect [192] because it has the same form as a quadrupole interaction between I and the molecular electric fields. In a simple $^1\Sigma$ linear molecule, for example, L may be thought of as precessing around the molecular axis, so that $(\mathbf{I}\cdot\mathbf{L})^2$ becomes proportional to the square of the cosine of the angle between I and the molecular axis, which is the same dependence on this angle shown by an electric quadrupole interaction. Hence experimentally the effect of this term cannot simply be distinguished from that of a nuclear quadrupole interaction. Fortunately, however, the pseudo quadrupole interaction is almost always negligibly small, since from (8-27) it is proportional to the square of a magnetic hyperfine interaction divided by the separation between electronic levels. It is hence not usually larger than a few cycles per second.

The pseudo quadrupole effect may be regarded as a magnetic polarization of the molecule by the nuclear magnetic moment, and then an interaction between the resulting molecular magnetic field and the nuclear moment. In principle the interaction discussed by Hebb (*cf.* page 182) in ρ-type tripling is identical with this nuclear effect, but it involves fine-structure rather than hyperfine-structure interactions and is consequently enormously greater.

The third term of (8-27) is an energy associated with the magnetic susceptibility or polarization of the molecule by an external field (*cf.* [38], p. 227) and is not of great interest here. It has no dependence on molecular rotation and corresponds to the interaction between the field H and the molecular magnetic dipole induced by H.

The fourth term of (8-27),

$$\sum_{g'} \sum_g \mu_0 I_g H_{g'} \frac{(0|aL_g'|n)(n|L_{g'}|0) + (0|L_{g'}|n)(n|aL_g'|0)}{W_0 - W_n}$$

also does not depend on the molecular rotation. It corresponds to a magnetic polarization of the molecule by an external field H, or creation of electronic angular momentum L as a result of this field, and then an interaction between the nuclear magnetic moment and the magnetic field produced by the angular momentum L. These effects are usually unimportant to microwave spectroscopy of gases, since they are normally smaller than the direct interaction $\boldsymbol{\mu}_I \cdot \mathbf{H}$ between an external field H and a nuclear magnetic moment by a factor of 10^4. However, for nuclear magnetic resonances in solids or liquids such effects are measurable and

are generally called "chemical effects," since they do not depend simply on the nucleus, but vary from one molecule to the next [569], [515].

The remaining two terms of (8-27),

$$-\sum_{g'}\sum_{g}\frac{\hbar^2 I_g J_{g'}}{A_{g'}}\frac{(0|aL_g'|n)(n|L_{g'}|0)(0|L_{g'}|n)(n|aL_{g'}'|0)}{W_0 - W_n}$$

and $-2\sum_{g'}\sum_{g}\frac{\mu_0\hbar^2 J_g H_{g'}}{A_{g'}}\frac{(0|L_g|n)(n|L_{g'}|0)}{W_0 - W_n}$, are both dependent on the rotational angular momentum J of the molecule and are interesting terms from the point of view of microwave spectroscopy. They may be thought of as due to an excitation of electronic orbital angular momentum L by the rotation J. This electronic angular momentum produces an internal molecular magnetic field which interacts with the nuclear magnetic moment, and also a molecular magnetic moment which interacts with the external field H. The latter term, linearly proportional to H and to J, is a Zeeman effect which will be discussed at length in Chap. 11. The term linearly proportional to I and J is part of the common variety of magnetic hyperfine structure in $^1\Sigma$ molecules which for simple linear molecules reduces to the form $C_I\mathbf{I}\cdot\mathbf{J}$, where C_I is a constant dependent on the molecule. This interaction is often called the "I dot J" interaction and will be discussed at length below.

8-8. Effect of Electronic Motion on Rotational Energy. We shall digress from magnetic effects briefly to examine parts of the energy (8-26) of the type illustrated by the second term of (8-27), *i.e.*,

$$W_2' = \sum_{g}\sum_{g'}\frac{\hbar^2 J_g J_{g'}}{A_g A_{g'}}\sum_{n}\frac{\hbar^2(0|L_g|n)(n|L_{g'}|0)}{W_0 - W_n} \tag{8-28}$$

These terms give the effect of electrons on the rotational energy of the molecule, and illustrate some of the properties of the terms involved in magnetic hyperfine structure. For simplicity, consider a linear molecule and take the z direction along the molecular axis. Then $L_z = 0$, and the terms of (8-28) of the type

$$\sum_{n}\frac{\hbar^2}{W_0 - W_n}[(0|L_x|n)(n|L_y|0) + (0|L_y|n)(n|L_x|0)]$$

are also zero. The latter may be shown by a rotation of the molecule about the z axis by $\pi/2$. After the rotation, x becomes y, and y becomes $(-x)$. Since the directions x and y are equivalent, this term has changed sign but cannot have changed value, so that it must equal zero. The only nonzero terms of (8-28) are therefore

$$W_2' = \hbar^2\frac{J_x^2}{A_x^2}\sum_{n}\frac{\hbar^2|(0|L_x|n)|^2}{W_0 - W_n} + \hbar^2\frac{J_y^2}{A_y^2}\sum_{n}\frac{\hbar^2|(0|L_y|n)|^2}{W_0 - W_n}$$

or, since the x and y directions are equivalent,

$$W_2' = \hbar^2\frac{J(J+1)}{A^2}\sum_{n}\frac{\hbar^2|(0|L_x|n)|^2}{W_0 - W_n} \quad \text{or}$$

$$4J(J+1)\hbar^2B^2\sum_{n}\frac{|(0|L_x|n)|^2}{W_0 - W_n} \tag{8-29}$$

where $J(J+1) = J_x^2 + J_y^2$ is the square of the total angular momentum, $A = A_x = A_y$, and $B = h/8\pi^2 A$ is the rotation constant.

The "slippage" of electrons with respect to the nuclei as the molecule rotates may be seen from (8-29). If the electron distribution and the fields were completely spherical about the center of mass, then $(0|L_x|n)$ would be zero. The fractional part of the valence electrons which is spherically distributed may be considered, as noted in Chap. 1, to slip with respect to the molecule and not contribute to the rotational energy.

The inner shells of electrons attached to a nucleus are not at all spherical with respect to the center of mass and may be more easily discussed with a coordinate system centered at this nucleus. Let r be the distance from the center of mass to the nucleus. Then

$$\hbar L_x = \hbar L_x' - rp_y \tag{8-30}$$

where L_x' is the electronic angular momentum (in units of $\hbar$) of the spherical shell about the nucleus in question and p_y is the linear momentum in the y direction. But if we consider only a spherical closed shell of electrons in the spherical field of a nucleus, $(0|L_x'|n) = 0$ for any n, so that, using (8-30), for closed shells

$$\sum_{n}\frac{\hbar^2}{W_0 - W_n}|(0|L_x|n)|^2 = r^2\sum_{n}\frac{|(0|p_y|n)|^2}{W_0 - W_n} \tag{8-31}$$

This can be simplified by the general identity* for any particle of mass m

$$\sum_{n}\frac{|(0|p_y|n)|^2}{W_0 - W_n} = \frac{-m}{2} \tag{8-32}$$

*This identity may be proved as follows:

$$p_y = m\frac{dy}{dt} = \frac{m}{i\hbar}(yH - Hy)$$

or

$$(0|p_y|n) = \frac{mi}{\hbar}(W_0 - W_n)(0|y|n)$$

(*cf.* [408], p. 139).

Hence

$$\sum_{n}\frac{(0|p_y|n)(n|p_y|0)}{W_0 - W_n} = \sum_{n}\frac{mi}{\hbar}\frac{(0|y|n)(n|p_y|0) - (0|p_y|n)(n|y|0)}{2} = \frac{-m}{2}$$

since $yp_y - p_y y = i\hbar$.

Hence (8-29) becomes for N electrons in spherical orbits around a nucleus which is a distance τ from the center of mass

$$W'_2 = \frac{-\hbar^2 J(J+1)Nm\tau^2}{2A^2} \tag{8-33}$$

This is a small decrease in the energy of rotation due to the presence of the electrons which should be added to the kinetic energy of the nuclei. Thus

$$W = W_0 + W'_2 = \frac{\hbar^2 J(J+1)}{2A} - \frac{\hbar^2 J(J+1)}{2A^2} Nm\tau^2 \approx \frac{\hbar^2 J(J+1)}{2(A + Nm\tau^2)} \tag{8-34}$$

Of course, (8-34) as written includes the effect of only those electrons "bound" to one particular nucleus, and all other closed electron shells should be similarly treated. This expression is sufficient to show, however, how the bound electrons add to the moment of inertia, and that, as stated in Chap. 1, the spherical closed electron shells in a molecule behave as if they follow the nuclei during molecular rotation, but remain fixed in orientation in space like the chairs on a rotating Ferris wheel.

For the valence shell of electrons, the sum in (8-29) cannot be so easily evaluated. One approximation which is often made involves the "pure-precession" hypothesis. In this case the electronic angular momentum L is assumed to have a fixed value and to precess around the molecular axis with a projection of zero on this axis for the ground state. The only low-lying electronic state for which $(0|L_x|n)$ is not zero is the Π state corresponding to a unit projection of L on the molecular axis. In this case $|(0|L_x|n)|^2 = L(L+1)/4$, so that (8-29) may be written

$$W'_2 = -J(J+1)B^2\left[8\pi^2 \sum_s N_s m\tau_s^2 + \frac{L(L+1)h^2}{(W_\Pi - W_\Sigma)}\right] \tag{8-35}$$

where the sum is over all "bound" electrons in closed shells around nuclei of distance τ_s from the center of gravity of the molecule, and J is the quantum number for the total angular momentum. The last term of (8-35) gives the contribution of valence electrons under the restrictive assumption of pure precession. $W_\Pi - W_\Sigma$ is the excitation energy of the lowest electronic state.

In nonlinear polyatomic molecules the full form (8-28) must be used to obtain the effect of electrons on the rotational kinetic energy. However, for almost all purposes sufficient accuracy may be obtained by assuming the electrons associated with each nucleus to be located at the nucleus and using moments of inertia which include these electrons in calculating rotational energy. Only for the valence electrons does this involve some small error, and usually only by very accurate measurements on diatomic molecules can such small effects be detected. In more complex molecules other inaccurately known effects tend to mask these errors.

8-9. Magnetic Hyperfine Interaction (I · J) in $^1\Sigma$ Molecules. We shall examine now in more detail the term in (8-27) which is linearly proportional to I and J, and which represents a magnetic hyperfine interaction between a nucleus and electrons even in $^1\Sigma$ molecules. It is

$$W'_5 = -\sum_n \sum_{g'} \sum_g \frac{\hbar^2 I_g J_{g'}}{A_{g'}} \frac{(0|aL'_g|n)(n|L_{g'}|0) + (0|L_{g'}|n)(n|aL'_g|0)}{W_0 - W_n} \tag{8-36}$$

where the summation over all excited states n has been included rather than over only one state as in (8-27).

Now an angular velocity about the center of mass of the molecule is equivalent to the same angular velocity about any nucleus in the molecule plus an appropriate instantaneous linear velocity v. The magnetic fields produced at the nucleus by rotation about the two different points should differ only by the effect of the velocity v. At the nucleus the average electric field is zero (because there is no average force on the nucleus at equilibrium), so that the velocity v in fact produces no magnetic field at the nucleus [magnetic field $\approx (v/c) \times$ electric field]. Hence it may be expected that the angular momentum $L_{g'}$ about the center of mass can be replaced in (8-36) by the angular momentum $L'_{g'}$ about the nucleus in question without changing the magnetic energy given by this expression.* Furthermore, since the quantity a depends on $1/r^3$, but not on the angular position of the electron with respect to the nucleus, the part of the matrix element which depends on a may be factored out, that is, $(0|aL'_g|n) = a_{0n}(0|L'_g|n)$. a_{0n} may be taken as real so that $a_{0n} = a_{n0}$. Hence (8-36) becomes

$$W'_5 = -2\sum_n \sum_{g'} \sum_g \frac{\hbar^2 I_g J_{g'}}{A_{g'}} a_{0n} \frac{(0|L'_g|n)(n|L_{g'}|0)}{W_0 - W_n} \tag{8-37}$$

The nature of expression (8-37) is perhaps most easily understood by applying it to the simple case of a diatomic molecule. It is evident that closed shells of electrons about the nucleus being considered do not contribute magnetic hyperfine structure, since for them $(0|L_g|n)$ is zero. Closed shells of electrons around other nuclei can be treated in a way similar to that used in reducing (8-28) for a diatomic molecule, and their contribution to (8-37) can be shown to be

$$-\frac{\mu_I \hbar \mathbf{I} \cdot \mathbf{J}}{IA} \sum_s \frac{e}{cr_s} = -4\pi \frac{\mu_I}{I} B\mathbf{I} \cdot \mathbf{J} \sum_s \frac{e}{cr_s}$$

Here e is the electron charge in esu (negative sign) and r_s is the distance of the center of the sth electron distribution from the nucleus of spin I

* For a more detailed discussion, see [686], Secs. 7 and 8.

and g factor g_I. Valence electrons which are not spherically distributed about any nucleus cannot be so simply treated and their contributions must be left in essentially the form (8-37). The charges on nuclei contribute in the same way as those of electrons in closed shells about the nuclei, as may be seen by formally considering their changes to be due to closed shells of positively charged electrons tightly bound to the nucleus. Therefore for the diatomic or linear molecule, the combined effect of electrons from (8-37) and the nuclear charges gives

$$W'_5 + \text{effects of nuclear charges} = \mathbf{I}\cdot\mathbf{J}B\left[4h\sum_n \frac{a_{0n}|(0|L_x|n)|^2}{W_n - W_0} - 4\pi\frac{\mu_I}{I}\sum_s \frac{q_s}{cr_s}\right] \quad (8\text{-}38)$$

where r_s is the distance between the nucleus for which (8-38) gives the magnetic hyperfine energy and any other nucleus in the molecule, and q_s is the net charge of the sth nucleus plus the electrons which are in closed shells about it. Assuming the pure precession approximation, (8-38) may be written

$$W'_5 + \text{nuclear effects} = \mathbf{I}\cdot\mathbf{J}B\left[\frac{ha_{\Sigma\Pi}L(L+1)}{W_\Pi - W_\Sigma} - 4\pi\frac{\mu_I}{I}\sum_s \frac{q_s}{cr_s}\right] \quad (8\text{-}39)$$

The general form of the magnetic hyperfine interaction of a nucleus in a linear $^1\Sigma$ molecule (with no vibrational angular momentum) is, from (8-38)

$$W_{mag} = C_I\mathbf{I}\cdot\mathbf{J} \quad (8\text{-}40)$$

where the constant C_I is dependent on molecular parameters shown in (8-38). This type of interaction was first found in the hydrogen molecule by the use of molecular-beam techniques [91], and the constant C_I has now been evaluated for a number of molecules by both molecular beam and the usual microwave spectroscopic techniques. Table 8-1 shows the values of C_I for molecules so far measured, which vary from near 1 kc to somewhat greater than 100 kc. A few additional values of C_I have been reported for the alkali halides from measurements of line widths in molecular-beam magnetic resonance experiments. However, such measurements are subject to uncertainties in interpretation and hence these values have been omitted from Table 8-1. White [999] has shown that a number of interesting trends can be established from present measurements of C_I.

Examples of $\mathbf{I}\cdot\mathbf{J}$ *Interaction.* Usually μ_I for the nucleus is positive, and hence the first term of (8-38) due to the valence electrons is positive, while the second term due to nuclei and bound electrons is negative. In most cases C_I is positive. O^{17} and Se^{79} are the only nuclei with a negative μ_I for which C_I has been measured. It may be seen from Table 8-1 that,

with the exception of hydrogen nuclei in H_2, these are precisely the only cases where C_I has been found to be negative. Hence except in the special cases of hydrogen the first term in (8-38), due to excitation of the valence electrons by rotation, always dominates.

TABLE 8-1. VALUES OF MAGNETIC HYPERFINE CONSTANTS C_I IN $^1\Sigma$ MOLECULES (Magnetic hyperfine energy = $C_I\mathbf{I}\cdot\mathbf{J}$)

Molecule	Nucleus	C_I, kc	$\frac{C_I}{g_I B(1/r^3)_{av}}$, 10^{-33} cm^3	Reference
Li^6F	F^{19}	37.3 ± 0.3	3.4	[753]
Li^7F	F^{19}	32.9 ± 0.1	3.3	[999]
KF	F^{19}	0 ± 10	0 ± 7	[463]
$Rb^{85}F$	F^{19}	11 ± 3	10	[476]
$Rb^{87}F$	F^{19}	14 ± 4	13	[476]
CsF	F^{19}	16 ± 2	14	[331]
Li^7F	Li^7	2.2 ± 0.6	90	[999]
DI	I^{127}	140	11	[999]
ClF	Cl^{35}	22 ± 3	54	[366] [999]
CS	S^{33}	19 ± 15	54	[999]
$Tl^{205}Cl^{35}$	Cl^{35}	1.4 ± 0.1	20	[676*b*]
$Tl^{205}Cl^{35}$	Tl^{205}	73 ± 2	110	[676*b*]
H_2	H	−113.904 ± 0.030	−40.8	[91] [716*a*] [807]
HD	H	−87.00 ± 0.85	−41.4	[91*a*]
HD	D	−12.6 ± 0.3	−39.0	[91*a*]
D_2	D	−8.445 ± 0.056	−39.1	[91*a*] [716*a*] [807]
OCS	O^{17}	−4.0 ± 1.5	28	[999]
OCS	S^{33}	2 ± 1	23	[999]
OCSe	Se^{79}	−3.2 ± 1.0	42	[999]
HCN	N^{14}	10 ± 4	34	[999]
DCN	N^{14}	8 ± 3	33	[999]
$Cl^{35}CN^{14}$	N^{14}	2.5 ± 0.8	62	[999]
$Cl^{35}CN^{14}$	Cl^{35}	3.0 ± 1.0	19	[999]
$Cl^{35}CN^{15}$	Cl^{35}	3.5 ± 0.6	24	[999]
$Cl^{35}CN^{15}$ (in excited state $v_2 = 1$)	Cl^{35}	8 ± 5	52	[999]
NH_3	N^{14}	$6.1 \pm 0.2 + (0.4 \pm 0.2)\frac{K^2}{J(J+1)}$	3.1	[999]
NH_3	H	See discussion in text		[999]

The proportionality of C_I to μ_I/I or to the gyromagnetic ratio

$$g_I = \frac{\mu_I}{I\mu_n}$$

and the rotational constant B is illustrated by comparing its value for H_2 and for D_2. The ratio of $g_I B$ for the two cases is 13.0, whereas the

ratio of the value of C_I observed is 13.5. The small difference between these two values is due to the slightly different average internuclear distances for H_2 and D_2.

Since the dominant contribution to C_I in all molecules except H_2 comes from the valence electrons,

$$\frac{C_I}{g_I B} \text{ should be proportional to } \sum_n \frac{|(0|aL_x|n)|^2}{W_n - W_0}$$

To a rough approximation we may assume that only the first excited state is important in this summation and that a is proportional to the average value of $1/r^3$ for a valence p electron of the atom. Hence

$$\frac{C_I}{g_I B(1/r^3)_{av}} \text{ should be proportional to } \frac{|(0|L_x|1)|^2}{W_1 - W_0}$$

It may be seen from Table 8-1 that this quantity is of the same order of magnitude for most molecules.

For a given atom it may be assumed that the matrix elements $(0|aL_x|n)$ are approximately the same in a series of chemically similar molecules. The value of C_I for fluorine in LiF, RbF, and CsF represents such an example. The fact that $\frac{C_I}{g_I B(1/r^3)_{av}}$ for F increases regularly in progressing from LiF to the larger molecules RbF and CsF is evidently due to decreasing separations $W_n - W_0$ of the energy levels which can be expected for the larger molecules. Another similar series is provided by the values of $\frac{C_I}{g_I B(1/r^3)_{av}}$ for Cl in CH_3Cl, SiH_3Cl, and GeH_3Cl [999]. However, for these cases C_I is not yet very accurately known.

For O^{17} and S^{33} in the same molecule OCS, one would expect $\frac{C_I}{g_I B(1/r^3)_{av}}$ to be essentially the same, since O and S are very similar chemically, and hence their electronic surroundings are very similar. Table 8-1 shows that this expectation is correct. On the other hand, Tl and Cl in the same molecule TlCl as well as Cl and N in ClCN have very different values of $\frac{C_I}{g_I B(1/r^3)_{av}}$ since their electronic surroundings are quite dissimilar.

Certain types of molecular rotation may result in relatively little electronic angular momentum. Such is the case for the rotation of H_2, where the "slip effect" is quite important. Another case occurs in the bending mode of ClCN ($v_2 = 1$). Here the bent ClCN molecule rotates very rapidly about the symmetry axis with a frequency roughly 100 times greater than the normal molecular rotational frequency. However, since the bending is slight, the rapid rotational motion does not excite much electronic angular momentum. This is shown by the fact that C_I in the bending mode is not much greater than C_I for the ground vibrational state of ClCN.

Relation between C_I and g_J. Even though magnetic hyperfine-structure interactions are complex and involve excited electronic states, the discussion above shows that reasonable correlations with certain molecular properties can be observed. Furthermore, the coefficients C_I are connected with other measurable quantities. If one low-lying excited electron state dominates in the sum $\sum_n \frac{|(0|L_x|n)|^2}{W_n - W_0}$, then C_I may be expected to be closely related to the molecular magnetic moment produced by electron excitation. For, from (8-38), (11-15), and (11-19),

$$C_I = \frac{g_J \mu_n a_{0n}}{\mu_0} = 2 g_J g_I (\mu_n)^2 \left(\frac{1}{r^3}\right)_{av} \tag{8-41}$$

Here g_J strictly includes only the contributions to g_J from the excited valence electrons. There should in addition be a connection between C_I and part of the rotational energy due to electrons as may be seen by comparing (8-29) or (8-35) with (8-39). OCS and OCSe are the only linear molecules in which both quantities C_I and g_J have already been measured so that a test of the relation (8-41) can be made. Assume that the electron which produces g_J spends half its time on the oxygen and half its time on the sulfur atom in OCS, so that $(1/r^3)_{av}$ is just one-half that for an atomic electron in each case. Then (8-41) predicts from the measured value $g_J = 0.025$ for OCS that C_I for O^{17} should be -2.3 kc and that for S^{33} C_I should be 1.5 kc. These values are very satisfactorily close to the measured values given in Table 8-1. Similarly, one may calculate the values of C_I for Se^{79} from relation (8-41) and the observed value of g_J for OCSe, which is $g_J = 0.019$. The result is $C_I = -1.4$ kc, again in reasonable agreement with the observed value of C_I for Se^{79} found in Table 8-1.

8-10. Magnetic Hyperfine Structure of Nonlinear Molecules in $^1\Sigma$ States. We now return to the general form (8-36) for any molecule. Since the hyperfine energy is a scalar and linearly proportional to the components of **I** and of **J**, it must be of the form

$$W_{mag} = \mathbf{I} \cdot \mathfrak{A} \cdot \mathbf{J} = \sum_{gg'} \mathfrak{A}_{gg'} I_g J_{g'} \tag{8-42}$$

where $\mathfrak{A}$ is a dyadic, or $\mathfrak{A}_{gg'}$ are components of a tensor which can be seen to be symmetric from inspection of (8-36). For a nucleus on the axis of a symmetric-top molecule, the principal axes of $\mathfrak{A}$ must coincide with the principal axes of inertia, so that

$$W_{mag} = \mathfrak{A}_{xx} I_x J_x + \mathfrak{A}_{yy} I_y J_y + \mathfrak{A}_{zz} I_z J_z \tag{8-43}$$

Since from the molecular symmetry, $\mathfrak{A}_{xx} = \mathfrak{A}_{yy}$ (z is parallel to the molecular axis), (8-43) may be written

$$W_{mag} = \mathfrak{A}_{xx}\mathbf{I}\cdot\mathbf{J} + (\mathfrak{A}_{zz} - \mathfrak{A}_{xx})I_zJ_z \tag{8-44}$$

Now $J_z = K$, and using the vector model $I_z = \mathbf{I}\cdot\mathbf{J}[K/J(J+1)]$ so that for a nucleus on the axis of a symmetric top, the energy is of the form given by Henderson [283]

$$W_{mag} = \mathbf{I}\cdot\mathbf{J}\left[a + (b - a)\frac{K^2}{J(J+1)}\right] \tag{8-45}$$

For the general asymmetric rotor, (8-42) does not simplify.

N^{14} in NH_3 affords a particularly good test of the dependence of magnetic interaction on J and K, since inversion lines for this molecule with many different values of J and K appear in the microwave region. Accurate measurement [930] of the NH_3 hyperfine structure for values of J and K up to 6 shows that the relation (8-45) holds within the experimental error of about 5 per cent. The constants a and b are given in Table 8-1.

NH_3 also displays an interesting magnetic hyperfine structure associated with magnetic moments of the hydrogen nuclei. A rather complete treatment and examination of hyperfine effects in NH_3 has been given by Gunther-Mohr *et al.* [930], [931]. Still more refined measurements and additional theoretical discussion are given by Gordon [925]. We shall discuss the various effects involving the hydrogen nuclei one at a time for the sake of simplicity.

Consider first the rotational states for which $K \neq 1$ in order to avoid the complication of hyperfine doubling. Since the N^{14} spin I_N is coupled to J by a quadrupole interaction, I_N and J couple to form F_1, which then couples with the sum I_H of the three hydrogen spins to form the total angular momentum F. When K is a multiple of 3, the total spin I_H of the three hydrogens can only be $\frac{3}{2}$ because of the exclusion principle (see Sec. 3-4). When K is not a multiple of 3, I_H can only be $\frac{1}{2}$.

There is an interaction between the hydrogen magnetic moments and the nitrogen moment which is given by expressions (8-15*b*). A somewhat larger interaction occurs between the moments of the hydrogen nuclei themselves, which can change in magnitude when I_H changes orientation with respect to J or F_1. This interaction has the form [925]

$$W = \frac{3}{4}\frac{g_I^2\mu_n^2}{r^3}(I_z^2 - \tfrac{5}{4}) \tag{8-46}$$

where I_z is the component of I_H along the symmetry axis of the molecule and r is the distance between hydrogen nuclei. When K is not a multiple of 3, $I_H = \frac{1}{2}$ and $I_z^2 = \frac{1}{4}$ for all hyperfine states, so that (8-46) produces

no variation of energy. When K is a multiple of 3, however, $I = \frac{3}{2}$ and (8-46) is given [925] by

$$\Delta W_{I_H=\frac{3}{2}} = \frac{3}{4}\frac{g_I^2\mu_n^2}{r^3}\left[\frac{3K^2}{J(J+1)} - 1\right]\cdot\frac{4(\mathbf{I}\cdot\mathbf{F}_1)^2 + 2(\mathbf{I}\cdot\mathbf{F}_1) - 5F_1(F_1+1)}{2F_1(F_1+1)(2F_1-1)(2F_1+3)}$$
$$\cdot\frac{6(\mathbf{F}_1\cdot\mathbf{J})^2 - 3(\mathbf{F}_1\cdot\mathbf{J}) - 2F_1(F_1+1)J(J+1)}{(2J-1)(2J+3)} \tag{8-47}$$

The coefficient $\frac{3}{4}\frac{g_I^2\mu_n^2}{r^3}$ in ΔW corresponds to 20.7 kc for hydrogen in NH_3, and hence spin-spin interactions of this type can be detected only by microwave spectroscopy of the highest resolution.

Rotation of the NH_3 molecule also creates a magnetic field which interacts with the moments of the hydrogen nuclei. Since the hydrogens are not on the molecular axis, the complete dyadic form (8-42) of this $\mathbf{I}\cdot\mathbf{J}$ interaction must be considered. From symmetry, one can immediately identify the principal axes of the dyadic for an individual hydrogen nucleus. One is the symmetry axis of the molecule, which we shall call z; a second is the perpendicular direction from the z axis through the nucleus, which we shall call x, and the y direction is of course perpendicular to each of these. Rotation of the molecule about the x, y, or z axis each produces a different magnetic field at the nucleus and hence a different $\mathbf{I}\cdot\mathbf{J}$ interaction energy. If, with respect to these principal axes, the dyadic $\mathfrak{A}$ of Eq. (8-42) is taken to be $\alpha\mathbf{ii} + \beta\mathbf{jj} + \gamma\mathbf{kk}$, the energy of the three hydrogens due to molecular rotation when $K = 1$ is [931]

$$\Delta W_{\mathbf{I}\cdot\mathbf{J}} = \left[\alpha + \beta + \frac{(\gamma - \alpha - \beta)K^2}{J(J+1)}\right]\mathbf{I}_H\cdot\mathbf{J} \tag{8-48}$$

Here $\mathbf{I}_H\cdot\mathbf{J} = \dfrac{\mathbf{I}_H\cdot\mathbf{F}_1\,\mathbf{F}_1\cdot\mathbf{J}}{F_1(F_1+1)}$ can be evaluated by the vector model.

The hydrogen spin I can take on the usual orientations with respect to F_1 which are allowed by quantum mechanics, giving a total angular momentum $F = F_1 + I, F_1 + I - 1, \ldots, |F_1 - I|$. The usual selection rules $\Delta F_1 = 0, \pm 1$ and $\Delta F = 0, \pm 1$ and intensity relations such as (6-6) apply. The resulting spectrum is indicated in Fig. 8-5, and compared with experimental observations made in a high-resolution beam spectrometer [925]. It may be seen that the maximum splitting of the 3,3 inversion line due to energy of the type given by (8-48) is about 60 kc, and hence these effects are observable only with resolution higher than that of the usual microwave spectrometer.

When $K = 1$, hyperfine doubling can occur. A small doubling is due to spin-spin interaction between the N and H nuclei, of the type discussed in Sec. 8.6. Even though $I_H = \frac{1}{2}$, the interaction is just twice that given by (8-16), since three protons are involved rather than a single

one [931]. Additional doubling occurs because of the variation of the $\mathbf{I}_H \cdot \mathbf{J}$ interaction with orientation. When $K = 1$, a distribution of hydrogen nuclear spin occurs which is similar to that of electron spin in Fig. 8-2. If $\mathbf{I}_H$ is fixed in orientation with respect to $\mathbf{J}$, it may be seen from this figure and the inequivalence of magnetic effects in the x and y directions that the two otherwise degenerate K states do not have the same energy.

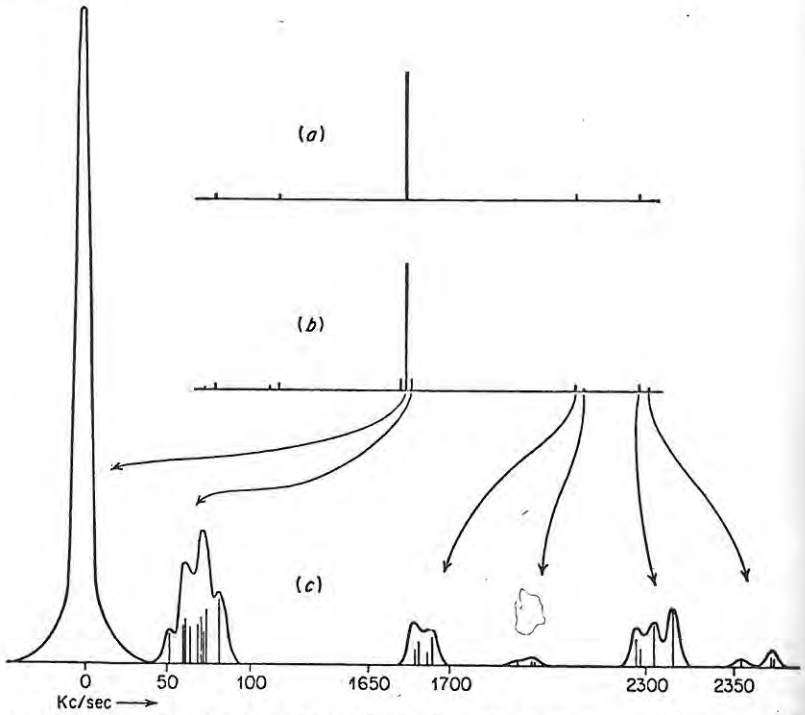

FIG. 8-5. Hyperfine structure of the NH_3 3,3 inversion spectrum. (*a*) Structure due to N^{14} quadrupole coupling alone. (*b*) Grosser features of structure due to N^{14} quadrupole coupling plus magnetic coupling of the three hydrogens. (*c*) Spectrum observed in a beam spectrometer, showing finer features of the individual lines of (*b*). (*After Gordon, Zeiger, and Townes* [925].)

A diagram of the energy levels of NH_3 for the 3,1 inversion transition and a particular value of F_1 is given in Fig. 8-6. Without hyperfine doubling, the stronger transitions would involve no change in magnetic energy (*cf.* Fig. 8-6*b*). Inversion transitions occur between different members of the two K-type levels, and hence the hyperfine doubling adds to the transition frequency for $F = \frac{7}{2}$, and subtracts from it for $F = \frac{5}{2}$, giving an appreciable doubling. The dotted levels of Fig. 8-6*c* are forbidden for $J = 3$ by the fact that hydrogen nuclei follow Fermi-Dirac

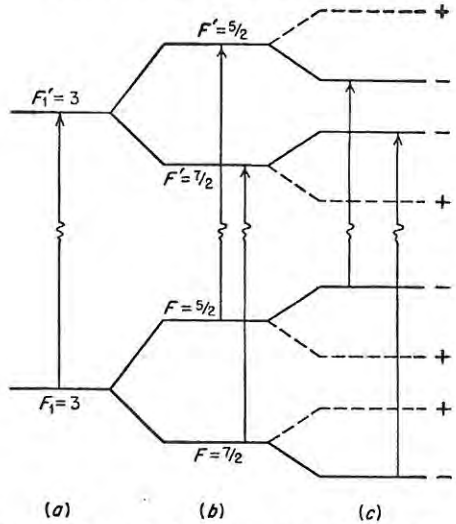

FIG. 8-6. Hyperfine structure of the 3,1 inversion transition of NH_3. Quantum numbers are $J = 3$, $K = 1$, $F_1 = |\mathbf{J} + \mathbf{I}_N| = 3$, $I_H = \frac{1}{2}$. (*a*) represents energies due to inversion and N^{14} quadrupole coupling only. (*b*) includes part of magnetic interaction with hydrogen moments which is the same for the two degenerate K states. (*c*) includes hyperfine doubling effects due to hydrogen moments. Only the stronger hyperfine transitions are shown. Dotted levels are forbidden by the exclusion principle.

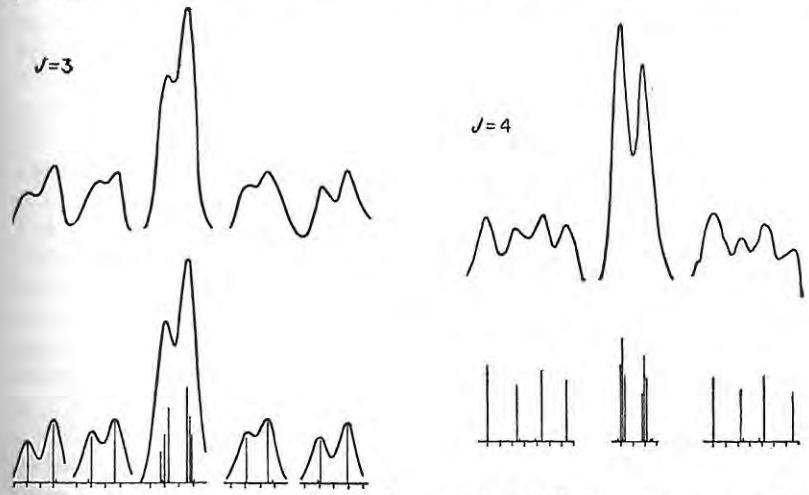

FIG. 8-7. Structure and hyperfine doubling of the $N^{14}H_3$ inversion spectrum for $J = 3$, $K = 1$, and $J = 4$, $K = 1$. Upper curves show experimental observations, and lower part of figure the theoretical expectations. Frequency increases from left to right with 60-kc intervals indicated. (*From Gunther-Mohr, White, Schawlow, Good, and Coles* [930].)

statistics (see Sec. 3-4 for a detailed explanation). The levels indicated by a minus sign are antisymmetric with respect to interchange of two hydrogen nuclei; those labeled with a plus sign are symmetric with respect to such an interchange. For $J = 4$, or any even value of J, the symmetry of the levels is reversed, so that the dotted levels of Fig. 8-6c are allowed, and the solid ones forbidden (*cf.* page 71).

Hyperfine structure of the 3,1 and 4,1 inversion lines of NH_3 is shown in Fig. 8-7, where the hyperfine doubling is quite prominent. The alternation in relative intensity of the doublets in changing from $J = 3$ to $J = 4$ is due to the alternation in the levels permitted by statistics which was noted above.

The magnitude of the energy shift of each level due to this type of hyperfine doubling is given [931] by

$$\Delta W = \pm(\beta - \alpha)\mathbf{I}_{\mathrm{H}} \cdot \mathbf{J} = \pm(\beta - \alpha)\frac{(\mathbf{F}_1 \cdot \mathbf{I})(\mathbf{F}_1 \cdot \mathbf{J})}{F_1(F_1 + 1)} \tag{8-49}$$

When the magnetic interaction is the same for the x and y directions, $\beta - \alpha = 0$, and this doubling disappears.

In the particular case of NH_3, $\beta - \alpha = -14.4$ kc. From this value and the $\mathbf{I}_{\mathrm{H}} \cdot \mathbf{J}$ interaction of the type given by (8-48) for hydrogen in inversion lines for which $K \neq 1$, one can obtain the values $\alpha = -1$ kc, $\beta = -16$ kc, and $\gamma = -19$ kc. As for C_I in H_2, the $\mathbf{I} \cdot \mathbf{J}$ interaction constants here are negative, indicating a large amount of slippage of the valence electrons as the hydrogens rotate in NH_3.

CHAPTER 9

INTERPRETATION OF HYPERFINE COUPLING CONSTANTS IN TERMS OF MOLECULAR STRUCTURE AND NUCLEAR MOMENTS

Hyperfine structure in molecular spectra can be theoretically predicted with high accuracy if the rotational state of the molecule, the spin of the nucleus producing the hyperfine structure, and certain coupling coefficients between molecule and nucleus are known. The coupling coefficients are dependent on either the magnetic dipole or electric quadrupole moment of the nucleus and on various properties of the molecule. The purpose of this chapter is to examine in detail the dependence of these hyperfine coupling coefficients on molecular structure, and to show how they may be theoretically estimated or, when measured, how they may be interpreted to obtain information about molecular structure and nuclear moments. For most molecules hyperfine structure due to nuclear quadrupole moments is considerably more prominent than that due to magnetic moments. Hence we shall begin with a discussion of quadrupole coupling.

9-1. Introductory Remarks on Quadrupole Coupling. From measurement of hyperfine structure, the quadrupole coupling eqQ may be evaluated. The nuclear quadrupole moment Q is a property of the nucleus which depends on the state of the nucleus and may be considered fixed since nuclei will almost always be encountered in their ground state. The sign and magnitude of Q can be very roughly estimated for some nuclei ([326] and [513]), but present knowledge of nuclear structure allows only the crudest estimates of Q from nuclear theory. The quantity e is the proton charge, and q, or $(\partial^2 V/\partial z^2)_{\mathrm{av}}$, is a molecular property, depending on the distribution of charges in the molecule. It cannot be exactly evaluated, but Townes and Dailey ([239] and [422]) have shown how it can be evaluated accurately enough in certain molecules to allow a useful determination of Q from the molecular coupling constant eqQ. In some cases Q may also be approximately determined from optical atomic spectra and with more accuracy from radio-frequency atomic-beam spectroscopy. Once Q for a given nucleus is known, it can provide a very convenient probe to test the electronic distribution in various molecules, since the quadrupole coupling allows a very direct measure-

CHAPTER 12

THE AMMONIA SPECTRUM AND HINDERED MOTIONS

12-1. Introduction. Because of the intensity and richness of its spectrum, ammonia has played a major role in the development of microwave spectroscopy. It has provided a large number of easily observable lines on which to try both experimental techniques and theory. NH_3 also provides the simplest and most thoroughly worked out example of a class of spectra which will continue to occupy and puzzle microwave spectroscopists for many years—spectra involving hindered motions.

The most important hindered motions all involve the quantum-mechanical tunneling effect. That is, they are motions which cannot occur in classical mechanics because of energy considerations, but are allowed by the wave nature of quantum mechanics. For example, in the ground vibrational state of NH_3, the molecule does not have enough energy to allow the nitrogen to be found in the plane of the hydrogens because of the large potential-energy hump at this position, as indicated in Fig. 12-1. Its actual penetration of the plane of the hydrogens and rapid vibration from one side of it to the other is called the tunnel effect because, if the nitrogen cannot climb the potential hill, it must "tunnel" in order to get through. In principle, the NH_3 inversion is a vibrational motion. Although vibrations normally give frequencies in the infrared region, the NH_3 inversion is so much slowed down by the hindering potential that its frequency lies in the microwave region. The qualitative change from ordinary vibrational levels where there is no hump in the potential to vibrational levels occurring in pairs when the hindering hump occurs is discussed in Chap. 3. When the vibrational energy is so great that the NH_3 molecule has sufficient energy to invert classically, the vibrational levels no longer occur in close pairs but are similar to more normal equally spaced vibrational levels. However, they are still markedly influenced by the presence of the potential hump, and hence in this case of no "tunneling," one may still speak of some hindering of the motion.

Another type of hindered motion is the rotation of one part of a molecule with respect to the remainder. Thus the hydrogen attached to oxygen in CH_3OH (Fig. 12-2) has three possible positions of equal energy but must tunnel through a potential hump between them as indicated in Fig. 12-3. Hence the rotation of this hydrogen around the C—O bond

is hindered. Similarly, the methyl group in CH_3CF_3 (Fig. 12-4) has three positions of equal energy separated by potential humps. Usually hindered motions do involve two or more positions of equal energy. If these positions are only minima, which are not equal in energy, many of

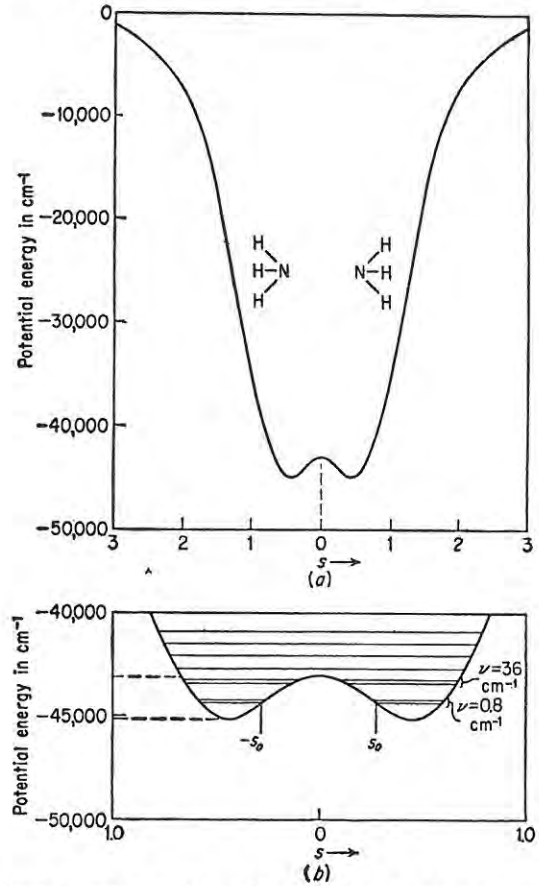

FIG. 12-1. Potential curve of NH_3. The variable s is a measure of the distance between the nitrogen and the plane of the hydrogens. (*b*) shows the lower part of the potential curve in more detail, and the energy levels.

the characteristic properties and interesting features of the hindered motions considered here do not occur.

When hindered motions have frequencies in or near the microwave region, the spectra are often quite difficult to interpret because the number of lines falling in the microwave region is greatly increased, and because there is no exact solution for the energy levels in these cases. In

addition, the frequencies of these motions are so strongly dependent on the potential humps or barriers that usually no helpful estimates of the frequency to be expected in a molecule can be made. However, hindered motions are of considerable importance to a knowledge of molecular structure and to chemistry. The difficulties they produce will be frequently encountered since hindered motions occur in a sizable fraction of the more complex gaseous molecules.

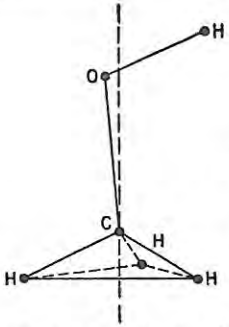

FIG. 12-2. Structure of methyl alcohol. The O—H bond may rotate about the axis with respect to the CH_3 group, but this rotation is hindered by mutual interaction.

12-2. Inversion Frequency of NH_3. Consider now the vibration of NH_3 in which the N moves perpendicular to the plane of the hydrogens, and which would lead to inversion if the N crossed this plane. As a function of the distance s of the nitrogen from the plane of the hydrogens, the potential is approximately as shown in Fig. 12-1. The molecule may vibrate at a fairly rapid rate in the potential minima with N on one side of the hydrogen plane, and after a large number of such vibrations, it may penetrate the potential barrier and begin oscillations on the other side. The rapid vibrations lie in the infrared region (950 cm^{-1}), whereas the frequency of penetration back and forth is the inversion frequency which occurs for the ground state in the microwave range (0.8 cm^{-1}). The approximate energy of the ground vibrational state is indicated in Fig. 12-1, and equals the potential energy $V(s)$ at $s = \pm s_0$, so that classically the nitrogen atom cannot be closer to the plane of the hydrogens than s_0.

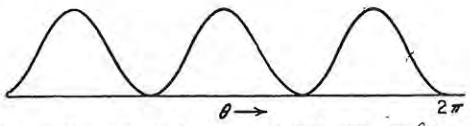

FIG. 12-3. Variation of the potential energy of CH_3OH with the relative rotation θ of the O—H bond and CH_3 group about the molecular axis. Probably the potential minima correspond to the hydrogen in O—H being a maximum distance from the nearest hydrogen of CH_3.

The inversion frequency has been calculated approximately by Dennison and Uhlenbeck [33] as

$$\nu = \frac{\nu_0}{\pi A^2} \tag{12-1}$$

where $A = \exp\left\{\frac{2\pi}{h}\int_0^{s_0} [2\mu(V(s) - W)]^{\frac{1}{2}}\, ds\right\}$

ν_0 = frequency of vibration in one of the potential minima
μ = reduced mass for the vibrational motion
W = total vibrational energy

This expression was obtained by the Wentzel-Kramers-Brillouin (WKB) method which uses approximate wave functions in the various regions of the motion and matches them at the boundaries of these regions. The significance of (12-1) may perhaps better be made clear by the following approach.

Let the wave function corresponding to the lowest state of simple harmonic oscillation with the nitrogen on the left side of the hydrogens be u_L and that for the nitrogen on the right be u_R. The true molecular wave functions, having a definite energy, must be either symmetric or antisymmetric with respect to the inversion, so the wave functions for the two inversion levels of the lowest vibrational state must be the combinations

$$\psi_0 = (1/\sqrt{2})(u_L + u_R)$$

and $$\psi_1 = (1/\sqrt{2})(u_L - u_R),$$

as shown in Fig. 3-8. If now the N is definitely placed on the left side at a time $t = 0$, the appropriate wave function describing the system at that time (and not having one definite energy) is $\psi = u_L = (1/\sqrt{2})(\psi_0 + \psi_1)$. If, as noted in Chap. 3, the time variation of the wave function is included, it becomes

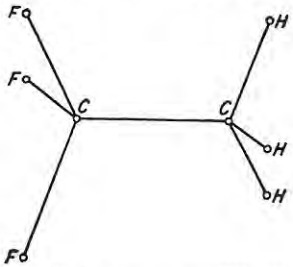

FIG. 12-4. Structure of CH_3CF_3 where rotation of the CH_3 group with respect to the CF_3 group is hindered by mutual interaction.

$$\psi = \frac{1}{\sqrt{2}}[\psi_0 + \psi_1 e^{2\pi i\nu t}]e^{2\pi i W_0 t/h} \tag{12-2}$$

where $h\nu$ is the energy difference between the two inversion states and W_0 is the energy of the lower state, which corresponds to ψ_0. After a time $t = 1/2\nu$, the wave function (12-2) becomes

$$\psi = \frac{1}{\sqrt{2}}[\psi_0 - \psi_1]e^{2\pi i W_0 t/h} = u_R e^{2\pi i W_0 t/h} \tag{12-3}$$

so that the nitrogen has moved over to the right side. Only a short time after the nitrogen has been initially placed on the left, the part of (12-2) in brackets may be written by expanding the exponential

$$\begin{aligned}\psi &= \left[\frac{1}{\sqrt{2}}(\psi_0 + \psi_1) + \psi_1\frac{2\pi i\nu t}{\sqrt{2}} + \cdots\right]e^{2\pi i W_0 t/h} \\ &= u_L + \pi i\nu t(u_L - u_R) + \cdots\end{aligned} \tag{12-4}$$

so that the amplitude of the wave function on the right has grown to $\pi\nu t$. This gives a measure of the rate of penetration of the potential

barrier in terms of the frequency of inversion. This rate of penetration may also be calculated from the "tunnel effect."

Consider now the nitrogen striking the barrier at $s = -s_0$ from the left. Its wave function will partly penetrate the barrier and extend over into the right-hand potential minimum. The amount of penetration can be roughly evaluated by examining Schrödinger's equation in the classically forbidden region.

$$\frac{d^2\psi}{ds^2} - \frac{2\mu}{\hbar^2}(V - W)\psi = 0 \tag{12-5}$$

An approximate solution to (12-5) is

$$\psi = \exp\left\{-\frac{1}{\hbar}\int_{-s_0}^{s}[2\mu(V(s) - W)]^{\frac{1}{2}}\,ds\right\} \tag{12-6}$$

if V does not vary too rapidly with s. Since $V - W$ is positive in the classically forbidden region, this corresponds to an exponentially decreasing function which has unity value at the boundary where the nitrogen strikes (the increasing exponential which is also a solution is omitted, since it would give the N the largest probability of being found on the right). The amplitude of the wave function which penetrates the boundary is then

$$\begin{aligned}\psi_{s=s_0} &= \exp\left\{-\frac{1}{\hbar}\int_{-s_0}^{s_0}[2\mu(V - W)]^{\frac{1}{2}}\,ds\right\}\\ &= \exp\left\{-\frac{2}{\hbar}\int_{0}^{s_0}[2\mu(V - W)]^{\frac{1}{2}}\,ds\right\} = \frac{1}{A^2}\end{aligned} \tag{12-7}$$

Now in a time t which is large enough for the nitrogen to oscillate on the left side many times, but small compared with the time required for inversion, the nitrogen will strike the left side of the potential barrier $\nu_0 t$ times, where ν_0 is the vibrational frequency. Each time it may be considered to partially penetrate and transmit an amplitude $1/A^2$ to the right side. The transmitted amplitudes add up to give a total amplitude after time t of $\nu_0 t/A^2$, so that the probability of penetration in time t is $(\nu_0 t/A^2)^2$. This is similar to, but differs slightly from, the usual expression for radioactive decay or other types of barrier penetration by tunneling ([305], p. 22), because the transmitted wave on the right-hand side of the barrier is trapped in an identical potential minimum and is added to by successive transmitted waves. Equating the amplitude $\nu_0 t/A^2$ to the amplitude for u_R in (12-4), we have

$$\pi\nu t = \frac{\nu_0 t}{A^2} \qquad \text{or} \qquad \nu = \frac{\nu_0}{\pi A^2} \tag{12-8}$$

which is the result obtained by Dennison and Uhlenbeck.

In the ground state of NH_3, $\nu/\nu_0 \approx 1200$, so that $A^2 \approx 400$ or e^6.

Because A^2 is large and varies exponentially with $\mu^{\frac{1}{2}}$ or $(V - W)^{\frac{1}{2}}$, changes in either of these quantities can very drastically affect the inversion frequency ν. For example, if the reduced mass μ is increased by a factor of 2, such as would be roughly done by changing from NH_3 to ND_3, ν decreases by $e^{6(\sqrt{2}-1)}$ or a factor of 11. The inversion frequency is correspondingly sensitive to the potential, and most molecules have such high potentials and heavy masses that the inversion frequencies are less than 1 cycle/sec. Many molecules invert so slowly that they have not succeeded in inverting during the few billion years' life of our planet.

NH_3 in the first excited level of this vibrational mode has a much higher inversion frequency because of the increased value of W. Dennison and Uhlenbeck [33] were able to assume a simple shape for the potential barrier and obtain values for the inversion frequencies in the ground and excited states which agreed roughly with experimental observations.

The exact form of the potential barrier assumed is not critical, since A depends only on an integral of this energy, and not on details of shape. However, Manning [61] found a potential function which has the general shape to be expected for NH_3, and for which the wave equation could be more easily solved and accurate values for the energies obtained. Manning's potential function is

$$\frac{V}{hc} = 66{,}551\ \text{sech}^4\frac{x}{2\rho} - 109{,}619\ \text{sech}^2\frac{x}{2\rho} \tag{12-9}$$

where V/hc = potential in units of cm^{-1}

x = a coordinate which is dependent on the distance of the nitrogen from the plane of the hydrogens

$\rho = 6.98 \times 10^{-8}/\mu^{\frac{1}{2}}$ where μ is the reduced mass in atomic mass units

This potential is zero for large s (or x), is symmetric about $s = 0$, and has a peak at $s = 0$, where the potential is $-43{,}068\ cm^{-1}$. It has two minima where the potential is $-45{,}140\ cm^{-1}$. The constants in (12-9) are also chosen to give close to the correct equilibrium configuration for the molecule, the vibration frequency, and the correct inversion frequency for one level.

If the distance between hydrogens is assumed to stay constant during the motion so that they move together as a rigid triangle, then x is taken as equal to s, the distance between the nitrogen and the plane of this triangle. If m is the mass of the hydrogens and M that of nitrogen, then the reduced mass for this case is simply $\mu = 3mM/(3m + M)$. However, probably a better approximation to the motion is to assume the N—H distance remains constant, and only the H—N—H angles change with vibration [110]. In this case x is taken as the distance along an arc moved by the hydrogens from the median plane, *i.e.*, a plane through the nitrogen and perpendicular to the molecular axis. If the angle between

this plane and the N—H bond is taken as α, the proper reduced mass can be shown to be $\mu = 3m(M + 3m \sin^2 \alpha)/(3m + M)$. This reduced mass varies only a small amount with α, and its value may be assumed to be that at the equilibrium angle of $\alpha_0 = 21°49'$. Different reduced masses in Manning's potential will give different equilibrium heights for the NH_3 pyramid. However, these heights do not deviate significantly from the observed value.

The values of inversion frequency for various isotopic species of ammonia calculated from Manning's potential are shown in Table 12-1

TABLE 12-1. INVERSION FREQUENCIES OF AMMONIA IN MEGACYCLES

The "first excited vibrational state" ($v_2 = 1$) corresponds to approximately 950 cm^{-1} excitation of the vibration of the nitrogen against the plane of the hydrogens. The calculated values are given by Manning [61] and Newton and Thomas [306] except for the calculation of $N^{14}D_3$ with the Manning potential, which was done by A. Javan and J. Lotspeich.

	Ground state			First excited vibrational state	
	$N^{14}H_3$	$N^{14}D_3$	$N^{15}H_3$	$N^{14}H_3$	$N^{14}D_3$
Observed value, Mc	23,786	1600	22,705	1,095,000	117,000
Calculated from Manning potential	25,000	1250	.....	780,000	83,000
Calculated from Newton-Thomas potential	23,800	....	22,700	690,000	

and compared with experimental results. The potential constants have been chosen to fit some of the data, including the energy of the first vibrational level. The excited vibrational levels are fitted rather satisfactorily by this potential [61]. Although the inversion frequencies are given approximately correctly, it does not seem possible to obtain a really satisfactory fit of all the data with a potential of Manning's type. This will be seen again when fine structure of the inversion spectrum is discussed.

Newton and Thomas [306] used a potential of the form

$$\frac{V}{hc} = \left\{\left[\frac{(0.377)^2 - s^2}{0.536 + s^2}\right]^2 - 1\right\} \times 3.17 \times 10^4 \text{ cm}^{-1} \qquad (12\text{-}10)$$

where s is measured in angstrom units. Here the hydrogens are considered to move as a rigid triangle. Values for some of the inversion frequencies calculated by an approximate method [306] from this potential are given in Table 12-1. Form (12-10) for the potential appears to give results which are comparable in accuracy with those from the potential (12-9).

12-3. Inversion of Other Symmetric Hydrides. A very simple form of potential has been found by Costain and Sutherland [678] to give fairly accurate values for the inversion frequency of NH_3, and has been used to estimate the inversion frequencies of PH_3 and AsH_3. This is a potential of the form

$$V = \tfrac{3}{2}k_r(\Delta r)^2 + \tfrac{3}{2}k_\delta(\Delta\delta)^2 \qquad (12\text{-}11)$$

where Δr = change in the N—H bond length
$\Delta\delta$ = change in the H—N—H bond angle

The force constants k_r and k_δ, as well as the ratio of Δr to $\Delta\delta$, can be obtained by a normal coordinate treatment of the observed vibrational frequencies of NH_3. Their evaluation gives

$$V = 3.89 \times 10^4(\Delta\delta)^2 \quad \text{cm}^{-1} \qquad (12\text{-}12)$$

where δ is measured in radians. This gives a potential hill of 2077 cm^{-1} between the two minima in good agreement with Manning's value of 2072 cm^{-1}. In fact, the entire potential curve given by (12-12) is very close to that given by (12-9).

A similar evaluation of the potential hill from vibrational constants and molecular geometry for PH_3 and AsH_3 gives the following results [678].

For PH_3:

$$V = 5.3 \times 10^4(\Delta\delta)^2 \text{ cm}^{-1} \qquad (12\text{-}13)$$

Height of potential hill above minimum = 6085 cm^{-1}
Inversion frequencies:
Ground state = 0.14 Mc
First excited state = 7.2 Mc

For AsH_3:

$$V = 4.56 \times 10^4(\Delta\delta)^2 \text{ cm}^{-1} \qquad (12\text{-}14)$$

δ_0 = 0.585 radian
Height of potential hill above minimum = 11,220 cm^{-1}
Inversion frequencies:
Ground state = 1/2 cycle/year
First excited state = 1 cycle/day

Thus the inversion splitting of PH_3 is probably large enough to give a splitting in microwave measurements of the rotational spectrum, whereas AsH_3 would take two years to go through a cycle of inversion and should hence have no observable splitting. These numbers illustrate the very rapid variation in frequency as the potential barrier height is changed.

12-4. Fine Structure of the Ammonia Inversion Spectrum Rotation-Vibration Interactions. Discussion of the inversion spectrum has so far

neglected the rotational motion of the molecule. There is, of course, an interaction between rotation and vibration which in most molecules shows up as a series of closely spaced lines in the rotational spectrum, each being due to different vibrational states. In an inversion spectrum, a type of vibration, there is similarly a series of lines at different inversion frequencies, each corresponding to a different rotational state.

A good qualitative view of the effect of rotation on the inversion spectrum of NH_3 (or any other molecule) may be obtained from a classical discussion. The rotational frequencies of NH_3 are considerably higher than the inversion frequencies of the ground state, so that no peculiar resonant interactions occur, but rather the centrifugal forces due to rotation simply change the effective potential in which the molecule vibrates. Consider first a rotation of the molecule about the symmetry axis. The resulting centrifugal force tends to distort the molecule by flattening it or increasing the H—N—H angle. Hence as a result of the centrifugal force the hydrogens can somewhat more readily move past the nitrogen and the inversion frequency is increased. The centrifugal force is proportional to the square of the angular momentum about this axis, or to K^2, so the inversion frequency can be expected to be increased roughly by an amount bK^2, where b is some positive constant. Now consider a rotation about an axis perpendicular to the molecular axis. In this case the centrifugal force tends to elongate the NH_3 pyramid, or decrease the H—N—H angle. It is then more difficult for the hydrogens and nitrogen to move into the same plane, and the inversion frequency is decreased. Since the square of the angular momentum perpendicular to the symmetry axis is proportional to $J(J+1) - K^2$, where J is the total angular momentum quantum number, this type of motion can be expected to decrease the inversion frequency roughly by an amount $a[J(J+1) - K^2]$, where a is a positive constant. Thus the frequency should be of the form

$$\nu = \nu_0 - a[J(J+1) - K^2] + bK^2 + \text{higher powers of } J \text{ and } K \qquad (12\text{-}15)$$

A quantitative calculation of the effects of rotation can be made by considering in detail how the centrifugal forces act on the vibrational and inversion motion. They will affect the inversion frequency through the quantity A in expression (12-1). Allowing for rotation, A may be written [110]

$$A = \exp\left\{\frac{2\pi}{h}\int_0^{s_0+\delta s} [2\mu(V + \delta V - W - \delta W)]^{\frac{1}{2}}\, ds\right\} \qquad (12\text{-}16)$$

where δV and δE represent the respective changes in the potential and vibrational energy as a result of rotation. δs is the change due to value of s where the kinetic energy is zero. The change in effective potential V due to centrifugal forces equals simply the change in kinetic energy of

rotation as the molecule vibrates, or

$$\delta V = \hbar^2[J(J+1) - K^2]\left(\frac{1}{2I_A} - \frac{1}{2I_A^0}\right) + \hbar^2K^2\left(\frac{1}{2I_C} - \frac{1}{2I_C^0}\right) \qquad (12\text{-}17)$$

where I_A and I_C are the moments of inertia of the molecule as a function of the vibrational coordinate, while I_A^0 and I_C^0 are the values for the molecule in the equilibrium condition. The change δW contributes only a small amount to A, and δs is quite negligible; so both these quantities will be neglected here. If (12-16) is expanded, assuming δV is small, and the new value of A is inserted into (12-1), the change in inversion frequency ν is

$$\delta\nu = -\frac{2\nu}{\hbar}\int_0^{s_0} \mu\, \delta V[2\mu(V - W)]^{-\frac{1}{2}}\, ds \qquad (12\text{-}18)$$

Expression (12-18) must be numerically integrated, after inserting δV from (12-17) and allowing for the dependence of I_A and I_C on the parameter s. In addition, various possible paths for the motion of the hydrogens with respect to the nitrogen may be assumed. Sheng, Barker, and Dennison [110] choose a path intermediate between that obtained by considering the hydrogens as a rigid triangle and the path for the N—H

TABLE 12-2. VALUES OF THE FINE-STRUCTURE COEFFICIENTS FOR AMMONIA
$\nu = \nu_0 - a[J(J+1) - K^2] + bK^2 +$ higher powers in J and K

		Isotope				
		$N^{14}H_3$		$N^{15}H_3$	$N^{14}D_3$	
		Ground state	Excited state	Ground state	Ground state	Excited state
Experimental value, Mc	a	151.5	4860	141.9	7.16	
	b	59.9	1800	55.8	2.88	
Calculated value	a	102	4680	.....	3.61	267
Manning potential, Mc	b	55.5	1980	.....	2.60	187
Calculated value	a	180	....	186		
Newton-Thomas potential, Mc	b	27	....	6		

bond fixed in length during the inversion. The expression resulting from (12-18) is of the form (12-15) expected qualitatively. Calculated values of the coefficients a and b in (12-15) are compared in Table 12-2 with the experimentally determined constants.

Newton and Thomas [306] have calculated the fine structure of the inversion spectrum of $N^{14}H_3$ and $N^{15}H_3$ by introducing the centrifugal terms somewhat earlier in the calculation. These terms can be conveniently combined with their form of the potential (12-10) so that

rotational effects are included in the calculation of inversion frequencies *ab initio*. Their values for the fine-structure constants are also given in Table 12-2.

Although the agreement between theory and experiment in Tables 12-1 and 12-2 is reasonably good, it is clear that none of the potentials assumed is capable of giving the behavior of the inversion spectrum for all isotopes and vibrational states to an accuracy better than about 10 per cent. Hadley and Dennison [157] have tried some modifications in the potentials assumed here, but with no marked improvement in the results. It appears that probably a treatment which is not restricted to one dimension as are all those so far used will be necessary in order to obtain much improvement in the theoretical results. The relative success of a one-dimensional treatment comes from the fact that there is one normal mode of vibration which is primarily involved in its inversion. However, other normal modes of vibration are of some importance in affecting inversion.

About 65 lines of the NH_3 inversion spectrum which have so far been measured are listed in Table 12-3 with their approximate intensities at room temperature. In computing relative intensities, it has been assumed that expression (13-61) is correct for the half widths of the lines. The extensive spectrum is often useful in calibrating wavemeters, checking the performance of spectrometers, and as standard frequency references in measuring accurately other spectra. Use of the NH_3 spectrum in testing has the disadvantage, however, that NH_3 tends to persist in the spectrometer absorption cell sometimes long after it is wanted.

The expression (12-15) is too much simplified to fit accurately all the lines of Table 12-3. A more complete expansion of the type indicated by (12-15), but including higher powers of $J(J+1)$ and K^2 can be made to fit the experimental frequencies reasonably well. A number of expansions of this general type have been given [141], [155], [172], [236], [317], [410]. One example [317] containing five terms in J and K is

$$\nu = 23{,}787 - 151.3J(J+1) + 211.0K^2 + 0.5503J^2(J+1)^2 - 1.531J(J+1)K^2 + 1.055K^4 \quad (12\text{-}19)$$

This fits the low J and K values best and gives deviations for some of the larger values of 25 to 50 Mc. The exponential dependence of (12-1) on the potential suggested to Costain that an exponential of various powers of $J(J+1)$ and K^2 might fit the frequencies [564]. His expansion

$$\nu = 23{,}785.88 \exp\left[-6.36996 \times 10^{-3}J(J+1) + 8.88986 \times 10^{-3}K^2 + 8.6922 \times 10^{-7}J^2(J+1)^2 - 1.7845 \times 10^{-6}J(J+1)K^2 + 5.3075 \times 10^{-7}K^4\right] \text{ Mc} \quad (12\text{-}20)$$

fits the lines in Table 12-3 with a mean deviation of 1.3 Mc and should hence predict other unmeasured lines with some accuracy.

There is a certain group of lines, those for which $K = 3$, which shows

TABLE 12-3. OBSERVED $N^{14}H_3$ INVERSION LINES

Rotational state		Frequency, Mc	Intensity, cm^{-1}
J	K		
9	5	16,798.3	8.7×10^{-6}
7	1	16,841.3	3.5×10^{-6}
7	2	17,291.6	1.0×10^{-5}
8	4	17,378.1	1.5×10^{-6}
7	3	18,017.6	4.3×10^{-6}
12	9	18,127.2	4.7×10^{-6}
11	8	18,162.6	4.8×10^{-6}
13	10	18,178.0	1.1×10^{-6}
10	7	18,285.6	9.4×10^{-6}
14	11	18,313.9	4.5×10^{-7}
6	1	18,391.6	4.2×10^{-6}
9	6	18,499.5	3.4×10^{-5}
15	12	18,535.1	3.6×10^{-7}
8	5	18,808.7	2.8×10^{-5}
16	13	18,842.9	6.6×10^{-8}
6	2	18,884.9	2.6×10^{-5}
7	4	19,218.52	4.0×10^{-5}
6	3	19,757.56	1.1×10^{-4}
5	1	19,838.4	1.8×10^{-5}
5	2	20,371.48	5.6×10^{-5}
8	6	20,719.20	1.0×10^{-4}
9	7	20,735.46	3.3×10^{-5}
7	5	20,804.80	7.4×10^{-5}
10	8	20,852.51	1.9×10^{-5}
6	4	20,994.62	9.9×10^{-5}
11	9	21,070.73	2.0×10^{-5}
4	1	21,134.37	4.0×10^{-5}
5	3	21,285.30	2.3×10^{-4}
12	10	21,391.55	5.2×10^{-6}
4	2	21,703.34	1.1×10^{-4}
13	11	21,818.1	6.0×10^{-7}
3	1	22,234.51	6.9×10^{-5}
14	12	22,355	2.2×10^{-6}
5	4	22,653.00	2.2×10^{-4}
4	3	22,688.24	4.4×10^{-4}
6	5	22,732.45	1.7×10^{-4}
3	2	22,834.10	2.0×10^{-4}
7	6	22,924.91	2.9×10^{-4}
15	13	23,004	4.8×10^{-7}
2	1	23,098.78	1.1×10^{-4}

TABLE 12-3. OBSERVED $N^{14}H_3$ INVERSION LINES (*Continued*)

Rotational state		Frequency, Mc	Intensity, cm^{-1}
J	K		
8	7	23,232.20	9.9×10^{-5}
9	8	23,657.46	6.5×10^{-5}
1	1	23,694.48	1.9×10^{-4}
2	2	23,722.61	3.2×10^{-4}
16	14	23,777.4	1.9×10^{-7}
3	3	23,870.11	7.9×10^{-4}
4	4	24,139.39	4.3×10^{-4}
10	9	24,205.25	7.8×10^{-5}
5	5	24,532.94	4.0×10^{-4}
17	15	24,680.1	1.1×10^{-7}
11	10	24,881.90	2.2×10^{-5}
6	6	25,056.04	6.9×10^{-4}
12	11	25,695.23	1.3×10^{-5}
7	7	25,715.14	2.7×10^{-4}
8	8	26,518.91	2.0×10^{-4}
13	12	26,655.00	1.3×10^{-5}
9	9	27,478.00	2.8×10^{-4}
14	13	27,772.52	3.0×10^{-6}
10	10	28,604.73	9.0×10^{-5}
15	14	29,061.14	1.4×10^{-6}
11	11	29,914.66	5.5×10^{-5}
12	12	31,424.97	6.2×10^{-5}
13	13	33,156.95	1.7×10^{-5}
14	14	35,134.44	8.7×10^{-6}
15	15	37,385.18	8.3×10^{-6}
16	16	39,941.54	1.9×10^{-6}

peculiar and systematic deviations from expressions (12-19) or (12-20) [198], [236]. The magnitude of this deviation increases rapidly with J and is alternately positive or negative according to whether J is odd or even, as may be seen from Table 12-4. The deviations for high J values are very much greater than the average error in expression (12-20) of 1.3 Mc, and have consequently not been averaged into this error.

H. H. Nielsen and Dennison [223] have shown that the deviations of lines for which $K = 3$ are due to still another rotation-vibration interaction of high order and hence small magnitude. It may be thought of as a splitting of the K degeneracy, *i.e.*, of the two levels corresponding to $K = \pm 3$. As explained in Chap. 3, the statistics and spin of the

hydrogen nuclei make only one of these levels possible in NH_3, so one displaced line is seen rather than two separated lines. From the discussion in Chap. 3, it may be remembered that the type of wave function that is allowed by the nuclear properties depends on the oddness or evenness of J and on the inversion level. Hence in the lowest inversion level for odd J the higher-frequency K doublet occurs, whereas for even J only the lower frequency doublet appears. In the upper inversion level the situation is reversed. A transition, therefore, gives one line shifted to higher frequency for even J by an amount equal to the K doubling, and shifted to a lower frequency for odd J.

Symmetry considerations can show quite generally that no K-type doubling or further splitting due to rotation-vibration interactions can

TABLE 12-4. DEVIATIONS OF AMMONIA LINES WITH $K = 3$ FROM NORMAL INVERSION FREQUENCIES AS GIVEN BY FORMULA (12-20)
Calculated shift for NH_3 is according to expression (12-21).

J	NH_3		ND_3
	Calculated shift, Mc	Measured shift [564], Mc	Calculated shifts [223], Mc
3	− 0.25	− 0.21	±0.03
4	1.76	1.76	±0.24
5	− 7.06	− 7.03	±0.95
6	21.18	21.18	±2.85
7	−52.9	−52.39	±7.14

occur for levels where K is not a multiple of 3 (*cf.* [66]). In addition, although levels with $K = 6$ or 9 can, in principle, be split, the effect of vibration-rotation interaction in splitting these levels is very much smaller than their effect on the levels with $K = 3$. Even when $K = 3$, the disturbance of the levels by vibration-rotation interaction is a very small perturbation; Nielsen and Dennison [223] have shown that it is proportional to the fourth power of the ratio of rotational to vibrational energy: They obtain a value for the splitting of the two degenerate levels and hence for the shift in frequency of the observed lines

$$\Delta\nu = 3.50 \times 10^{-4} J(J+1)[J(J+1) - 2][J(J+1) - 6] \quad \text{Mc} \qquad (12\text{-}21)$$

The constant in (12-21) can be evaluated to about 10 per cent accuracy from known rotational and vibrational constants of the NH_3 molecule, but its precise value is picked to fit the data of Table 12-4 [564]. This table shows that expression (12-21) agrees quite well with the observed deviations of lines with $K = 3$.

In the case of ND_3, the nuclear spin of D is unity and both the K doublets are allowed. These have not yet been observed, but the calcu-

lated deviation of each member from normal frequency is given in Table 12-4.

12-5. Asymmetric Forms of Ammonia. In addition to the symmetric forms of ammonia NH_3 and ND_3, the asymmetric rotors NH_2D and NHD_2 occur and have inversion spectra. However, in these cases the inversion spectrum tends to be mixed up with rotational energies. Examination of the transitions allowed for NH_3 in Fig. 3-9 shows that rotational transitions occur only at the same time as an inversion (or vibrational) transition. In addition, an inversion transition occurs only with a rotational transition, since upper and lower inversion levels have different rotational wave functions. In the case of NH_3, the molecular symmetry gives the two different rotational wave functions the same rotation energy. However, it can be shown to be always true that only transitions with a change of both rotational and inversion states occur, and in the cases of NH_2D and NHD_2 the rotational transition contributes to the frequency of the observed lines because of their asymmetry [662].

If the energy difference due to the rotational transition $J'_{\tau'} \leftarrow J_\tau$ is small, then a pair of lines is observed of frequency $\nu_i \pm \nu_{J_\tau J'_{\tau'}}$, where ν_i is the inversion frequency and $\nu_{J_\tau J'_{\tau'}}$ the rotational frequency. If the inversion frequency is much smaller than that due to the rotational frequency, the observed spectrum has a pair of lines of frequencies $\nu_{J_\tau J'_{\tau'}} \pm \nu_i$. In the extreme and very common case of an unobservably small inversion frequency, this last doublet becomes the single observed rotational frequency $\nu_{J_\tau J'_{\tau'}}$. A number of lines of both the above types have been found in partially deuterated ammonia, and from these rotational constants and inversion frequencies have been obtained [662]. The rotational constants are consistent with the structural parameters of NH_3 usually assumed [130] after some allowance is made for centrifugal distortion.

The inversion frequencies of the asymmetric forms of ammonia cannot be treated as easily as those for NH_3 and ND_3. In the vibration which inverts the asymmetric forms, the N does not move strictly perpendicularly to the plane of the hydrogens. However, an approximate calculation of the inversion frequencies of these molecules, assuming the same motion and potential for the inversion as in the symmetric cases, gives surprisingly good agreement with the observed frequencies as shown in Table 12-5. The inversion frequencies for the ground states are in very close agreement, although the excited state frequencies show a sizable discrepancy.

It is also more difficult to calculate the fine structure, or rotation-vibration interaction, in the asymmetric ammonias because both the vibrational and the rotational motions are rather complex. Weiss and Strandberg [662] have obtained a reasonably good empirical approximation to the fine structure, however, by assuming it to be of the form

$$\nu = \nu_0 - a[J(J+1) - (P_c^2)_{av}] + b(P_c^2)_{av} \qquad (12\text{-}22)$$

where $(P_c^2)_{av}$ is the average square of the angular momentum in units of $h/2\pi$ parallel to the principal axis of largest moment of inertia. This axis differs by only about 10° from the "symmetry" axis perpendicular to the plane of the hydrogens. $(P_c^2)_{av}$ is the analog of the quantity K^2 in expression (12-15) for the symmetric ammonias. The more intense microwave transitions in NH_2D and NHD_2 involve very little change in $(P_c^2)_{av}$ and no change in J, again in analogy with the symmetric cases where $\Delta K = 0$ and $\Delta J = 0$. Hence $(P_c^2)_{av}$ and J can be assumed the same for upper and lower states of the transition. Empirical values for a and b of expression (12-22) for NH_2D and NHD_2 are listed in Table 12-5.

TABLE 12-5. CONSTANTS OF THE INVERSION SPECTRUM OF NH_2D AND NHD_2 (From Weiss and Strandberg [662])

	NH_2D		NHD_2	
	Observed	Calculated	Observed	Calculated
Inversion frequency of ground state, Mc	12,182	12,100	5,111	5,160
Fine-structure constant of ground state, Mc a	23.6		8.1	
b	76.7		26	
Inversion frequency of first excited state, Mc	592,000	465,000	295,000	204,000

The quantity $(P_c^2)_{av}$ is just $(\alpha_{zc}^2)_{av}J(J+1)$, where α_{zc} is the cosine of the angle between the total angular momentum J and the molecular axis c of largest principal moment of inertia. $(\alpha_{zc}^2)_{av}$ can be evaluated as in Chap. 6 [*cf.*, for example, expression (6-16)].

12-6. Hindered Torsional Motions in Symmetric Rotors. Another common type of hindered motion is the rotation of one part of a molecule with respect to the remainder, which, when hindering is large, becomes a torsional oscillation. An example is the relative rotation of CH_3 and CF_3 about the symmetry axis of the molecule $H_3C—CF_3$. Hindered torsional motion can also occur in an asymmetric rotor, as in CH_3OH, where the OH bond may rotate with respect to the CH_3 group.

Consider first a symmetric top such as H_3CCF_3 having an "internal" torsional motion of one end of the molecule with respect to the other end. In either one of the two extreme cases where the CH_3 rotates perfectly freely about the molecular axis, or where it interacts strongly with the CF_3 group so that it can scarcely rotate at all with respect to this group, the energy levels are relatively simple. We shall examine these two

extreme cases first before proceeding to the more complex intermediate case where tunneling effects are prominent.

If the two parts of the molecule are bound together tightly, the energy may be obtained in a straightforward way as the sum of the rotational energy of a symmetric top and various molecular vibrational energies. We shall consider only the torsional vibration. The reduced moment of inertia for the CH_3 twisting with respect to CF_3 is

$$I_r = \frac{I_1 I_2}{I_1 + I_2} \text{ or } \frac{I_1 I_2}{I}$$

where I_1 is the moment of inertia for CH_3 about the symmetry axis, I_2 is that for CF_3, and $I = I_1 + I_2$. The potential energy has three minima corresponding to the three equivalent positions 120° apart of the CH_3 with respect to CF_3, and there is a very high potential hump between each minimum—so high that tunneling from one minimum to another is negligibly small. In one of the minima, the potential energy can then be written $V = \frac{1}{2}k\alpha^2$, where $\alpha = \chi_1 - \chi_2$ is the difference in the angular position χ_1 of CH_3 about the symmetry axis and the angle χ_2 of CF_3. The force, or rather torque, constant is k. The frequency of torsional oscillation is then

$$\omega = \frac{1}{2\pi}\sqrt{\frac{kI}{I_1 I_2}}$$

and the energy of torsional and rotational motions is simply

$$W = hB[J(J+1) - K^2] + hCK^2 + h\omega(v + \tfrac{1}{2}) \qquad (12\text{-}23)$$

where B and C are the usual rotation constants ($C = h/8\pi^2 I$) and v is the vibrational quantum number for the torsional motion. Each torsional vibrational level is triply degenerate since there are three equivalent positions in which the oscillation may occur.

In the other extreme case, CH_3 and CF_3 can rotate freely about the molecular axis. Let the angular momentum about the axis for CH_3 be $m_1\hbar$ and that of CF_3 be $m_2\hbar$ so that the total angular momentum about the symmetry axis is $(m_1 + m_2)\hbar = K\hbar$. The usual quantum-mechanical conditions require that m_1, m_2, and K be integers. The energy of rotation is

$$W = hB[J(J+1) - K^2] + \frac{(m_1\hbar)^2}{2I_1} + \frac{(m_2\hbar)^2}{2I_2}$$

or

$$W = hB[J(J+1) - K^2] + hCK^2 + \frac{I\hbar^2}{2I_1 I_2}\left(m_1 - \frac{KI_1}{I}\right)^2 \qquad (12\text{-}24)$$

The energies due to deviations from these ideal cases, or in the intermediate case when the barrier is of moderate height, remain to be calculated. Connections between the energy levels for the two extreme cases

are shown in Fig. 12-5. It may be seen from this figure that some of the degenerate levels of the extreme cases split in the intermediate case of moderate potential barrier heights. The amount of splitting must be obtained from a solution of the wave equation which, of course, gives (12-23) or (12-24) in the two extreme cases.

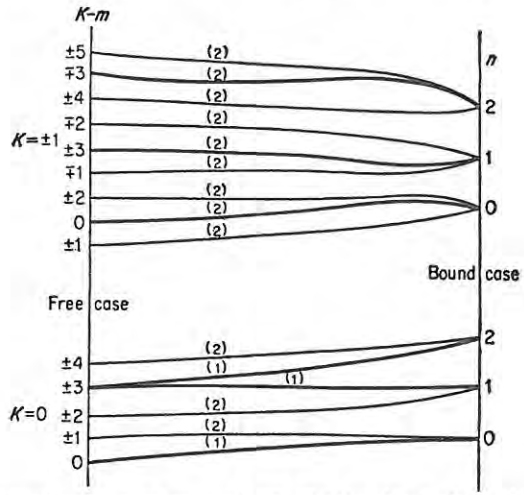

FIG. 12-5. Connections between energy levels with free internal rotation and those for torsional oscillation. Three potential minima are assumed, as in the molecule CH_3CF_3. Intermediate barrier heights, corresponding to neither very strong nor negligible interaction between the CH_3 and CF_3 groups, can be seen to split certain levels. Numbers (1) and (2) indicate the number of levels of the same energy. (*After Koehler and Dennison* [99].)

The kinetic energy due to rotation is

$$T = \tfrac{1}{2}I_x\omega_x^2 + \tfrac{1}{2}I_y\omega_y^2 + \tfrac{1}{2}I_1\dot{\chi}_1^2 + \tfrac{1}{2}I_2\dot{\chi}_2^2 \qquad (12\text{-}25)$$

where I_x and I_y are the principal moments of inertia perpendicular to the axis and ω_x and ω_y, the angular velocities. I_1 and I_2 are the moments of inertia of the two parts of the molecule about which relative rotation occurs, and which is taken as the z direction with respect to the axis. χ_1 and χ_2 are angles specifying the rotation of these two parts about this axis. If new variables are defined so that

$$\chi = \frac{I_1\chi_1 + I_2\chi_2}{I} \qquad \alpha = \chi_1 - \chi_2 \qquad (12\text{-}26)$$

Then the energy is, from (12-25)

$$W = \tfrac{1}{2}I_x\omega_x^2 + \tfrac{1}{2}I_y\omega_y^2 + \tfrac{1}{2}I\dot{\chi}^2 + \tfrac{1}{2}\frac{I_1 I_2}{I}\dot{\alpha}^2 + \tfrac{1}{2}V_0(1 - \cos 3\alpha) \qquad (12\text{-}27a)$$

and the Hamiltonian is

$$H = \frac{1}{2}\frac{P_x^2}{I_x} + \frac{1}{2}\frac{P_y^2}{I_y} + \frac{1}{2}\frac{P_z^2}{I} + \frac{1}{2}\frac{I}{I_1 I_2}p_\alpha^2 + \tfrac{1}{2}V_0(1 - \cos 3\alpha) \quad (12\text{-}27b)$$

where the symbols involved have been defined above. It may be observed that α gives the angle of torsion within the molecule, and that $I\dot{\chi} = I_1\dot{\chi}_1 + I_2\dot{\chi}_2$ is the total angular momentum about the symmetry axis.

Here the potential energy for torsional motion is assumed to be $V = \frac{1}{2}V_0(1 - \cos 3\alpha)$, corresponding to three potential minima with intervening barriers of height V_0. The shape of the potential barrier will not, of course, be given perfectly by the $\cos 3\alpha$ variation but more generally should be written as a Fourier series

$$V = \sum_p (a_p \cos 3p\alpha + b_p \sin 3p\alpha)$$

However, the energy levels of the molecule will not depend strongly on minor details of the potential. In addition, potential curves which have been calculated on the basis of simple assumptions about the origin of the hindering forces are in fact fitted extremely well by a $\cos 3\alpha$ curve. There is some experimental evidence from the barrier in CH_3NO_2, to be discussed below, that the term proportional to $\cos 6\alpha$ in this Fourier expansion is not more than a few per cent as large as that proportional to $\cos 3\alpha$.

Properties of Quantum States with Hindered Torsional Motion. It may be seen that the first three terms of (12-27) have just the same form as Eq. (3-2), which gives the energy of rotation for a rigid top. In this case, $I_x = I_y$ so that the top is symmetric. Consequently the wave function describing the rotation and torsion of the molecule has the form [36], [99]

$$\psi = \frac{1}{2\pi} e^{iK\chi} e^{iM\phi}\Theta_{JKM}(\theta)\mathfrak{M}(\alpha) \quad (12\text{-}28)$$

where θ and ϕ are the usual Eulerian angles and $e^{iK\chi}e^{iM\phi}\Theta(\theta)$ is identical with expression (3-12a), the wave function for a rigid symmetric top $\mathfrak{M}$ satisfies the equation

$$\frac{I\hbar^2}{2I_1I_2}\frac{d^2\mathfrak{M}}{d\alpha^2} + \left[W_\alpha - \frac{V_0}{2}(1 - \cos 3\alpha)\right]\mathfrak{M} = 0 \quad (12\text{-}29)$$

The energy is

$$W = W_R + W_\alpha = hB[J(J+1) - K^2] + hCK^2 + W_\alpha \quad (12\text{-}30)$$

where W_R is the rotational energy of the molecule considered as a rigid symmetric top and W_α the torsional energy. B and C are the usual

rotational constants with

$$C = \frac{h}{8\pi^2(I_1 + I_2)}$$

Hence, the only new problem is to solve (12-29), a form which is equivalent to Mathieu's equation, and hence to obtain W_α. Characteristics of the functions $\mathfrak{M}(\alpha)$ have been discussed by Koehler and Dennison [99], whose treatment we shall follow.

Solutions of equation (12-29) are known from Floquet's theorem (see [65] and *Tables Relating to Mathieu Functions*, Columbia University Press, New York, 1951) to be of the type

$$\mathfrak{M}(\alpha) = e^{i\sigma\alpha}F(\alpha) \quad (12\text{-}31)$$

where $F(\alpha)$ is periodic with period $2\pi/3$, that is, $F(\alpha)$ may be expanded in the form

$$F(\alpha) = \sum_p a_p e^{3ip\alpha} \quad (12\text{-}32)$$

where p is any integer. The constant σ must be real in order to make the wave function finite everywhere. The other conditions imposed on the wave function by the physical situation it must describe are that it must be unchanged when either end of the molecule is rotated any number of complete rotations, that is, when

$$\chi_1 \to \chi_1 + 2\pi n_1 \quad \text{and} \quad \chi_2 \to \chi_2 + 2\pi n_2 \quad (12\text{-}33)$$

Making these substitutions into (12-28) and (12-31),

$$e^{iK\chi}e^{iM\phi}\Theta(\theta)e^{i\sigma\alpha}F(\alpha) = e^{iK\chi}e^{iM\phi}\Theta(\theta)e^{i\sigma\alpha}F(\alpha)e^{2\pi i\left[\frac{K(n_1I_1+n_2I_2)}{I} + \sigma(n_1-n_2)\right]}$$

so that

$$\frac{K(n_1I_1 + n_2I_2)}{I} + \sigma(n_1 - n_2) = p \quad (12\text{-}34)$$

where p is an integer.

Equation (12-34) can hold only if K is an integer (as would be expected since $K\hbar$ is the total angular momentum around the symmetry axis) and if

$$\sigma = s - \frac{KI_1}{I} \quad (12\text{-}35a)$$

where s is any integer.

There are only three types of solutions, which may be obtained with values of $s = 0$, 1, or 2; that is, with

$$\sigma = -\frac{KI_1}{I},\ 1 - \frac{KI_1}{I},\ \text{or}\ 2 - \frac{KI_1}{I} \quad (12\text{-}35b)$$

For, if $\sigma = 3p + s - KI_1/I$, where p is an integer, the exponent $3p$ may be taken as part of $F(\alpha)$ in (12-31), so that the solution is equivalent to

that with $\sigma = s - KI_1/I$. (These three types of solutions have in previous treatments often been designated by a quantum number τ, with $\tau = 1, 3$, and 2, corresponding to $s = 0, 1$, and 2, respectively.) The solutions (12-31) are also periodic in K with a period $3I/I_1$, for if $K = 3I/I_1$, $\sigma = s - 3$, which is equivalent to the solution with $\sigma = s$.

Actual solutions $\mathfrak{M}(\alpha)$ must be obtained by using the expanded form (12-32) of $F(\alpha)$, substituting into the Eq. (12-29), and evaluating the coefficients a_p (or from tabulations). This also gives the various allowed values of the "internal" energy W_α associated with the angle α. There are an infinite number of allowed values of W_α, but for reasonably high barriers the lower values are grouped in threes near the energies to be expected from the bound case with vibrational quantum numbers $v = 0, 1, 2, 3, \ldots$. The calculated values of these energies for a particular case where

$$V_0 = 770 \text{ cm}^{-1} \qquad \frac{Ih}{8\pi^2 I_1 I_2 c} = 24.8 \text{ cm}^{-1} \qquad \frac{I_1}{I} = 0.21$$

are plotted in Fig. 12-6. The lower energy levels correspond essentially to vibrational levels which are slightly split into three levels. The higher levels (*e.g.*, with vibrational quantum number $v = 2$ or 3) are still partly grouped by vibrational quantum numbers but are far enough above the hindering potential to correspond fairly closely to the levels of a free rotor which are plotted in the same figure for comparison. The internal energy of the free rotor is, from (12-24),

$$W_x = \frac{I\hbar^2}{2I_1I_2}\left(m_1 - \frac{KI_1}{I}\right)^2$$

For a fixed value of m_1 and varying K, this gives a parabola with a minimum energy at $K = Im_1/I_1$. The various parabolas in Fig. 12-6 correspond to different integral values of m_1.

Figure 12-6 also illustrates the rapid decrease in the frequency of tunneling as the energy sinks farther below the top of the potential barrier. Both sets of levels $v = 1$ and $v = 0$ are below the top of the barrier, and the spread in frequency in each set corresponds to the tunneling frequency. For $v = 0$, the tunneling frequency is very low, and it would be decreased further, of course, if the potential barrier were assumed to be higher.

The three different types of levels, with $s = 0$, 1, or 2, are indicated by solid, short-dashed, or long-dashed curves, respectively, as are their counterparts in the free-rotor levels. The effect of a hindering potential is to separate groups of the free-rotor levels at the points where levels of like types cross in Fig. 12-6. Each type of level may be seen to be periodic in K with a period as shown above of $3I/I_1$, or approximately 14.

There are many molecules having hindered torsional motions with

more or fewer equilibrium positions than the three which apply to our present example. The ethylene molecule H_2CCH_2 has only two equilibrium positions, while F_3CSF_5 has twelve equilibrium positions of the CF_3 group with respect to the four off-axis fluorines bonded in the SF_5

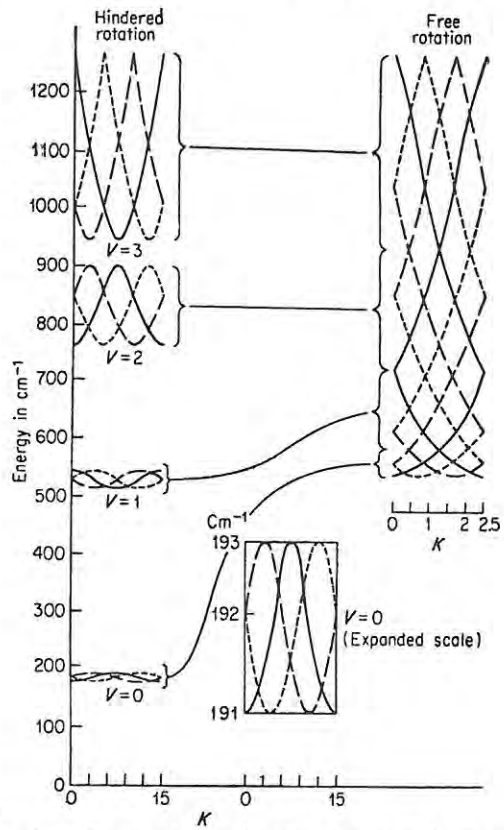

FIG. 12-6. Comparison of energy levels of torsional motion of a molecule of the type H_3CCF_3 with free rotation and with a hindering potential. The hindering potential is assumed to have a height $V_0 = 770$ cm^{-1}, $\frac{Ih}{8\pi^2 I_1 I_2 c} = 24.8$ cm^{-1}, and $\frac{I_1}{I} = 0.21$. (*Adapted from Koehler and Dennison* [99].)

group (Fig. 12-7). The general structure of the energy levels is similar to that of the case discussed above, but the number of levels is, of course, changed. If there are n equilibrium positions the potential may be written

$$V = \frac{V_0}{2}(1 - \cos n\alpha) \tag{12-36}$$

There are then n levels in each vibrational group, which repeat as K increases with a period of nI/I_1.

A truly symmetric rotor has a dipole moment only along the symmetry axis; hence a microwave field is not able to change the angular momentum around the symmetry axis of any part of the symmetric molecule with hindered rotation discussed here. It can only induce transitions in the total angular momentum J, so that the selection rules are $\Delta J = 0, \pm 1$, $\Delta K = \Delta m_1 = \Delta v = 0$. The frequencies observed are therefore just $\nu = 2BJ$, and one might suppose the above discussion of internal energies which do not give spectra has been fruitless. This is not the case, however, because the same energy levels are good approximations to those of the slightly asymmetric rotor with hindered torsional motion, where dipole transitions between these levels do occur. In addition, the effects of the torsional motions on the rotational constant B are often seen.

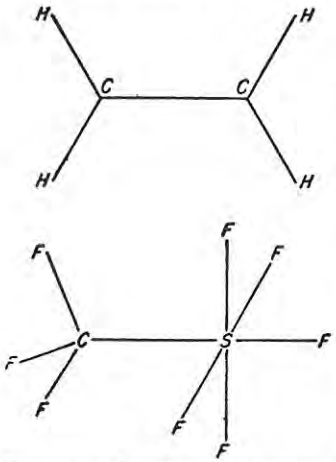

FIG. 12-7. Structure of ethylene with two potential minima and CSF_8 with 12 minima.

12-7. Heights of Hindering Barriers. In the simplest case of strongly hindered torsion, where the levels are essentially those of a harmonic oscillator, their effect on B is expressible in terms of a rotation-vibration constant α and the vibrational quantum number v, that is,

$$B = B_e - \alpha(v + \tfrac{1}{2})$$

One can be sure that the effect of torsional vibrational will be to push the two interfering parts of the molecule farther apart on the average, which will almost always give a positive sign to α. Very frequently also, the torsional motion is the lowest-frequency vibration in the molecule, so that one can identify the lines with $v = 1, 2, \ldots$ as the strongest set of excited vibrational lines in the rotational spectrum with a positive value of α. A measurement of the relative intensities of the ground state rotational line and one or more of the excited states at a given temperature allows a determination of the torsional frequency ω, since the intensities are proportional to the Boltzmann factor $e^{-\hbar\omega/kT}$. A knowledge of the torsional frequency and the approximate moments of inertia involved in turn allows a determination of the barrier height, since approximately

$$\omega = \frac{1}{2\pi}\sqrt{\frac{kI}{I_1 I_2}} \tag{12-37}$$

where k is the torque constant at the position of the potential minimum,

If the potential has n minima, and is of the form (12-36), then

$$k = \left(\frac{d^2V}{d\alpha^2}\right)_{\alpha=0} = \frac{n^2 V_0}{2}$$

and from (12-37),

$$V_0 = \frac{8\pi^2\omega^2}{n^2}\frac{I_1 I_2}{I} \tag{12-38}$$

The barrier heights for a number of molecules determined by measurement of intensity ratios and use of (12-38) are listed in Table 12-6 with values of α for the torsional vibration. Table 12-6 also lists some barrier

TABLE 12-6. BARRIER HEIGHT AND ROTATION-VIBRATION CONSTANT α FOR HINDERED MOLECULAR VIBRATIONS

All barrier heights listed have been determined by microwave methods except for those in [130].

Molecule	Barrier height, cm^{-1}	Rotation-vibrational constant α, Mc./sec.	Reference
CH_3NO_2	2.10	.....	[986]
CF_3SF_5	220	0.05	[713]
CH_3CCl_3	950	.....	[130]
CH_3SiF_3	410	4.2	[618] [641]
CH_3OH	375	.....	[561] [817]
CH_3SH	400	.....	[978a] [949a]
CH_3SiH_3	558	30	[604]
CH_3SnH_3	....	10.8	[603]
CH_3CF_3	1200	.....	[618]
CH_3CH_3	960	.....	[130]
$(CH_3)_2O$	1000	.....	[130]
CH_3CHF_2	1200	.....	[978]
CH_3NH_2	685	.....	[976]
H_2O_2	113	.....	[960]

heights which have been more precisely determined from spectroscopic observations, and some obtained by thermodynamic techniques. Usually the intensity ratios have not been determined more accurately than ± 10 per cent, so that there are sizable uncertainties in V_0. However, this method is one of the best available for barrier-height determinations, since the torsional frequencies do not often give detectable effects in either vibrational or Raman spectra (*cf.* [130], p. 496), and a determination from thermodynamic measurements, which has sometimes been used, is often tedious and inaccurate (*cf.* [130], p. 520).

Of course (12-38) assumes the particular form (12-36) for the potential. However, as pointed out above, calculations of potential shapes with

reasonable assumptions about the interactions give curves very close in shape to (12-36), so that actual potential curves are not likely to differ greatly from it. Expression (12-38) also assumes that the excited vibrational states whose relative intensities are measured lie sufficiently close to the bottom of the potential for a harmonic-oscillator approximation to apply. If this is not true, then the intensity ratios of successive excited states will not be constant, nor will α be constant. In one or two cases so far measured, such deviations seem to have been observed.

The separation between the three levels in an individual vibrational state may be sufficient to produce slightly different values of the rotation-vibration constant α. For example, Lide and Coles [604] report that in excited torsional vibrational states the $J = 1 \leftarrow 0$ transition of CH_3SiH_3 splits into two lines representing slightly different values of α, and that the $J = 1 \leftarrow 0$, $K = 1$ transitions split into three components, corresponding to expectations from Fig. 12-6 (see also [948a]).

12-8. Hindered Torsional Motions in Asymmetric Rotors. Consider now the case where one of the two parts of the molecule with hindered torsional motion is not a symmetric rotor. Let the hindered motion involve rotation of the part which is a rigid symmetric rotor about its axis and with respect to a second part of the molecule which comprises a rigid asymmetric rotor. Also let the asymmetric rotor have a plane of symmetry which includes the axis of the symmetric rotor. Such a model is of course not completely general, but it includes a wide variety of interesting cases such as CH_3OH, CH_3NO_2, CH_3NH_2, and CF_3CH_2Cl. Our treatment will follow closely that of Hecht and Dennison [934a], which in turn relies heavily on a discussion by Burkhard and Dennison [561].

The kinetic energy due to rotation of such a molecule is

$$T = \tfrac{1}{2}I_x\omega_x^2 + \tfrac{1}{2}I_y\omega_y^2 + \tfrac{1}{2}I_1\dot{\chi}_1^2 + \tfrac{1}{2}I_2\dot{\chi}_2^2 - D\omega_y\dot{\chi}_1 \tag{12-39}$$

where, as in Eq. (12-25), I_x is the principal moment of inertia of the entire molecule about an axis perpendicular to the plane of symmetry and to the axis of hindered motion which is the z direction, and I_y is the moment of inertia about an axis perpendicular to x and z. The corresponding angular velocities are ω_x and ω_y. I_1 and I_2 are the moments of inertia of the two parts of the molecule about the axis or z direction, χ_1 is the angle specifying the rotation of the asymmetric part about the axis and χ_2 is the similar angle for the symmetric part. Since I_1 is not necessarily a principal moment of inertia of the asymmetric rotor, the term $-D\omega_y\dot{\chi}_1$ is needed in (12-39), where D is the product of inertia

$$D = \sum_i m_i y_i z_i \tag{12-40}$$

Here m_i is the mass of an atom of the asymmetric rotor and y_i, z_i the coordinates of this mass with respect to the center of gravity of the entire

molecule. No products of inertia involving the x axis occur in (12-39), because the yz plane is taken to be the plane of symmetry of the molecule so that these products of inertia are zero.

Suitable rotations of axes and introduction of the variable $\alpha = \chi_1 - \chi_2$ as in (12-26) transform [934a] the Hamiltonian derived from (12-39) to

$$\begin{aligned}
H = {} & \left.\begin{aligned}
&\left[\frac{1}{4I_x} + \frac{I_y}{4(I_y^2 + D^2)}\right](P_{x'}^2 + P_{y'}^2) \\
&\quad + \frac{1}{2}\left[\frac{I_y + I}{I_yI - D^2} - \frac{I_y}{I_y^2 + D^2}\right]P_{z'}^2 \\
&\qquad + \frac{(I_yI - D^2)}{2I_2(I_yI_1 - D^2)}\,p_\alpha^2 + V(\alpha)
\end{aligned}\right\} \text{(I)} \\
&+ \frac{1}{4}\left(\frac{1}{I_x} - \frac{I_y}{I_y^2 + D^2}\right)\left[(P_{x'}^2 - P_{y'}^2)\cos 2\left(\frac{I_2}{I}\right)^* \alpha \right. \\
&\qquad \left. + (P_{x'}P_{y'} + P_{y'}P_{x'})\sin 2\left(\frac{I_2}{I}\right)^* \alpha\right] \\
&+ \frac{D}{2(I_y^2 + D^2)}\left[(P_{y'}P_{z'} + P_{z'}P_{y'})\cos\left(\frac{I_2}{I}\right)^* \alpha \right. \\
&\qquad \left. - (P_{x'}P_{z'} + P_{z'}P_{x'})\sin\left(\frac{I_2}{I}\right)^* \alpha\right]
\end{aligned} \quad \text{(II)} \tag{12-41}$$

where $P_{x'}$, $P_{y'}$, and $P_{z'}$ are components of the total angular momentum operator, p_α is the momentum which is canonically conjugate to α or $\chi_1 - \chi_2$, $I = I_1 + I_2$, and $\left(\frac{I_2}{I}\right)^* = \frac{I_2\sqrt{I_y^2 + D^2}}{I_yI - D^2}$. The potential $V(\alpha)$ is assumed to have the form $V(\alpha) = (V_0/2)(1 - \cos n\alpha)$, where n is an integer.

The part of the Hamiltonian indicated by (I) is identical in form with (12-27b) for the completely symmetric hindered rotor and hence has solutions and energy values of the same type. In solutions of (12-41), however, the following quantities which occur in the symmetric-rotor cases will be replaced by their equivalents:

$$\frac{I}{I_1I_2} \text{ is replaced by } \left(\frac{I}{I_1I_2}\right)^* = \frac{I_yI - D^2}{I_2(I_1I_y - D^2)} \tag{12-42a}$$

$$\frac{I_2}{I} \text{ by } \left(\frac{I_2}{I}\right)^* = \frac{I_2\sqrt{I_y^2 + D^2}}{I_yI - D^2} \tag{12-42b}$$

and

$$\frac{I_1}{I} \text{ by } \left(\frac{I_1}{I}\right)^* = 1 - \frac{I_2\sqrt{I_y^2 + D^2}}{I_yI - D^2} \tag{12-42c}$$

Solutions of part (I) are

$$\psi_{JKMvs} = \frac{1}{2\pi}e^{iK\chi'}e^{iM\phi'}\Theta_{JKM}(\theta')e^{i\sigma\alpha}F_{Kvs}(\alpha) \tag{12-43}$$

where χ', ϕ', and θ' are Eulerian angles for the system corresponding to the transformed axes x', y', and z'. $F_{Kvs}(\alpha)$ is a function of the form (12-32) appropriate to a particular value of K, a particular torsional-vibrational quantum number v, and a particular value of s. The quantum number s is defined as $\sigma + K(I_1/I)^*$ in analogy with (12-35a). In the common case when the potential has three minima, $s = 0$, 1, or 2 [*cf.* expression (12-35b)]. The energies are given by

$$H_{JKvs}^{J,Kvs} = hB[J(J+1) - K^2] + hCK^2 + W_\alpha^{Kvs} \tag{12-44}$$

where $B = \dfrac{h}{16\pi^2}\left(\dfrac{1}{I_x} + \dfrac{I_y}{I_y^2 + D^2}\right)$

$$C = \frac{h}{8\pi^2}\left(\frac{I_y + I}{I_y I - D^2} - \frac{I_y}{I_y^2 + D^2}\right)$$

W_α^{Kvs} = the torsional or internal energy for the particular state designated by the quantum numbers K, v, and s.

The terms of the Hamiltonian (12-41) designated as (II) may be treated as perturbations of the solutions (12-43) for the symmetric case. Part (II) has no matrix elements diagonal in J, K, v, s, and the off-diagonal elements are

$$H_{JKvs}^{J,K\pm1,v,s'} = \frac{h^2 D(2K \pm 1)\sqrt{(J \mp K)(J \pm K + 1)}}{16\pi^2(I_y^2 + D^2)} \int_0^{2\pi} e^{i(s'-s\mp1)\alpha} F_{Kvs}^*(\alpha) F_{K\pm1,v,s'}(\alpha)\, d\alpha \tag{12-45}$$

$$H_{JKvs}^{J,K\pm2,v,s'} = \frac{-h^2}{32\pi^2}\left(\frac{1}{I_x} - \frac{I_y}{I_y^2 + D^2}\right) \sqrt{(J \mp K)(J \mp K - 1)(J \pm K + 1)(J \pm K + 2)} \int_0^{2\pi} e^{i(s'-s\mp2)\alpha} F_{Kvs}^*(\alpha) F_{K\pm2,v,s'}(\alpha)\, d\alpha \tag{12-46}$$

When the potential has three minima, $F_{Kvs}(\alpha)$ from (12-32) is a sum of terms of the type $a_p e^{3ip\alpha}$, where p is an integer. Hence the integral in (12-45) is different from zero only when $s' - s \mp 1 = 3p$, and that in (12-46) is nonzero only when $s' - s \mp 2 = 3p$. Therefore, for $K \to K \pm 1$, $s' - s = \pm 1$ or ∓ 2, and for $K \to K \pm 2$, $s' - s = \pm 2$ or ∓ 1 (*cf.* [561]). These rules may also be expressed as $\Delta s = \Delta K \pm 3p$, where p is an integer.

In principle, energies W of all levels can be found from the secular equation of the determinantal form

$$|H_{JKvs}^{JK'v's'} - W\delta_{Kvs}^{K'v's'}| = 0 \tag{12-47}$$

where the matrix elements $H_{JKvs}^{JK'v's'}$ are given by (12-44), (12-45), and (12-46). The symbol $\delta_{Kvs}^{K'v's'}$ equals unity when $K' = K$, $v' = v$, and $s' = s$, but otherwise it is zero. For such a calculation, however, the

functions F_{Kvs} must be obtained and the integrals indicated in (12-45) and (12-46) carried out. This procedure is not practical except in individual cases, or when special conditions make simplifying approximations appropriate. However, before considering such approximations, we shall discuss the general nature of the solutions of the secular equation.

When the hindering potential has three minima

$$[V(\alpha) = \tfrac{1}{2}V_0(1 - \cos 3\alpha)]$$

the levels for which $K = s \pm 3p \pm 1$, where p is an integer, are always doubly degenerate. This degeneracy corresponds in the symmetric-rotor case to the degeneracy of the $\pm K$ states but is not removed by

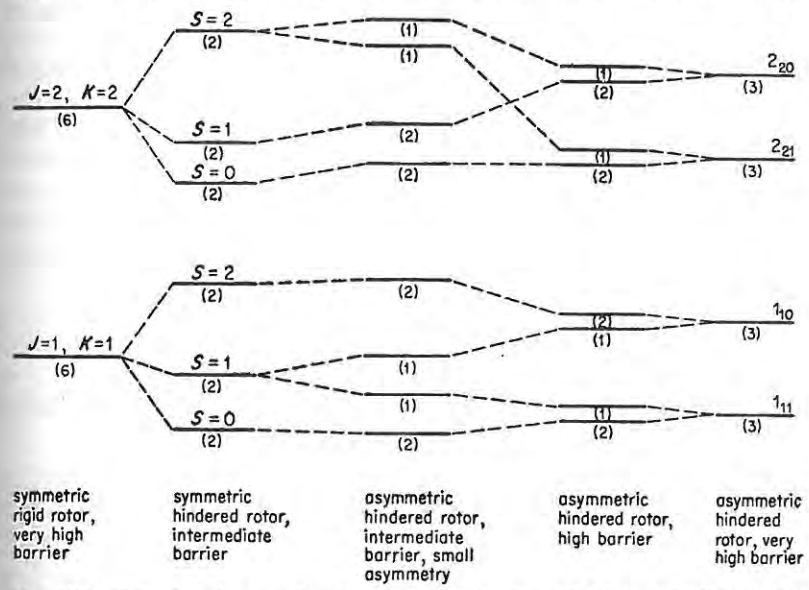

FIG. 12-8. Behavior of energy levels of a hindered rotor with three potential minima and with various asymmetries and barrier heights. Numbers in parentheses under energy levels represent the multiplicity of the level. (*After Ivash and Dennison* [817].)

asymmetry. However, for the states having $K = s \pm 3p$, asymmetry does remove the K degeneracy and splits the two levels by an amount which increases with asymmetry and decreases rapidly with increasing values of K. The general behavior of these levels for various barrier heights and asymmetries is illustrated in Fig. 12-8.

In the limit of a very high barrier, the molecule becomes a rigid asymmetric rotor. The energies W_α^{Kvs} become simply the energies of torsional oscillation in a single potential minimum, and the integrals in the matrix elements (12-45) and (12-46) both equal unity.

Whether or not a barrier is "high" or "low" depends on the ratio of its height V_0 to the kinetic energy associated with torsional momentum, or hence to the ratio

$$V' = \frac{V_0}{\frac{\hbar^2}{2}\left(\frac{I}{I_1 I_2}\right)^*} \tag{12-48}$$

where

$$\left(\frac{I}{I_1 I_2}\right)^* = \frac{I_y I - D^2}{I_2(I_1 I_y - D^2)}$$

For a barrier with $V' > 200$, the molecule may be treated as a rigid rotor for the lowest torsional-vibrational state. If $V' \leq 100$ the lowest torsional-vibrational state will be appreciably split, and the rigid-rotor approximation is not accurate. When $V' \approx 50$, the lowest vibrational state is split by many megacycles and the third vibrational state lies near the top of the barrier. If V' is less than unity, the barrier is low enough for something like free rotation to exist in the lower torsional states.

The High-barrier Case. Good approximations for the energies when $V' \geq 50$ have been worked out by Hecht and Dennison [934*a*]. They obtain for the torsional or internal energy

$$\begin{aligned} W_\alpha^{Kv0} &= W^v - \tfrac{2}{3}\Delta_v \cos\frac{2\pi K}{3}\left(\frac{I_1}{I}\right)^* \\ W_\alpha^{Kv1} &= W^v - \tfrac{2}{3}\Delta_v \cos\frac{2\pi}{3}\left[K\left(\frac{I_1}{I}\right)^* - 1\right] \\ W_\alpha^{Kv2} &= W^v - \tfrac{2}{3}\Delta_v \cos\frac{2\pi}{3}\left[K\left(\frac{I_1}{I}\right)^* + 1\right] \end{aligned} \tag{12-49}$$

where

$$W^v = \frac{\hbar^2}{\frac{2(I_1 I_2)^*}{I}}\left\{3\sqrt{V'}\,(v + \tfrac{1}{2}) - \tfrac{9}{8}[(v + \tfrac{1}{2})^2 + \tfrac{1}{4}]\right.$$
$$\left. - \frac{27}{64}\frac{1}{\sqrt{V'}}[(v + \tfrac{1}{2})^3 + \tfrac{3}{4}(v + \tfrac{1}{2})] + \cdots \right. \tag{12-50}$$

and, for the ground vibrational state ($v = 0$), Δ_0 is given to within a few per cent accuracy by

$$\Delta_0 = 7.05(V')^{\frac{1}{2}} \exp\left(-1.379\sqrt{V'}\right) \tag{12-51}$$

A general expression for Δ_v by use of the *WKB* approximation has also been obtained [934*a*]. The matrix elements (12-45) and (12-46) can be evaluated for the ground vibrational state of the high-barrier case from

the following values of the integrals which are involved:

$$\int_0^{2\pi} F_{K0s}(\alpha) e^{i(s'-s\mp 2)\alpha} F_{K\pm 2,0,s'}(\alpha)\, d\alpha = 1 - \frac{2}{3\sqrt{V'}}\left[1 - \left(\frac{I_1}{I}\right)^*\right]^2$$
$$- \frac{4}{9V'}\left\{\frac{9}{8}\left[1 - \left(\frac{I_1}{I}\right)^*\right]^2 - \frac{1}{2}\left[1 - \left(\frac{I_1}{I}\right)^*\right]^4\right\} + \cdots \tag{12-52a}$$

$$\int_0^{2\pi} F_{K0s}(\alpha) e^{i(s'-s\mp 1)\alpha} F_{K\pm 1,0,s'}(\alpha)\, d\alpha = 1 - \frac{1}{6\sqrt{V'}}\left[1 - \left(\frac{I_1}{I}\right)^*\right]^2$$
$$- \frac{1}{9V'}\left\{\frac{9}{8}\left[1 - \left(\frac{I_1}{I}\right)^*\right]^2 - \frac{1}{8}\left[1 - \left(\frac{I_1}{I}\right)^*\right]^4\right\} + \cdots \tag{12-52b}$$

These integrals are approximately independent of the value of s. Hecht and Dennison [934*a*] have given explicit expressions for the energies in the high-barrier case for states with $J = 1$ and $J = 2$.

Barriers of Intermediate Height. When the barrier is intermediate or low, that is, when V_0 is not much greater than $h^2 I_1 I_2/2I$, the formulation and matrix elements discussed above may still be used. However, the approach of Burkhard and Dennison [561] may be advantageous in actual calculation of energy levels. They do not make the transformation of Eq. (12-39) required to eliminate the cross term $D\omega_y\dot{\chi}_1$ but rather divide the Hamiltonian into two parts H_0 and H', where

$$H = H_0 + H' = \frac{(I_x + I_y)I_1 - D^2}{4I_x(I_y I_1 - D^2)}(P_x^2 + P_y^2) + \frac{1}{2(I_1 + I_2)}P_z^2$$
$$+ \frac{I_1 + I_2}{2I_1 I_2}p_\alpha^2 + V(\alpha) + H' \tag{12-53}$$

H_0 in this expression is identical in form with Eq. (12-27*b*) for the completely symmetric hindered rotor with the two equal moments of inertia replaced by I_B, where

$$I_B = \frac{2I_x(I_y I_1 - D^2)}{(I_x + I_y)I_1 - D^2} \tag{12-54}$$

Wave functions identical with Eq. (12-28) are therefore appropriate and matrix elements of $H = H_0 + H'$ for these functions can be evaluated. They are

$$H_{JKvs}^{JKvs} = \frac{h^2}{8\pi^2 I_B}[J(J+1) - K^2] + \frac{h^2K^2}{8\pi^2(I_1 + I_2)}$$
$$- \frac{h^2D^2}{8\pi^2 I_1(I_y I_1 - D^2)}\int_0^{2\pi} e^{-is\alpha}F_{Kvs}^{*(\alpha)}\frac{d^2}{d\alpha^2}(e^{is\alpha}F_{Kvs}^{(\alpha)})\, d\alpha \tag{12-55}$$

$$H_{JKvs}^{JKv's} = -\frac{h^2D^2}{8\pi^2 I_1(I_y I_1 - D^2)}\int_0^{2\pi} e^{-is\alpha}F_{Kvs}^{*(\alpha)}\frac{d^2}{d\alpha^2}(e^{is\alpha}F_{Kv's}^{(\alpha)})\, d\alpha \tag{12-56}$$

$$H^{J,K\pm1,v's'}_{JKvs} = \frac{\hbar^2 D\sqrt{(J\mp K)(J\pm K+1)}}{8\pi^2(I_yI_1 - D^2)}\int_0^{2\pi}\left[\pm\frac{e^{-i(s\pm1)\alpha}}{i}F^{*(\alpha)}_{Kvs}\frac{d}{d\alpha}\right.$$
$$\left.(e^{is'\alpha}F_{K\pm1,v's'}) - \frac{e^{i(s'-s\mp1)\alpha}}{2}F^{*(\alpha)}_{Kvs}F^{(\alpha)}_{K\pm1,v',s'}\right]d\alpha \quad (12\text{-}57)$$

$$H^{J,K\pm2,v',s'}_{JKvs} = \hbar^2\cdot\frac{(I_xI_1 - I_yI_1 + D^2)}{32\pi^2 I_x(I_yI_1 - D^2)}\sqrt{(J\mp K)(J\mp K-1)}$$
$$\times\sqrt{(J\pm K+1)(J\pm K+2)}\int_0^{2\pi}e^{i(s'-s\mp2)\alpha}F^{*(\alpha)}_{JKvs}F_{J,K\pm2,v',s'}\,d\alpha \quad (12\text{-}58)$$

As for Eqs. (12-45) and (12-46), these matrix elements are nonzero only when $\Delta S = \Delta K \pm 3p$, where p is an integer. Energy levels may be determined from them by solution of a secular equation of the form (12-47).

The previous treatment, which eliminated the cross term $D\omega_y\dot{\chi}_1$ and gave (12-41), is of advantage in avoiding matrix elements between states of different vibrational quantum number v. These are especially troublesome only in the high-barrier case, where their elimination affords considerable simplification.

The Low-barrier Case. When the barrier is very low, that is, when $V_0 \leq \frac{\hbar^2}{2(I/I_1I_2)^*}$, the most appropriate starting point for approximations is free internal rotation. If V_0 is assumed to equal zero, the part of the wave function for the internal motion, which is equivalent to (12-29), becomes

$$\frac{\hbar^2}{2}\left(\frac{I}{I_1I_2}\right)^*\frac{d^2\mathfrak{M}}{d\alpha^2} + W_\alpha\mathfrak{M} = 0$$

Hence

$$\mathfrak{M}(\alpha) = \frac{1}{\sqrt{2\pi}}e^{\pm i[m_1 - K(I_1/I)^*]\alpha} \quad (12\text{-}59)$$

and

$$W^{m_1}_\alpha = \frac{\hbar^2}{2}\left(\frac{I}{I_1I_2}\right)^*\left[m_1 - K\left(\frac{I_1}{I}\right)^*\right]^2 \quad (12\text{-}60)$$

To satisfy boundary conditions, as in (12-35*a*), m_1 must be an integer. $F_{Kvs}(x)$ is just $1/\sqrt{2\pi}\,e^{3ip\alpha}$, where $s + 3p = m_1$. It may be seen from (12-24) that m_1 is just the angular momentum in units of $\hbar$ of the asymmetric part of the molecule about the z' axis. From the similarity of the two parts of the molecule, $m_1 - K(I_1/I)^*$ in (12-59) and (12-60) might have been replaced by $m_2 - K(I_2/I)^*$, where $m_2\hbar$ is the angular momentum of the symmetric part and $m_1 + m_2 = K$. The quantum numbers v and s may be replaced by the number m_1 or m_2. The matrix elements (12-45) and (12-46) then become

$$H^{J,K\pm1,m_1\pm1}_{JKm_1} = H^{J,K\pm1,m_2}_{JKm_2} = \frac{\hbar^2 D(2K\pm1)\sqrt{(J\mp K)(J\pm K+1)}}{16\pi^2(I_y^2 + D^2)} \quad (12\text{-}61)$$

$$H^{J,K\pm2,m_1\pm2}_{JKm_1} = H^{J,K\pm2,m_2}_{JKm_1} = \frac{-\hbar^2}{32\pi^2}\left(\frac{1}{I_x} - \frac{I_y}{I_y^2 + D^2}\right)$$
$$\sqrt{(J\mp K)(J\mp K-1)(J\pm K+1)(J\pm K+2)} \quad (12\text{-}62)$$

If the barrier is low, but not zero, then it may be considered a small perturbation. The largest effects of such a perturbation are to add a constant $V_0/2$ to W^m_α, and to split pairs of levels which are close together and for which m differs by n, where n is the number of potential minima. This splitting is due to the existence of off-diagonal matrix elements of

$$V(\alpha) = \frac{V_0}{2}(1 - \cos n\alpha)$$

which are

$$V^{J,K,m\pm n}_{JKm} = -\frac{V_0}{4} \quad (12\text{-}63)$$

Matrix elements such as (12-63) are most important when there is a near degeneracy of the two levels which they connect.

Other Cases. A number of other useful approximations can be obtained for various special cases. Wilson, Lin, and Lide [1,000*a*] have discussed the case of a hindered asymmetric rotor with the product of inertia D equal to zero. They use a similar but somewhat different approach from that adopted above and give useful approximations for cases of small asymmetry and of high and low barriers.

Burkhard [782*a*] has formulated the rather general case of two asymmetric parts of a molecule with a potential hindering their relative motion, and with the sole limitation that the center of mass of one of these parts must lie on the axis of hindered rotation. He has written out the wave equation for this case and the matrix elements needed for a solution. Burkhard has also written down the wave equation and matrix elements for the still more general case of hindered rotation of two asymmetric parts with the center of gravity of neither part on the axis of rotation [908*a*]. However, this case is too unwieldy to be very useful unless simplifying approximations apply.

12-9. Selection Rules. For hindered rotors, the usual selection rule $\Delta J = 0, \pm1$ for the total angular momentum applies, as well as

$$\Delta M = 0, \pm 1$$

for the projection of J on a space-fixed axis. One other general rule can be stated for transitions of a hindered rotor of which one part is a symmetric top. It was pointed out in discussion of the matrix elements (12-45) and (12-46) that if the potential has three minima these matrix

elements connect only states for which

$$\Delta K = \Delta s \pm 3p$$

where p is an integer. This rule breaks up the states into three types which may be divided as follows:

$$K = s \pm 3p \qquad K = s \pm 3p + 1 \qquad K = s \pm 3p - 1 \qquad (12\text{-}64)$$

For a potential with n minima, the states may similarly be divided into n groups. There are also no electric dipole transitions between the different types of states specified by (12-64), so that one may write the selection rule $\Delta K = \Delta s \pm 3p$, or more generally

$$\Delta K = \Delta s \pm np \qquad (12\text{-}65)$$

where p is an integer and n is the number of potential minima. It should be noted that, if the rotor is asymmetric, it will involve a sum of symmetric-rotor states of various values of K so that K is not a well-defined quantity. However, from (12-64) a given state involves values of $K - s$ which differ only by $\pm 3p$, so that the selection rule (12-65) is meaningful.

For the general asymmetric rotor, all transitions are allowed which satisfy (12-65) and for which $\Delta J = 0$ or ± 1 and $\Delta M = 0$ or ± 1. However, unless the rotor is very asymmetric, the stronger transitions are given by the somewhat more restrictive selection rules of a symmetric rotor, which will now be discussed.

The electric dipole moment of a strictly symmetric rotor will always be parallel to the molecular axis. However, since we are also concerned with nearly symmetric tops, it will be assumed that the dipole moment may have a component perpendicular to the axis as well as one parallel to the axis. Selection rules are different for the two types of dipole moments, and intensities are in each case proportional to the square

TABLE 12-7. SELECTION RULES FOR SYMMETRIC OR NEARLY SYMMETRIC ROTORS WITH HINDERED ROTATION

The rules $\Delta J = 0, \pm 1$ and $\Delta M = 0, \pm 1$ apply to all transitions. $m_1\hbar$ is the angular momentum about the molecular axis of that part of the molecule which may have a dipole moment perpendicular to the axis.

	Very high barrier	Free rotation (zero barrier)	Intermediate barrier
Dipole moment parallel to molecular axis	$\Delta K = 0$ $\Delta s = 0$ $\Delta v = 0$	$\Delta K = 0$ $\Delta m_1 = \Delta m_2 = 0$	$\Delta K = 0$ $\Delta s = 0$ $\Delta v = 0$
Dipole moment perpendicular to molecular axis	$\Delta K = \pm 1$ $\Delta v = 0, \pm 1$	$\Delta K = \pm 1$ $\Delta m_1 = \pm 1$ $\Delta m_2 = 0$	$\Delta K = \pm 1$ $\Delta K = \Delta s \pm np$ $\Delta v =$ anything

of the component of the dipole moment involved. The selection rules are given in Table 12-7. The very-high-barrier case with the dipole moment parallel to the axis corresponds to the normal rigid symmetric rotor. In the case of free rotation with a dipole perpendicular to the axis, the angular momentum about the axis $m_1\hbar$ of only the asymmetric part of the molecule changes, since it alone would allow a perpendicular component of the dipole moment.

12-10. Examples of Hindered Torsional Motion in Asymmetric Rotors. The case of hindered torsional motion which has received by far the most complete and detailed analysis is CH_3OH. This is the molecule to which Koehler and Dennison [99] applied the symmetric-rotor approximation. However, little quantitative progress could be made until the advent of microwave spectroscopy allowed measurement of the CH_3OH spectrum under high resolution. Burkhard and Dennison [561] first worked out the CH_3OH hindered motion in detail, and quantitatively fitted the rather extensive microwave spectrum measured by Hughes, Good, and Coles [590] and by others. From this work the structure of CH_3OH, the components of the dipole moment perpendicular and parallel to the CH_3 axis, and the barrier height listed in Table 12-6 was obtained. A similar but still more complete discussion of CH_3OH has been given by Ivash and Dennison [817].

The CH_3OH lines of primary interest here make up an intense series beginning near 25,000 Mc, extending to about 31,000 Mc, and then returning toward lower frequencies. Thirty members of the series have been found. Stark effects of these lines show that the series corresponds to $\Delta J = 0$ transitions, that for the first line of the series $J = 2$, and that others involve successively higher values of J. The frequencies of the first dozen members of this series (for the common isotopic species of CH_3OH) are fairly accurately given [561] by

$$\nu = 24{,}948.13 - 2.9656J(J+1) + 0.11258J^2(J+1)^2 - 0.4094 \times 10^{-4}J^3(J+1)^3 - 0.3168 \times 10^{-6}J^4(J+1)^4 \quad \text{Mc} \qquad (12\text{-}66)$$

Burkhard and Dennison [561] showed that the only explanation of the origin of this series consistent with reasonable parameters for the CH_3OH molecule is a transition of the type $v = 0, \Delta J = 0, K = 2 \leftarrow 1, s = 0 \leftarrow 2$. The increase of rotational energy due to the transition $K = 2 \leftarrow 1$ is approximately 10 cm^{-1}, which is almost canceled by the decrease in internal energy of about 9 cm^{-1} due to the transition $s = 0 \leftarrow 2$. The difference between these two quantities depends to some extent on J, which allows the series of lines for different values of J. The lowest value of J for such a series equals, of course, the maximum value of K, which is 2. This is in agreement with the results of Stark-effect measurements.

The value of $V' = \dfrac{V_0}{\hbar^2 I/2I_1I_2}$ in CH_3OH is approximately 13, so that the barrier is of intermediate height, and neither the high-barrier nor low-barrier approximations discussed above are accurate. Burkhard and Dennison [561] have, however, worked out approximate expressions for the torsional energy.

An interesting example of a low barrier is afforded by CH_3NO_2, which has been studied by Tannenbaum, Johnson, Myers, and Gwinn [986]. CH_3NO_2 has a potential with 6 minima and a height of 2.1 cm^{-1}. The quantity $\hbar^2 I/2I_1I_2$ is approximately 5.8 cm^{-1}, so that $V' = 0.36$, and the low-barrier approximation is appropriate. Table 12-8 gives observed components of the $J = 2 \leftarrow 1$ transition of this molecule and calculated frequencies assuming either a zero barrier or a barrier of height $V_0 = 2.10$ cm^{-1}. Since NO_2 has no dipole moment perpendicular to the molecular axis, the torsional energy does not appear very directly in the transition frequencies, and hence the free-rotation approximation is fairly accurate. However, the potential does strongly affect the energy levels with $m_2 = \pm 3 = \pm n/2$. These levels are split by an interaction of the type indicated by (12-63).

TABLE 12-8. STRUCTURE OF THE $J = 2 \leftarrow 1$ TRANSITION OF CH_3NO_2, A MOLECULE WITH HINDERED TORSION AND A LOW BARRIER

Frequencies are calculated assuming $B + C = 16{,}419.3 - 0.32m_2^2$ Mc, $B - C = 4{,}666.0$ Mc, $h/8\pi^2 I_1 = 13{,}277.5$ Mc, and $h/8\pi^2 I_2 = 160{,}000$ Mc. (From Tannenbaum, Johnson, Myers, and Gwinn [986].)

K	m_1	m_2	Calculated frequencies, Mc		Measured frequencies, Mc
			$V_0 = 0$	$V_0 = 2.10$ cm^{-1}	
0	0	0	30,010.7	30,011.5	30,035.6
±1	±2	∓1	32,033.4	32,034.1	32,034.1
±1	0	±1	33,642.5	33,643.5	33,643.5
0	∓2	±2	32,959.8	32,959.8	32,959.2
±1	∓2	±3	33,174.4	33,474.6	33,476.5
∓1	±2	∓3	33,174.4	31,676.2	31,677.3
±1	±4	∓3	32,491.6	32,191.4	32,189.7
∓1	∓4	±3	32,491.6	33,989.8	33,988.5
0	∓4	±4	32,856.6	32,856.6	32,859.5

In CH_3NO_2, the zero spin and Bose-Einstein statistics of O^{16} require that only levels with even m_1 are permitted. For, if two oxygens in the NO_2 group are interchanged, this is equivalent to a rotation about the axis of 180°, so that the wave function is changed by $e^{im_1\pi}$. Since the O^{16} spins are zero and only a symmetric-spin wave function can be formed, the spatial partial of the wave function must also be symmetric. This requires that $e^{im_1\pi} = 1$, or that m_1 is an even integer.

The magnitude of V_0 gives some interesting qualitative information about the nature of barriers in molecules with three potential minima. Consider the simplified molecule CH_3NO, which would have three potential minima, with a potential of the general form

$$V = \sum_p V_p \cos 3p\alpha \tag{12-67}$$

Presumably the height of the barrier would be approximately the same as found in most molecules of this geometry, that is, V_1 equals a few hundred wave numbers. If a second oxygen 180° away from the first is added to the molecule to produce CH_3NO_2, the potential is

$$\begin{aligned} V &= \sum_p V_p[\cos 3p\alpha + \cos 3p(\alpha + \pi)] \\ &= \sum_p 2V_{2p} \cos 6p\alpha \end{aligned} \tag{12-68}$$

Since experimentally $2V_2 = 2.1$ cm^{-1}, we have a good indication that V_2/V_1 is only a few parts in 100; therefore, higher terms in a series such as (12-67) are probably not important. In view of this it is very surprising, however, that the 12-minima potential of CF_3SF_5 is as large as is given in Table 12-6.

CHAPTER 13

SHAPES AND WIDTHS OF SPECTRAL LINES

A truly isolated, undisturbed, and stationary molecular system would have the attractive feature of definite and fixed energy levels, but various types of unavoidable disturbances do in fact vary the energy levels, giving a width to spectral lines and varying their average or center frequencies. The sources of spectral line broadening which need to be considered are:

1. Natural line breadth
2. Doppler effect
3. Pressure broadening, *i.e.*, disturbances due to interactions between molecules
4. Saturation broadening
5. Collisions between molecules and the walls of a containing vessel.

13-1. Natural Line Breadth. The natural line breadth may be interpreted classically as due to radiation damping, or quantum-mechanically as a disturbance of the molecule by zero-point vibration of electromagnetic fields which are always present in free space. For a transition of frequency ν from an excited state to the ground state of the system, zero-point electromagnetic fields give an absorption line a half width at half maximum intensity of

$$\Delta\nu = \frac{32\pi^3\nu^3}{3hc^3}|\mu|^2 \qquad \text{cycles/sec} \tag{13-1}$$

where μ is the quantum-mechanical matrix element of the dipole moment —usually of the order of 1 debye unit, or 10^{-18} esu. For radiation of 1 cm wavelength $\Delta\nu$ is, from Eq. (13-1), approximately 10^{-7} cycle/sec. For radio frequencies and ordinary temperatures, thermal radiation consists of stronger electromagnetic fields than the usual zero-point fields, since each mode of vibration of the field has a mean energy kT rather than $\frac{1}{2}h\nu$. This increases the value of $\Delta\nu$ by a factor $2kT/h\nu$, or approximately 400 for room temperature, giving a "natural" width of 4×10^{-5} cycle/sec. This width is quite negligible in comparison with that caused by other types of broadening.

The natural line breadth is often regarded as an unchangeable effect of disturbance of the system by electromagnetic fields, which are uni-

formly present in all space. However, in the radio-frequency range the zero-point electromagnetic fields need not be uniform because cavities or circuits may be as small as one wavelength. Thus in a cavity with perfectly reflecting walls only certain resonant frequencies can occur, and a particular frequency necessary to cause a particular microwave transition may not occur. In this case no "spontaneous" emission of this frequency can occur, and the natural line breadth is zero. Similarly natural line breadths may be increased by the presence of resonant circuits which increase the local strength of zero-point electromagnetic vibrations.

Radiation broadening is of importance for microwave spectroscopy when transitions between levels of excited electronic states are observed. Then the line width is large because it is proportional to ν_0^3, where ν_0 is now the frequency of the transition to the ground electronic state. For instance, the $2p\ ^2P_{\frac{3}{2}}$ state of hydrogen, discussed in connection with the Lamb-Retherford experiment in Chap. 5, has a natural half width of 50 Mc.

13-2. Doppler Effect. The Doppler effect occurs when a molecule is moving parallel to the direction of propagation of the radiation being absorbed, and gives a frequency shift of $\pm\nu(v/v_p)$, where ν is the resonant frequency without Doppler shift, v the molecular velocity, and v_p the velocity of phase propagation of the radiation. Although under some conditions v_p may be larger than c (*e.g.*, for propagation in a waveguide near cutoff), usually $v_p \approx c$, and the fractional frequency shifts are simply v/c. The probability that a molecule in a gas at temperature T has a velocity v in a particular direction is proportional to $e^{-mv^2/2kT}$, where m is the molecular mass. Hence the line intensity as a function of change ϵ from the resonance frequency is $e^{-\frac{mc^2}{2kT}\left(\frac{\epsilon}{\nu}\right)^2}$. The line is consequently symmetric and has a half width at half maximum of

$$\Delta\nu = \frac{\nu}{c}\sqrt{\frac{2kT}{m}\ln 2} = \frac{\nu}{c}\sqrt{2kN_0\ln 2}\sqrt{\frac{T}{M}} = 3.581 \times 10^{-7}\sqrt{\frac{T}{M}}\,\nu \tag{13-2}$$

where M is the molecular weight and N_0 is Avogadro's number. For an ammonia molecule at room temperature, $\Delta\nu/\nu = 1.5 \times 10^{-6}$. Doppler effect can be decreased to some extent by use of heavier molecules and lower temperatures, but a decrease in line width of more than a factor of 2 can hardly be expected because at low temperatures molecules have not sufficient vapor pressure ($\sim 10^{-2}$ mm Hg) to absorb radiation. A great decrease in Doppler width is obtained in some optical spectroscopy experiments by observing an atomic beam at right angles to its direction of motion [238]. This method is not so easy to apply or so popular in microwave spectroscopy, but it has been used in two different types of microwave spectrometers [709], [925], [982]. Newell and Dicke [622] have also developed a technique of selecting absorption only from

molecules in a certain narrow velocity range and thus decreasing the effect of Doppler broadening on the line width by a factor of 10 or more. Although these techniques sacrifice sensitivity to eliminate Doppler effect and obtain narrow lines, they should be useful for resolving very closely spaced lines in strong microwave spectra.

13-3. Pressure Broadening. The most important source of broadening in many microwave experiments is pressure broadening. It is also the most interesting because it provides information about how molecules behave in intermolecular collisions and hence about molecular force fields. This broadening arises from collisions between molecules.

The spectral distribution of a molecular oscillation of finite lifetime was first considered by Lorentz [2]. For an oscillator whose amplitude decreases exponentially with time ($a = a_0e^{-t/\tau}$), the radiation distribution corresponds to the well-known resonance-type curve with a half width in frequency of $1/2\pi\tau$. Exactly the same result is obtained for a group of oscillators, each of which oscillates with a constant amplitude but is abruptly stopped after time t, where the number oscillating for time t is given by $n_t = n_0e^{-t/\tau}$. The theory assumes that after a collision, when the oscillation is stopped, it starts again with a phase having no relationship to the phase before collision; *i.e.*, "strong" collisions are assumed. When applied to the case of rotating molecules, this assumption is equivalent to assuming that the orientation of the molecules after collision is random.

A fairly complete qualitative description of pressure broadening in the microwave and radio-frequency region can be obtained with the simple assumption that collisions are very brief, but so strong that the behavior of the molecule after collision has no particular relationship to that before collision. We shall first explore the consequences of collisions of this type to obtain a general description of pressure broadening, and then return to examine in more detail what happens during a collision and the relation between pressure broadening and intermolecular forces.

Debye ([12], Chap. 5) considered the case of the fixed dipole with no rotation or translation energy. After each collision the dipole is assumed to be not completely random in orientation, but oriented with respect to the electric field present at the moment in accordance with the Boltzmann distribution $\exp(-\mathbf{E}\cdot\boldsymbol{\mu}/kT)$, where $\mathbf{E}$ is the electric field strength existing at the time, $\boldsymbol{\mu}$ is the dipole moment, and k and T are the Boltzmann constant and the absolute temperature, respectively. If the field has oscillated many times before the molecule makes another collision, the dipole has no special orientation with respect to the field at the time of this next collision. During the next collision, however, it is again oriented with respect to the field present, again absorbing a small quantity of energy from the field during this orientation process. Such a process is repeated many times and thus absorbs energy although there

is no characteristic resonance peak. Debye calculated the theoretical expression for this type of absorption (*cf.* Van Vleck and Weisskopf [136] for some discussion and generalization). In this case, the absorption per unit length is

$$\gamma = \frac{\omega}{c}\frac{4\pi N\mu^2}{3kT}\frac{\omega\tau}{1+\omega^2\tau^2} \tag{13-3}$$

where ω is the angular frequency ($2\pi\nu$) of the incident radiation, τ is the mean lifetime between collisions, N is the number of molecules per cubic centimeter, μ is the dipole moment of a molecule, c is the velocity of light, k is the Boltzmann constant, and T is the absolute temperature.

The Van Vleck–Weisskopf Line Shape. The Debye and Lorentz theories have been synthesized by Van Vleck and Weisskopf ([136]; see also H. Fröhlich [154] for another derivation). Assuming that the molecule undergoes a violent collision the phase of its oscillation after such a collision will not be greatly dependent on its phase at the start of the collision. In this case there must be thermodynamic equilibrium between the molecule and the existing electric field immediately after each collision somewhat like the assumed equilibrium distribution in the orientation of the fixed dipole mentioned above. Using this assumption rather than Lorentz's assumption that the phase after a collision is arbitrary, an expression similar to Lorentz's formula may be obtained which is consistent with the Debye case.

Since the rotation of a molecule can always be resolved into two perpendicular vibrations, it is sufficient to consider a linear vibrator. To determine the absorption and the dielectric constant associated with a vibrating charge in a classical way, one needs only to solve the equation of motion of the oscillator in the field subject to the right boundary conditions. The equation is of the type

$$\ddot{x} + \omega_0^2 x = \frac{eE}{m}\cos\omega t \tag{13-4}$$

where $\omega_0 = 2\pi$ times the natural molecular frequency
$\omega = 2\pi$ times the frequency of oscillation of the field E

Before solving Eq. (13-4) we shall show how the absorption and dielectric constant may be obtained from the solution for x. The dielectric constant is defined as usual

$$K = \frac{D}{E} = 1 + 4\pi\frac{P}{E} \tag{13-5}$$

where P is the polarization per unit volume. After x has been averaged over all molecules, it will be of the form

$$\bar{x} = aE\cos\omega t + bE\sin\omega t \tag{13-6}$$

The real part of the polarization is $P = naEe \cos \omega t$, so that

$$K = 1 + 4\pi nae \tag{13-6a}$$

where n is the number of such oscillators per unit volume.

To obtain the fractional absorption of power per unit distance, consider a cube of unit volume with the radiation traveling through it perpendicular to one of the faces. The radiation absorbed during a time T will be

$$n \int_0^T e\dot{x}E \cos \omega t \, dt$$

The total radiation energy passing into the cube will be $c(E^2/8\pi)T$, where c is the velocity of light, so that the fractional absorption per unit distance or the absorption coefficient will be

$$\frac{neE \int_0^T \dot{x} \cos \omega t \, dt}{c(E^2/8\pi)T}$$

Remembering again the form of $\bar{x}$ and integrating over a long period of time the absorption coefficient is seen to be

$$\gamma = \frac{4\pi nebw}{c} \tag{13-7}$$

We return to a solution of the equation of motion. For ease of solution we use a complex quantity $e^{i\omega t}$ for $\cos \omega t$ in the equation of motion so that x will be the real part of the solution, which is of the form

$$\frac{eEe^{i\omega t}}{m(\omega_0^2 - \omega^2)} + c_1 e^{i\omega_0 t} + c_2 e^{-i\omega_0 t} \tag{13-8}$$

where c_1 and c_2 depend on the initial values of x and $\dot{x}$. The average initial value of x and $\dot{x}$ can be found from the energy

$$H = \frac{m}{2}(\dot{x})^2 + \frac{m}{2}(\omega_0 x)^2 - exE \cos \omega t \tag{13-9}$$

thus

$$\bar{x}_0 = \frac{\int x e^{-H/kt} \, dx \, d\dot{x}}{\int e^{-H/kt} \, dx \, d\dot{x}} = \frac{Ee \cos \omega t}{m\omega_0^2} \tag{13-10}$$

and similarly

$$\bar{\dot{x}}_0 = \bar{\dot{x}}_0 = 0 \tag{13-11}$$

For some time of interest t the constants c_1 and c_2 will be functions of t_1, the time of last collision of the molecule. We must average then over all values of t_1. The distribution of collisions in time can be written according to kinetic theory

$$n(t_1) = \frac{1}{\tau} e^{-(t-t_1)/\tau} \, dt_1 \tag{13-12}$$

where τ is the mean time between collisions, where $n(t_1)$ is the probability that a molecule made its last collision between time t_1 and $t_1 + dt_1$. Our expression for x must be averaged over this distribution. After performing the average one can find the in-phase and the quadrature terms of the real part of $\bar{x}$ to be

$$a = \frac{e}{m(\omega_0^2 - \omega^2)} \left\{1 - \frac{\omega}{2\omega_0^2\tau^2}\left[\frac{\omega_0 + \omega}{(1/\tau)^2 + (\omega_0 - \omega)^2} + \frac{\omega - \omega_0}{(1/\tau)^2 + (\omega_0 + \omega)^2}\right]\right\} \tag{13-13}$$

$$b = \frac{e\omega}{2m\omega_0^2\tau}\left\{\frac{1}{(1/\tau)^2 + (\omega_0 - \omega)^2} + \frac{1}{(1/\tau)^2 + (\omega_0 + \omega)^2}\right\} \tag{13-14}$$

Correspondingly, from Eq. (13-6a) the dielectric constant is

$$K = 1 + \frac{ne^2}{\pi m(\nu_0^2 - \nu^2)}\left\{1 - \frac{\nu}{2\nu_0^2(2\pi\tau)^2}\left[\frac{\nu_0 + \nu}{(1/2\pi\tau)^2 + (\nu_0 - \nu)^2} + \frac{\nu - \nu_0}{(1/2\pi\tau)^2 + (\nu_0 + \nu)^2}\right]\right\} \tag{13-15}$$

and the absorption coefficient from Eq. (13-7) is

$$\gamma = \frac{ne^2\nu^2}{mc\nu_0^2}\left[\frac{1/2\pi\tau}{(\nu - \nu_0)^2 + (1/2\pi\tau)^2} + \frac{1/2\pi\tau}{(\nu + \nu_0)^2 + (1/2\pi\tau)^2}\right] \quad \text{cm}^{-1} \tag{13-16}$$

This is the complete expression for a classical oscillator. They must be modified to some extent, however, for the quantum-mechanical case. In such equations it is found that e^2/m in a classical expression corresponds to $(8\pi^2/3h)|\mu_{ij}|^2\nu_0$ in the corresponding quantum-mechanical expression. This may be seen by comparing Eq. (19) on p. 38 with Eq. (19) on p. 180 of Heitler's *The Quantum Theory of Radiation* [936]. Here μ_{ij} is the matrix element of the dipole moment, or may be called the dipole moment for the transition from state i to state j. These substitutions give the proper transition to the quantum-mechanical expression. It should be noted that $|\mu_{ij}|^2$ is an average of the square of the matrix element for a transition from the lower state i to the upper state j. It is defined, as in Eq. (1-76), by

$$|\mu_{ij}|^2 = \sum_{M'} |\mu_x(JMJ'M')|^2 + |\mu_y(JMJ'M')|^2 + |\mu_z(JMJ'M')|^2$$

We have assumed so far that oscillators are absorbing energy only and not emitting energy. From the quantum-mechanical viewpoint there must be oscillators in the upper state of the transition as well as those in the lower state, and it can be shown that the electromagnetic field induces the oscillators in the upper state to emit with the same probability that the oscillators in the lower state absorb. Our net absorption is then

proportional to the difference in the number of oscillators in the upper and lower state, which is

$$\Delta n = (1 - e^{-h\nu_0/kT})n \tag{13-17}$$

where n is the number of molecules per unit volume in the lower state. In the radio-frequency region $h\nu_0 \ll kT$, so that this can be well approximated by

$$\Delta n = \frac{h\nu_0}{kT} n \tag{13-18}$$

In addition to these two states there may be many other molecular states which are occupied by molecules of our material. We may represent by f the fraction of the total which is in the lower of the two states of interest, so that n in the above equations may be replaced by Nf, where N is the total number of molecules per unit volume. Making this substitution we obtain the final expression

$$\gamma = \frac{8\pi^2 Nf}{3ckT} |\mu_{ij}|^2 \nu^2 \left[\frac{1/2\pi\tau}{(\nu - \nu_0)^2 + (1/2\pi\tau)^2} + \frac{1/2\pi\tau}{(\nu + \nu_0)^2 + (1/2\pi\tau)^2}\right] \quad \text{cm}^{-1} \tag{13-19}$$

This can be shown to reduce to the Debye case when ν_0 is 0, for then γ becomes

$$\gamma = \frac{8\pi N f \mu^2}{3ckT} \frac{\omega^2\tau}{1 + \omega^2\tau^2} \quad \text{cm}^{-1} \tag{13-20}$$

In that case also $f = \frac{1}{2}$ and

$$\gamma = \frac{4\pi N \mu^2}{3ckT} \frac{\omega^2\tau}{1 + \omega^2\tau^2} \quad \text{cm}^{-1} \tag{13-21}$$

which is identical with expression (13-3) derived directly from the Debye theory.

At low pressures (*i.e.*, where $1/2\pi\tau \ll \nu_0$), the first term in Eq. (13-19) is the predominant one. The intensity at the line center is then proportional to N, where N is the number of molecules per unit volume and τ is the mean time between molecular collisions. But the time between collisions is inversely proportional to the pressure, so that γ is independent of pressure. Thus the intensity at the peak of a microwave line is independent of pressure over a wide range of pressures. Moreover the line width is proportional to $1/2\pi\tau$, and therefore to the pressure.

The first term of Eq. (13-19) was given in Chap. 1 without proof as Eq. (1-49). It is the most commonly used expression because it does fit the observed microwave line intensities and widths well at low and medium pressures. Karplus and Schwinger [297] have given a quantum-mechanical derivation of the Van Vleck–Weisskopf formula for the shape

and intensity of a microwave spectral line. The assumptions are the same, *i.e.*, collisions so strong that the Boltzmann energy distribution is restored after each collision, and that the duration of a collision is short enough that the field does not change appreciably during the collision. It is not necessary that $\Delta\nu$ be less than ν, and the theory would appear to apply even at quite high pressures.

Van Vleck and Margenau [424] have also examined the Van Vleck–Weisskopf theory. They evaluated separately the work done between collisions and that done impulsively by sudden changes of position of the molecule in the electric field at collisions.

The dielectric constant K and absorption coefficient γ are both given for a particular line shape by (13-15) and (13-16). There are general relations between the dielectric constant and absorption coefficient for any system [8*a*], [135*a*], of which these equations are a special case. The general expressions are known as the Kramers-Kronig relations, and may be written

$$K(\omega) - 1 = \frac{2c}{\pi} \int_0^\infty \frac{\omega'\gamma(\omega')d\omega'}{\omega[\omega'^2 - \omega^2]}$$

$$\gamma(\omega) = \frac{-2\omega^2}{\pi c} \int_0^\infty \frac{[K(\omega') - 1]d\omega'}{\omega'^2 - \omega^2}$$

13-4. Absolute or Integrated Line Intensity. The Van Vleck–Weisskopf equation (13-19) in the region of ν_0 can be approximated

$$\gamma = \frac{8\pi^2 Nf}{3ckT} |\mu_{ij}|^2 \nu^2 \frac{\Delta\nu}{(\nu - \nu_0)^2 + (\Delta\nu)^2} \tag{13-22}$$

if $\Delta\nu \ll \nu_0$. This is the form of a typical resonance absorption of half width $\Delta\nu = 1/2\pi\tau$. If one integrates over the absorption line, assuming $\Delta\nu \ll \nu_0$, the integral $\int\gamma\, d\nu$ becomes

$$\frac{8\pi^3 Nf}{3ckT} |\mu_{ij}|^2 \nu_0^2 \tag{13-23}$$

which is often called the absolute or integrated line intensity.

The approximation $\Delta\nu \ll \nu_0$ is good in the infrared and optical regions, but not always good in the microwave region. In fact, sometimes $\Delta\nu > \nu_0$ at high pressures. Absolute or integrated line intensity may be more appropriately defined as

$$\int_0^\infty \frac{\gamma}{\nu^2} d\nu$$

It may be noted that the first term of the expression in brackets in Eq. (13-19) corresponds to a resonant absorption at frequency ν_0, and the second term to a resonant absorption at frequency $-\nu_0$. Integrating the sum of the two terms from 0 to ∞ is equivalent to integrating either

one from $-\infty$ to $+\infty$. Hence

$$\int_0^\infty \frac{\gamma}{\nu^2}\,d\nu = \frac{8\pi^2 Nf}{3ckT}\,|\mu_{ij}|^2 \int_{-\infty}^{\infty} \frac{1/2\pi\tau}{x^2 + (1/2\pi\tau)^2}\,dx = \frac{8\pi^3 Nf}{3ckT}\,|\mu_{ij}|^2 \qquad (13\text{-}24)$$

This is independent of τ and hence of the line width $\Delta\nu$. The invariance of the absolute intensity with perturbations such as collisions is connected with the principle of "spectroscopic stability." This principle is usually applied to a spectroscopic line split by Zeeman, Stark, or other effects into a fine structure. It states that the sum of intensities of all fine-structure components of a line is equal to the intensity of the unsplit line which would occur if the cause of fine structure were removed, or if the fine structure were not resolved.

13-5. Comparison of the Van Vleck–Weisskopf Line Shape with Experiment. The following general features of collision or pressure broadening have been demonstrated from microwave measurements and are predicted from the Van Vleck–Weisskopf theoretical shape [Eq. (13-19)].

1. The half width $\Delta\nu$ is proportional to pressure over a wide range of low pressures.
2. The peak absorption intensity is independent of pressure over a wide range of low pressures.
3. The apparent resonant frequency ν_0 is constant over a wide range of low pressures.
4. At low pressure the line shape is fitted very accurately by a simple resonant expression.
5. At moderate pressures (1 atm) the absorption-line shape is very asymmetric and given qualitatively by Eq. (13-19).
6. At high frequencies ($\nu \gg \nu_0$) the absorption is constant and has the value

$$\gamma_\infty = \frac{8\pi Nf}{3ckT\tau}\,|\mu_{ij}|^2 \qquad (13\text{-}25)$$

The theoretical line shapes for several values of $\Delta\nu$ are shown in Fig. 13-1. It should be noted that properties 1 to 4 are characteristic of impact theories in general, and only 5 and 6 distinguish the Van Vleck–Weisskopf formulation.

The observed shape of a line in the inversion spectrum of ammonia is compared at pressures near 1 mm Hg with a Lorentz resonance line shape in Fig. 13-2. The Van Vleck–Weisskopf line shape reduces to this Lorentz shape at these low pressures, since $\Delta\nu \ll \nu_0$.

At a pressure of 0.27 mm, the fit is good. When the pressure is raised to 0.83 mm, both the frequency and the intensity of the peak absorption remain unchanged, as predicted, and the line shape fits the theory, except on the low-frequency side where there is overlapping with the edge of a neighboring line [172]. Bleaney and Penrose [180] have shown that $\Delta\nu/p$

is a constant from 0.5 mm up to 10 cm pressure while others have shown that this holds down to about 10^{-3} mm Hg. Below this pressure other causes of broadening become important.

A more complete test of theoretical line shapes and discrimination between the Lorentz shape and its modification by Van Vleck and Weisskopf must be made at higher pressures. Only when the lines are so broad

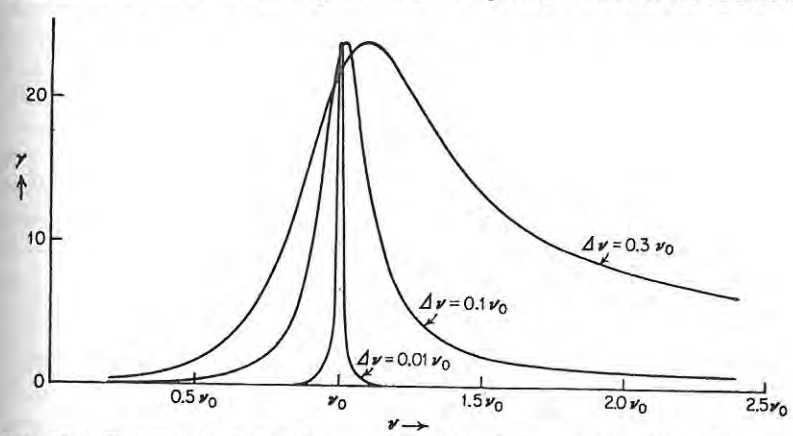

FIG. 13-1. Theoretical shape of pressure-broadened line. (*After Van Vleck and Weisskopf* [136].)

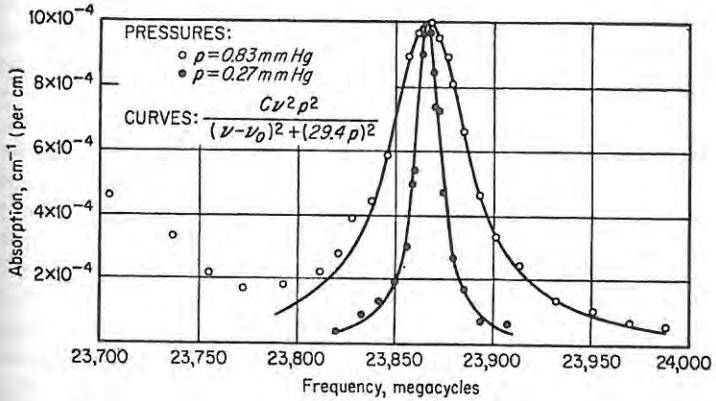

FIG. 13-2. Effect of pressure broadening on the NH_3 3,3 absorption line. (*From Townes* [172].)

that $\Delta\nu$ is comparable with ν_0 do the effects of the ν^2 factor and the "negative frequency resonance" term in (13-19) become apparent. The shape of a microwave line between 15,000 and 35,000 Mc for water vapor in air is compared in Fig. 13-3 with theoretical line shapes. Here $\Delta\nu \approx \nu_0$, and it is evident that the Van Vleck–Weisskopf line shape is

different from the Lorentz theory and more nearly correct. However, there is a deviation from the Van Vleck–Weisskopf line shape on the high-frequency side of the water line.

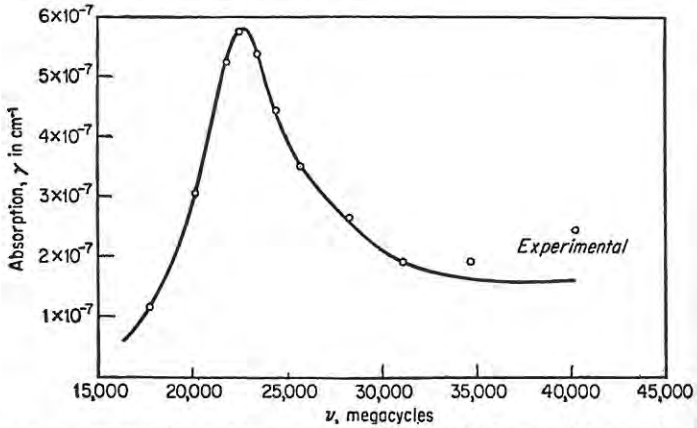

FIG. 13-3. Absorption by water vapor in air (10 g of H_2O per cubic meter). (*From Becker and Autler* [137].)

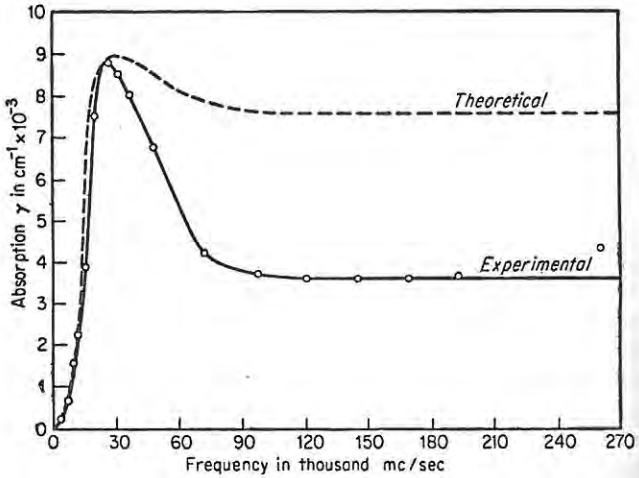

FIG. 13-4. Absorption in NH_3 at 1 atm pressure. (*From Bleaney and Loubser* [439] *and Nethercot, Klein, Loubser, and Townes* [734].)

The microwave spectrum of ammonia at a pressure of 1 atm is shown in Fig. 13-4 [439], [734]. Since at this pressure the width of any one line is considerably greater than the over-all spacing of the individual lines, the spectrum should fit a Van Vleck–Weisskopf curve fairly well with a single value of ν_0 and of $\Delta\nu = 1/2\pi\tau$. Qualitatively the spectrum does

have the predicted shape. In particular the flat "tail," or region of constant absorption at high frequencies, is observed. However, a close comparison shows many deviations from the Van Vleck–Weisskopf line shape. If the line shape is fitted near the peak of the line, the theoretically expected absorption in the flat region should be considerably larger than the observed value. Birnbaum and Maryott [780] have shown that at pressures of 5 to 30 cm of Hg, the low-frequency tail of the ammonia absorption is about 40 per cent larger than that given by the Van Vleck–Weisskopf shape. Too large an observed intensity is, of course, necessary on the low-frequency side of the line to compensate for too small an intensity on the high-frequency side if the integrated intensity (13-24) is to remain constant. Furthermore, the magnitude of $\Delta\nu$ used for the theoretical fit in Fig. 13-4 is only 14,000 Mc, whereas from measurements of line widths at lower pressures, and assuming $\Delta\nu/p$ is constant, it would be expected to be 22,000 Mc. The fact that $\Delta\nu/p$ is less at atmospheric pressure than at low pressure indicates that collisions of more than two molecules at a time have become important, a circumstance not allowed for by Van Vleck and Weisskopf.

Still another complication is that the best fits of the experimental absorption curves to the Van Vleck–Weisskopf shape require a decrease in ν_0 with pressures as high as 1 atm. At 2 atm pressure and higher, ν_0 must be taken as zero [255], [321], [338]. For ND_3, which has a lower inversion frequency than NH_3, the shift in ν_0 has been found [779] to occur at a proportionally lower pressure. This is in accord with the theory of Margenau [394] and Anderson [341]. They show that when the average energy of interaction between molecules is comparable with the inversion energy, the wave functions are sufficiently disturbed to shift the microwave absorption to lower frequencies. Such effects should occur for all gases of sufficient density, since the microwave absorption must approach that given by Debye (13-20) for the liquid state. The density at which such shifts occur can be expected to depend on the strength of the intermolecular interactions and to be approximately proportional to the frequency of the microwave transition.

13-6. Pressure Broadening and Intermolecular Forces. Even if a Lorentz-type theory were developed which fits the line shapes exactly, it would still not be completely satisfactory because the quantity $\Delta\nu$ or $\Delta\nu/p$ is taken as an empirical parameter. A more complete theory should evaluate $\Delta\nu$ in terms of intermolecular forces or some known molecular properties. One might expect that the time between collisions, τ, and hence $\Delta\nu$ could be obtained from classical kinetic theory and measurements of collision diameters from viscosity or from van der Waals' equation of state. However, observed line widths are in most cases greater than those obtained by such methods, so that collision diameters for broadening of microwave lines are sometimes several times larger

than diameters calculated from kinetic theory (see table of values in [473]). This may be expected since kinetic-theory diameters are determined by the requirement that molecules come close enough for intermolecular forces to cause a transfer of most of the kinetic energy kT. Microwave lines on the other hand are disturbed by more distant collisions which transfer considerably less energy since $h\nu \ll kT$.

A complete treatment of pressure broadening and evaluation of $\Delta\nu$ is so complex that a variety of different types of treatments and approximations have been developed to account for the wide range of phenomena encountered. Some approximations are suitable in the optical and infrared regions, others in the microwave region.

One is forced into making simplifying assumptions and approximations. However, no one approximate theory can be used for the wide range of phenomena encountered. Many of the earlier theories use approximations which are appropriate for optical and infrared frequencies, but not for the very different microwave frequencies. In addition some theories are nicely applicable to some types of intermolecular forces but must give way to other approximations for other types of forces.

All intermolecular forces are usually called van der Waals forces. This name includes a number of short-range interactions [93] which depend in various ways on the relative angles of orientation of the two interacting molecules and the distance r between them. The most important types are listed in Table 13-1. Note that each different type of force depends on the distance in a different way except types 4, 5, and 6 which are variations on the same basic type of interaction between a dipole and induced dipole. When the longer-range forces (dependent on lower inverse powers of r) are present they are generally more important than the shorter-range forces in producing collisions simply because of the larger radius of effectiveness. For this reason it is often possible to attribute the major responsibility for pressure broadening to one or two types of interaction rather than all types which are known to be present. One of the reasons for studying pressure broadening is the information about the occurrence and relative importance of the various types of van der Waals forces which may be obtained.

13-7. Comparison of Methods of Treating Pressure Broadening. The pressure-broadening problem can be formulated in general terms without approximations. In arriving at useful numerical results, however, simplifying approximations must always be introduced. Jablonski [130*a*], [161] has pointed out that an entire volume of gas may be considered as one system with bands of energy levels between which transitions occur. Interactions between molecules are just part of the Hamiltonian of the complete system whose energy levels need to be determined. The mathematical difficulty of obtaining energy levels and transition intensities of the entire collection of molecules treated as one system is so great,

TABLE 13-1. TYPES OF VAN DER WAALS FORCES IMPORTANT TO PRESSURE BROADENING

Type of interaction	Variation of potential with r	Discussion
1. Dipole-dipole	r^{-3}	Interaction between two dipoles fixed in orientation, or "resonant," so that they may vary synchronously
2. Quadrupole-dipole	r^{-4}	Dipole and quadrupole fixed in orientation
3. Quadrupole-quadrupole	r^{-5}	Interaction between two quadrupoles
4. Keesom alignment	r^{-6}	Two dipoles not fixed in orientation. One dipole induces an alignment of the other and hence a second-order dipole-dipole interaction
5. Dipole–induced dipole	r^{-6}	Molecular dipole which perturbs electronic wave function of second molecule thus inducing and interacting with a dipole moment. Same as type 4 but induced dipole due to perturbation of electron state
6. London dispersion	r^{-6}	Electrons in molecule or atom inducing electronic dipole moment. Same as type 4 but both dipoles due to electronic motions rather than being fixed molecular dipoles
7. Quadrupole–induced dipole	r^{-7}	Dipole moment of first molecule induces dipole moment in second molecule which reacts back on quadrupole moment of first molecule
8. Exchange forces	Exponential or very high power of $1/r$	Strong, usually repulsive, forces due to direct interaction of electronic distributions in two molecules

however, that his approach has been used only in approximations which give essentially the same results obtained by the Kuhn-London statistical theory discussed below.

All other treatments of pressure broadening can be classified as collision or statistical theories. Collision theories assume that, during most of the time a molecule is sufficiently far from other molecules, it may be

considered free. Occasionally it comes close enough to one or more other molecules for the intermolecular fields to perturb its energy levels appreciably. After collision the molecule may be in the same state as before the encounter, with only a change in phase of its wave function, or a transition to another state may have been induced by the collision. Both types of collision contribute to pressure broadening. Collision theories usually assume that the radiation takes place only while the molecule is undisturbed by intermolecular interactions, the collisions being so brief and infrequent that they serve only to interrupt or change the phase of the normal process of radiation. Statistical theories, on the other hand, consider that molecules are always under the influence of intermolecular interactions, even though these may be weak, and that the frequency radiated depends on the amount of interaction occurring during radiation. The intensity emitted at a particular frequency ν depends simply on the probability that a molecule is perturbed by other molecules just the correct amount to make its frequency ν. Statistical theories hence always involve finding the probabilities of molecules being within a range R and $R + \Delta R$ apart with various possible angles of orientation and hence of their levels being perturbed by various amounts. Collision theories, on the other hand, require calculation of the probability of various types of collisions, the changes in molecular states which occur during these collisions, and a Fourier analysis of the molecular radiation which has intermittent disturbances due to collisions.

Either the collision or statistical approach can give fairly complete and accurate theories if they are developed sufficiently far. However, collision theories usually neglect radiation during a collision and hence become poor approximations at pressures of a few atmospheres where molecules are always close together and collisions are frequent. Statistical theories cannot very well take into account the changes of interactions with time due to molecular motion and hence are good only when molecular velocities are so low that the rate of change of intermolecular interactions may be neglected. We shall see below that this limitation prevents the statistical approach from being very accurate in the microwave range, although it can be used as a guide and rough approximation.

Let us examine now the effect of collisions on microwave radiation, assuming that pressures are low enough so that only collisions between two molecules are important. Using classical language, assume the first molecule is oscillating or rotating so that it radiates a frequency of interest and that it collides with a second molecule. During the collision its oscillation is somewhat modified in frequency because of the interaction, but if the oscillation continues without loss in energy, the molecule emerges from the collision oscillating as before, but with a change in phase due to the changes in frequency during the collision. Such a collision is called adiabatic since no energy has been lost from the

oscillation of interest during collision. The radiated wave is as intense as before the collision, but new frequencies have been introduced because the change in phase due to the collision can be represented as a Fourier distribution of frequencies. Quantum-mechanically, this change of frequency during collision corresponds to a change in energy separation between the ground and excited states due to intermolecular interactions, and the change in phase is a change in relative phases of the ground and excited-state wave functions. The molecule could also appreciably change its energy of oscillation during collision, *i.e.*, make a transition from the excited to the ground state as a result of the collision or vice versa. Such a collision is diabatic.* In this case the radiation emitted, if any, after collision will have no particular relation to that emitted before the disturbance.

In order for a change in phase as large as 1 radian to occur during an adiabatic collision,

$$2\pi\epsilon t \geq 1 \qquad \text{or} \qquad \epsilon \geq \frac{1}{2\pi t} \tag{13-26}$$

where ϵ is an average change in frequency during the collision and t is the duration of the collision. A rough measure of ϵ from the energy of the interaction W is

$$\epsilon = \frac{W}{h} \tag{13-27}$$

The time of collision is given approximately by

$$t = \frac{R}{v} \tag{13-28}$$

where R is the distance between molecules required to produce an appreciable interaction, and v is the thermal velocity of the molecule. Since R is a few angstroms and v near 10^5 cm/sec, t is approximately 10^{-13} sec. Hence $1/2\pi t$ is greater than any microwave frequency ν, and from (13-26), (13-27), and (13-28),

$$W > h\nu \tag{13-29}$$

This shows that the energy of interaction required to give an appreciable change in phase during collision is greater than enough to cause a transition between the ground and excited states. Furthermore this energy fluctuates in a time short compared with the period of oscillation $1/\nu$, and hence the fluctuation has frequency components which can easily produce transitions. Another requirement for transitions to occur is that the kinetic energy of the molecules be sufficiently high to provide the

* Adiabatic means without a transfer of energy. To describe the case where energy is transferred we use diabatic rather than the more usual but clumsy double negative nonadiabatic.

necessary energy, or

$$kT > h\nu \tag{13-30}$$

This condition is, of course, fulfilled for microwave frequencies. For these reasons, almost all collisions which are effective in broadening a microwave line are also strong enough to leave the molecule more or less randomly in the upper or lower state. That this is true can be shown from experimental measurements of saturation discussed below, as well as from comparison of observed line shapes with those predicted by various theories.

When energy levels are so far separated that transitions occur in the infrared or optical region, the situation is very different. There $1/t$ is smaller than the radiated frequency ν', and hence for a change of phase of approximately 1 radian

$$W < h\nu' \tag{13-31}$$

In addition the interactions fluctuate too slowly to excite frequencies as high as those of interest, and the kinetic energy is usually insufficient to cause these higher-frequency transitions ($kT < h\nu'$). Thus, in contrast to the microwave region, adiabatic collisions are the common type of importance to pressure broadening of optical or infrared lines. It is for this reason that most of the early theories of pressure broadening, which were developed for the optical and infrared region, are not very good when applied to pressure broadening of microwave lines. Furthermore, such theories can be expected to be inadequate whenever fine structure is resolved which is so small that diabatic collisions producing transitions between the fine structure levels commonly occur.

Since statistical theories of pressure broadening have not been developed to take into account the variations of intermolecular interactions with time, they suffer the same difficulty as collision theories which allow only adiabatic collisions. In fact the two can be shown to be equivalent for slow collisions or for frequencies far removed from the line center [104], [472], [494]. However, these types of approximations are in some cases simpler than a theory of diabatic collisions, which should be more accurate for microwave lines, and hence are still of value.

The statistical method was introduced by Kuhn and London [50], [51] in a very simple form. Let the transition frequency be ν_0 and its change due to intermolecular interactions be of the form

$$\nu - \nu_0 = \frac{B}{r^n} \tag{13-32}$$

where B and n are constants and r is the distance between two molecules. If only two molecules are considered, the probability that the intermolecular distance will lie between r and $r + dr$ is

where A is a constant. Then the fraction of the radiation intensity with frequency between ν and $\nu + d\nu$ is, from (13-32) and (13-33),

$$I = \frac{AB^{3/n}}{n(\nu - \nu_0)^{(n+3)/n}} \tag{13-34}$$

This simple form of the statistical theory gives an infinite relative intensity at $\nu = \nu_0$ because there is an infinite probability of two molecules being separated by an infinite distance. Finite molecular densities must be taken into account to remove this divergence. In addition, expression (13-34) gives a shift of frequency only to one side of the resonance frequency ν_0, and hence a very asymmetric line. Such asymmetric lines are observed in some optical spectra, but this type of asymmetry never occurs in the microwave region because of the prominence of diabatic collisions. However, the tail of a microwave line can be approximately fitted by an expression of the type (13-34). The tail is sometimes fitted to the tail of a resonance-shaped curve, and from this a half width of the resonance can be obtained.

Margenau has given a much more sophisticated statistical theory of the pressure broadening of the ammonia inversion spectrum [393] in case collisions between more than two molecules are negligible. The energy of interaction of the dipole moments of two symmetric tops is [82]

$$V(JKJ'K'\lambda) = \frac{\mu^2}{r^3}\frac{KK'}{J(J+1)J'(J'+1)}\epsilon_\lambda \tag{13-35}$$

where J, K and J', K' are the quantum numbers of the two molecules, each of which has a dipole moment μ. λ is an index replacing the individual M's of the molecules, which are not good quantum numbers during close approaches because the separate angular momenta about the intermolecular axis are not conserved. ϵ_λ is a numerical factor for each λ state. The frequency of the line absorbed by one of the molecules (J,K) is then

$$\nu = \nu_0 + \frac{B_{\lambda\lambda'}}{r^3} \tag{13-36}$$

where ν_0 is the unperturbed resonance frequency and

$$B_{\lambda\lambda'} = \frac{\mu^2}{h}\frac{KK'}{J(J+1)J'(J'+1)}(\epsilon_\lambda - \epsilon_{\lambda'}) \tag{13-37}$$

In passing from one inversion state to the other the dipole changes its orientation so that the system of two molecules changes from state λ to state λ'. By averaging over all possible types of collisions, or hence over all λ, λ', K', and J', and using the same basic statistical approach discussed above, Margenau obtains

$$\frac{\Delta\nu}{\ldots} = 33.9\left[\frac{K^2}{J(J+1)}\right]^{\frac{1}{2}} \quad \text{Mc/mm Hg at 20°C} \tag{13-38}$$

where $\Delta\nu$ is the half width of the line at half maximum intensity and p is the pressure in millimeters of mercury. This theory gives line widths of the right order of magnitude and varying in roughly the right way with K and J, as shown by the comparison with experimental line widths in Table 13-3 (page 362). However, a systematic deviation between the theoretical and experimental results can be seen in this table.

Collision theories for the optical and infrared region have been given by Lindholm [131] and Foley [153]. They consider the phase shifts produced during collisions, and assume that diabatic collisions are unimportant, so that their approximations are not good for pressure broadening of microwave lines, although they apply well in the higher-frequency infrared and optical regions. This type of theory considers the approach of a perturbing molecule during a collision to change the energies of both ground and excited states of the emitting molecule, the difference between their changes being $W(t)$. This changes the frequency of the emitting molecule by $W(t)/h$, and if the change in frequency persists for a time dt, there is a phase change of $[2\pi W(t)/h]\,dt$ over what would have occurred for normal oscillation without a collision. The total phase shift due to the collision may be obtained by integrating over the duration of the collision as

$$P_1 = 2\pi \int_{-\infty}^{\infty} \frac{W(t)\,dt}{h} \tag{13-39}$$

The straight-line paths of the colliding molecules are assumed to be unaffected by the collision.

P_1 is a function of the impact parameter b (distance of closest approach), being large when b is small. If b is so small that the phase shift is very large, then the phase after collision has no very close connection with that before collision, and the collision can be considered strong, producing a complete and arbitrary interruption of the emitted wave train. Weisskopf, who originated this type of calculation [44], assumes that a phase shift larger than 1 radian is equivalent to a complete interruption of the radiation, and obtains an approximate collision diameter as the value of b for this particular phase shift, considering a collision to occur only for b less than this value.

The strong collisions, giving large phase shifts, produce a symmetrical line broadening of the Lorentz type with no shift in the central frequency. By taking into account the phase shifts produced by all types of collisions, including the weaker ones, and making a Fourier analysis of the resulting wave trains, Foley and Lindholm showed, however, that there is often an appreciable shift of the central line frequency due to phase shifts during collisions. Thus if $W(t)/h$ corresponds to a decrease in frequency during a distant collision, the line will be both broadened and shifted slightly to lower frequencies by the distant or weak collisions.

These distant collisions are much less important than closer collisions if the potential drops off very rapidly with r, that is, when $V = B/r^n$, if n is large. The phase-shift approximation therefore gives an absorption line of the form

$$\gamma = \frac{A}{(\nu - \nu_0 \pm a\,\Delta\nu)^2 + (\Delta\nu)^2} \tag{13-40}$$

where the change in the center of the line $a\,\Delta\nu$ is proportional to the line width and dependent on the force law as shown in Table 13-2. When n is 3, no frequency shift is observed because only "resonant" type interactions give $n = 3$ (*cf.* Table 13-1), and they give a symmetrical splitting of energy levels. Although this type of frequency shift is often observed in infrared or optical spectra, no such frequency shifts have yet been found in the microwave region. They are in most cases certainly less than $0.05\,\Delta\nu$. This is because adiabatic collisions are of little importance in broadening microwave lines. However, some collisions of this type occur, and they undoubtedly produce small frequency shifts which may be found with refined techniques.

TABLE 13-2. RATIO a OF SHIFT IN FREQUENCY TO LINE BREADTH $\Delta\nu$ ON PHASE-SHIFT THEORY

Potential of interaction of two molecules is assumed to be of the form $V = B/r^n$

n	3	4	5	6	7	∞
a	0	0.866	0.500	0.363	0.289	0

13-8. Impact Theory—Anderson's Treatment. Anderson has given a more complete treatment of pressure broadening of the collision type which allows adequately for diabatic collisions, *i.e.*, those which induce transitions [342], [343]. Where the computations involved are not too complex, Anderson's theory may be very satisfactorily applied to pressure broadening in the microwave region. In some cases this approach, combined with experimental measurements, can be used to determine the magnitude of certain intermolecular interactions. However, there are always minor contributions to collision effects which involve computations that are prohibitively complex, and in many cases even the major sources of pressure broadening still involve such difficulties.

Anderson makes some assumptions usual to collision theories:

1. Colliding molecules follow definite classical paths. In very close collisions this is a poor assumption, but the errors introduced are unimportant since any path giving a close collision involves complete interruption of the radiation, and details of the path are unnecessary. Collisions near the limit of the effective collision radius are the ones which must be accurately treated, and the quantum-mechanical wave packet for each molecule may in almost all cases be considered sufficiently small compared with this distance to make the classical path a very good approximation.

2. The duration of a collision is small compared with the time between collisions. This is always true at sufficiently low pressures, and is true for most molecules if the pressure is below about 1 atm.

A line shape similar to that of Van Vleck and Weisskopf is obtained, but with the possibility of a shift in the central frequency,

$$\gamma = \frac{8\pi^2 Nf}{3ckT} |\mu_{ij}|^2 \nu^2 \left[\frac{\Delta\nu}{(\nu - \nu_0 - a\,\Delta\nu)^2 + (\Delta\nu)^2} + \frac{\Delta\nu}{(\nu + \nu_0 + a\,\Delta\nu)^2 + (\Delta\nu)^2} \right] \tag{13-41}$$

However, the frequency change $a\,\Delta\nu$ is not so prominent as in the phase-shift theory or (13-40), and is usually negligible for microwave lines.

The number of collisions per second is given by $Nv\sigma_2$, where σ_2 is an effective cross section, v the molecular velocity, and N the number of molecules per unit volume. Hence

$$\Delta\nu = \frac{Nv\sigma_2}{2\pi} \tag{13-42}$$

Similarly, the frequency shift is

$$a\,\Delta\nu = \frac{Nv}{2\pi}\sigma_1 \tag{13-43}$$

where σ_1 is the effective cross section for frequency shifts. These cross sections may be written

$$\sigma = \int_0^\infty 2\pi b S(b)\, db \tag{13-44}$$

where b is the impact parameter, or distance of closest approach of the molecules, so that $2\pi b\, db$ is proportional to the probability of a collision with impact parameter b, and $S(b)$ is a weight factor which indicates whether or not a collision of this type is effective in disturbing the molecular radiation. $S(b)$ is unity when b is small since every such collision is effective in broadening the spectrum and for larger b the most important parts of S are given by

$$S_2(b) = \tfrac{1}{2} \sum_{l,M} \left[\frac{|(iM|P|l)|^2}{2J_i + 1} + \frac{|(fM|P|l)|^2}{2J_f + 1} \right] \tag{13-45}$$

where i,M represent all the quantum numbers of the initial state, and f,M those of the final state of the radiating transition. J_i and J_f are the angular momenta of initial and final states. l represents the quantum numbers of any state to which transitions are induced by the perturbing intermolecular interaction. The matrix elements $(i,M|P|l)$ are

$$(a|P|b) = \frac{2\pi}{h} \int_{-\infty}^{\infty} [a|V_1(t)|b] \exp(2\pi i \nu_{ab} t)\, dt \tag{13-46}$$

where $V_1(t)$ is the perturbing interaction, and ν_{ab} is the frequency of a transition between states a and b. The sum over M divided by $2J + 1$ involved in (13-45) is simply an average over the $2J + 1$ different possible values of the magnetic quantum numbers M.

From (13-45), $S_2(b)$ may be interpreted as the probability that the collision at a distance b produces a transition, averaged over the ground and excited states, and over the various possible orientations of the angular momentum. This is because $|(iM|P|l)|^2$ is just the quantity which gives the transition probability (*cf.* [153]). It has been suggested [536] that a simplifying assumption might be applied to Anderson's theory by considering an effective collision to take place for any b small enough

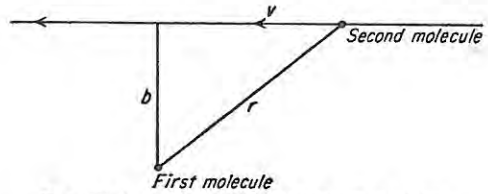

FIG. 13-5. Geometry of molecular collision.

to make this probability (S_2) larger than $\frac{1}{4}$. This gives approximately the same result as an integration of (13-44) over all collision parameters. However, for force laws of the form $1/r^n$ this approximation gives little simplification.

The expression for frequency shift similar to (13-45) is

$$S_1 = \sum_M \left[\frac{(iM|P|iM)}{2J_i + 1} - \frac{(fM|P|fM)}{2J_f + 1} \right] \tag{13-47}$$

which is zero for most of the common interactions because the matrix elements in the sum are zero.

The relative positions of the two colliding molecules and the path over which the time integral in (13-46) is made is indicated by Fig. 13-5. The path of the second molecule with respect to the first is assumed to be a straight line since only the closer collisions which always interrupt the radiation will involve appreciable curvature of the path. Then

$$r(t)^2 = b^2 + v^2 t^2 \tag{13-48}$$

For an interaction energy which varies as $1/r^n$ with the distance between molecules, $[a|V_1(t)|b]$ is the form $K/[r(t)]^n$. Letting $x = vt/b$ and $k = (2\pi b/v)\nu_{ab}$, (13-46) becomes

$$(a|P|b) = \frac{2\pi K}{hb^{n-1}v} \int_{-\infty}^{\infty} \frac{e^{ikx}\, dx}{(1 + x^2)^{n/2}} \tag{13-49}$$

When $k \approx 0$, the collision might be called "fast," and the P matrix element tends to be large if the interaction energy K/b^n is large. This value does not decrease much for values of k up to 1, but then falls off rapidly, being very small for k as large as 4 or 5.

The parameter k is roughly the ratio of the time b/v required for the collision to be completed to the time $1/\omega$ required for the radiation to change phase. For a collision parameter b as large as 10 A, and v a typical thermal velocity of 10^5 cm/sec, $b/v \approx 10^{-12}$ sec. This is considerably smaller than $1/\omega$ for 1 cm wavelength radiation, which is $1/\omega = 3 \times 10^{-11}$.

One may see from (13-49) two criteria for a transition to occur during collision: first the interaction energy must be large, and secondly the collision must be "fast," *i.e.*, the time variation of the interaction must involve frequencies as high as the transition frequency ν_{ab}. For microwave transitions, k is almost always less than unity, so that diabatic collisions occur, and the exponential in (13-49) may be ignored. However, for optical frequencies the exponential could not be ignored, and the integral in (13-49) would take on a very different character.

Letting $k = 0$, S_2 is of the form

$$S_2 = \frac{A}{b^{2n-2}} \tag{13-50}$$

where b is the impact parameter and A is a quantity depending on various properties of the molecules and the quantum states involved. With some approximations which introduce errors of 10 per cent or less, the cross section and half width $\Delta\nu$ may then be found from (13-42), (13-44), and (13-50) as

$$\sigma = \pi\left(\frac{n-1}{n-2}\right)A^{1/(n-1)} \qquad \Delta\nu = \frac{Nv}{2}\left(\frac{n-1}{n-2}\right)A^{1/(n-1)} \tag{13-51}$$

The problem is then reduced to finding A, or evaluating the sum in (13-45). Since a particular molecule of interest may collide with molecules in a variety of states, each having a different effective cross section, $\Delta\nu_a$ must be obtained for each different type of molecule with which collisions may occur, and weighed according to the fractional abundance f_a of each type. Then

$$\sigma = \sum_a f_a\sigma_a \qquad \Delta\nu = \sum_a f_a\,\Delta\nu_a \tag{13-52}$$

In some cases the sum in (13-45) is very difficult to obtain, especially when both colliding molecules may make a variety of transitions. It has been worked out, however, for the important cases of dipole-dipole, dipole–induced dipole, and quadrupole–induced dipole interactions (types 1, 5, and 7 of Table 13-1).

The interaction energy of two dipole moments $\boldsymbol{\mu}_1$ and $\boldsymbol{\mu}_2$ separated by a distance r is

$$V_1 = \left[\boldsymbol{\mu}_1\cdot\boldsymbol{\mu}_2 - \frac{3(\boldsymbol{\mu}_1\cdot\mathbf{r})(\boldsymbol{\mu}_2\cdot\mathbf{r})}{r^2}\right]r^{-3} \tag{13-53}$$

For two interacting symmetric-top molecules, this energy is of the first order and proportional to $1/r^3$. This is because a symmetric-top molecule has a component of the dipole moment along the angular momentum J, which is fixed in orientation. For a linear molecule, no component of the dipole moment is fixed in direction, and the energy (13-53) averages to zero in the first order unless two interacting molecules happen to be rotating at essentially the same rate. Even two molecules like ammonia, which invert at microwave frequencies and thus reverse the direction of their dipole moments, give a first-order dipole-dipole interaction. Averaging over a long period of time would give no first-order interaction because unless the two ammonia molecules are in the same rotational state they invert at different frequencies and would change relative orientation with time. However, over the short duration of a collision, they may be considered to invert synchronously and remain with the same relative orientation. The matrix elements needed to evaluate these first-order interactions produced by dipole-dipole interactions [V_1 given by (13-53)] turn out to be just those given by Table (4-4) for dipole radiation. After the time integration indicated by (13-46) is done, the matrix elements inserted and summed according to (13-45), one obtains [342], [343]

$$S_2(b) = \frac{8}{9}\,\frac{\mu_1^2\mu_2^2}{b^4v^2(h/2\pi)^2}\,\frac{K_1^2K_2^2}{J_1(J_1+1)J_2(J_2+1)} \tag{13-54}$$

where K_1, J_1, K_2, J_2 are the usual angular-momentum quantum numbers for molecules 1 and 2, respectively, which are involved in the collision. v is the relative velocity of the two molecules.

Letting the molecule with index 1 be the one emitting microwave radiation of interest, and summing over all other colliding molecules, from (13-51), (13-52), and (13-54),

$$\Delta\nu = \frac{4\pi\sqrt{2}\,N|\mu_1K_1|}{3h\sqrt{J_1(J_1+1)}}\sum_{\mu_2,J_2,K_2}\frac{|\mu_2K_2|}{\sqrt{J_2(J_2+1)}}f_{J_2K_2\mu_2} \tag{13-55}$$

where $f_{J_2K_2\mu_2}$ is the fraction of molecules having dipole moment μ_2 and quantum numbers K_2, J_2 and N is the number of molecules per unit volume. The cross section σ may be easily obtained from $\Delta\nu$ by (13-42) if some average velocity v is assumed. Sometimes an effective diameter b_e is calculated for collisions, which is given by

$$\sigma = \pi b_e^2 \tag{13-56}$$

Another case where the dipole moments of two molecules interact strongly, or in first-order perturbation approximation, is the case of "rotational resonance." Two molecules in rotational resonance may be considered classically to be rotating at the same rate so that the interaction between their dipole moments when averaged over time is not zero. Quantum-mechanically, rotational resonance requires two identical molecules with angular momenta differing by one unit ($J_1 = J_2 \pm 1$). Using the interaction (13-53), this gives [342], [343], for collisions with $J_2 = J_1 - 1$,

$$S_2(b) = \frac{8}{9}\frac{\mu_1^4}{b^4v^2(h/2\pi)^2}\frac{(J_1^2 - K_1^2)(J_1^2 - K_2^2)}{J_1^2(2J_1 + 1)(2J_1 - 1)} \tag{13-57}$$

$$\Delta\nu = \frac{4\pi\sqrt{2}}{3h}\frac{N\mu_1^2}{J_1}\left[\frac{(J_1^2 - K_1^2)}{(2J_1)^2 - 1}\right]^{\frac{1}{2}}\sum_{K_2}(J_1^2 - K_2^2)^{\frac{1}{2}} f_{J_1-1,K_2} \tag{13-58}$$

When $J_2 = J_1 + 1$, the number J_1 in (13-58) need only be replaced by $J_1 + 1$. The notation is the same as in Eqs. (13-54) and (13-55).

"Rotational-resonance" interactions can occur with either symmetric tops or linear molecules ($K = 0$) and tend to be large when the dipole moments μ_1 and μ_2 are large and the fraction f of molecules in the proper state is not too small. However, for most rotational lines of molecules falling in the microwave region, $f \approx h\nu/kT$, or $\frac{1}{200}$ [*cf.* (1-56)], and the rotational-resonance effects are usually small. The case of ammonia is somewhat unusual since its microwave lines show large effects due to rotational resonance. This is because the ammonia lines in the microwave region are due to inversion rather than rotational transitions, and the molecule is so light that for some rotational states f is as large as $\frac{1}{16}$. Other molecules do show a quasi resonance, because collisions are so short that the frequency cannot be established accurately. If a collision lasts 10^{-12} sec, all levels within about 10^{11} cycles are near enough to behave as resonant.

Other types of interactions which have been treated by Anderson's method involve a dipole moment induced by the distortion of the distribution of electrons on one molecule, which we shall label 1, by the molecular dipole moment of a second molecule labeled 2. The induced dipole moment on molecule 1 may interact back on the dipole moment of molecule 2, with an energy proportional to $1/r^6$ (type 5 of Table 13-1). Because of certain symmetry relations, this type of interaction usually contributes a negligible amount to pressure broadening [342], [343], [428].

The induced dipole moment of molecule 1 of the last paragraph may also interact with the electric quadrupole moment of molecule 2 (type 7, Table 13-1). If molecule 2 is symmetric, the interaction energy is then

$$V_1 = -\frac{6\alpha_1\mu_2Q_2}{r^7}\cos^3\theta \tag{13-59}$$

where α_1 = polarizability of molecule 1
μ_2, Q_2 = dipole and quadrupole moments, respectively, of molecule 2
r = radius between the two molecules
θ = angle between r and the axis of molecule 2

Anderson has obtained [428]

$$S_2 = \frac{3}{b^{12}}\left(\frac{15\pi^2\alpha_1\mu_2Q_2}{64vh}\right)^2\frac{K^2}{J(J+1)}\left\{1 + \frac{22}{5}\frac{K^2}{J(J+1)} + \frac{121}{21}\frac{K^4}{J^2(J+1)^2} - \frac{K^2}{3J^2(J+1)^2}\left[\frac{22}{5} + \frac{121}{7}\frac{K^2}{J(J+1)}\right] + \frac{121}{63}\frac{K^4}{J^4(J+1)^4}\right\} \tag{13-60}$$

which is of the form given by (13-50)

$$S_2 = \frac{A}{b^{12}}$$

so that from (13-51)

$$\sigma = 1.2\pi A^{\frac{1}{2}}$$

Leslie [602] has given a treatment of pressure broadening similar to that of Anderson but has eliminated the assumption of a classical path and used a Boltzmann distribution of velocities throughout rather than assuming an average molecular velocity. Although such a treatment is naturally more complicated because of elimination of these two simplifying assumptions, Leslie has obtained results similar to those discussed above.

13-9. Comparison of Theories with Experiment. After the above lengthy discussion of theoretical evaluation of line widths, the reader might expect extensive confirming comparisons between theory and experiment. Unfortunately, successful comparisons are rather limited, and many attempts to fit particular calculations to observations have been inconclusive. One of the reasons for this is that there are few cases in which only one of the wide variety of possible interactions predominates, and even the rough magnitudes of some of the molecular constants required by theory are unknown. In addition, there has been much conflicting experimental data. The one outstanding exception to these uncertainties is dipole-dipole broadening in NH_3, which is so far the only microwave case for which extensive quantitative agreement between theory and experiment seems to have been achieved.

The NH_3 $J = 3$, $K = 3$ inversion line in pure NH_3 at a pressure of 1 mm Hg and 0°C has a measured half width at half maximum of 30 ± 1 Mc.* The half width calculated from expression (13-54) is 31 Mc for the

* This value is an average of the results of Bleaney and Penrose [179] and of Townes [172]. Both the directly measured line widths and those calculated from the measured intensities were averaged. A dipole moment of 1.468 debye units [562] was used. The reported widths were reduced to 0°C assuming the width is inversely proportional to temperature.

same conditions. Rotational-resonance terms (13-57) are zero for this line because $J = K$. The agreement between theory and experiment is well within the accuracy of the theoretical approximations and the experimental uncertainties.

The variation of the NH_3 line-breadth parameter $\Delta\nu$ with J and K is shown in Table 13-3 and compared with predictions of several types of theories. It may be seen that Anderson's approach, using broadening

TABLE 13-3. COMPARISON BETWEEN EXPERIMENTAL AND THEORETICAL LINE WIDTHS FOR AMMONIA SELF-BROADENING

Experimental values apply to a temperature of 20°C.

Line		Line breadth, Mc/mm Hg					
J	K	Experimental, Bleaney and Penrose [179]	Anderson [342]	Anderson (neglecting rotational resonance) [342]	Bleaney and Penrose [257]	Margenau [393]	Mizushima [619]
2	1	16	16	13	16	14	12
3	1	14	14	9	13	10	9
3	2	19	20	18	20	20	16
3	3	27	27	27	27	29	23
4	4	27	28	28	28	30	24
5	1	11	11	6	10	6	6
5	2	16	15	11	15	12	11
5	3	20	20	17	20	19	16
5	5	28	29	29	28	31	24
6	3	19	17	14	19	15	13
6	4	22	21	19	22	21	17
6	6	28	29	29	28	31	24
7	5	25	22	21	23	23	18
7	6	23	26	25	26	27	22
8	7	25	26	26	26	28	22
10	9	25	27	27	27	29	23
11	9	17	25	25	25	27	21

of type (13-54) and allowing for rotational resonance (13-57), gives rather good agreement with experimental results. Omitting the rotational-resonance type of interaction (column 5 of Table 13-3) gives poor agreement when $K < J$. The values in Table 13-3 are measured by Bleaney and Penrose [257], and all the results of Anderson's theory have been multiplied by a constant factor to give exact agreement between this theory and the experimental value for the 3,3 line.

The closest fit to the experimental data is a formula given by Bleaney and Penrose (column 6, Table 13-3)

$$\Delta\nu = 30\left[\frac{K^2}{J(J+1)}\right]^{\frac{1}{2}} \tag{13-61}$$

where $\Delta\nu$ is the half width in megacycles for a pressure of 1 mm Hg. The form of this expression is derived on the assumption that a collision occurs when two molecules approach closely enough for the interaction of their dipoles to reach some critical value W. However, since any effect of the perturbation depends on its duration, the criterion for a collision should be that the product of the interaction energy W and the duration of the collision reaches some critical value. With this modification, Bleaney and Penrose's approach becomes similar to the statistical theory and gives an expression of the form $\Delta\nu \propto K/\sqrt{J(J+1)}$. This is the type of variation found by Margenau from a statistical type of theory (column 7, Table 13-3). It does not fit so well as (13-61). Bleaney and Penrose's formula must be regarded essentially as empirical since their assumption in deriving it is quite artificial. Moreover, as may be seen from the discussion below, it gives the wrong temperature dependence of line width. Mizushima's calculation of line breadths (Table 13-3) is based on an adiabatic type of collision theory. The similarity between the results of Bleaney and Penrose, Mizushima, Margenau, and Anderson shows that approximate agreement with experiment can be obtained under a variety of assumptions. However, the line widths calculated by Anderson are clearly more accurate than those given by Margenau or Mizushima in the cases where rotational resonance is of importance.

Broadening of ammonia lines by foreign gases is treated in exactly the same manner as self-broadening if the perturbing molecule is a symmetric top with a reasonably large dipole moment (*e.g.*, CH_3Cl or $CHCl_3$) and similarly good agreement is obtained ([536], Table 1). Line breadths and effective collision diameters for pressure broadening of NH_3 by a number of gases are given in Table 13-4. These collision diameters are in many cases larger than the collision diameters given by kinetic theory, which are listed in Table 13-4 for comparison. This is because for pressure broadening the long-range and weak interactions can be important, whereas in processes of significance to kinetic theory the shorter-range stronger interactions are necessary. In the cases where the collision diameter for broadening is large, one can expect to obtain a relatively simple theory of the collision since the many short-range forces can be neglected. In the case of self-broadening in NH_3, for example, the collision diameter is more than three times as large as the kinetic theory diameter, or the cross section about ten times as large. The importance of long-range dipole-dipole forces in the case of NH_3 self-broadening is the reason it can be treated so successfully with a theory that neglects other types of interactions.

Smith and Howard [536] have shown that the large effective collision diameters between NH_3 and N_2, CO_2, COS, and CS_2 are very probably due to interaction between the NH_3 dipole moment and the molecular quadrupole moments of these molecules [536]. This type of interaction has not yet been treated accurately, but if broadening of the NH_3

TABLE 13-4. COLLISION DIAMETERS AND LINE-WIDTH PARAMETERS FOR BROADENING OF THE NH_3 3,3 LINE BY VARIOUS GASES*

$\Delta\nu$ is the half width at half maximum intensity for a small amount of NH_3 in 1 mm Hg pressure of the colliding molecule. Collision diameters computed from kinetic theory are included for comparison.

Colliding molecule	Dipole moment, debye units, or 10^{-18} esu	$\Delta\nu$, Mc	Effective collision diameter b_e, angstroms	Kinetic theory collision diameter b, angstroms
NH_3	1.47	27	13.8	4.43
He	0	1.3	2.4	3.31
A	0	1.7	3.7	4.04
H_2	0	3.0	3.1	3.59
N_2	0	3.8	5.5	4.09
O_2	0	2.3	4.3	4.02
CO_2	0	6.8	7.6	4.46
COS	0.720	6.5	7.6	
CS_2	0	6.5	7.7	
HCN	2.96	13	10.0	
ClCN	2.80	16	11.9	
CH_3Cl	1.87	15	11.3	5.14
CH_2Cl_2	1.59	12	10.3	
$CHCl_3$	0.95	20	13.7	
CCl_4	0	5.5	7.2	
SO_2	1.7	12	10.4	

* W. V. Smith and R. Howard [536]. Where other measurements have been published [658], [627] the results have been averaged with those of Smith and Howard. The numbers presumably all apply to room temperature.

3,3 line is due to the quadrupole moment Q of a foreign molecule, then approximately

$$|Q| = 5.3 \times 10^5 b_e^3 \left(\frac{M_1 + M_2}{M_1 M_2}\right)^{\frac{1}{2}} \tag{13-62a}$$

(*cf.* [536]). Here M_1 and M_2 are the molecular weights of the colliding molecules. The quadrupole moment of a symmetric molecule is defined as

$$Q = \int \rho(3z^2 - r^2)\, dv \tag{13-62b}$$

where ρ is the charge density at a point z,r in the molecule. Coordinates are measured from the center of mass and z is in the direction of the

molecular-symmetry axis. This definition is that commonly used in molecular theory but differs by a factor of the electron charge from that used for nuclear quadrupole moments.

Table 13-5 gives the molecular quadrupole moments for some molecules which have been measured by their effectiveness in broadening the ammonia 3,3 line [536], [586].

The values in the table are those measured directly for the normal rotating molecule. On the other hand, theoretical calculations [using (13-62)] of molecular quadrupole moments for a known or postulated molecular structure assume that the molecule is at rest. The effective quadrupole moment for a classically rotating linear molecule, averaged over the rotation, is one-half of that for the stationary molecule. This

TABLE 13-5. MOLECULAR QUADRUPOLE MOMENTS

Q' is the effective quadrupole moment for rotating molecules. For a linear molecule, $Q' = Q/2$, where Q is defined by (13-62*b*).

Molecule	$b \times 10^8$, cm, kinetic theory	$b \times 10^8$, cm, from NH_3 3,3 line broadening	Molecular Q', 10^{-26} esu
N_2	4.09	6.0	1.5
O_2	4.02	4.18	<0.55
NO	3.90	5.64	1.4
CO	3.96	5.97	1.6
CO_2	4.46	7.59	3.1
COS	....	7.56	2.9
CS_2	....	7.72	3.1
N_2O	4.35	9.1	4.4
HCN	....	10.0	7.7
ClCN	....	11.9	11.5
C_2H_2	....	8.79	5.3
C_2H_4	4.79	6.67	2.3
C_2H_6	4.86	5.64	<1.3

classical average is usually adequate in pressure-broadening studies, since the most abundant states of the perturbing molecules are usually those with high J values for which the classical approximation is good. Sometimes, particularly in molecular theory, the molecular quadrupole moment is defined as half the value given here.

Estimates of molecular quadrupole moments using what is known about molecular structures and bonding are consistent with the measured values [582].

For collisions between NH_3 and H_2, He, or A, interactions of the quadrupole–induced dipole type discussed above [*cf.* (13-60)] may be of importance. The rather large dipole moment of NH_3 may induce a dipole moment in a He or A atom, and this induced dipole moment

reacts back on the quadrupole moment of the NH_3 molecule. It is perhaps surprising that such an interaction is more important than the reaction of the induced dipole back on the NH_3 dipole. This is because the symmetry of the dipole–induced dipole interaction is such that it produces no inversion transitions and hence a small disturbance of the inversion spectrum [428]. The quadrupole–induced dipole interaction has such a symmetry that it can cause inversion transitions and is therefore of more importance. Unfortunately the quadrupole moment of NH_3 is not accurately known. Estimates of this quadrupole moment and application of expressions (13-59) and (13-60) show that the collision diameters for broadening of the NH_3 3,3 line by the gases H_2, He, A, and O are of approximately the magnitude to be expected from this type of interaction [428]. However, these collision diameters are not larger than the kinetic theory diameters (*cf.* Table 13-4), so other short-range interactions such as type 8 of Table 13-1 may also be of importance.

13-10. Self-broadening of Linear Molecules. Self-broadening of linear molecules in the infrared region has received considerable attention, and dipole-dipole interactions of the Keesom alignment type have been rather completely worked out for adiabatic collisions, which predominate in the infrared region. Rotational-resonance-type interactions are also of importance for the infrared spectra of these molecules and have been fairly completely treated [93], [153].

For microwave transitions adiabatic collision approximations are not very satisfactory. It might be thought that rotational resonance is unimportant because at room temperature the most abundant molecular states have high J values ($J \approx 30$), whereas only molecules with low J values give microwave transitions. Hence an encounter between a molecule absorbing microwaves and another molecule differing by one unit in J is a rare event and contributes little to the line breadth. However, the short duration of collisions between molecules (10^{-12} sec) makes the requirements for rotational resonance much less stringent. That is, during a collision lasting τ sec, the energy levels are uncertain by about $h/2\pi\tau \approx 5$ cm^{-1}. Thus all levels within this distance are effectively in resonance with the transition being studied. For OCS, where $B = 0.2$ cm^{-1}, the first five J levels are effective in rotational-resonance broadening of the lowest rotational level. The number of molecules with energies near enough to cause resonance broadening increases as J increases.

These qualitative expectations are confirmed by the measurements of Johnson and Slager [706] on OCS line widths. It is found that line widths increase with increasing J, which is to be expected as the number of molecules within the resonance interval is greater for those with higher values of J. The relative increase with J is greater at lower temperatures where the peak of the population distribution is shifted toward lower J.

By considering interactions between a given rotational state and all other rotational states which may be considered resonant, Smith, Lackner, and Volkov [to be published] have calculated collision diameters for OCS and BrCN in good agreement with experimental observations. Thus for the $J = 3 \leftarrow 2$ transition of BrCN, the theoretical collision diameter is 19.3 A while the experimental value is 19.0 A. Recent measurements on OCS by R. S. Anderson [to be published] give similarly good agreement.

No complete treatment of broadening of microwave lines by either dipole-quadrupole or Keesom alignment forces is available. However, Keesom alignment forces have been approximately treated by adiabatic theories [153], [303], [398], [499], [619].

Keesom alignment interactions are difficult to evaluate from Anderson's theory because of the particular matrix elements involved. While the mean of the diagonal elements of the square of the interaction matrix is desired, some idea of the magnitude of these effects may be obtained from the ordinary linear average of the energy which is more easily computed [93]. It is

$$(W_{dd})_{\text{av}} = \frac{2\mu^4}{3Br^6} \frac{J_1(J_1+1) + J_2(J_2+1)}{(J_1+J_2)(J_1+J_2+2)(J_1-J_2-1)(J_1-J_2+1)} \tag{13-63}$$

where μ is the permanent dipole moment, B the rotational constant, J_1 and J_2 the rotational quantum numbers of the two colliding molecules, and r the distance between them. The most important collisions involve large quantum numbers J_2 for the colliding molecules, or $J_2 \gg J_1$. For this case

$$(W_{dd})_{\text{av}} = \frac{\mu^4}{3r^6 E_{J_2}}$$

where E_{J_2} is the rotational energy of the colliding molecule, which may be approximated as kT, or

$$(W_{dd})_{\text{av}} = \frac{\mu^4}{3kTr^6} \tag{13-64}$$

An average value for the dipole-quadrupole interaction is [536]

$$(W_{dq})_{\text{av}} = \frac{1}{3}\frac{\mu Q_e}{r^4} \tag{13-65}$$

In many typical collisions the energies of interaction W_{dd} and W_{dQ} are comparable in magnitude. However, for small dipole moments and distant collisions the longer-range dipole-quadrupole interactions may predominate. Thus for the collision diameter of OCS, $b_e = 7.6$ A and $Q = 0.6 \times 10^{-16}$ cm^2, the dipole moment μ must be as large as 2 debyes for W_{dd} to equal W_{dq}. Since the dipole moment of OCS is only 0.7 debye,

the dipole-quadrupole interactions may be expected to dominate. For dipole moments as large as 2 or 3 debyes, the dipole-dipole Keesom alignment interactions usually are most important. While dipole moments are readily measurable, quadrupole moments have so far only been estimated roughly from the molecular structure [382] or deduced from ammonia pressure broadening. Smith and Howard [536] have estimated the quadrupole moments of several molecules in this way from their effectiveness in broadening the NH_3 3,3 line and have used the resulting values to calculate dipole-quadrupole self-broadening in these gases. They obtained fair agreement with experiment.

13-11. Oxygen Line Breadths. The oxygen spectrum is unusual in that it arises from a molecule having a zero electric dipole moment. It might therefore be expected to have unusually narrow lines, and this is indeed the case. Because of its importance to atmospheric transmission, breadths of oxygen lines in pure oxygen and in air have been studied since the early days of microwave spectroscopy [139], [244], [301], [416], [576]. Half widths of the microwave oxygen lines are about 2 Mc per mm of Hg and are approximately independent of the rotational quantum numbers [667], [669], [770]. This, plus theoretical estimates of the magnitudes of various interactions, indicate that the width of these lines is mainly caused by the same short-range repulsive forces responsible for kinetic energy transfer [770]. Even though they decrease very rapidly with distance, they are probably large enough to cause rotational transitions (which involve little energy) at a distance $1\frac{1}{2}$ times the kinetic theory radius, and so to cause the observed line widths.

13-12. Temperature Dependence of Line Widths. An elementary model of the collision process might be two colliding "hard" molecules of definite boundaries, so that the collision cross section is independent of the velocity of collision. Then since the number of molecules at a given pressure is inversely proportional to the temperature, and the velocity is proportional to the square root of the temperature,

$$\Delta\nu \propto nv\sigma \propto \frac{1}{\sqrt{T}}$$

In contrast to expectations from this model, experimentally the ammonia line width of fixed pressure is approximately proportional to $1/T$ [536] so the collision cross section cannot be independent of velocity. Some such variation is to be expected from a more refined collision theory. A slow molecule spends more time near the radiator and so causes more disturbance than one which passes quickly.

The dependence of the collision cross section on velocity for an intermolecular potential proportional to $1/r^n$ may be readily obtained. For such a potential, a measure of the disturbance is the matrix element $(a|P|b)$ whose square is the probability of a collision-induced transition.

From (13-49),

$$(a|P|b) = \frac{\text{const}}{b^{n-1}v} \tag{13-66}$$

For a collision just strong enough to be effective in line broadening or to give a critical value of $(a|P|b)$, the collision parameter b is the effective collision diameter b_e. From (13-66)

$$b_e^{n-1} \propto \frac{1}{v}$$

Hence the line-breadth parameter is

$$\Delta\nu \propto nvb_e^2 \propto nv^{1-2/(n-1)}$$

Remembering that the average velocity is proportional to $T^{\frac{1}{2}}$ and n to T^{-1},

$$\Delta\nu \propto T^{-(n+1)/2(n-1)} \tag{13-67}$$

For $n = 3$ (the ammonia case), $\Delta\nu \propto T^{-1}$; for $n = 6$, $\Delta\nu = T^{-0.7}$. If T is increased by a factor of 2, $\Delta\nu$ would change to 0.5 or 0.62, respectively, of its original value. Thus the temperature dependence of line width, when accurately measured, may give information about the force law between molecules. However, if it were to be so used, very precise line widths would be needed.

Furthermore, the measured collision diameter varies with temperature whenever resonance collisions between molecules are important because the distribution of molecules among the rotational or other quantum states changes with temperature. For the $J = 2 \leftarrow 1$ transition of OCS the line-width parameter $\Delta\nu$ varies as $T^{-0.9}$ [921], so that, from Eq. (13-67), the collision diameter is approximately proportional to $T^{-0.2}$. About half of this temperature variation of collision diameter has been shown to be due to the change in first-order (resonant) dipole interactions [921].

13-13. Effect of Temperature on Intensities. Temperature enters into the peak intensity of a microwave line [Eq. (19)] through $\Delta\nu$, kT, N, and f, where f is the fraction of molecules in the lower state of the transition and N is the number of molecules per cubic centimeter. From the above discussion, at a given pressure $\Delta\nu$ varies with temperature as $T^{-\frac{1}{2}}$ for a very short-range force law, and as T^{-1} for the longer-range force laws. Assuming $\Delta\nu \propto T^{-1}$, Eq. (1-77) shows that for a diatomic or linear molecule the variation of intensity with T is

$$\gamma_{max} \propto \frac{1}{T^2} \tag{13-68}$$

For a symmetric rotor, from (3-52),

$$\gamma_{max} \propto \frac{1}{T^{\frac{5}{2}}}$$

In these expressions most of the variation with temperature is due to the change in the Boltzmann distribution which populates lower rotational states more fully at lower temperatures. That portion of the variation which is caused by changes in population of the vibrational state has not been taken into account. Although population of vibrational states is also affected by temperature, its variation can be neglected in the important case where the vibrational frequency is so high that almost all molecules are in the ground vibrational state.

For linear and symmetric rotor molecules in the ground vibrational state, intensity is always increased by operating at as low a temperature as possible, consistent with a reasonable vapor pressure. For microwave transitions between high-energy rotational levels of asymmetric tops, or those involving excited vibrational states, a decrease in temperature may decrease the intensity or leave it relatively unchanged.

13-14. High Pressures. Pressures may be called high from the point of view of line breadths when collisions involving more than two molecules become frequent enough to be important. In such cases the line width is no longer proportional to pressure, since the number of effective collisions undergone by one molecule is not simply proportional to the density of molecules. "High" pressure may occur as low as $\frac{1}{2}$ atm for molecules with large collision diameters. For example, at 1 atm the average distance between molecules is approximately 30 A, which is only twice the effective collision diameter for NH_3. "Low" pressure conditions may still apply at 1 atm to other gases such as O_2 which have very small collision diameters. Collision theories which assume two-body impacts only and a long interval of time between impacts are, of course, not strictly applicable to high-pressure conditions. Statistical types of theories may be more appropriate since the radiating molecule is almost continually perturbed. However, as yet no quantitative theory of line broadening at high pressures is available.

The ammonia spectrum has been studied experimentally at pressures up to a few atmospheres by several observers [779], [257], [439], [321], [734]. It is found that the spectrum is fitted near the peak by a Van Vleck–Weisskopf shape but that ν_0 may be assumed to decrease with increasing pressure. For pressures equal to or greater than 2 atm $\Delta\nu$ increases less than linearly with pressure and the best fit is obtained with $\nu_0 = 0$. This shift in ν_0 is proportional to the square of the pressure rather than its first power as might be expected from phase-shift theories. Diabatic collisions, of course, predict no shift at all. The observed shift in frequency has been explained qualitatively by Anderson [341] and by Margenau [393]. They point out that, with the small intermolecular distances which are common at high pressures, the perturbations are large enough to cause a change in molecular wave functions and hence in selection rules. In a strong field the molecule is characterized by either

of the wave functions ψ_{+K} or ψ_{-K} rather than by their weak-field combinations $\psi = \psi_{+K} \pm \psi_{-K}$. In other words, the inversion is eliminated and the nitrogen is held on one side of the hydrogens by the electric field. The only allowed transitions are changes in orientation or of one unit in magnetic quantum number. These transitions involve much smaller frequencies than inversion. At 1 atm pressure, where this effect begins to appear experimentally, the interaction between dipole moments is greater than the inversion splitting so that the strong-field approximation holds for about 50 per cent of the time. The importance of this effect and interpretation of the high-pressure line shape has, however, been questioned [504] on the basis of infrared measurements.

13-15. Saturation Effects. The well-known Lambert's law states that each layer of material of equal thickness absorbs an equal fraction of radiation which traverses it. From Lambert's law is derived the exponential decrease in intensity

$$I = I_0 e^{-\gamma x} \tag{13-69}$$

where γ is constant. In optical spectra departures from Lambert's law are usually associated with polychromatic radiation, individual components of which are absorbed at different rates. In the microwave region, however, Lambert's law breaks down even for monochromatic radiation because of saturation effects. The intensity of radiation can be made so large that absorbing molecules of a gas cannot get rid of the absorbed energy rapidly enough and γ becomes dependent on I.

Consider a molecular ground state in which there are n_0 molecules per unit volume and an excited state containing n_1 molecules per unit volume, with a microwave transition possible between the two states. From the derivation of Eq. (13-19), it can be seen that

$$\gamma = \frac{8\pi^2}{3ch}(n_0 - n_1)|\mu_{01}|^2 \frac{\nu(1/2\pi\tau)}{(\nu - \nu_0)^2 + (1/2\pi\tau)^2} \tag{13-70}$$

where the "negative frequency resonance" term of Eq. (13-19) has been omitted since it is quite unimportant under the low-pressure conditions which show saturation effects.

If essentially no microwave radiation is present, then collisions maintain an equilibrium between n_0 and n_1 such that

$$n_1 = n_0 e^{-h\nu/kT} \tag{13-71}$$

If $1/t_{01}$ and $1/t_{10}$ are the probabilities per second that a molecule is transferred from state 0 to state 1 or from state 1 to state 0, respectively, by collision, then for equilibrium with no radiation

$$\frac{n_0}{t_{01}} = \frac{n_1}{t_{10}} \tag{13-72}$$

If radiation of intensity I (in units of quanta per second per unit cross section of area) is absorbed with an absorption coefficient γ, then a new equilibrium condition must be set up

$$\frac{n_0}{t_{01}} + I\gamma = \frac{n_1}{t_{10}} \tag{13-73}$$

From Eqs. (13-71) and (13-72), $1/t_{01} = (1 - h\nu/kT)/t_{10}$, assuming $h\nu/kT$ is small, so that Eq. (13-73) becomes

$$(n_0 - n_1) = n_0 \frac{h\nu}{kT} + I\gamma t_{10} \tag{13-74}$$

Furthermore, when no radiation is present but $n_0 - n_1$ is disturbed from its equilibrium value $(n_0 - n_1)_{\text{equ}}$,

$$\frac{d(n_0 - n_1)}{dt} = \frac{-2}{t_{10}} [(n_0 - n_1) - (n_0 - n_1)_{\text{equ}}]$$

so that $t = t_{10}/2$ gives the rate of approach to equilibrium.

Combining Eqs. (13-74) and (13-70), and letting $t = t_{10}/2$

$$\gamma = \frac{8\pi^2}{3ch}\left(n_0 \frac{h\nu}{kT} - 2I\gamma t\right) |\mu_{01}|^2 \nu \frac{1/2\pi\tau}{(\nu - \nu_0)^2 + (1/2\pi\tau)^2} \tag{13-75}$$

or

$$\gamma = \gamma_0 \left(1 - \frac{2I\gamma kTt}{n_0 h\nu}\right) \tag{13-76}$$

where γ_0 is the absorption coefficient when I is very small. When I is very large then $\gamma \ll \gamma_0$ and the quantity in the parentheses in Eq. (13-76) approaches zero; so that for large radiation flux

$$\gamma \approx \frac{n_0 k\nu}{2IkTt} \tag{13-77}$$

This equation written

$$\gamma I \approx \frac{n_0}{2t} \frac{h\nu}{kT}$$

is simply equivalent to saying that the total number of quanta absorbed per unit time must equal the rate at which the energy of these quanta can be transformed into kinetic energy by collision.

Solving Eq. (13-75) for γ gives

$$\gamma = \frac{8\pi^2 n_0}{3ckT} |\mu_{01}|^2 \nu^2 \frac{1/2\pi\tau}{(\nu - \nu_0)^2 + (1/2\pi\tau)^2 + \dfrac{16\pi^2 t}{3ch} |\mu_{01}|^2 \nu I (1/2\pi\tau)} \tag{13-78}$$

Thus, as a result of saturation, γ is decreased at all frequencies. The most noticeable effects occur, of course, near the peak absorption $\nu = \nu_0$. The line shape is altered only in that the maximum intensity is decreased

by the factor

$$\frac{1}{1 + \dfrac{16\pi^2 |\mu_{01}|^2 \nu I t}{3ch} 2\pi\tau}$$

and the half width increased by the factor

$$\sqrt{1 + \frac{16\pi^2 |\mu_{01}|^2 \nu I t 2\pi\tau}{3ch}} \tag{13-79}$$

Essentially the same result is given by a more sophisticated quantum-mechanical treatment [297], [322].

At high pressures, saturation is generally unobservable. It becomes noticeable when

$$\frac{16\pi^2 |\mu_{01}|^2 \nu I t 2\pi\tau}{3ch} \approx 1$$

Since both t and τ are inversely proportional to the number of collisions per second, the radiation intensity I at which saturation occurs is proportional to the pressure squared. Experimentally, saturation is often noticed when the power flux is as high as one milliwatt per square centimeter and the pressure low enough to give line widths less than 1 Mc [172]. It is not uncommon for saturation effects to set a lower limit on the width of microwave lines. In order to obtain very narrow lines, the radiation intensity must be kept low.

In considering saturation, each Zeeman (or Stark) component of a line should be treated individually. Although individual components all have the same frequency, their matrix elements differ (*cf.* page 23) so that some components saturate more readily than others [295]. However, saturation effects may be described approximately by taking some average matrix element $|\mu_{10}|^2$ for the entire transition.

Measurement of saturation effects allows determination of $1/t$, the rate at which the molecular distribution approaches equilibrium. In ammonia, it has been shown that $t \approx \tau$ [172], [256], [294], [295], so that each collision which is effective in producing line broadening is also effective in restoring an equilibrium distribution to the colliding molecules. This is the result to be expected from the discussion on pages 351 and 352.

Saturation effects may also be used to obtain an estimate of the matrix element $|\mu_{01}|^2$ in certain cases. The intensity of a line is influenced both by the dipole matrix elements $|\mu_{01}|^2$ and by the number of molecules in the particular ground state from which transitions occur. Saturation effects may be seen from (13-78) or (13-79) not to depend on the number of molecules normally in the ground state, but they do depend on the matrix element. Thus the relative ease with which two different lines can be saturated affords some information about the relative sizes of their dipole matrix elements.

13-16. Broadening by Collisions with Walls. If a gas molecule strikes a wall of the cavity or waveguide in which it is contained, the process of absorption is interrupted.

A good approximate treatment of the broadening effects of wall collision can be obtained by assuming that the line shape due to wall collisions is the same as that produced by intermolecular collisions, *i.e.*

$$\gamma = \frac{\gamma_{\max}(\Delta\nu)^2}{(\nu - \nu_0)^2 + (\Delta\nu)^2} \tag{13-80}$$

Here the line-breadth parameter is given by $\Delta\nu = 1/2\pi\tau$, where τ is the mean time between collisions. τ may be evaluated from kinetic theory.* The number of molecules hitting the surface of total area A in each second is

$$n = \tfrac{1}{4}N\bar{v}A \tag{13-81}$$

where N is the number of molecules per cubic centimeter of gas, $\bar{v}$ is the average molecular velocity $= 4(RT/2\pi M)^{\frac{1}{2}}$, R is the gas constant, T is the absolute temperature, and M is the molecular weight. Hence the number of collisions per second is

$$n = NA\left(\frac{RT}{2\pi M}\right)^{\frac{1}{2}} \tag{13-82}$$

But the total number of molecules in the absorption cell is NV, where V is the volume of the cell. Thus the average time between collisions for any molecule is

$$\tau = \frac{NV}{NA(RT/2\pi M)^{\frac{1}{2}}} = \frac{V}{A}\left(\frac{2\pi M}{RT}\right)^{\frac{1}{2}} \tag{13-83}$$

so that

$$\Delta\nu = \frac{A}{V}\left(\frac{RT}{8\pi^3 M}\right)^{\frac{1}{2}} \tag{13-84}$$

At 300°K,

$$\Delta\nu = 1.00 \times 10^4 \frac{A}{V} M^{-\frac{1}{2}} \tag{13-85}$$

As an example, for ammonia in a cell with a spacing of 4 mm between a Stark plate and the opposite face, and all other dimensions considerably larger, $\Delta\nu = 12$ kc.

A more rigorous treatment of wall broadening has been given by Danos and Geschwind [788]. The line shape is shown to be close to the Lorentz shape and the line width is about 10 per cent greater than that given by the elementary treatment above.

If both Doppler and collision widths are appreciable, the total line-

* See, for instance, M. Knudsen, *Kinetic Theory of Gases*, Methuen & Co., Ltd., London, and John Wiley & Sons, Inc., New York, 1950.

width parameter is given very nearly by*

$$\Delta\nu \approx [(\Delta\nu_{\text{Doppler}})^2 + (\Delta\nu_{\text{collision}})^2]^{\frac{1}{2}} \tag{13-86}$$

Wall-collision broadening is ordinarily much less than pressure broadening. Where necessary for high-resolution spectroscopy it can always be reduced as much as desired by using a sufficiently large absorption cell.

13-17. Microwave Absorption in Nonpolar Gases. A nonpolar gas ordinarily does not absorb microwaves. However, if the gas molecules are sufficiently polarizable, some dipole moment may exist during collisions. At high pressures, the molecules are in collision for a large part of the time, so that an appreciable absorption occurs. Such a pressure-dependent absorption has been found in CO_2 by Birnbaum, Maryott, and Wacker [905]. The observed absorption was approximately proportional to the square of the pressure and reached 2.3×10^{-5} at 3.3 cm wavelength for a pressure of 45 atm and a temperature of 25°C.

* See numerical tabulation in M. Born, *Optik*, pp. 486, 431*ff.*, Springer-Verlag OHG, Berlin, 1933.

CHAPTER 14

MICROWAVE CIRCUIT ELEMENTS AND TECHNIQUES

14-1. Introduction. Electromagnetic Fields and Waves. Although microwaves were produced by Hertz in the very earliest demonstration of electromagnetic waves, for many years waves of these short lengths were not much used. The interesting features of wavelengths comparable with the dimensions of laboratory apparatus (1 to 1000 mm) were recognized but could not easily be studied because of the lack of suitable generators.

With the development of klystron and magnetron oscillators and of waveguide techniques near the beginning of World War II, large-scale military applications of radar became possible. The attendant intensive development program saw the introduction or development of most of the microwave techniques currently used in spectroscopy. The status of the art at the end of the war is described most completely in the 28 volumes of the Massachusetts Institute of Technology Radiation Laboratory Series (McGraw-Hill Book Company, Inc., New York, 1947). A number of shorter treatments of microwave theory and practice on various levels have appeared since the war. Many of these are listed at the end of the present chapter.

Because the basic microwave techniques are described in detail elsewhere, they will be only outlined here except for those peculiar to microwave spectroscopy. References will for the most part be to books where fairly complete treatments are available rather than to original papers.

Devices with dimensions comparable with the radiation wavelength cannot usually be treated by the lumped circuit-element approximation used in ordinary electrical-circuit theory. On the other hand, microwave devices are seldom large enough in comparison with the wavelength for the approximations of geometrical optics to be employed. Both limiting cases do occasionally occur, but most microwave apparatus has to be discussed in terms of electromagnetic wave theory.

The behavior of the entire electromagnetic spectrum may be obtained from a study of Maxwell's equations combined with additions from quantum mechanics which are necessary to understand interactions between radiation and matter. In Gaussian units (for comparison with

mks units see, for instance, [537]), Maxwell's equations are

$$\nabla \times \mathbf{H} = \frac{4\pi \mathbf{i}}{c} + \frac{1}{c}\frac{\partial \mathbf{D}}{\partial t} \tag{14-1}$$

$$\nabla \times \mathbf{E} = -\frac{1}{c}\frac{\partial \mathbf{B}}{\partial t} \tag{14-2}$$

$$\nabla \cdot \mathbf{B} = 0 \tag{14-3}$$

$$\nabla \cdot \mathbf{D} = 4\pi\rho \tag{14-4}$$

where $\mathbf{H}$ = magnetic field
$\mathbf{B}$ = magnetic induction
$\mathbf{E}$ = electric field
$\mathbf{D}$ = electric displacement
$\mathbf{i}$ = electric current
ρ = electric charge density
∇ = the operator $\mathbf{a}(\partial/\partial x) + \mathbf{b}(\partial/\partial y) + \mathbf{c}(\partial/\partial z)$

$\mathbf{a}$, $\mathbf{b}$, and $\mathbf{c}$ are unit vectors along the x, y, and z axes, respectively. To these equations must be added relationships which have to do with the properties of matter:

$$\mathbf{E} = \tau \mathbf{i} \tag{14-5}$$

$$\mathbf{B} = \mu \mathbf{H} \tag{14-6}$$

$$\mathbf{D} = \epsilon \mathbf{E} \tag{14-7}$$

where τ = resistivity
μ = permeability and
ϵ = dielectric constant

From these seven equations the following important relations may be derived:

Energy density of an electric field $= \epsilon \mathbf{E}^2/8\pi$
Energy density of a magnetic field $= \mu \mathbf{H}^2/8\pi$

Energy flow from a volume bounded by a surface $S = \dfrac{c}{4\pi}\displaystyle\int_S \frac{\mathbf{E} \times \mathbf{B}}{\mu}\, ds$

The quantity $\dfrac{c\mathbf{E} \times \mathbf{B}}{4\pi\mu}$ is called Poynting's vector and usually can be regarded as the energy flux vector per unit surface, although it can be rigorously used only with integrations over a closed surface. For nonisotropic, ferromagnetic, or ferroelectric material, the relations (14-5), (14-6), and (14-7) are replaced by more complicated expressions. In addition, when one proceeds to a detailed study of interactions between microwaves and matter, a number of interesting cases appear in which τ, μ, and ϵ may no longer be usefully regarded as constants. However, in developing the general characteristics of microwave propagation, we shall accept τ, μ, and ϵ as constant properties of bulk matter.

If there are no free charges in a material ($\rho = 0$), by taking the curl of Eq. (14-1) or Eq. (14-2) and using Eqs. (14-3), (14-4), (14-5), (14-6), and

(14-7), one obtains the wave equations

$$\nabla^2\mathbf{E} = \frac{4\pi\mu}{c^2\tau}\frac{\partial\mathbf{E}}{\partial t} + \frac{\mu\epsilon}{c^2}\frac{\partial^2\mathbf{E}}{\partial t^2} \tag{14-8}$$

$$\nabla^2\mathbf{B} = \frac{4\pi\mu}{c^2\tau}\frac{\partial\mathbf{B}}{\partial t} + \frac{\mu\epsilon}{c^2}\frac{\partial^2\mathbf{B}}{\partial t^2} \tag{14-9}$$

A solution of Eq. (14-8) for the electric field **E** is a satisfactory solution of Maxwell's equations if it is paired with the proper solution of Eq. (14-9) for the magnetic field, if it satisfies Eq. (14-4), and if the appropriate boundary conditions are satisfied. The proper solution for **B** may be obtained from **E** by using Eq. (14-2).

Focusing attention on solutions of Eqs. (14-8) or (14-9) which involve a wave of definite frequency $\nu = \omega/2\pi$ traveling along the z axis, we substitute the form $E = E_0 e^{j(\omega t - \gamma z)}$ into Eq. (14-8), where $j = \sqrt{-1}$. The wave equation (14-8) is satisfied if

$$\gamma = \pm\sqrt{\frac{\mu\epsilon}{c^2}\omega^2 - \frac{4\pi\mu}{c^2\tau}j\omega} \tag{14-10}$$

This solution is given in the complex notation commonly employed in electrical theory. The actual physical quantities are the real parts of these expressions.

If the propagation constant γ is positive and real, the wave progresses in the positive z direction without damping or diminution. If γ is negative, the direction of propagation is in the negative z direction. If $\gamma = j\alpha + \beta$ is complex, then $E = E_0 e^{j(\omega t - \beta z) - \alpha z}$ represents an exponentially increasing or exponentially decreasing wave. To prevent violation of the principle of conservation of energy, the wave must usually decrease as it progresses, so that α and β must have opposite signs. An exceptional case occurs inside the traveling-wave amplifier or oscillator tube where energy is supplied to the wave as it advances.

If the wave is in a good dielectric material (resistivity τ very large), the propagation constant $\gamma = \pm(\omega/c)\sqrt{\mu\epsilon}$ is real, giving an undamped wave in a medium with index of refraction $\sqrt{\mu\epsilon}$.

If the wave is propagated in a good conductor (resistivity τ small), then usually $4\pi/\tau \gg \epsilon\omega$, and the first term under the radical of Eq. (14-10) can be neglected so that $\gamma = \pm\sqrt{\frac{2\pi\mu\omega}{c^2\tau}}(1 - j)$. Such a propagation constant corresponds to a very strongly damped wave since E decreases by $1/e$ in a distance

$$\delta = \sqrt{\frac{c^2\tau}{2\pi\mu\omega}} \tag{14-11}$$

Because of the large damping, such a wave is usually appreciable only at the surface of a conductor, and δ is called the skin depth since it gives the amount of penetration of the wave into the material. For a good conductor and microwave frequencies $\delta = 10^{-3}$ cm or less.

14-2. Waveguides. We shall now proceed to show by means of these relations that electromagnetic waves of suitable length are propagated in a hollow rectangular metal pipe or "waveguide." Figure 14-1 shows the coordinate system. In these coordinates the boundary conditions are

$$E_x = 0 \quad \text{at } y = 0 \text{ and at } y = b \tag{14-12}$$

$$E_y = 0 \quad \text{at } x = 0 \text{ and at } x = a \tag{14-13}$$

of the walls are perfect conductors.

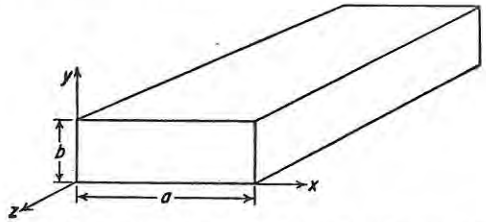

FIG. 14-1. Rectangular hollow metal pipe waveguide.

For a perfect dielectric (infinite resistivity) inside the waveguide $\tau = \infty$ and the wave equation (14-8) becomes

$$\nabla^2\mathbf{E} = \frac{\mu\epsilon}{c^2}\frac{\partial^2\mathbf{E}}{\partial t^2} \tag{14-14}$$

Assume a solution of this wave equation, subject to the boundary conditions, of the form of a traveling wave with no longitudinal electric-field component.

$$\begin{aligned} E_x &= -E_0\frac{k_y}{k_x}\cos k_x x \sin k_y y\, e^{+j(\omega t - \gamma z)} \\ E_y &= E_0 \sin k_x x \cos k_y y\, e^{+j(\omega t - \gamma z)} \\ E_z &= 0 \end{aligned} \tag{14-15}$$

These satisfy the wave equation provided that

$$k_x^2 + k_y^2 + \gamma^2 = \frac{\mu\epsilon\omega^2}{c^2} = \left(\frac{2\pi}{\lambda_0}\right)^2 \tag{14-16}$$

where λ_0 is the wavelength in the free dielectric without walls.

From the boundary conditions at $x = a$ and at $y = b$

$$k_x = \frac{m\pi}{a} \qquad k_y = \frac{n\pi}{b} \tag{14-17}$$

where m and n are integers. Then

$$\gamma = 2\pi \sqrt{\frac{1}{\lambda_0^2} - \left(\frac{m}{2a}\right)^2 - \left(\frac{n}{2b}\right)^2} \tag{14-18}$$

For waves whose λ_0 is sufficiently small, γ is real and propagation occurs. Longer waves are not propagated through the guide, for γ is imaginary when γ_0 is greater than a critical "cutoff" value designated λ_{0c}. The cutoff wavelength is given by

$$\frac{1}{\lambda_{0c}^2} = \frac{m^2}{(2a)^2} + \frac{n^2}{(2b)^2} \tag{14-19}$$

The length of the wave in the guide λ_g is related to the propagation constant by

$$\lambda_g = \frac{2\pi}{\gamma} = \frac{\lambda_0}{\sqrt{1 - (m\lambda_0/2a)^2 - (n\lambda_0/2b)^2}} = \frac{\lambda_0}{\sqrt{1 - (\lambda_0/\lambda_{0c})^2}} \tag{14-20}$$

λ_g approaches infinity when λ_0 approaches the cutoff wavelength. For shorter wavelengths, λ_g decreases and eventually approaches λ_0 when both are much smaller than λ_{0c}.

It is interesting at this point to compare the behavior of low-frequency electromagnetic waves and of light in a hollow tube with that of microwaves. A low-frequency wave requires two insulated conductors for propagation. It cannot go down a single-conductor waveguide because its wavelength is beyond cutoff. Microwaves can be propagated down a waveguide, but the propagation is usually strongly affected by the boundary conditions required by the walls; *i.e.*, the microwaves are somewhat constrained in being made to "fit into" a waveguide. For optical wavelengths, however, the walls have relatively little effect since the fields vary rapidly with distance, and boundary conditions in a tube of ordinary dimensions are easily met. A tube of 1 cm dimension is almost equivalent to free space for light waves.

As mentioned above, Eq. (14-20) shows that, for λ_0 just slightly smaller than the cutoff wavelength, γ is very small and hence the apparent wavelength measured along the z axis is very large. Since the phase velocity equals ω/γ, the phase velocity may become very large and is always greater than $c/\sqrt{\mu\epsilon}$, the velocity of light in the free medium. Of course, the group velocity must obey the principles of relativity and cannot exceed $c/\sqrt{\mu\epsilon}$. The group velocity may be shown in the usual way to be $v_g = (c/\sqrt{\mu\epsilon})(\lambda_0/\lambda_g)$. The group velocity is always less than $c/\sqrt{\mu\epsilon}$, approaching this value when $\lambda_0 \ll a$, or for very short wavelengths.

The modes which have been discussed are those for which $E_z = 0$, that is, the electric field is purely transverse, and are designated TE_{mn} modes (transverse electric). Equation (14-15) gives the components of **E**, and

the components of **H** may be obtained from Eq. (14-15) and Eq. (14-2) as

$$\begin{aligned} H_x &= -\frac{c\gamma}{\mu\omega} E_0 \sin k_x x \cos k_y y \, e^{j(\omega t - \gamma z)} \\ H_y &= -\frac{c\gamma k_y}{\mu\omega k_x} E_0 \cos k_x x \sin k_y y \, e^{j(\omega t - \gamma z)} \\ H_z &= \frac{cj(k_x^2 + k_y^2)}{\mu\omega k_x} E_0 \cos k_x x \cos k_y y \, e^{j(\omega t - \gamma z)} \end{aligned} \tag{14-21}$$

where $k_x = m\pi/a$, $k_y = n\pi/b$, $k_x^2 + k_y^2 + \gamma^2 = \mu\epsilon\omega^2/c^2$, and m and n are integers.

For any given rectangular waveguide having $a > b$, the lowest frequency, or longest λ_0, mode of the TE type which can be propagated is the one for which $m = 1$, $n = 0$. It is known as the TE_{10} mode, or the dominant mode, and is almost the only one used for microwave transmission and spectroscopy.

The complete set of field equations for the dominant mode may be written

$$\begin{aligned} E_x &= 0 & H_x &= -\frac{c\gamma}{\mu\omega} E_0 \sin k_x x \, e^{j(\omega t - \gamma z)} \\ E_y &= E_0 \sin k_x x \, e^{j(\omega t - \gamma z)} & H_y &= 0 \\ E_z &= 0 & H_z &= \frac{cjk_x}{\mu\omega} E_0 \cos k_x x \, e^{j(\omega t - \gamma z)} \end{aligned} \tag{14-22}$$

Except near cutoff, H_z is considerably smaller than H_x, and the wave may be visualized as an electric and a magnetic vector both approximately perpendicular to the direction of propagation and traveling down the waveguide in phase. Actually H_z is by no means negligible.

An instructive viewpoint is provided by realizing that the fields in the dominant mode given above are the same as those due to two plane waves reflected successively from the walls of the waveguide so that each zigzags its way down the guide in the z direction. The velocity with which power is propagated down the waveguide is slowed up an amount appropriate to the zigzag motion of the hypothetical plane waves.

Figure 14-2 shows the instantaneous electric field and wall currents in a rectangular waveguide carrying a TE_{10} wave. Magnetic fields, which can also be obtained from the wave equations, are shown by broken lines. Wall currents are perpendicular at every point to the magnetic field.

Other modes satisfying the wave equation and boundary conditions exist, including some with a purely transverse magnetic field. The latter are designated TM waves, with the particular mode indicated by subscripts analogous to those used for TE modes. Their cutoff wavelength is also given by Eq. (14-20), but m and n must be greater than zero, so

that no TM mode has a cutoff wavelength as long as that of the dominant TE mode.

Circular-cylinder waveguides also can propagate microwaves in various modes governed by the boundary condition that the electric field at the wall must be perpendicular to the wall. Both TE and TM modes exist and are designated by those letters with added subscripts. The first subscript is the number of maxima of the field in a 180° angle measured

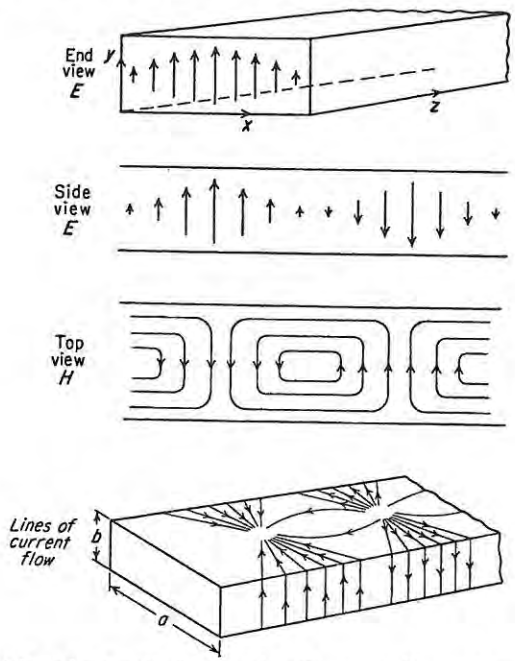

FIG. 14-2. Electric and magnetic fields and wall currents in a rectangular waveguide ($TE_{1,0}$ mode). (*After Pollard and Sturtevant* [308].)

in a plane perpendicular to the axis of the cylinder. The second subscript is the number of maxima between the center and the wall of the waveguide. The fields of some of the circular modes are shown in Fig. 14-3, along with their cutoff wavelengths. As in the rectangular waveguide, λ_g is related to λ_0 and λ_{0c} by Eq. (14-20), *i.e.*,

$$\lambda_g = \frac{\lambda_0}{\sqrt{1 - (\lambda_0/\lambda_{0c})^2}}$$

While each of these modes has uses, most microwave spectrographs employ the TE_{01} mode in a rectangular guide. This mode has the advantage that, if the size of the pipe relative to the wavelength is properly chosen, no other mode can be propagated. In addition, no current flows

across the center of the broad face, so that a longitudinal slot may be cut there without disturbing the fields. Finally, the electric field is always perpendicular to the broad face, so that a metal plate parallel to that face may be put inside the guide without disturbing the fields.

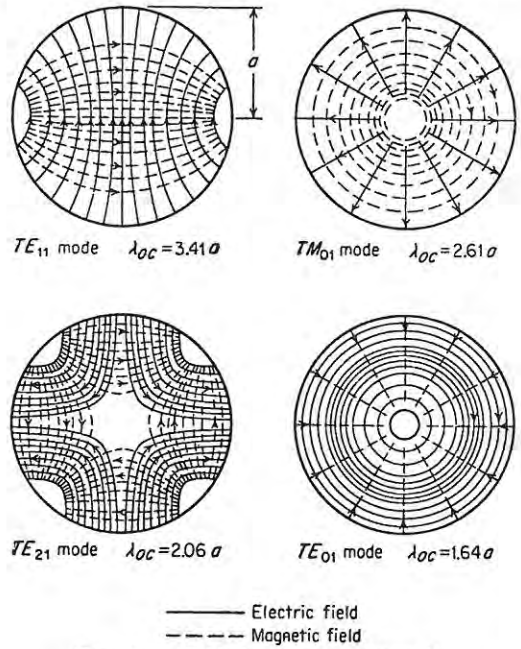

FIG. 14-3. Fields in circular waveguides.

14-3. Attenuation. Waveguide walls made of copper, brass, or silver approximate perfect conductors well enough that the field distributions discussed above are good approximations. However, since currents flow in the walls it is evident that some loss of power will accompany propagation of the wave. These losses give a small imaginary contribution to the propagation constant γ which may be fairly accurately determined by assuming that the fields in the waveguide are those appropriate to the perfectly conducting waveguide and computing the ohmic losses due to current flow.

The boundary conditions at the surface of a perfect conductor require that **H** must be parallel to the surface. Considering any small area of a waveguide wall over which the oscillating magnetic field has essentially constant amplitude, the solution of Eq. (14-9) inside the conducting wall (analogous to the solution discussed for **E** in conducting material) is

$$H_y = H_{0y} e^{j(\omega t - z/\delta) - z/\delta} \tag{14-23}$$

where $\delta = \sqrt{c^2\tau/2\pi\mu\omega}$ is the skin depth. For copper $\delta = 3.8 \times 10^{-5}\sqrt{\lambda}$ cm, where δ and λ are in centimeters. Axes have been oriented so that the origin is at the surface, y is in the direction of $\mathbf{H}$ over the small element of area having $\mathbf{H}$ essentially constant, and the positive z axis extends perpendicularly into the wall.

From Eq. (14-1), since $\partial\mathbf{D}/\partial t \approx 0$ in the conductor,

$$i = \frac{c}{4\pi}\nabla \times \mathbf{H} \qquad \text{or} \qquad i_x = \frac{c}{4\pi\delta}(1 + j)H_{0y}e^{j(\omega t - z/\delta) - z/\delta} \tag{14-24}$$

The power loss due to ohmic resistance per unit volume is $(i_R^2)_{av}\tau$ or $\frac{1}{2}ii^*\tau$, where i_R is the real part of Eq. (14-24). Integrating over z from 0 to ∞, the power loss per unit area is obtained as

$$\text{Power loss/area} = \int_0^\infty \frac{ii^*}{2}\tau\, dz = \frac{c^2\tau}{32\pi^2\delta}H_{0y}^2 = \frac{\mu\nu\delta}{8}H_{0y}^2 \tag{14-25}$$

where ν is the frequency. The last expression for power loss has a simple interpretation. The total energy per unit area built up in the magnetic field inside the metal on every half cycle is approximately $(\mu H_{0y}^2/8\pi)\delta$ since $\mu H_{0y}^2/8\pi$ is the energy density at the metal surface and δ is approximately the depth of penetration of the field. If all this energy associated with the magnetic field in the metal were dissipated in the metal on every half cycle, then the rate of power loss per unit area would be

$$2\nu\frac{\mu H_{0y}^2}{8\pi}\delta$$

which is approximately the same as Eq. (14-25). Thus the energy of the electromagnetic field penetrating the metal may be considered lost on every half cycle.

If the behavior of some field component of a microwave is described by $E = E_0e^{j(\omega t - \beta z) - \frac{\alpha}{2}z}$, where α and β are real, the constant $\frac{\alpha}{2}$ is sometimes called the attenuation constant. Its unit is nepers per unit length. More commonly the quantity α is called the attenuation constant, since the power or energy associated with the wave depends on the square of field strength, or as $P = P_0e^{-\alpha z}$. The attenuation constant α for power is given in units of inverse length, such as cm^{-1}. It can be calculated by computing the power flow through a waveguide and the power loss per unit length. Thus

$$\alpha = \frac{\displaystyle\int_{S_1}\frac{\mu\nu\delta}{8}H_{S_1}^2\, dS_1}{\displaystyle\int_{S_2}\frac{c}{4\pi\mu}\mathbf{E} \times \mathbf{B} \cdot d\mathbf{S}_2} \tag{14-26}$$

where H_{S_1} is the component of $\mathbf{H}$ at the surface of the waveguide, S_1 is the surface of the waveguide walls of unit length, S_2 is the cross-sectional surface of the waveguide (perpendicular to the direction of power flow).

Evaluation of α for the TE_{10} mode gives, for a silver waveguide at wavelengths well below the cutoff wavelength

$$\alpha = \frac{3.384 \times 10^{-4}}{a^{\frac{3}{2}}}\left\{\frac{(a/2b)(2a/\lambda_0)^{\frac{3}{2}} + (2a/\lambda_0)^{-\frac{1}{2}}}{[(2a/\lambda_0)^2 - 1]^{\frac{1}{2}}}\right\} \quad \text{cm}^{-1} \tag{14-27}$$

where a is the long dimension and b is the short dimension of the waveguide, both being measured in centimeters. λ_0 is the free-space wavelength (in centimeters) of the radiation. To obtain the power loss in decibels per centimeter, the α given by Eq. (14-27) should be multiplied by 4.343.

For metals other than silver, the attenuation is similar to that given by (14-27), but is proportional to the square root of the resistivity. For copper waveguide, the attenuation given by Eq. (14-27) is to be multiplied by 1.05; for gold the factor is 1.26 and for brass it is 2.08.

At the cutoff frequency, the attenuation given by this expression is infinite, and for slightly higher frequencies the attenuation falls rapidly. The large attenuation near the cutoff wavelength is to be expected from the equivalence of the wave to two plane waves zigzagging across the waveguide. Near cutoff the plane waves are reflected back and forth between the walls many times while moving down the waveguide one wavelength. There is consequently opportunity for considerable loss of power. The attenuation passes through a minimum at higher frequencies and then rises approximately proportionally to the frequency. For typical "K-band" copper waveguide, having inside dimensions 0.420 by 0.170 in., Eq. (14-25) gives for $\lambda_0 = 1.25$ cm, $\alpha = 1.1 \times 10^{-3}\ \text{cm}^{-1}$, or 0.48 db/meter. The actual measured attenuation is likely to be between 20 and 100 per cent greater because of surface imperfections ([312], pp. 117, 191). Similar expressions may be given for other modes and other types of waveguides, most of which give attenuation of the same order of magnitude, and with analogous frequency dependence. An exceptional case is the TE_{01} mode in a circular waveguide for which the attenuation decreases without limit as the frequency increases. If, in going to higher frequencies, the size of the waveguide is changed in proportion to the wavelength, the attenuation increases as $a^{-\frac{3}{2}}$, or $\lambda_0^{-\frac{3}{2}}$. If the size of guide is not changed, the attenuation increases for smaller wavelength only as $\lambda_0^{-\frac{1}{2}}$. A waveguide larger than that required to avoid cutoff is often used in the millimeter-wavelength region because of its lower attenuation. For wavelengths beyond cutoff ($\lambda_0 > \lambda_{0c}$), the attenuation is given by $\alpha = 54.6[1/\lambda_{0c}^2 - 1/\lambda_0^2]^{\frac{1}{2}}$ db/unit length and the impedance is reactive. Waveguides beyond cutoff are sometimes used as standards of attenuation.

14-4. Reflections in Waveguides. Reflection occurs whenever a wave in a guide encounters any irregularity. The irregularity may be a change in guide size, a bend or twist, or an obstacle. A treatment of reflection at irregularities is very complicated for the general waveguide case because the obstacle is likely to introduce higher modes into the reflected and transmitted waves. Very great simplifications are possible, however, when only one mode can be propagated at the wavelength considered. Then a reflected wave can be propagated only in the same mode as the incident wave, as in the case of a low-frequency transmission line. The analogy between a single-mode waveguide and a transmission line is very far-reaching and is quite useful because of the familiarity of transmission-line theory and behavior.

A transmission line for electrical impulses usually consists of two parallel conductors with current flowing along each conductor. Current also flows between the two conductors either because of current paths purposely introduced or because of the inevitable interconductor capacitance and leakage resistance. Let the series impedance of the line per unit length be T, and the shunt impedance per unit length be S. Then (*cf.* [117], Chap. 1) the instantaneous current at any point distant z along the line is given by

$$i = i_0 \exp j\omega t \pm \sqrt{T/S}\, z \tag{14-28}$$

where $i_0 e^{j\omega t}$ represents the current at $z = 0$. The potential difference V between the conductors at any point is obtained by multiplying their shunt impedance per unit length by the current flowing through this impedance. The latter is $-di/dz$ since the shunt current is that which is lost from the main line. Therefore

$$V = \mp \sqrt{TS}\, i \tag{14-29}$$

The characteristic impedance of the transmission line is defined as $Z = V/i$. If the wave travels toward positive z $(i = i_0 e^{j\omega t - \sqrt{T/S}z})$, $Z = \sqrt{TS}$, and if the wave is traveling toward negative z the impedance appears to be $Z = -\sqrt{TS}$. Actually the impedance is usually taken as positive for both directions and $V = Zi$ for the wave advancing in the z direction, $V = -Zi$ for the reversed wave.

If the transmission line is not lossy, then T is usually purely inductive and may be written $T = j\omega L$, while S is purely capacitive and is $S = 1/j\omega C$. Hence $Z = \sqrt{L/C}$ and

$$i = i_0 e^{j(\omega t \pm \gamma z)} \tag{14-30}$$

where $\gamma = \sqrt{LC}$ is the propagation constant. Expressed in this form, it is clear that propagation of electromagnetic waves along a transmission line has much in common with the propagation of microwaves in a waveguide or in free space.

Instead of propagation on an infinitely long uniform transmission line, consider now the behavior of a current wave at a junction between two transmission lines of impedance Z_0 and Z_1 as indicated in Fig. 14-4. At the junction itself the current and voltage can be computed from the point of view of either transmission line, which must of course give equivalent results. Thus the current is either the algebraic sum of an incident current wave i_i and the reflected wave i_r or equals the transmitted wave i_t. Hence when $z = 0$,

$$i_i - i_r = i_t \tag{14-31}$$

and

$$i_i Z_0 + i_r Z_0 = i_t Z_1 \tag{14-32}$$

FIG. 14-4. Currents at a junction of transmission lines of impedance Z_0 and Z_1.

where the subscripts i, r, and t denote, respectively, the incident, reflected, and transmitted currents. It is important to remember that in Eq. (14-32) for a wave traveling to the right in Fig. 14-4, $V = iZ$, but for one traveling to the left, $V = -iZ$. Solving Eqs. (14-31) and (14-32) for i_t and i_r when $z = 0$,

$$i_t = \frac{2Z_0}{Z_1 + Z_0} i_i \tag{14-33}$$

$$i_r = \frac{Z_1 - Z_0}{Z_1 + Z_0} i_i \tag{14-34}$$

At any point z to the left of the junction a new impedance may be defined as the ratio of voltage to current

$$Z = \frac{V}{i} = \frac{i_i Z_0 + i_r Z_0}{i_i - i_r} = \frac{Z_0\left(e^{-j\gamma z} + \dfrac{Z_1 - Z_0}{Z_1 + Z_0} e^{+j\gamma z}\right)}{e^{-j\gamma z} - \dfrac{Z_1 - Z_0}{Z_1 + Z_0} e^{+j\gamma z}}$$

$$= Z_0 \left[\frac{-\sinh j\gamma z + (Z_1/Z_0)\cosh j\gamma z}{\cosh j\gamma z - (Z_1/Z_0)\sinh j\gamma z}\right] \tag{14-35}$$

It is to be noted that, for points to the left of $z = 0$, z is a negative quantity. If $Z_1 = Z_0$, from Eq. (14-34) it is seen that there is no reflected wave. This condition is usually desirable because it gives a maximum power transfer and because it avoids standing waves on the transmission line.

If the transmission line to the right of $z = 0$ consists simply of a short circuit ($Z_1 = 0$) and γ is real, then from Eq. (14-35), $Z = -Z_0 j \tan \gamma z$, so that the impedance changes from zero to infinity when z varies from 0 to $-\pi/2\gamma$. Thus the short circuit at $z = 0$ produces what appears to be an open-circuited line at $z = -\pi/2\gamma$ (or $-\lambda/4$), and the impedance varies periodically with z between the extremes of zero and infinity. If, however, there is some loss in the transmission line to the left of $z = 0$,

γ is partly imaginary ($\gamma = j\alpha/2 + \beta$), and some distance from the junction $z = 0$ the periodic impedance variation decreases in magnitude and Z approaches a constant value Z_0.

The impedance concept is particularly useful for transmission lines because Eq. (14-35) permits calculation of the effects of a discontinuity at any point on the line, provided that the propagation constant γ is known. That is, any discontinuity can be expressed as an equivalent impedance at that place, or by Eq. (14-35) at any other place on the line.

For microwave transmission in waveguides these impedance concepts and formulas are still useful. Since there is only one conductor and since different current densities flow over the various waveguide surfaces, both voltage and current are difficult to define. Although no unique definition of impedance can be made, it is customary to define the impedance as the ratio of electric to magnetic field strengths (E/H) at some point in the guide. It is not strictly necessary to define the characteristic impedance. Z_0 can be taken as an arbitrary constant, and other impedances, such as those due to obstacles in the guide, can be expressed in terms of Z_0 because Eq. (14-35) involves only ratios Z/Z_0 and Z_1/Z_0. Discontinuity in the guide propagation due to a sudden change of dielectric properties is easily interpreted as a sudden change in impedance, and the reflected-wave characteristics are given by Eq. (14-34).

However, if the waveguide suddenly changes dimensions, the reflected wave is not so easily obtained since it depends on the particular geometry at the discontinuity. Near the discontinuity the fields are complicated and can be represented as a combination of higher-order propagation modes with the fundamental modes. However, if the higher-order modes cannot be propagated, a wavelength or two from the discontinuity on the incident side one finds only an incident and a reflected wave in the dominant mode. As in a transmission line, these waves can be expressed in terms of an effective impedance at the position of the discontinuity which replaces the discontinuity for the calculation of the fields in the waveguide. Near the discontinuity higher modes are present and this approach cannot be used. It makes difficulty also if two discontinuities occur within a half wavelength or so, for then the higher-order waves from one discontinuity can reach the other before being completely attenuated. If several modes can be propagated, a different discontinuity impedance and propagation constant must be given for each mode; so the concept loses much of its usefulness. Moreover, a reflection can introduce a mode which was not present in the original wave.

In many cases it is desirable to minimize reflections at the junctions of transmission lines by making the terminating impedance for the first line equal to its characteristic impedance. This may be done at low frequencies by a simple transformer involving mutual inductance between two coils. A quarter wavelength of transmission line of characteristic

impedance Z' between the two lines of characteristic impedances Z_0 and Z_1 can also act as a matching transformer. Thus if the junction between Z' and Z_1 is at $z = 0$ and Z' extends one-quarter wavelength in the negative z direction the impedance of the combination is, from Eq. (14-35), $Z = (Z')^2/Z_1$. If it is desired to make Z equal Z_0 so that the transmission lines may be joined with no reflections, then $Z' = \sqrt{Z_1 Z_0}$. Reflection can be eliminated by a number of other types of "transformers." Generally it is necessary to have two independent variables such as, in this case, the length and characteristic impedance of the auxiliary transmission line.

In many cases another approach based on simple ideas of wave interference and diffraction can be used to investigate microwave behavior at a discontinuity. For example, the quarter-wave transformer discussed above may be viewed as setting up two reflected waves. These waves are of equal magnitude because the ratios of characteristic impedance at the two reflecting discontinuities are equal. They are just opposite in phase and hence cancel because the path length for one is one-half wavelength (two quarter wavelengths) longer than for the other. The principle is the same as that used for making nonreflecting glass, where a quarter wavelength of surface material with index of refraction intermediate between air and glass produces two canceling reflections, or "matches impedances."

In many cases it is desirable to have a transformer produce little reflection over a wide range of frequencies. The quarter-wave transformer and many other impedance matching devices depend somewhat critically on the ratio of certain distance parameters to the wavelength and hence are not useful over a very wide frequency range. However, any change in waveguide dimensions or impedance which is so gradual that only a small fractional change occurs over one wavelength affords a good transformer from one impedance to another and shows approximately the same characteristics over a wide frequency range. A gradual change of impedance such as a long taper from one dimension of waveguide to another can easily be seen to produce very little reflection of power because for any reflecting point in the taper an essentially similar reflecting point can be found one-quarter wavelength farther down the taper and the reflected waves from these two will cancel.

Still another important method of reducing reflection is by means of attenuation. Equation (14-35) shows that the impedance approaches the characteristic impedance as z decreases if there is attenuation in the transmission line. This is because any reflected wave decreases as a result of the attenuation. A short section of highly attenuating waveguide will give the same effect. Such a section is customarily inserted between a klystron oscillator and a waveguide to minimize the effect of reflected waves in the guide on the operation of the klystron.

14-5. Cavity Resonators. A hollow space enclosed by metallic walls can support electromagnetic waves of some particular wavelengths in modes which fit the boundary conditions. Consider, for example, a section of rectangular waveguide which is closed at both ends by flat conducting plates (Fig. 14-5). The boundary conditions at the side walls are satisfied for any TE_{mn} waves provided only that their wavelength is short enough for propagation. If the length of the waveguide is l and the wavelength in the guide is λ_g for a particular TE_{mn} mode, the end boundary conditions require that E_z and E_y vanish at $z = 0$ and $z = l$. From Eq. (14-15) this will be satisfied if $e^{j(\omega t - \gamma l)} = \pm e^{j\omega t}$, or $\gamma l = \pi p$, where p is an integer. Since $\gamma = 2\pi/\lambda_g$,

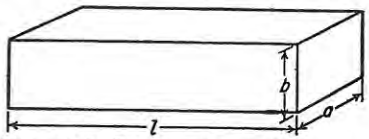

FIG. 14-5. Rectangular cavity resonator.

$$p = \frac{2l}{\lambda_g} \tag{14-36}$$

This relation is just what would be expected for a wave of length λ_g which is reflected with a 180° change of phase at the end of the guide so that a standing wave is produced. For nodes at $z = 0$ and $z = l$, the guide must contain an integral number of half wavelengths.

From Eqs. (14-36) and (14-20), the values of λ_0 for which the cavity is resonant may be obtained.

$$l = \frac{p\lambda_g}{2} = \frac{p\lambda_0}{2\sqrt{1 - (m\lambda_0/2a)^2 - (n\lambda_0/2b)^2}} \tag{14-37}$$

so that

$$\left(\frac{m\lambda_0}{2a}\right)^2 + \left(\frac{n\lambda_0}{2b}\right)^2 + \left(\frac{p\lambda_0}{2l}\right)^2 = 1 \tag{14-38}$$

From this relation, the wavelength λ_0 at which the cavity is resonant may be determined if its dimensions are known.

Rectangular cavities are not much used as resonators although a section of waveguide with partial reflections at each end behaves somewhat like a resonator.

Circular cylindrical cavities are more often used because they can easily be accurately machined and are suitable for wavelength measurements. As for a rectangular cavity, the resonance condition is that the length of the cavity be an integral multiple of $\lambda_g/2$. For either a TE or TM mode in a circular waveguide, the free-space resonant wavelength is given by

$$\lambda_0 = \frac{2}{\sqrt{(2x_{mn}/\pi D)^2 + (p/L)^2}}$$

where D = the diameter and L the length of the cavity
m = the number of half-period variations of E_r with respect to θ (of H_r for TM modes)
n = the number of half-period variations of E_θ with respect to r (of H_θ for TM modes)
p = the number of half-period variations of E_r with respect to z (of H_r for TM modes)
x_{mn} = the nth root of $J_m'(x) = 0$ for the TE modes or of $J_m(x) = 0$ for the TM modes; the J's are Bessel functions

Table 14-1 gives the values of some of the roots. For modes with $p = 0$ the field does not vary in the z direction and so the resonant wavelength does not depend on the length of the cavity, but only on its diameter. This can occur only for TM modes. For wavemeter applications, the TE_{01p} mode is commonly used.

TABLE 14-1. ROOTS OF $J_m(x)$ AND $J_m'(x)$

TE mode	x_{mn}	TM mode	x_{mn}
11p	1.841	01p	2.405
21p	3.054	11p	3.832
01p	3.832	21p	5.136
31p	4.201	02p	5.520
41p	5.318	31p	6.380
12p	5.332	12p	7.016

A useful figure of merit for a resonator is the Q, defined as

$$Q = 2\pi \frac{\text{electromagnetic energy}}{\text{energy lost per cycle}} = -2\pi W \frac{\nu\, dt}{dW} \tag{14-39}$$

From this definition it follows that the energy in a freely oscillating resonator decays according to the equation

$$W = W_0 e^{-\omega t/Q} \tag{14-40}$$

where W is the energy remaining after time t and W_0 is the initial energy at $t = 0$. Q is also a measure of the sharpness of resonance, for the width in frequency $\Delta\nu$ of the resonance curve between points at which the response is one-half that at maximum is

$$\frac{\Delta\nu}{\nu_0} = \frac{1}{Q} \tag{14-41}$$

where ν_0 is the resonant frequency (*cf.* [121], p. 137).

Q may be calculated from Eq. (14-39) by a procedure resembling that used to calculate attenuation (*cf.* [486], pp. 73–77). For instance, for a rectangular box with $l = a$, for the TE_{101} mode (**E** parallel to the b

dimension)

$$Q = 0.71 \frac{\lambda_0}{\delta} \frac{b}{a + 2b} \tag{14-42}$$

where δ is the skin depth and λ_0 the wavelength. Since for copper $\delta = 3.8 \times 10^{-5} \sqrt{\lambda_0}$ when δ and λ_0 are in centimeters, a cubic resonator in this mode at $\lambda = 1$ cm would have a Q value of 6200. This Q is much higher than those obtainable with coils and condensers at frequencies where the latter are appropriate, but still higher Q's can be obtained with other shapes or larger dimensions ([221], Chaps. 5 and 6). In general the Q is roughly proportional to the volume divided by the surface area because stored energy depends on the volume while losses occur only at the walls. An exceptional case is the TE_{01p} mode of a circular cylinder at high frequencies. For this mode the side-wall losses decrease continuously with increasing frequency, and it may be used to obtain very high Q's.

14-6. Coupling of Cavities to Waveguide. In practice a cavity must be coupled to a microwave system. Then, in addition to the losses at the walls, there will be some energy delivered from the cavity to the system, so that the energy loss is greater, and the Q less, than for a completely enclosed cavity. As before, $Q_E = 2\pi \times$ (electromagnetic energy in the cavity)/(energy lost per cycle), where the denominator is the total energy lost and the subscript E denotes the "external" Q with a coupling connection. This may be expressed in terms of the "internal" unloaded Q_U, involving only wall losses, and the "radiation" Q_R involving only losses from the cavity to the external circuit, for

$$\frac{1}{Q_E} = \frac{1}{Q_U} + \frac{1}{Q_R} \tag{14-43}$$

The resonant frequency of the cavity may also be affected by the connection to the microwave circuit if the latter is reactive. However, the coupling is often not large enough to affect greatly either the Q or the resonant frequency ([221], Chap. 5), although in some applications these effects must be considered.

Coupling to a cavity is usually accomplished by one or two holes in the cavity wall. At lower frequencies (3000 Mc or less), coupling loops entering through a suitable hole provide a direct connection to a coaxial line. Usually the coupling is designed to excite preferentially some particular mode by making the electric or magnetic lines of force at the coupling region coincide with those of the desired mode. For instance, the TE_{01p} mode in a cylindrical cavity may be excited by two diametrically opposite holes in the end wall [178]. These holes coincide with holes in the narrow face of the waveguide approximately $\lambda_g/2$ apart. The only field existing at the narrow edge of a waveguide carrying the dominant mode is a longitudinal magnetic field. Through the coupling holes

this field is transmitted to the cavity with opposite phases for the two holes, and so matches the TE_{01p} mode, but not other possible modes except the TE_{02p} mode. The latter may be avoided in a transmission-type resonator by taking the output from a coupling hole in the curved wall of the cylinder at a 45° angle to the input holes. Then an output is obtained only if the cavity is at or very near resonance for the desired mode.

The TE_{01p} mode has the advantage for wavemeter applications of a high Q, so that resonances are sharp. Moreover, there are no radial currents at the edges of the end plates, so that the latter need not make good contact with the walls. This is particularly useful in wavemeters where one end plate must be movable for tuning.

Another mode which is often used for wavemeters is the TE_{11p} mode. This is the lowest-frequency mode for a given cavity, and so the diameter of the cavity may be chosen to permit only this mode over an appreciable band of wavelengths (around 25 per cent—*cf.* Table 14-1). However, this mode is polarized in that it has a plane of symmetry containing the axis of the cylinder (*cf.* Fig. 14-3) and can be resolved into similar modes in any pair of perpendicular directions. If the cylinder is slightly elliptical, these modes have different propagation constants and so give slightly different resonant frequencies. A horseshoe-shaped strap across the coupling hole perpendicular to the electric vector in the waveguide produces a large effective eccentricity so that these resonances are far apart and cross coupling is prevented. Only the mode with polarization parallel to the electric vector in the waveguide is excited.

Good effective contact between the walls and the plunger is obtained by a quarter-wave "choke." That is, the plunger is one-half wavelength long, and in the back is cut a groove one-quarter wavelength deep. The wavelength involved here is the free-space wavelength since either in the groove or in the space between the plunger and the walls waves travel in the coaxial TE_{11} mode for which λ_g is very close to λ. The effect of the groove is to produce a high impedance at the edge of the plunger for waves flowing toward the back of the plunger and so to confine the radiation to the region in front of the plunger. Any radiation which does reach the region behind the plunger and might cause spurious resonances is further reduced by some suitable absorbing material such as "polyiron" ([221], p. 723).

Resonant cavities may be used as either transmission or reaction wavemeters. For use as a transmission-type wavemeter, the cavity of Fig. 14-6 is modified to use two coupling holes, diametrically opposed on the curved wall $\lambda_g/4$ from the base. Then the transmission is almost zero until near resonance it rises to a large value. A typical wavemeter might transmit 25 per cent of the incident power at resonance.

Alternatively, the wavemeter may be coupled to a hole in the side

of the waveguide. At the end of the waveguide is a crystal detector which matches the waveguide well enough to absorb most of the power reaching it. In the guide directly opposite the wavemeter is a post or "iris" diaphragm which is designed to cancel out as nearly as possible the reflections produced by the wavemeter when not in resonance. At resonance the wavemeter absorbs some power and reflects more, so that the power reaching the detector is reduced. Sometimes the detector is also coupled to the side of the waveguide before the wavemeter and detects a change in the reflected power. Depending on the relative phases of the wavemeter reflection and other reflections in the system, the crystal current may either increase or decrease at resonance. In either

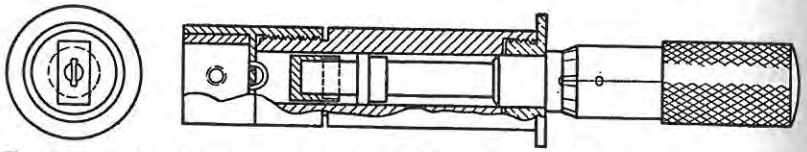

FIG. 14-6. A typical wavemeter for the 1.25-cm region (MIT Radiation Laboratory type TFK-2). Barrel diameter (inside) = 0.3750 ± 0.0002 in. Coupling hole diameter = 0.111 in.

case the detector used with a reaction wavemeter may also be used to monitor the output of the microwave oscillator, for a signal is obtained as long as the wavemeter is not at resonance.

A loaded Q of the order of 3500 may be expected from a wavemeter in the 1-cm region, such as that shown in Fig. 14-6. As the plunger is moved by the micrometer screw two or three resonances separated by $\lambda_g/2$ are reached, and from λ_g the wavelength λ is readily calculated. In practice, if many wavelength readings are to be made, a conversion table from λ_g to wavelength or frequency is worth the trouble required to make it.

14-7. Directional Couplers. It is often desirable to monitor the power delivered by a microwave generator to a waveguide system. For this purpose a directional coupler is very useful, for it permits a sampling of the power from the oscillator without any of the reflected waves from the system reaching the monitor detector.

The easiest type of directional coupler to understand is analogous to directional antennas. Two holes approximately $\lambda_g/4$ apart are cut in the narrow edge of a waveguide which is to carry waves in the dominant mode. The holes match similar holes in the narrow edge of another waveguide (Fig. 14-7). Then a wave traveling from left to right in waveguide (1) will reach hole B one-quarter of a period later than hole A. A wave in the same direction starting at the same time and passing through hole A will reach hole B at the same time and the two will reinforce to produce a combined wave in waveguide (2) in the same direction.

On the other hand, a wave going through (1) to hole B and then back to A will arrive at A one-half wavelength behind a wave which passes directly through A and so be canceled by the wave from A. Thus a wave traveling from left to right in waveguide (1) will produce only a wave in the same direction in waveguide (2). A reflected wave traveling from right to left in (1) will produce only a wave traveling from right to left in (2), which will be absorbed by a suitable termination of the left end of (2). A wedge-shaped strip of lossy dielectric can be made to absorb this wave without serious reflection.

A detector at the right end of (2) then receives only waves from the oscillator, and none of the reflected power. It is thus suitable for monitoring the oscillator output power. A cavity wavemeter connected at

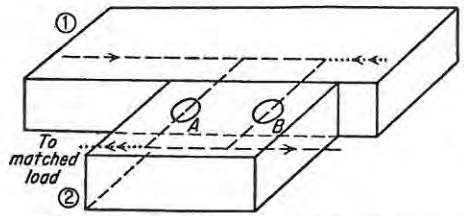

FIG. 14-7. Two-hole directional coupler.

this point is assured of a reliable power input regardless of reflections and in turn causes a minimum disturbance to the rest of the microwave circuit. For wavemeter connection a directional coupler which transmits from 1 to 10 per cent of the incident power into (2) is useful ("a 20-db" or "a 10-db" coupler).

Other types of directional couplers have been used which are merely variants of that described. For instance, the coupling holes may be in the broad face of the waveguide as long as they are far enough from the center line or wide enough to provide sufficient radiation. It should be mentioned that for either type the holes are usually large enough so that they cannot be treated exactly as points, and so their optimum spacing may not be exactly $\lambda_g/4$. In any case the spacing is not excessively critical so that the coupler is useful over a considerable wavelength band. However, better directivity (forward wave to back wave amplitude ratio) over a wide wavelength band can be obtained by using more than two coupling holes, with neighboring holes $\lambda_g/4$ apart [222]. The diameters of the holes are chosen so that α_r, the amplitude of the wave originating at the rth hole, is given by

$$\alpha_r = \alpha_0 \frac{n!}{r!(n-r)!} \tag{14-44}$$

where $n + 1$ is the number of holes. That is, the amplitudes are pro-

portional to the binomial-expansion coefficients. Then the amplitude of the reflected wave is proportional to $\cos^n (2\pi d/\lambda_g)$, where d is the distance between successive holes. The reflected wave is zero for $\lambda_g = 4d$ regardless of the number of holes, but the larger n is, the more slowly the reflected wave increases when λ_g deviates from $4d$. Many other varieties of directional coupler have been used, and several are described in [221], Chap. 14.

Another waveguide device related to the directional coupler is the "magic T" shown in Fig. 14-8. Its operation may be understood from the fact that the plane bisecting arms C and D is a plane of symmetry. Thus a wave entering through branch D in the principal mode has its electric vector symmetric about that plane. However, a wave which can be propagated in C must have an electric vector which is antisymmetric with regard to the symmetry plane. Thus a wave entering from either C or D will excite waves in A and B, either symmetrically or antisymmetrically, but waves will not pass directly from C to D. Similarly waves from A or B can excite waves in C or D, but the amplitude in C will be proportional to the difference, and in D to the sum, of the amplitudes of the waves entering through C and D.

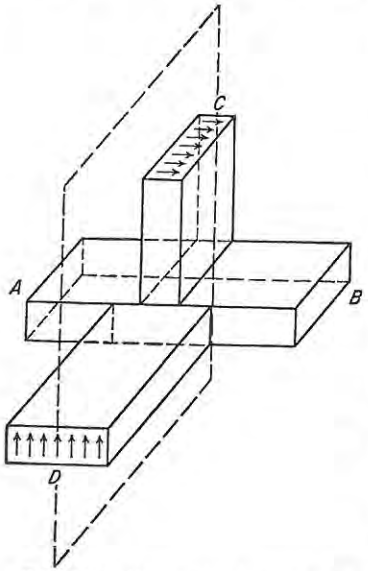

FIG. 14-8. Waveguide "magic T."

In a typical application as a directional coupler, the wave from the oscillator enters through A, and the waveguide system is connected to C. D has a power-monitoring crystal detector or wavemeter, and B has a matched load such as a tapered lossy plastic strip designed to prevent reflections. Power is then transmitted to C and D, but reflected power from C cannot enter D. A monitor in D measures only the power delivered by the oscillator to the load, regardless of reflections.

Another important application of the magic T is to balanced systems analogous to bridge circuits in ordinary electrical measurements. Use is made of the fact that arm C gives a signal depending on the difference of the signals in A and B. It can then be used to show departures from balance in arms A and B.

To prevent reflections by the magic T itself, it is usually necessary to match it to the waveguides by "irises" or diaphragms in the waveguide

positioned so as to reflect a wave of phase opposite to, and amplitude equal to, the reflection from the magic T.

14-8. Attenuators. Most waveguide systems contain at least one attenuator. Sometimes an attenuator is used to reduce power input to the system, *e.g.*, to prevent power saturation in a spectroscope absorption cell. Equally often, the attenuator is inserted principally to prevent reflections in the waveguide system from reaching the oscillator and affecting its operation.

It is always desirable, and sometimes very important, that standing waves be kept low to avoid variations in power at the detector as the frequency is varied. Attenuation in the system helps to reduce standing waves since reflected waves must pass an attenuator twice in each back-and-forth trip through the waveguide.

Most commonly attenuation is obtained by inserting a strip of lossy material such as bakelite coated with carbon (with surface resistance of a few hundred ohms per square) into the guide through a longitudinal slit in the center of the broad face. The strip is a few wavelengths long and is tapered to prevent reflections from the ends. Often it is pivoted at one end, and the attenuation is controlled by lowering the other end into the guide (see Fig. 14-9).

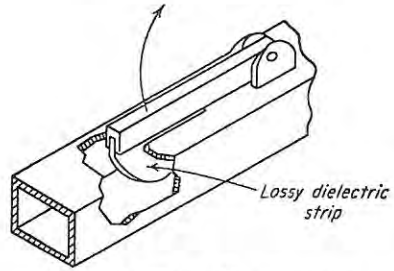

FIG. 14-9. Waveguide attenuator.

A fixed attenuator can be constructed in many ways. One of the simplest is to attach a strip of lossy dielectric to the narrow wall of the waveguide. In order that the attenuator will not itself introduce reflections its ends should be tapered. With carefully made attenuators of this type, it is possible to reduce the variation in transmitted power due to reflections to as low as about 1 per cent.

When the attenuation must be known absolutely, a short section of waveguide which is too small to propagate the wavelength produced by the oscillator may be used. The attenuation can then be calculated from the dimensions of the guide and the free-space wavelength (*cf.* page 385).

14-9. Joints in Waveguide Systems. Waveguide sections and devices are commonly joined by attaching suitable flanges and bolting them together. The flanges need only be large enough so that they can be conveniently bolted, but they must be soldered carefully flush with the ends of the waveguide. Especially if the guide is to transmit wavelengths short enough so that higher modes could be propagated, it is important to obtain good alignment of the two guides and locating pins may be provided for this purpose.

In a flat-flange joint, the longitudinal current components are carried by the capacitance between the flanges even if the contact between them is poor. However, there is a small voltage drop across the joint, and if the guide is to carry high power, as from a magnetron, arcing may occur at the joint, or there may be a small leakage of power. For these applications "choke" flanges are useful. A choke-flange joint is shown in Fig. 14-10. It differs from a flat-flange joint in that a groove $\lambda/4$ deep is cut in one flange. The inner and outer walls of this groove act as conductors of a quarter-wave coaxial line, short-circuited at one end and

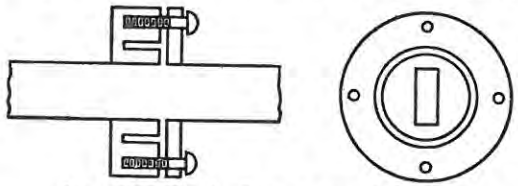

FIG. 14-10. Choke-flange waveguide joint.

thus having a very large impedance at the open end. This large impedance makes difficult a radial flow of power between the flanges. If, moreover, the distance from the groove to the waveguide is roughly another quarter wavelength, then the impedance at the waveguide wall is very small. This permits the wall currents to flow without large potential drops.

Since the dimensions of a choke flange depend on the wavelength, it is frequency-sensitive and so not well suited to equipment required to operate over large frequency ranges.

If leakage from flanges must be minimized, the completed joint may be wrapped in steel wool. If this is not done, waves radiated from the joint may be reflected from objects in the room and reenter the waveguide to cause a small change in the signal which varies as people move in the room. This precaution is usually needed only for spectrographs which do not employ modulation because they are sensitive to any change in microwave power at the detector, no matter how slowly the change occurs.

14-10. Waveguide Windows. It is often necessary to confine a gas to one section of a waveguide system. Windows for this purpose must be vacuumtight and yet reflect or absorb very little microwave power. A suitable window may be constructed of 0.001-in.-thick mica sheet sealed by a flat gasket stamped from rubber or polyethylene sheet a few mils thick and sandwiched between flat flanges. "Dental-dam" rubber obtained from dental supply houses is suitable for gaskets. A light coating of stopcock grease is used on the gasket.

For higher-temperature operation or for spectroscopy on certain reactive compounds, the rubber gaskets may be replaced by solder, lead, or

gold, and thin quartz windows have been used. A design for mica windows with lead gaskets has been described [637]. If the flanges are made sufficiently sturdy and the area of contact with the mica sufficiently small so that considerable pressure can be applied to the mica window, a good vacuum seal can be obtained without the use of a gasket. Mica windows may also be sealed permanently to metals. Such windows have been used in klystron tubes and might be applied to spectroscopy.

14-11. Plungers. Often, as in a cavity wavemeter or in a matching section, a waveguide must be terminated by a movable short-circuiting plunger. If the mode is such that currents flow across the gap between the plunger and the walls, care must be taken to provide a dependable low-impedance path for them. Sometimes, particularly at lower microwave frequencies, spring contacting fingers are sufficient. A good effective contact may be obtained by using the principle of the choke flange,

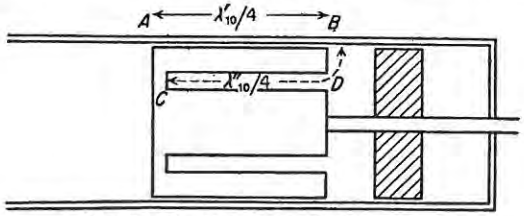

FIG. 14-11. Waveguide choke plunger.

as in Fig. 14-11, which shows a type of plunger often used in wavemeters. The inner and outer walls of the slot CD act as the conductors of a quarter-wave coaxial line short-circuited at C. Thus at D there is a high impedance which is transformed by the quarter-wave section BA to give a very low effective impedance at A. The lengths λ'_{10} and λ''_{10} are not free-space wavelengths and are not equal because the coaxial lines involved are not excited in the principal mode but in the TE_{10} mode for the appropriate coaxial waveguide ([312], Chap. 8). This type of device is of course designed for a particular wavelength but is fairly satisfactory over a wavelength range of 5 to 10 per cent.

14-12. Other Types of Guided Waves. It is possible to confine microwave radiation to a restricted region without requiring that region to be part of a hollow-tube waveguide. For instance, a horn radiator can be used to beam radiation toward a similarly directional receiving horn. A glass or quartz absorption cell between the horns could have the advantage of bringing no metal in contact with the sample, which would be helpful for corrosive materials.

If the radiation from the horns is polarized, thin metal plates can be placed in the path of the beam with their planes perpendicular to the electric vector without disturbing the fields. A low-frequency electric field can then be applied between the plates for Stark modulation.

When the horns are arranged to confine the radiation to the space between the plates, the plates constitute a parallel-plate waveguide. Alternatively the ordinary rectangular waveguide in the dominant mode may be imagined to have its width increased indefinitely. The electric field remains perpendicular to the broad faces and has a maximum value in the center, decreasing toward the now distant walls. If the extreme edges are then cut off at a point where the field is sufficiently small, the remaining portion behaves very much as the infinite-parallel-plate guide. The coupling horns serve to direct the waves from ordinary waveguides to the central region of the flat plate guide.

The use of parallel-plate waveguides for microwave spectroscopy has been suggested by Gordy [278] and investigated by Baird, Fristrom, and Sirvetz [430]. It has the advantage that small spacings can be used, and a large uniform d-c field can be applied between the plates. Moreover, the insulating spacers may be kept entirely outside the region occupied by the microwave energy so that their dielectric-loss properties are unimportant. For this reason, parallel-plate waveguides would appear to be

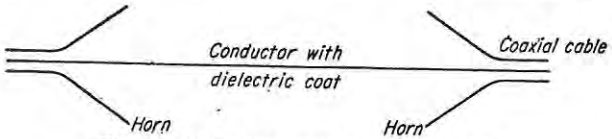

FIG. 14-12. Surface wave transmission line.

useful for operation at high temperatures where the insulators used to support Stark-effect electrodes inside ordinary waveguides give trouble. However, unless very large horns are used, the radiation tends to spread and produce rather bad frequency-sensitive reflections from obstacles outside the absorption cell.

Some of the advantages of the free-space waveguide cell, without the need for extremely large horns to provide high directivity, might be gained by using a single-conductor surface wave transmission line [575a]. This consists of a single wire with a thin coating of dielectric. The wave is launched and received by coaxial cables having their outer conductors flared to form horns (Fig. 14-12).

14-13. Microwave Applications of Ferrites. The name "ferrite" is applied to a group of materials which have high magnetic permeability and low electrical conductivity. Because of their low conductivity, microwaves can propagate through them without excessive loss. When a magnetic field is applied to a ferrite, the unpaired electron spins, which produce the high permeability, precess. A broad resonance of this precession is obtained at microwave frequencies in fields of a few thousand oersteds.

For fields lower than that needed to give resonance, a large Faraday

rotation of the plane of polarization is obtained. Figure 14-13 shows one way in which this rotation can be applied to provide variable attenuation.

The incoming wave is plane-polarized, and in a circular waveguide section the ferrite rotates the plane of polarization. If the plane of polarization is rotated 45° in one direction, the wave is transmitted by the output waveguide, but if it is rotated 45° in the opposite direction, the output waveguide cannot transmit it. Thus a control over the amplitude of the transmitted wave is obtained by varying the current in the solenoid and with it the degree of rotation.

If the magnetic field is adjusted to give 45° rotation for maximum transmission, then a reflected wave coming in the opposite direction is rotated a further 45° in the same sense. Thus the reflected wave emerges with its plane of polarization perpendicular to the short face of the input waveguide and so is not transmitted. The device therefore is a one-way

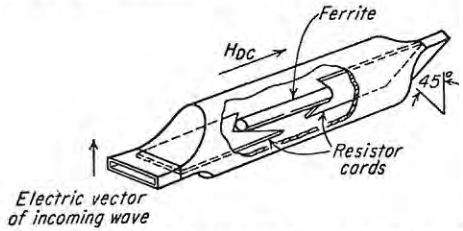

FIG. 14-13. A variable attenuator and one-way transmission device (isolator) using a ferrite. (*After Rowen* [860].)

transmitter and can be used, for instance, to isolate a klystron from a long waveguide section in which reflections can occur.

Other useful devices employing ferrites can be constructed and some of them will undoubtedly find applications in microwave spectroscopy [696a], [860].

14-14. Microwave Generators. More than any other one thing work in the microwave region is characterized by the electronic sources used for microwave generation. Heat sources used in the infrared region hardly produce usable amounts of energy for wavelengths beyond $\frac{1}{2}$ mm. The typical microwave sources provide milliwatts of power in a frequency band less than 1 Mc and sometimes less than $\frac{1}{100}$ Mc. The temperature required of a hot body to produce a similar radiation would be approximately 10^{14}°C.

Electronic generators have the advantage over heat sources that their radiation is entirely confined to a small portion of the spectrum. Hence even a small amount of power from an electronic generator may represent a very high effective temperature and be easily detectable. Moreover, this nearly monochromatic radiation makes possible the study of absorption spectra by tuning the source rather than by making a selection from the radiation of a broad source, as by a prism or grating.

However, microwaves lie just in the region of the high-frequency limit for satisfactory operation of a normal electronic tube. This is because the electrons take a time which is an appreciable part of a cycle to pass between the electrodes. At microwave frequencies the field may actually alternate many times during the electron transit time unless the electrode spacing is extremely small. The time average of the field acting on the electron is then zero regardless of the field strength. Thus the grid in a conventional triode cannot control at a microwave frequency the flow of the electrons through the tube. Triodes have been made to operate at 10,000 Mc by the use of extremely small grid-to-cathode spacing (less than the thickness of the oxide coating on most cathodes). However, with such close spacing interelectrode capacitance is a serious difficulty.

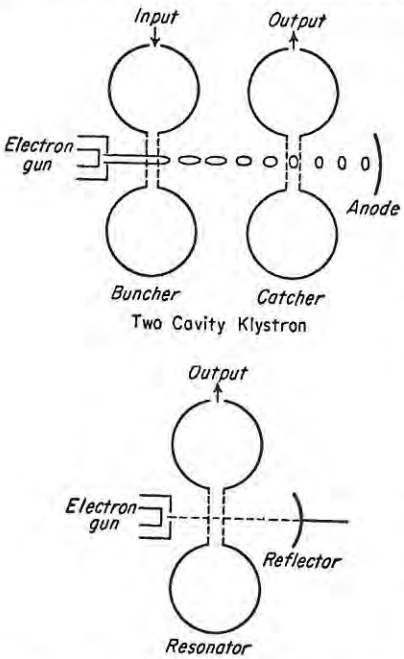

FIG. 14-14. Klystron oscillators.

14-15. Klystrons. Most microwave generators allow for and make use of the electron transit time. The klystron [281] has two resonant cavities through which an electron beam passes. A radio-frequency field in the first cavity bunches the electrons into groups which pass through the second cavity and induce radio-frequency fields in it. More exactly, the first cavity accelerates some electrons slightly and decelerates others, depending on what portion of the radio-frequency cycle they traverse. After a distance of some millimeters the fast electrons have caught up with the slower ones ahead and maximum bunching occurs. It is at this point that the second resonator is placed, for farther along the beam the accelerated electrons have passed the slow ones and the electrons are again debunched. The two-cavity and reflex klystrons are illustrated in Fig. 14-14.

If some of the radio-frequency energy from the second resonator is fed back to the buncher resonator in the right phase, as by a coaxial transmission line of suitable length, the klystron becomes an oscillator. The frequency of oscillation is determined primarily by the size of the cavities, *i.e.*, by their resonant frequency. It can also be influenced slightly by changing the electron velocity, but if the frequency is changed too much

from the center of the cavity resonance by changing the electron velocity, oscillations are not maintained.

The second cavity may be eliminated and the klystron considerably simplified if the electron beam is reversed by a suitable reflector electrode, negatively charged. After reflection, the beam retraverses the cavity, delivering to it more energy than originally received from the cavity if the beam velocity and reflector distance are right.

"Reflex" klystrons of this type have been by far the most commonly used microwave oscillators for spectroscopy. They are available commercially for almost all frequencies from below 3000 Mc to about 60,000 Mc (Sperry Gyroscope Co., Great Neck, N.Y.; Raytheon Manufacturing Co., Waltham, Mass.; Varian Brothers, San Carlos, Calif.). Individual types of reflex klystrons require accelerating voltages in the range from 300 to 3000 volts. The reflector is operated at a negative voltage which is usually between zero and 300 volts. It is necessary to stabilize the power supplies, and this is especially true for the reflector voltage. Most general spectroscopic work requires a stability such that possible short period changes in voltage (such as ripple from the alternating current which has not been perfectly filtered after rectification) can cause a frequency change not greater than $\frac{1}{50}$ Mc. This means that for the type 2K33 the accelerating voltage must be held within 0.1 volt and the reflector voltage within 0.01 volt. In addition, for this type of stability it is often helpful to operate the klystron cathode heater on direct current either from batteries or from a rectifier. Typical klystron power supplies suitable for general-purpose microwave spectroscopy use a series regulator tube controlled by reference to a voltage-regulator tube with a single stage of amplification ([221], Sec. 2-13, and [519]). An additional stage of d-c amplification in the control circuit may be needed for higher stability, particularly with 2K50 tubes.

The 2K33 family of tubes (Raytheon) has been most widely used because tubes are available for the entire wavelength region from 18,000 to 60,000 Mc with the same wiring connections and similar power requirements for all the members of the group. They have a variety of type numbers and each type covers a frequency range of only about 10 per cent. The tubes are reflex klystrons with a cavity partly inside and partly outside the vacuum. The cavity involves a bellows arrangement so that it can be compressed and thereby tuned. While the nominal range of the type 2K33 is 22,000 to 25,000 Mc, individual models sometimes may be found to oscillate anywhere in the range from 18,000 to 28,000 Mc. If a tube is not on hand for a particular desired frequency, it is possible to extend the range of another tube by loosening the locking screws which limit the range of the cavity adjustment (*cf.* [519]). Too large a change of this type may, however, damage the tube.

Another useful klystron type for the same region as the 2K33 is the

2K50. This is a smaller tube mechanically and somewhat more difficult to build. However, the completed tube is very convenient to use and requires only 300 volts on the accelerator and −150 volts on the reflector. Tuning is accomplished by changing the size of cavity thermally. One of the cavity supports is made the anode of an auxiliary triode. When this triode plate current is increased, this support is heated by electron bombardment and expands enough to tune the klystron cavity. The tube may be tuned in 2 or 3 sec over about 2000 Mc by changing the tuner grid current. The tuner grid has a sensitivity of about 120 Mc/volt [225] so that its voltage must be accurately regulated. This is not very difficult in practice, because the voltage is low and little current is drawn. Batteries may be used if a suitable power supply is not available. Moreover the tuner response is slow enough that the effect of power-supply ripple is greatly reduced. The 2K50 reflector regulation requirements are similar to those for the 2K33 family. This tube is now being manufactured by Bendix Red Bank, Eatontown, N.J.

The Varian klystrons (*e.g.*, types X-12 and X-13) are available only for frequencies below 20,000 Mc. However, they give somewhat more power than the preceding types and are therefore especially useful for driving crystal harmonic generators.

If it is desired to sweep a 2K33 slowly through a frequency band wider than can be obtained by reflector voltage variation, a suitably geared motor can be attached to the screw which varies the cavity size. A friction clutch must be included in the drive to allow slippage at the end of the tuning range and thus avoid damage to the tube. In thermally tuned klystrons, a wide frequency sweep is obtained by deriving the tuner grid voltage from a motor-driven potentiometer, preferably of the 10-turn type (*e.g.*, Helipot potentiometer).

The sources of noise and extraneous modulation in the output of klystrons are varied, and their noise spectra are poorly known at frequencies near the oscillator frequency itself. However, the noise generated by a klystron oscillator is not usually so large as that produced by the crystal detector. Occasionally an individual tube will produce exceptionally large noise, particularly near the end of a mode. In addition, klystron noise is larger than that generated by a bolometer detector and is the factor limiting the ultimate sensitivity of spectrographs using thermal detectors.

In case klystron noise has a harmful effect on a microwave measurement, it can usually be decreased by one of a number of techniques. Beyond 50 or 100 Mc from the center frequency it is usually negligible, so that noise from a local oscillator can be eliminated by using a sufficiently high intermediate frequency. Local oscillator noise can also be avoided by the use of a balanced mixer. Noise at low frequencies (*i.e.*, close to the frequency of klystron oscillation) may be eliminated by

dividing the emitted microwave into two parts, one part transversing, for example, an absorption cell before detection and the other part being separately detected. If the two detected signals are compared, variations due to oscillator noise may be eliminated and distinguished from effects of absorption in the cell (see [172]). A microwave bridge also tends to balance out noise.

14-16. Magnetrons. Multicavity magnetrons have been made to produce wavelengths as short as 2.6 mm. However, they have not been much used for spectroscopy because of the difficulty in tuning them [262]. Moreover, magnetrons are often rather noisy, and their large power output is seldom necessary.

Magnetrons have been used for spectroscopy in the millimeter region and may find further application for that purpose (see Chap. 15).

14-17. Traveling-wave and Backward-wave Tubes. A more recent type of tube which is not yet commercially available for the regions of most interest for spectroscopy is the traveling-wave oscillator. Several varieties have been constructed experimentally and they have been operated at wavelengths as short as 6 mm [511], [617]. In these tubes an electron beam is surrounded by a structure through which a wave travels more slowly than the electrons. At low frequencies (hundreds of megacycles) the wave may be guided by a helix; at higher frequencies a corrugated waveguide has been used. With suitable wave and electron velocities and appropriate coupling between them, the electron beam imparts energy to the wave, thereby increasing its amplitude. An amplification of 18 db has been obtained over a 3 per cent bandwidth near 6 mm wavelength, and such a tube can be used as an oscillator.

The "backward-wave" tube [830] is related to the traveling-wave tube. It can be constructed to give good amplification or oscillation at millimeter wavelengths and is tunable over a wide range of frequencies. In this device the electron beam passes along a corrugated waveguide to a collecting anode. An electromagnetic wave sent in from near the collecting anode emerges near the cathode and hence the wave is backward from that of a traveling-wave tube. Along its path it interacts with the electron beam at regular intervals, determined by the waveguide corrugations. The beam is thereby bunched and on traveling toward the collector interacts further with the electromagnetic wave. This provides a feedback which can be positive if rates of progress of the waves and hence phases are correct. Since the feedback phase and therefore the frequency of maximum amplification is determined by the electron-beam velocity, the frequency can be controlled by varying electrode voltages. One model has oscillated at wavelengths from 6 to 7.5 mm and has been used as an amplifier with a gain of 20 db. The power output of the oscillator is of the order of 10 mw.

Table 14-2 summarizes the microwave generators which have been

TABLE 14-2. CHARACTERISTICS OF MICROWAVE SOURCES

Source	Wavelength range	Average power output	Comments
Hot body	All wavelengths	$kT\,\Delta\nu$ (into transmission line) as long as $h\nu < kT$. For bandwidth $\Delta\nu = 10^6$ cycles/sec $kT\,\Delta\nu \leq 5 \times 10^{-14}$ watts	Of use only in exceptional cases for microwave work because of low power
Spark discharge*	∞–0.2 mm	$10^{-5} - 10^{-8}$ watt for bandwidth $\Delta\nu \approx 10^8$ cycles/sec	Low power and not monochromatic, but for short wavelengths one of the few available sources
Triode electronic tubes	∞ –3 cm	10–0.5 watts	Convenient for longer wavelengths
Klystrons	50 cm–5 mm	100–10^{-3} watts	Very convenient and tunable over about 10% range for high-frequency types
Klystrons plus crystal multipliers (harmonics)*	50 cm–0.6 mm	10^{-2}–10^{-9} watts	One of most convenient sources below 1 cm wavelength, and best source for spectroscopy below 4 mm
Magnetrons (fundamental)	50 cm–3 mm	100–1 watts	High power. Often pulsed with very high peak power. Usually tunable only over small range
Magnetron harmonics*	3 cm–1 mm	10^{-1}–10^{-9} watt	Good monochromatic source for wavelengths below 2.5 mm, but usually tunable only over small range
Traveling-wave and backward wave tubes	1 m–6 mm	100–10^{-3} watts	Expected performance similar to klystrons but not yet commercially available for short wavelengths. Tunable over wide range

* Discussed more fully in Chap. 15.

used or suggested for microwave spectroscopy. The higher powers quoted are representative of performance at the lower frequency end of the range of each type. Tubes for higher frequencies are necessarily smaller and so have reduced power, dissipation, and usually lower efficiency.

14-18. Detectors. Crystal rectifiers are used almost exclusively for detectors of microwave power in spectroscopy, although thermal detectors have been applied in some special cases. The crystal detector [325] consists of a fine wire in contact with a block of semiconducting material (most often silicon but sometimes germanium). The contact resistance is greater in one direction that in the reverse, and the current-voltage characteristic is very nonlinear near the origin so that rectification occurs when an alternating voltage is applied. Because the contact is a fine point, contact capacitance is small and the rectifier can be used up to extremely high frequencies. Nevertheless, in the millimeter-wavelength range the stray capacitance shunting the contact becomes a limiting factor.

The sensitivity of a crystal is determined by its forward and backward low-current impedances. However, the usable sensitivity is limited by crystal noise. Both these factors vary greatly between individual crystals, but a typical good type 1N26 crystal matched to a waveguide gives an output current of about 1 ma/mw. The internal output impedance is near 200 ohms when 1 mw of power is received, and considerably higher for lower received powers. The impedances which govern the performance at microwave frequencies differ from those at low frequencies by the effects of shunt capacitance and series inductance, so that low-frequency measurements are only a rough guide to the performance of a crystal at microwave frequencies. The noise power generated in a crystal may be divided into two parts. The first is the thermal agitation, or "Johnson" noise, $kT\,\Delta\nu$, where k is Boltzmann's constant $= 1.380 \times 10^{-23}$ joule per degree, T the absolute temperature, and $\Delta\nu$ the output frequency bandwidth. The second part of the noise is not strongly temperature-dependent but is approximately proportional to the square of the crystal current and inversely proportional to the output frequency. Thus the noise power of a crystal is given by

$$P = \left(kT + \frac{CI^2}{\nu}\right)\Delta\nu \tag{14-45}$$

where C = a constant
I = the d-c crystal current, amp
ν = output frequency

At room temperature (20°C), $kT = 4.04 \times 10^{-21}$ watt/cycle/sec. For a reasonably good K-band crystal C is about 10^{-7} ohms. Thus for an output frequency of 30 Mc, which is typical of superheterodyne detec-

tion, the second term of (14-45) is less than the first for normal crystal currents of 1 ma or less. For direct or "video" detection, however, lower output frequencies are used and the second term normally predominates. For $\nu = 6000$ cycles/sec, I must be reduced to a few microamperes to keep excess noise due to the second term less than "thermal" noise. Such low crystal currents have distinct disadvantages.

Since the current-voltage characteristic of a crystal is represented fairly well by $I = KV^2$, where K is some constant, the output power is approximately proportional to the square of the input power, that is, $P_{out} \propto I^2 \propto V^4 \propto P_{in}^2$. Hence, for small variations ΔP_{in} of the input power such as would be produced by gas absorption, the change in output signal is

$$\Delta P_{out} \propto P_{in}\Delta P_{in} \tag{14-46}$$

The conversion gain may be defined as $\Delta P_{out}/\Delta P_{in}$, which is a measure of the efficiency of the rectification process. It is usually considerably less than unity, and from (14-46) may be seen to decrease with decreasing power level. Hence usually the crystal current should be high enough to give good conversion and to make crystal noise predominate over amplifier noise. Since crystal noise power is proportional to the square of the current or input power from (14-45), and detected signal for a given fractional absorption is also proportional to the square of the power from (14-46), the precise value of crystal current does not affect the sensitivity or signal-to-noise ratio as long as the crystal current is large enough to make crystal noise predominate over other noise sources. Crystal currents as low as a few microamperes may hence still allow good sensitivity if exceptionally noise-free amplifiers are used. For very large crystal currents (greater than about 0.5 ma), the conversion gain no longer increases with current, which sets an upper limit to the desired crystal current.

The noise which is proportional to crystal current may be regarded as originating in a variable resistance of the rectifier. If, instead of a direct current through the rectifier, the microwaves are completely modulated with frequency ν_0 so that the rectified crystal current varies at frequency ν_0, the noise of this type becomes $\frac{CI^2}{\nu - \nu_0}\Delta\nu$ rather than $\frac{CI^2}{\nu}\Delta\nu$ as given in Eq. (14-45). For this reason amplitude modulation of the source of microwave power at a high frequency does not obviate the large crystal-produced noise in a narrow band about the frequency of modulation ν_0.

Figure 14-15 shows two typical crystal mounts for 1N26 crystals ([309], p. 171). The mount in Fig. 14-15*a* is tunable for optimum impedance match at a particular frequency, while the other is broadly resonant over

the K-band region. In the latter, especially, some adjustment may be obtained at the ends of the frequency band by moving the crystal slightly in or out of its holder.

Crystals are also used for harmonic generation, being well suited for these purposes because their nonlinear resistance characteristic persists to high frequencies, and for superheterodyne mixers. When superheterodyne detection is used, the beat oscillator should give adequate power (approximately 1 milliwatt) to the crystal to give good conversion

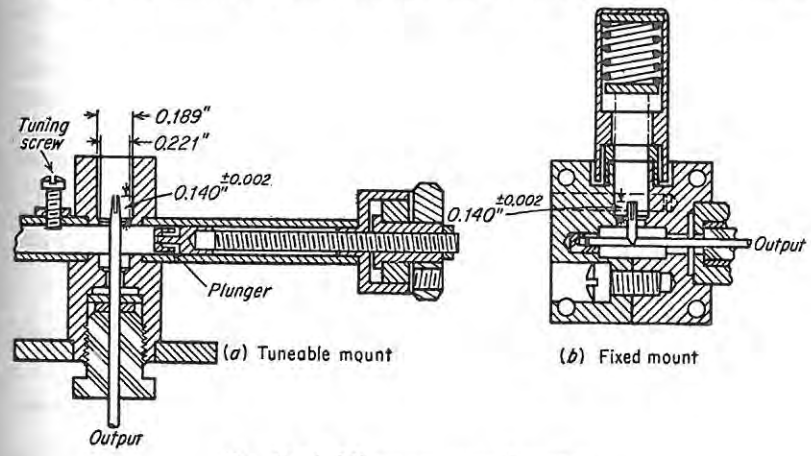

FIG. 14-15. Microwave crystal mounts.

gain [*cf.* (19-46)]. Its frequency should also differ from the signal frequency by an amount sufficiently large to prevent difficulty from crystal noise of the type indicated by the second term of (19-45) (*cf.* Sec. 15-7).

Welded contact germanium crystals have been used and are very sensitive and stable. However, they tend to have higher noise than good silicon crystals ([325], Chap. 13). When used as mixers, they may have a conversion gain greater than unity, giving an intermediate-frequency output power greater than the signal power, the local oscillator providing the difference. In the longer wavelength range, these crystals are very good for harmonic generation but unfortunately are no longer being manufactured.

Bolometers or barretters can also provide useful detection of microwaves if the power level is not too low. A bolometer consists of a small length of fine metal wire which is heated by the presence of a microwave signal, with a resulting change in resistance. The change in resistance can be detected as a voltage signal by passing a small current through the bolometer. Bolometers and their mounts are manufactured by the Sperry Gyroscope Company, Great Neck, N.Y., and by the Polytechnic Research and Development Co., Brooklyn, N.Y., with approximately

the following characteristics: resistance = 200 ohms; change of resistance = 8 ohms/milliwatt; maximum power before burnout = 15 milliwatts; time constant = 300 μsec. Units are made for microwave frequencies near 3 cm and near 1 cm which give satisfactory reception over variations in wavelength of ± 10 per cent or more. If 5 ma of current is passed through the bolometer, the above change of resistance gives a voltage change of 0.04 volts/milliwatt of microwave power.

One of the most important advantages of a bolometer is that, in contrast with crystal detectors, it gives very low noise at low (audio) frequencies. Thus the bolometer noise is not much larger than thermal noise, which is about 2×10^{-9} volts for a 1 cycle/sec bandwidth and the bolometer described above. If an amplifier is used with a noise figure of 100, this means that microwave power changes of about 5×10^{-10} watts can be detected. Bolometers will not generally respond well to changes in microwave power more rapid than about 1000 cycles/sec (time constant $\approx 10^{-4}$ sec), but for slower modulation frequencies they can be very convenient and sensitive. Additional discussion of their design and use can be found in reference [221].

References: Books on Microwaves

Barlow, H. M., and A. L. Cullen, *Microwave Measurements*, Constable & Co., Ltd., London, 1950.

Bronwell, Arthur B., and Robert E. Beam, *Theory and Application of Microwaves*, McGraw-Hill Book Company, Inc., New York, 1947.

Lamont, H. R. L., *Wave Guides*, 3d ed., Methuen & Co., Ltd., London, and John Wiley & Sons, Inc., New York, 1950.

MIT Radiation Laboratory Series, Vols. 1 to 28, members of the staff of the Massachusetts Institute of Technology Radiation Laboratory, McGraw-Hill Book Company, Inc., New York, 1947.

Principles of Radar, 3d ed., members of the staff of the Radar School, Massachusetts Institute of Technology, McGraw-Hill Book Company, Inc., New York, 1952.

Moreno, T., *Microwave Transmission Design Data*, McGraw-Hill Book Company, Inc., New York, 1948.

Pollard, Ernest C., and Julian M. Sturtevant, *Microwaves and Radar Electronics*, John Wiley & Sons, Inc., New York, and Chapman & Hall, Ltd., London, 1948.

Reich, H. J., P. F. Ordung, H. L. Kraus, and J. G. Skalnick, *Microwave Theory and Techniques*, D. Van Nostrand Company, Inc., New York, 1953.

Sarbacher, R. I., and W. A. Edson, *Hyper and Ultra-high Frequency Engineering*, John Wiley & Sons, Inc., New York, and Chapman & Hall, Ltd., London, 1943.

Skilling, H. H., *Fundamentals of Electric Waves*, 2d ed., John Wiley & Sons, Inc., New York, and Chapman & Hall, Ltd., London, 1948.

Slater, J. C., *Microwave Electronics*, D. Van Nostrand Company, Inc., New York, 1950.

Slater, J. C., *Microwave Transmission*, McGraw-Hill Book Company, Inc., New York, 1942.

Wind, M., and H. Rapaport, *Handbook of Microwave Measurements*, Polytechnic Institute of Brooklyn Microwave Research Institute, Brooklyn, 1954.

CHAPTER 15

MICROWAVE SPECTROGRAPHS

15-1. General Principles and Ultimate Sensitivity. Microwave absorption in gases is usually detected by passing microwave radiation from an oscillator through a long waveguide cell containing the gas, and measuring the amount of transmission as a function of the oscillator frequency. If the gas pressure is low enough so that the lines are not more than a megacycle or so wide, this is conveniently done by sweeping the oscillator frequency periodically and putting a voltage corresponding

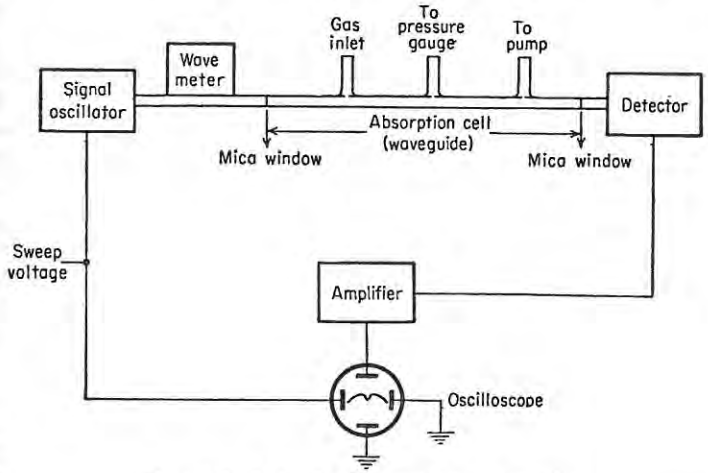

FIG. 15-1. A simple microwave spectrograph.

to this sweep on the horizontal axis of an oscilloscope, and a voltage corresponding to the transmitted power on the vertical axis. Such a system, shown in Fig. 15-1, thus plots the spectrum on the cathode-ray tube. The oscillator is swept over a region only 10 to 50 Mc wide, the center of its frequency being varied by hand to search for absorption lines or to move from one line to another. If, as is customary, the oscillator is a reflex klystron, a sweep of the order of 30 Mc is obtainable electrically by varying the repeller potential.

The type of spectrometer shown in Fig. 15-1 is simple and convenient

if the absorption lines are strong, *i.e.*, produce changes in power as large as 0.1 per cent. However, many lines give very weak absorption, so that, even with a cell length of several meters, changes in power due to gas absorption of 1 part in a million or less would have to be observed on the oscilloscope. Interfering variations in power can easily be produced by the variation in oscillator output as a function of frequency, or by variation in transmission due to reflections and standing waves in the waveguide. These difficulties generally limit a spectrometer of this type to detection of lines with absorption coefficients greater than 10^{-6} cm^{-1}, or producing a power change of 0.1 per cent in a 10-meter absorption cell. Another type of interfering fluctuation is "thermal noise." This is electromagnetic radiation in the waveguide and detector produced by thermal agitation of their electrons and is the only interfering variation of a fundamental nature. Other sources of variation can presumably be eliminated by sufficiently careful design and construction of a spectrometer, so that it is thermal noise which limits the ultimate sensitivity attainable. This limit on the minimum detectable absorption coefficient for a "perfect" spectrometer, *i.e.*, a spectrometer whose sensitivity is limited only by thermal noise, is discussed below.

If power P_0 is introduced into a waveguide it will be attenuated by losses in the waveguide walls and also by possible gas absorption. These two sources of attenuation are designated by attenuation coefficients α_0 and α_{gas}, respectively. The power after traversing a length L of the waveguide will therefore be

$$P = P_0 e^{-(\alpha_0+\alpha_{gas})L} \tag{15-1}$$

If the gas is removed, the power is $P = P_0 e^{-\alpha_0 L}$, so that the change in power due to the gas is

$$\Delta P = P_0 e^{-\alpha_0 L}(1 - e^{-\alpha_{gas} L}) \approx \alpha_{gas} L P_0 e^{-\alpha_0 L} \tag{15-2}$$

where the exponential has been expanded because we shall be interested in very weak absorptions such that $\alpha_{gas} L \ll 1$.

To find the minimum detectable absorption, we need also to calculate the fluctuations in power caused by thermal agitation. Consider a long waveguide of length L which, for simplicity, supports only one mode of propagation for frequencies near ν. The waveguide will be assumed to be lossless and to be shorted at both ends. This guide is in reality a cavity and its resonant modes are given by $n = 2L/\lambda_g$, where λ_g is the wavelength of radiation in the guide and n is an integer. Since λ_g is not very different from the wavelength λ in a vacuum (in most practical cases $\lambda_g \approx 1.2\lambda$), we shall write $n = 2L/\lambda$ and neglect the complications of modified wavelength and velocities in the waveguide. Then $n = 2L\nu/c$. As long as $kT \gg h\nu$, the classical equipartition law holds, and the average energy in each mode of oscillation is kT. Since the number of modes per

frequency interval is $dn/d\nu = 2L/c$, the energy per frequency interval is

$$\frac{dW}{d\nu} = \frac{2LkT}{c} \quad \text{or} \quad \Delta W = \frac{2LkT}{c}\Delta\nu \tag{15-3}$$

Each standing-wave mode can be resolved into two equal traveling waves moving in opposite directions. Each wave contains half the energy, so that the total energy per second moving down the guide in one direction is one-half the energy density per unit length times the velocity c, or

$$\frac{c\,\Delta W}{2L} = kT\,\Delta\nu \tag{15-4}$$

This is the thermal power in the frequency interval $\Delta\nu$ which travels in either direction down the waveguide. It is independent of the length of the waveguide and so holds equally well for an infinite waveguide or for its practical equivalent, a finite lossy waveguide or one terminated by matching impedances. For instance, the thermal power flowing from a waveguide into a matched crystal detector is given by (15-4). In addition the crystal must radiate an equal amount of power into the waveguide if the entire system is in thermal equilibrium.

This thermal energy $kT\,\Delta\nu$ produces a fluctuating signal at the crystal detector. It might, at first thought, appear that a signal due to gas absorption would be detectable as long as the change in power produced at the crystal was somewhat larger than the thermal power $kT\,\Delta\nu$. However, the thermal power is associated with a field strength in the waveguide which combines with the field strength due to the purposely transmitted microwave to produce apparent changes in power at the crystal considerably greater than $kT\,\Delta\nu$.

For convenience, let the transmitted microwave power from the signal oscillator be represented by a voltage defined so that $V^2 = 2ZP$, where P is the power and Z is the guide impedance. V is the voltage amplitude of the wave emitted by the oscillator. The similar voltage due to thermal radiation will then be $(\Delta V)^2 = 4ZkT\,\Delta\nu$, where an additional factor of 2 is required because there is a wave of thermal radiation in each direction along the guide which contributes to voltage fluctuations at the detector. The net power flow in the guide (assuming no gas absorption) is

$$\frac{(V \pm \Delta V)^2}{2Z} = P \pm 2\sqrt{2kTP\,\Delta\nu} + 2kT\,\Delta\nu \tag{15-5}$$

Equation (15-5) shows that the thermal radiation produces changes of power of magnitude approximately $\sqrt{PkT\,\Delta\nu}$, which is considerably larger than the thermal power itself, since usually $P \approx 10^{12}kT\,\Delta\nu$. For a signal to be noticeable, the power change involved must be approximately as large as or larger than $\sqrt{PkT\,\Delta\nu}$. Then using the change in power due to gas absorption given by Eq. (15-2), the smallest detectable

absorption coefficient for a waveguide of length L is given when

$$\alpha_{gas} L P_0 e^{-\alpha_0 L} \approx 4 \sqrt{2 P_0 e^{-\alpha_0 L} k T \, \Delta\nu} \tag{15-6}$$

or

$$\alpha_{gas} = \frac{4}{L} \sqrt{\frac{2kT \, \Delta\nu}{P_0 e^{-\alpha_0 L}}} \tag{15-7}$$

This expression is a minimum for a certain optimum waveguide length

$$L_{op} = \frac{2}{\alpha_0} \tag{15-8}$$

Then

$$\alpha_{gas}(\min) = 2e\alpha_0 \sqrt{\frac{2kT \, \Delta\nu}{P_0}} \tag{15-9}$$

for the optimum waveguide length $2/\alpha_0$. The same result follows from a more rigorous treatment ([328]; *cf.* also [445], [278]).

Instead of absorption, it is possible to use dispersion, or variation in dielectric constant, to detect a gas resonance. The ultimate sensitivity attainable can be shown to be essentially the same as by detection of absorption [653].

The optimum guide length $L = 2/\alpha_0$ is generally between 5 and 30 meters since $\alpha_0 \approx 10^{-3}$ cm^{-1}. If the power used in the waveguide is 1 mw, and the bandwidth of the detecting circuits is 30 cycles, the minimum detectable absorption coefficient would be $\alpha_{gas}(\min) \approx 10^{-10}$ cm^{-1}. Actual spectrometers have not reached this ideal sensitivity, the best being approximately 30 times less sensitive for bandwidths of 30 cycles as assumed here.

The actual sensitivity of microwave spectrometers is usually limited by one of the following instead of by fundamental thermal fluctuations:

1. Random fluctuations of power due to
   a. Noise in excess of thermal noise as a result of current flowing in the detecting crystal
   b. "Oscillator noise," or variations in oscillator output
   c. Noise in excess of thermal noise in the amplifying circuits
2. Changes in power which vary systematically with oscillator frequency as a result of
   a. Variation of oscillator power as a function of frequency
   b. Variation with frequency of transmission of the waveguide, absorption cell, and detecting crystal
3. "Conversion loss" in the crystal detector, *i.e.*, the loss in signal power when a microwave signal is converted into a lower-frequency signal by the detector.

The first and third difficulties are usually allowed for by introducing a noise figure N, which is the factor by which the ratio of noise to signal

power coming through the amplifying circuits has been changed by troubles of types 1 and 3. Thus for $N = 1$, a signal power of $kT \, \Delta\nu$ would appear as large as noise, but for $N = 20$, the signal power would have to be 20 times larger to equal noise power. Hence (15-9) becomes for a nonideal system

$$\alpha_{gas}(\min) = 2e\alpha_0 \sqrt{\frac{2kT \, \Delta\nu \, N}{P}} \tag{15-10}$$

The noise figure N can easily vary with conditions and usually depends to some extent on the power P and the frequency. In typical good microwave spectrographs N is as large as 10^3, as may be surmised from the discrepancy of a factor of 30 between $\alpha_{gas}(\min)$ observed and the ideal value. The fact that the crystal noise and hence the noise figure usually decreases with decreasing current means that optimum sensitivity is obtained with waveguides somewhat longer than that given by (15-8). However, from (15-7) the sensitivity varies only slowly with variations in lengths, which are near optimum, so that the precise value of the optimum length is not critical.

Usually the worst source of random noise is the detecting crystal, for which the noise at low frequencies is often much greater than thermal (*cf.* Chap. 14). Crystals vary by orders of magnitude; it is well worth while to select crystals for low noise. Oscillator-tube noise is usually less than crystal noise, but some klystrons have noisy frequency regions, particularly near the edge of a mode. Oscillator noise is also less serious than crystal noise because if necessary it can always be eliminated by bridge or compensating systems.

The most troublesome cause of systematic variation with frequency is usually reflections or standing waves in the absorption cell which vary the transmission from oscillator to crystal. As the signal oscillator frequency is varied, this produces a pattern of peaks and valleys in the power received by the crystal. If the waveguide cell is of length L and the offending reflections occur as usual near the two ends of the cell, the peaks and valleys repeat every time the oscillator frequency is varied by $c/2L$. If the cell is long, these reflection effects produce narrow peaks which closely resemble absorption lines. They may be reduced by introducing an attenuator between the two sources of reflections. The attenuator itself may, however, introduce new reflections. Carefully tapered attenuators can reduce power variations of this type to $\frac{1}{10}$ per cent, but even so reflections make it difficult to detect a total gas absorption much less than this amount. Thus the simple microwave spectrograph of Fig. 15-1 is suitable only for the stronger absorption lines.

Electrical filters can help discriminate between absorption lines and noise or reflections. In a waveguide which is not too long, reflections give a slower variation of power with frequency than does a line, so that

a high-pass filter tends to suppress reflections with respect to the line. Since noise occurs with all frequencies, much of the noise can be eliminated by filtering out all frequencies higher than those essential to pass the absorption line. Often noise can be best eliminated by sweeping very slowly over a small region about the absorption line and rejecting all frequencies higher than about ten times the sweep frequency, which is all that is necessary to reproduce the line. If the sweep frequency is ν_0, then this represents a bandwidth of $10\nu_0$, and if the noise power per frequency interval $P/\Delta\nu$ is constant as in thermal noise, ν_0 should be made as small as possible to minimize the bandwidth $\Delta\nu$. On the other hand, if crystal noise dominates as is often the case, the noise power depends on ν. From Eq. (14-45) the noise power per frequency interval is $P/\Delta\nu = C/\nu$, where C is a constant. The total noise power is the integral

$$P = \int_{\nu_1}^{\nu_2} \frac{CI^2}{\nu}\, d\nu = CI^2 \log \frac{\nu_2}{\nu_1}$$

The lower limit ν_1 of frequency passed should be not more than two or three times the sweep frequency ν_0, and the highest frequency ν_2 not much lower than $10\nu_0$. Hence $P = CI^2 \log (\nu_2/\nu_1) \sim CI^2 \log 5$, and is independent of the sweep rate. This independence of noise power on sweep frequency (with appropriate filtering) holds only under conditions where crystal noise predominates. If any other sources of noise are important, a slow sweep rate is usually advantageous.

It might be thought that modulating the klystron power at a high frequency (*i.e.*, 100 kc) and amplification of the 100-kc signal on the crystal would allow discrimination against this crystal noise since crystal noise has a maximum at low frequency from (14-45). Unfortunately such a system gives no particular advantage, however, because the crystal noise acts as if it were produced by a variable resistance. Hence the maximum noise always occurs at the frequency of the current flowing through the crystal. Modulating the amplitude of the microwave power at 100 kc simply produces a maximum of the objectionable noise at 100 kc, and no improvement in signal-to-noise ratio (*cf.* Sec. 14-18).

15-2. Source Modulation. Considerable improvement in signal-to-noise ratio can be obtained by a small frequency modulation of the klystron oscillator at, say, a frequency of the order of 100 kc in addition to the slower sweep frequency [278], [286]. This modulation can be achieved easily by adding to the klystron slow sweep a 100-kc sine-wave or square-wave sweep voltage. If at a particular instant the klystron is just at the peak of an absorption line and a voltage pulse is applied to the repeller, the klystron moves off the line and the absorption disappears so that more power reaches the crystal. With a 100-kc modulation the line appears and disappears 100,000 times a second. If a line is

present, the 100-kc frequency modulation is converted into amplitude variations at the crystal, which may be amplified by a tuned amplifier. If the amplifier is tuned to 100 kc, only noise components near that frequency are amplified and these are much smaller than the low-frequency components. Note that this frequency modulation does not produce a large modulation of the crystal current, as would amplitude modulation of the klystron source.

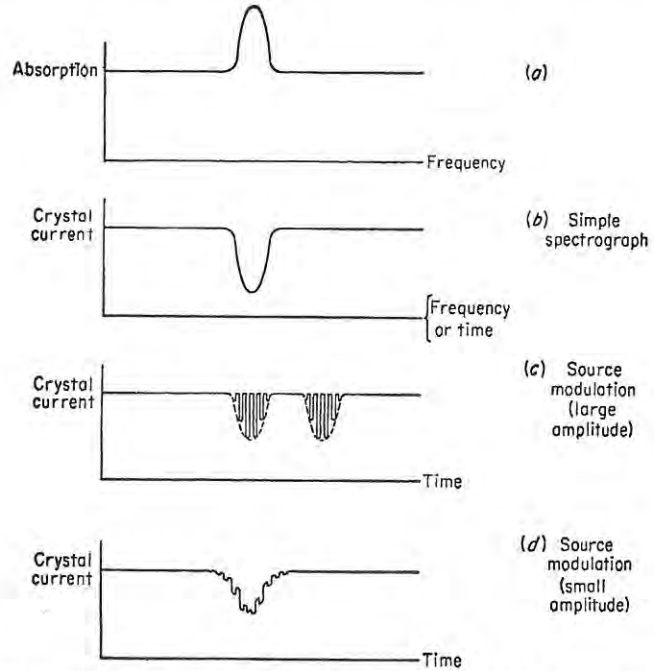

FIG. 15-2. Absorption and corresponding waveforms, one with a simple spectrograph and one using frequency modulation of the microwave source in addition to a slow frequency sweep.

Sharp variations in output power with frequency, as, for instance, those due to certain types of reflections, may also produce 100-kc components and such reflections have often been mistaken for lines. Transmitted power variations with frequency due to reflections are usually less rapid than those due to absorption lines and hence may often be distinguished from them. However, variations due to reflections are a serious limitation on the ultimate sensitivity of this type of spectrometer.

Figure 15-2 shows the crystal-current waveform for the simple spectrograph and for the frequency-modulated, or "double-modulated," spectrograph. In Fig. 15-2*c*, the modulation of the instantaneous klystron

frequency is assumed to be greater than the line width. The line first appears as one tip of the instantaneous frequency excursion strikes the absorption. However, the two appearances of the line are at opposite phases of the modulation frequency and if necessary they can be distinguished by a phase-sensitive detector.

If the modulation is small compared with the line width, the modulation-frequency component of the crystal current is proportional to the slope of the absorption curve. The line may be said to be differentiated, and the two modulation-frequency peaks occur at the points of largest slope, while the output at the peak absorption is zero. For a line with a Lorentz shape, as given by the first term of the Van Vleck–Weisskopf equation (13-19), these peaks occur at $\Delta\nu/\sqrt{3}$ from the center of the absorption line, where $\Delta\nu$ is the line-width parameter.

Square-wave modulation, which has been assumed, gives the most faithful reproduction of the line shape (or its derivative) [465]. However, sine-wave modulation may be used for simplicity [202], [248] with little loss of sensitivity, but with some distortion of the line shape.

15-3. Stark Modulation. If an electric field is applied to a polar molecule its absorption frequencies are shifted because of the Stark effect (Chap. 10). If at some instant the klystron frequency coincides with the peak of an absorption line, when the electric field is applied the absorption decreases. Thus high-frequency modulation can be obtained by subjecting the gas to a periodically interrupted electric field [210], [396]. In addition to the reduction in crystal and tube noise at the high modulation frequency, the method has the very great advantage of being almost completely insensitive to systematic power variations due to anything but spectral lines. Reflections and klystron power variations associated with the low-frequency sweep usually produce very small interfering signals at the high modulation frequency. This useful type of spectrometer was introduced by Hughes and Wilson [210].

Square-wave modulation is almost universally used with Stark spectrographs, with one tip of the square wave being at zero field. Then during this half of the cycle, the absorption pattern is that of the undisplaced line, while during the other half cycle the Stark spectrum occurs. With a phase-sensitive detector, the oscillograph pattern shows both the absorption line and the Stark pattern with the latter inverted. The Stark pattern may then be used to identify the transition or to measure the molecular dipole moment.

Figure 15-3 shows a cross section of a waveguide cell suitable for Stark modulation and a block diagram of the instrument. Stark spectrographs have been described by several authors [419], [396], [519]. The cell is usually a section of waveguide about 3 meters long, as the optimum length is reduced by the extra attenuation of the Stark plate and its supporting insulation. It may be constructed from ordinary waveguide, with the

addition of a central flat plate parallel to the broad faces of the guide and so perpendicular to the microwave electric field. The plate is supported by strips of good insulating material such as polystyrene or teflon in which guiding grooves are milled. Connection to the Stark electrode is made by a wire through a hermetic seal in the side wall, which may terminate in a screw threaded into the plate. An alternative support using mica strips rather than plastic is suitable for higher temperatures [637].

Most often the waveguide size chosen is that appropriate to the wavelength band being used, but larger sizes are sometimes desirable to reduce

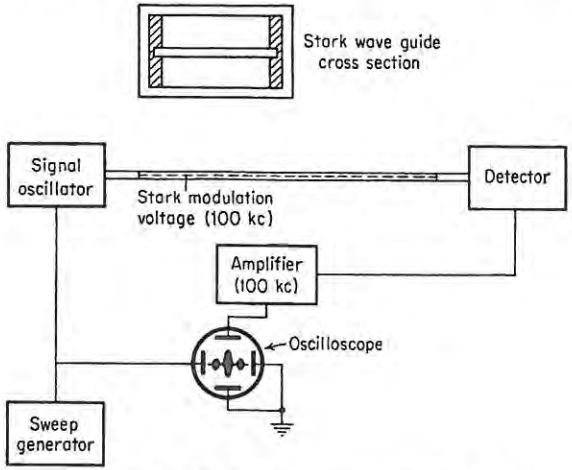

FIG. 15-3. Stark-modulation spectrograph.

the microwave energy density and so avoid saturation. However, larger sizes require larger applied voltages for a given Stark field, and this may be difficult to obtain. A large enough modulating field strength should be used so that all the Stark components are displaced more than the line width, if possible. Otherwise some of the Stark components (inverted by the phase-sensitive detector) will overlap the main line and subtract from it. A few volts per centimeter is usually sufficient for a line with a low J value having a first-order Stark effect. If only a second-order Stark effect occurs several hundred to several thousand volts per centimeter may be needed.

The requirements for the square-wave generator are made more severe by the capacitance between the central plate and the rest of the guide which may be as much as 1000 $\mu\mu$f. For this reason the square-wave generator must have a low output impedance and be capable of supplying large output currents. One such generator, constructed for the Columbia Radiation Laboratory by S. Geschwind, takes a sine wave from a

100-kc oscillator and clips it in several stages of pentode limiting amplifiers to produce a square voltage wave. The necessary low output impedance is obtained from a final cathode follower stage of two 829B or 3E29 tubes in parallel. Provision is made so that an adjustable direct voltage may be added to the square wave to ensure that one end of the square wave corresponds to zero voltage between the Stark plate and the waveguide. For lines which have only small second-order Stark effect, it is sometimes useful to adjust the d-c voltage so that the low-voltage half of the square wave is several hundred volts above zero. Since a second-order Stark effect is proportional to the square of the field, a given change in voltage produces a larger modulation at high field strengths, and so it may be useful to start from a nonzero field.

Another suitable type of square-wave generator [373], [585], [519] uses two sets of parallel output tubes. One set, connected to the high voltage, charges the capacitance of the Stark electrode while the other set discharges it on alternate half cycles. The two groups of output tubes are each triggered at the right time by a blocking oscillator controlled by a sine-wave input voltage of the same frequency as the desired square wave. If the square wave is to be very near zero on one half-cycle, an additional clamping diode is needed. Thus the plates of one group of triggered output tubes may be at a high positive voltage and the cathodes of the other group at about minus 40 volts. The diode clamping tubes are connected to ground so that the voltage cannot actually decrease to negative values, but is stopped sharply near zero. This type of circuit can provide a better and higher voltage square wave at high frequencies than the limiting amplifier, but the blocking oscillator must be readjusted if the frequency is changed.

15-4. Modulation-frequency Signal Amplifiers. The modulation-frequency amplifiers need to have sufficient gain and sufficiently low noise that crystal noise is the only limiting factor in the spectrograph's sensitivity. Since the signal is lowest in the first amplifier stage, that is the most critical one from the standpoint of noise. In fact, the signal voltage at the input may be as low as the crystal noise which, for a 30-cycle bandwidth and a few hundred microamperes of crystal current, is of the order of 10^{-9} volt. A considerable increase in signal voltage can be obtained by using a series-resonant input circuit tuned to the modulation frequency, as shown in Fig. 15-4. The device may be considered as a matching network from the low crystal impedance (300 to 5000 ohms) to the high input impedance of the amplifier. Since the matching network output impedance is high, the cable connecting it to the amplifier must be short and of low capacitance. It is important that the matching network be well shielded. The circuit of Fig. 15-4 also includes a separate low-pass filter to permit measurement of the direct crystal current. If, to avoid saturation of the spectral line, it is necessary to operate at low power levels so that the crystal noise and signal are both small, the resonant input circuit can be followed by a cascade amplifier using a low-noise tube such as the 12AY7 [460]. With this combination the amplifier noise is only slightly greater than the thermal noise of a resistor equal in value to the crystal impedance, *i.e.*, its noise figure is not much more than unity.

It is always easy to test whether or not the amplifier is sufficiently noise-free. If it is, then a decrease in crystal current should produce a decrease in noise voltage through the amplifier or on the oscilloscope which is approximately proportional to the change in current. If such a decrease occurs, the noise must originate either in the microwave oscillator or in the crystal, and for normal oscillators it will be crystal noise.

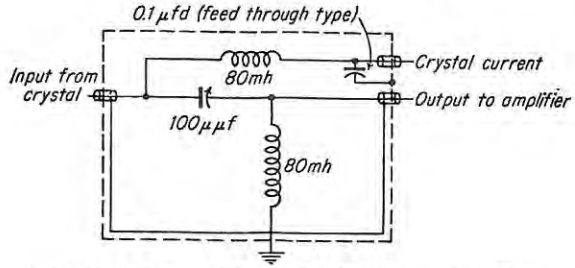

FIG. 15-4. Resonant input circuit for signal amplifier.

Various types of modulation-frequency amplifiers have been used. It is possible to use a commercial broad-band preamplifier followed by a tunable low-frequency radio receiver. Since the receiver does not need to be easily tunable and the preamplifier does not require a broad band, a specially constructed amplifier can be somewhat simpler. Many other amplifier combinations are possible, and some of them are described in the references [419], [396], [519], [460].

The bandwidth used in the receiver should, to reduce noise, be as low as possible. If it is too small, the line will not be faithfully reproduced unless the sweep rate is reduced. Moreover, a too narrow receiver band may lead to errors in frequency measurement [460]. The necessary ratio of bandwidth to sweep rate for good portrayal of a line cannot be specified uniquely, but is often of the order of 20. It is not difficult to have a sweep rate lower than 1 per second on a long-persistence oscilloscope. For use with a recorder on the receiver output, the klystron tuner may be driven slowly by a motor so as to cause the line to be traversed even more slowly. Bandwidths as low as 1 cycle/sec may then be usable. Since in this case the noise power is proportional to bandwidth, a narrow band and slow sweep are highly desirable for good sensitivity. Such a narrow effective bandwidth is most readily attained by means of a phase-sensitive detector (or "lock-in amplifier," as it is sometimes called).

Figure 15-5 is the circuit diagram of a simple type of phase-sensitive detector. The signal is applied to the control grid of a pentode amplifier. From the modulation generator a large voltage (10 to 100 volts depending on the tube used) is applied, through a phase shifter, to the suppressor grid. During one-half of the modulation cycle, the tube functions as a class A amplifier. During alternate half cycles, the lock-in voltage is sufficiently negative to cut off the plate current and with it the amplification.

In the absence of a signal, the plate current consists of a series of pulses once each cycle of the modulation frequency. If a signal of the same frequency and phase is present, the pulses are larger, while if it has opposite phase the pulses are smaller. The plate load resistance R and by-pass capacitor C produce an output voltage determined by the average

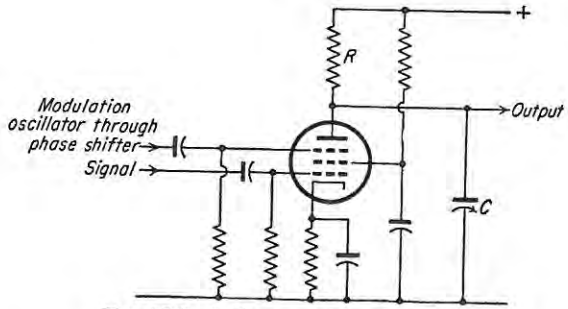

FIG. 15-5. A phase-sensitive detector.

size of these pulses averaged over a time determined by the time constant CR. Thus a signal of the modulation frequency will either increase or decrease this averaged output voltage, depending on its phase. A signal of any other frequency will have no fixed phase relative to the lock-in voltage and so will produce no effect on the average plate current or output voltage.

Interfering signals or noise at frequencies near the modulation frequency will produce fluctuations in output voltage if the time constant is not sufficiently large. The fluctuations might appear to be transient signals of the modulation frequency encountered during a sweep. It will be seen that the longer the time constant CR, the nearer an interfering signal must be in frequency to produce a signal, and so the narrower the effective bandwidth.

Figure 15-6 shows the signal waveforms at different places in a Stark spectrograph using a tuned amplifier and lock-in detector. Phases are indicated by "off" or "on" referring to the portions of the modulation cycle in which the Stark voltage, is, or is not, zero, respectively.

Both the line and its Stark components appear in the final output voltage. Since they occur at opposite phases, the Stark component is

inverted relative to the main line. The line shown in Fig. 15-6 is assumed to have only one Stark component, but commonly there are several.

To use a recording milliameter with a lock-in detector of the type shown, the average plate current in the absence of a signal must be balanced out by an auxiliary supply. The balancing current may be obtained by means of a potentiometer from the plate supply.

For greater stability, the signal and balancing voltages may be obtained from matched amplifiers; *i.e.*, the balancing voltage may be supplied

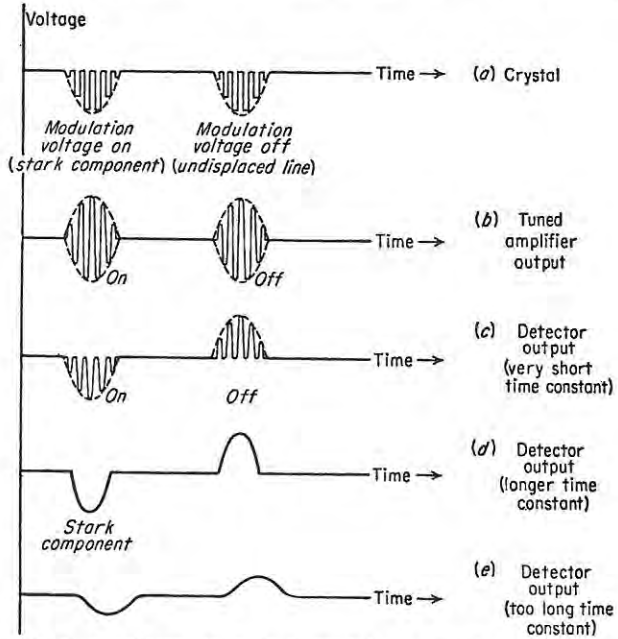

FIG. 15-6. Signal waveforms in a Stark-modulation spectrograph using a phase-sensitive detector.

by a second phase detector whose phase is such that its plate current charges in the opposite direction to the first one when a signal is received [396]. Inverse feedback may be applied to the amplifiers to improve the linearity and stability [737].

One of the primary advantages of a lock-in amplifier is that it provides an easy method for obtaining a very narrow bandwidth about any desired frequency. If a lock-in amplifier is used as part of an amplifying system, the effective bandwidth, *i.e.*, the band from which noise is received, is just half the reciprocal of the time constant, or $\Delta\nu_2 = 1/2CR$. (This assumes that $\Delta\nu_2$ is the smallest bandwidth of the system, which is almost always the case.) If a lock-in is not used, the signal would

typically be passed through an amplifier of bandwidth $\Delta\nu_1$, then rectified by a conventional detector followed by a filter of time constant CR or bandwidth $\Delta\nu_2$. The effective bandwidth may then be considerably greater than $\Delta\nu_2$. This is because pairs of noise components throughout the whole amplifier bandwidth $\Delta\nu_1$ are mixed in the detector to produce frequencies which lie within the band $\Delta\nu_2$. The effective bandwidth of this system is $\sqrt{\Delta\nu_1 \Delta\nu_2}$, so that the noise power may be considerably greater than that obtained with a lock-in amplifier.

If the detector time constant is too long relative to the time for a sweep, the output voltage cannot change fast enough to reproduce the line shape accurately. The line then appears to be broadened and reduced in height. Moreover, its peak is delayed and so comes at a point in the sweep corresponding to a different microwave frequency.

If a long time constant (*i.e.*, narrow bandwidth) must be used to reduce noise, the sweep rate must be proportionately lowered. The ultimate limit to the degree of improvement in signal-to-noise ratio which can be thus achieved is set by fluctuations in the klystron output frequency. Further improvement requires increased oscillator stability, which can be attained by use of an external stabilizing cavity resonator or by a controlling quartz-crystal oscillator with frequency multipliers.

15-5. Zeeman Modulation Spectrographs. For paramagnetic molecules such as NO, O_2, NO_2, ClO_2, and free radicals, a magnetic modulation

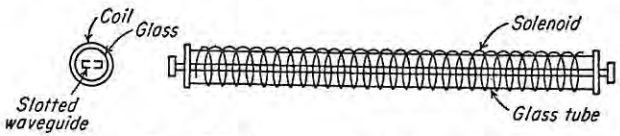

FIG. 15-7. Zeeman modulation cell.

analogue of the Stark spectrograph can be constructed. The high-frequency magnetic field is most easily applied by a solenoid surrounding the waveguide.

Unless the modulation frequency is quite low, the guide must be slotted longitudinally to reduce eddy currents; such a slot can be put in the center of the broad face without disturbing the microwave fields. A glass tube surrounding the waveguide serves as a support for the coil and keeps the sample gas in the guide region (Fig. 15-7). At modulation frequencies less than 1000 cycles/sec, it is often possible to operate without the slot and then the glass envelope is no longer needed.

Since a square current wave through an inductance is hard to generate at high frequencies, sine-wave modulation may be used with a direct current added so that one extreme of the sine wave occurs at approximately zero field. The coil can then be part of a series-resonant circuit if large currents are desired.

15-6. Choice of Modulation Frequency for Spectrographs. Although crystal noise is reduced as the modulation frequency is raised [Eq. (14-45)], the apparent line width is increased (Chap. 10). The line breadth due to a square-wave modulation is somewhat greater than the modulation frequency, so that for the fine structures commonly encountered in microwave spectroscopy, modulation frequencies much greater than 100 kc have seldom been found desirable. Indeed, for particularly small line spacings even considerably lower frequencies may be desirable, even though the crystal noise is increased.

Whatever the modulation frequency, the amplifier should if possible have a low enough noise figure so that it contributes less noise than the crystal. As long as this is so, decreasing the microwave power level decreases the signal and the noise proportionately. Thus the signal-to-noise ratio is nearly independent of power. Very low microwave power levels (a few microwatts) are sometimes required in high resolution spectrographs to avoid saturation broadening, and then special precautions for amplifier input circuits may be needed. If such a low level must be used that most noise comes from the amplifier, the noise is independent of the signal. In that case, for any given microwave absorption, the signal is proportional to the power level, and so the sensitivity is also proportional to the power.

15-7. Superheterodyne Detection. At low microwave power levels, crystals are inefficient detectors, as their output voltage is approximately proportional to the square of the radio-frequency amplitude. It is then advantageous to use superheterodyne detection to produce a signal as large as possible relative to noise in the following amplifiers. Moreover, if the intermediate frequency is reasonably high (*e.g.*, 30 to 60 Mc) crystal noise within the intermediate-frequency amplifier bandwidth is reduced practically to the thermal noise.

Superheterodyne detection requires an auxiliary microwave oscillator which is kept at a constant frequency difference from the signal oscillator. This local oscillator may be made to follow the signal oscillator by a discriminator and automatic frequency-control system ([308], Sec. 8.3; [573]). Then as the signal oscillator is tuned, the frequency difference between it and the local oscillator is always such that the mixer output is at the desired intermediate frequency.

The need for an extra oscillator and automatic frequency control makes the superheterodyne more complicated than the simple detector. It is not usually possible to make the local oscillator follow automatically over more than a limited region. Moreover, the local oscillator may be an additional source of noise, although this noise can always be eliminated by the use of a balanced mixer [309].

15-8. Bridge Spectrographs. It has been seen that superheterodyne detection can be employed as an alternative to modulation for reducing